HAL
open science

Décryptage des processus transcriptionel dans la sénescence cellulaire : le rôle de PARP1 dans la régulation de l'expression génique associée à la sénescence

Lucas Robinson

To cite this version:

Lucas Robinson. Décryptage des processus transcriptionel dans la sénescence cellulaire : le rôle de PARP1 dans la régulation de l'expression génique associée à la sénescence. Biologie du développement. Université Paris Cité, 2019. Français. NNT : 2019UNIP7099 . tel-03145221

HAL Id: tel-03145221

https://theses.hal.science/tel-03145221v1

Submitted on 18 Feb 2021

HAL is a multi-disciplinary open access archive for the deposit and dissemination of scientific research documents, whether they are published or not. The documents may come from teaching and research institutions in France or abroad, or from public or private research centers.

L'archive ouverte pluridisciplinaire **HAL**, est destinée au dépôt et à la diffusion de documents scientifiques de niveau recherche, publiés ou non, émanant des établissements d'enseignement et de recherche français ou étrangers, des laboratoires publics ou privés.

Université de Paris

Ecole doctorale BIOSPC ED 562

Laboratoire Institut Pasteur – Oncogenesis and Nuclear Organization / Senescence and Age-related Pathologies

Deciphering Gene-regulatory Processes in Cellular Senescence:

The role of PARP1 in the regulation of senescence-associated gene expression

Par: **Lucas Robinson**

Thèse de doctorat de Biologie Cellulaire

Dirigée par Oliver Bischof

Présentée et soutenue publiquement à Paris le 19/09/2019

Président du jury : Desdouets, Chantal (DR2 – Université Paris Descartes)
Rapporteur : Gil, Jesus (Professor – MRC London Institute of Medical Sciences – Imperial College)
Rapporteur: Mann, Carl (DR2 - Université Paris-Saclay)
Directeur de thèse : Bischof, Oliver (DR2 – Institut Pasteur)
Membre invités : Li, Han (G5 Group Leader – Instiut Pasteur)
Membre invités : Gilson, Eric (Professor/Director – Institut de Recherche sur le Cancer et Vieillissement)

Acknowledgements

As the clock has run down on my time as a PhD student, it is almost unimaginable to look back on my transformation over the past 4 years. I have come a long way in so many parts of my life. I have an enormous number of people to thank for being beside me along this path and helping me get through it all. I have gone through some ups and downs, mountains and valleys, and I would not be here today if it were not for my support network of incredible colleagues, friends, and family.

I would first thank my thesis jury: Chantal Desdouets, Carl Mann, Jesus Gil, Eric Gilson, Han Li for committing their time to evaluating my work and contributing to my academic journey. My PhD would not have been possible without support from the leader of our wonderful ONO unit, Anne Dejean.

Thank-you to my supervisor, Oliver, for helping me grow from my microbiologist background to what I am now. I have learned more than what I thought was possible in my time with you in the lab. I think you have pulled together an amazing team, pushing significant and valuable research. I appreciate our friendship, candidness and all the days in the lab. It's a great feeling when coming into the lab is exciting. It has made my time working together special, and for which I am very grateful. It is just like my opinion man, but it has been a pleasure.

Thanks, Ricardo, for mentoring me and pushing me to become who I am today. I feel like my journey through the fire was incredibly difficult, but I have become stronger, thanks to you. I am proud to call you a friend.

I want to thank everyone in the ONO group. I arrived as a young buck from the middle of nowhere Canada, and I was welcomed with such open arms. Pef, Greg and Ricardo, you guys immediately made me feel part of the team, and part of a family. Pef, I appreciate your friendship and having you as a colleague. It was an incredible experience to learn from you and to spend so much time in the lab together. I know for sure, that some of our experiences I will never forget. Greg, you helped me through so much, at every stage of this thesis, inside and outside of the lab. Your generosity and kindness are heartwarming. I have to thank our "office" team in the back corner: Nir and Jota. Coming into the lab and discussing everything under the sun has made my days in the lab unforgettable. Ilan, thank you for being a killer squash partner,

concert buddy, and amazing friend. I appreciate how you welcomed me into your life and introduced me to your own social network. Having all of you as friends is something I will appreciate for my whole life. Everyone in the ONO unit who helped me to adjust to life in Paris, and life in the lab: Thibault, Juan-Pablo, Jacob, Pablo, Jack, Victoria, Ying, Elma, Tatiana, Alexandra, Pascal, Agnes, Samia, Coraline, Cathy, Monique, Nacho! Thanks!

And finally, thank you to my friends and family from Canada. I can't thank you enough for the support over the past 4 years from abroad. May the TiltQueens continue to thrive. Living with you Ross will always be an amazing memory, our time in Paris has been fantastic. Thank-you Mom and Dad for always being there when I am on the up slope or the down slope. You have supported me completely to realize this goal. Through all of it, you have been there, thank-you.

Table of Contents

ACKNOWLEDGEMENTS ..... **II**

LIST OF FIGURES AND TABLES ..... **VI**

LIST OF ABBREVIATIONS ..... **VII**

FOREWORD **1**

GENERAL INTRODUCTION **3**

1.1. A Brief History of Cellular Senescence 5
1.2 Markers of Senescence 8
1.2.1. Senescence-Associated Growth Arrest (SAGA) *8*
1.2.2. Apoptosis Resistance *9*
1.2.3. Cytomorphological Changes *9*
1.2.4. Senescence-Associated Beta-Galactosidase (SAβG) *10*
1.2.5. Metabolism *11*
1.2.6. Chromatin Conformation: SAHF/SAD/SDF/TIFS/LADS *12*
1.2.7. Senescence-Associated Secretory Phenotype (SASP) *13*
1.3 Causes of Senescence 15
1.3.1. Replicative Senescence (RS) *15*
1.3.2. Stress-Induced Premature Senescence (SIPS) *16*
1.3.3. Oncogene-Induced Senescence (OIS) *16*
1.3.4. DNA Damage Induced Senescence (DDIS) *18*
1.3.5. Therapy-induced senescence (TIS) *20*
1.3.6. Mitochondrial Dysfunction-Associated Senescence (MiDAS) *21*
1.3.7. Development *22*
1.3.8. Tissue Regeneration, Repair and Maintenance of Plasticity and Stemness *22*
1.5. Mechanisms and Regulation of Cellular Senescence 24
1.5.1. Senescence arrest *24*
1.4.2. TP53 and the Senescence Arrest *25*
1.4.3. pRB and the Senescence Arrest *27*
1.4.4. Other Critical Players Regulating the Senescence Arrest *29*
1.5. Mechanisms and Effects of the SASP 30
1.5.1. Paracrine/Juxtracrine Effects of the SASP *32*
1.5.2. Immune Surveillance of Senescent Cells *33*
1.5.3. SASP and Tumor Promotion *35*
1.6. Regulation of the SASP 36
1.6.1. NF-κB and SASP Regulation *37*
1.6.2. CEBPβ and SASP Regulation *38*
1.7. Regulation of the Senescence-Associated Gene Expression Program 41
1.8. Clinical Relevance of Senescence 43
1.8.1 Senescence and Pathology 47
2.1 Poly (ADP-ribose) Polymerase 1 (PARP1) 51
2.2 PARP1 Protein Structure 51
2.3. ADP-ribose 54
2.4. Modes of PARP1 Regulation 55
2.5. Functions and mechanisms of PARP1 and ADP-ribosylation 57
2.6. PARP1 binding and catalytic activity play a multi-facetted role in the nucleus 58
2.6.2. PARP1 is a key player in DNA damage repair *59*
2.6.3. Chromatin remodeling during DNA damage *60*
2.6.4 PARP1 and ADP-ribosylation and the Regulation of Gene Expression 62
2.6.5 PARP1-Driven Chromatin Decondensation at D. melanogaster heat-shock protein 70 (HSP70) loci . *62*
2.6.6. PARP1 and the Regulation of Histones and DNA Modification *63*
2.6.6. PARP1 and Chromatin insulation *65*
2.6.7 PARP1 and Heterochromatin *66*
2.6.8 Interactions with Histones *67*

2.6.10 PARP1 Binding and Enzymatic Interactions with Transcription Factors 68
2.6.9 PARP1 Regulation of Inflammatory Gene Expression 72
2.7 Role of PARP1 Binding and Catalytic Activity in Physiology and Pathophysiology 75
2.7.1 Role of PARP1 in Cancer 76
2.7.2. PARP1 Inhibitors in Cancer Therapy 76
2.7.3. PARP1 and Aging 77
3. Thesis Rationale, Aims and Hypothesis 79
3.1. Thesis Aims 80
3.2. Hypothesis: 81

4. RESULTS 82

4.1 PARP1 enzymatic activity and ADP-ribosylation are increased in OIS 83
4.2 Experimental outline to measure the differential impact of PARP1 depletion and enzymatic inhibition on the RAS-OIS gene expression program 87
4.3 Differential impact of PARP1 depletion and enzymatic inhibition on the RA-OIS gene expression program 90
4.4 PARP1 regulates chromatin-associated ADP-ribosylation at enhancers to fine-tune the transcription of lowly expressed genes 93
4.5 PARP1-mediated ADP-ribosylation modulates chromatin accessibility of active RAS-OIS enhancers 96
4.6 Active ADP-ribosylated RAS-OIS enhancers are enriched for select TF binding sites 98
4.7 PARP1 binding is enriched at transcription start-sites to regulate the RAS-OIS transcriptional program 100
4.8 Repositioning PARP1-inhibitors as potential senolytics 102

5. DISCUSSION AND FUTURE DIRECTIONS 105

5.1. PARP1 is enzymatically activated during OIS 108
5.2. Distinct PARP1 catalytic and chromatin-binding activities control the RAS-OIS gene expression program. 109
5.3. Genome-wide mapping of ADP-ribosylation 110
5.4. PARP1 catalytic activity localizes to active enhancers of lowly expressed genes 111
5.5. PARP1 catalytic activity influences chromatin accessibility at active enhancers of senescence-associated genes through a context-dependent mechanism 112
5.6. ADP-ribosylation co-localizes with TFs at enhancers during OIS 114
5.7. PARP1 binds globally across the genome, but exerts a regulatory role at the TSS by maintaining stable nucleosome positioning at TSSs through its chromatin-binding activity 115
5.8. PARP inhibitors selectively eliminate senescent cells from cell culture through prolonged exposure 116
5.9. Future Directions: 118

6. MATERIALS AND METHODS 121

7. BIBLIOGRAPHY 134

8. APPENDIX 164

8.1 CONTRIBUTIONS TO PUBLICATIONS: 165

8.1.1 AP-1 Imprints a Reversible Transcriptional Program of Senescent Cells 166
8.1.2 Necroptosis Microenvironment Directs Lineage Commitment in Liver Cancer 256
8.1.3 Cell Snapshot: Cellular Senescence Pathways 257
8.1.4 Cell Snapshot: Cellular Senescence in Pathophysiology 288

List of Figures and Tables

INTRODUCTION FIGURE 1. HALLMARKS OF AGING 5
INTRODUCTION FIGURE 2. MARKERS OF SENESCENCE 8
INTRODUCTION FIGURE 3. METABOLIC CHARACTERISTICS OF SENESCENT CELLS 12
INTRODUCTION TABLE 1. NOTABLE SASP FACTORS 14
INTRODUCTION FIGURE 4. CHARACTERISTIC DNA-DAMAGE RESPONSE DURING SENESCENCE 20
INTRODUCTION FIGURE 5. PATHWAYS OF SENESCENCE 24
INTRODUCTION FIGURE 6. IMMUNE SURVEILLANCE OF SENESCENT CELLS 34
INTRODUCTION FIGURE 7. SASP PATHWAYS. OUTLINING THE PATHWAYS INVOLVED IN REGULATING SASP EXPRESSION 36
INTRODUCTION FIGURE 8. TWO-PHASES OF SASP GOVERNED BY NOTCH SIGNALING 39
INTRODUCTION FIGURE 9. INK-ATTAC MICE: 44
INTRODUCTION FIGURE 10. CELLULAR SENESCENCE IN PATHOPHYSIOLOGY 46
INTRODUCTION FIGURE 11. STRUCTURE OF PARP1 52
INTRODUCTION FIGURE 12. ADP-RIBOSYLATION METABOLISM 55
FIGURE 1: OUTLINE AND VALIDATION OF CHROMATIN ADP-RIBOSYLATION AFFINITY PURIFICATION (CRAP) METHOD 84
FIGURE 2: PARP1 ENZYMATIC ACTIVITY AND ADP-RIBOSYLATION LEVELS ARE INCREASED IN OIS CELLS 86
FIGURE 3: DIFFERENTIAL IMPACT OF PARP1 DEPLETION AND ENZYMATIC INHIBITION ON THE SENESCENCE GENE EXPRESSION PROGRAM. 89
FIGURE 4: VALIDATION OF K/S METRIC TO MEASURE CHANGES IN ADP-RIBOSYLATION IN RAS-OIS. 92
FIGURE 5. PARP1 REGULATES CHROMATIN-ASSOCIATED ADP-RIBOSYLATION AT ENHANCERS TO FINE-TUNE THE TRANSCRIPTION OF LOWLY EXPRESSED GENES. 95
FIGURE 6: ADP-RIBOSYLATION MODULATES CHROMATIN ACCESSIBILITY OF ACTIVE RAS-OIS ENHANCERS. 97
FIGURE 7: ACTIVE ADP-RIBOSYLATED RAS-OIS ENHANCERS ARE ENRICHED FOR SELECT TF BINDING SITES. 99
FIGURE 8: PARP1 BINDING IS ENRICHED AT TRANSCRIPTION START-SITES TO REGULATE THE RAS-OIS TRANSCRIPTIONAL PROGRAM. 101
FIGURE 9: REPOSITIONING PARP1-INHIBITORS AS POTENTIAL SENOLYTICS. 104
DISCUSSION FIGURE 1: WELL-POSITIONED NUCLEOSOMES AT TSS FACILITATE TRANSCRIPTION. 116

List of Abbreviations

5-mc	5-methylcytosine
53BP1	TP53-binding protein 1
aa	Amino acid
AD	Automodification domain
ADP	Adenosine diphosphate
ADPr	ADP-ribose
AGO-2	Argonaute RISC Catalytic Component *2*
AKT	Protein-kinase B
ALC1	Chromodomain-helicase-DNA-binding protein 1-like
AMP/ADP:ATP	Adenosine monophosphate/diphosphate:triphosphate
ANRIL	anti-sense ncRNA in the INK4 locus
AP1	Activator protein 1
AREG	Amphiregulin
ATAC-seq	Assay for transposase accessible chromatin
ATM	Ataxia telangiescasia mutated
ATPase	Adenosine triphosphatase
ATR	Ataxia telangiesctasia and Rad 3 related
ATTAC	Apoptosis through targeted activation of caspase
BCL-2	B cell lymphoma 2
BCL6	B cell lymphoma 6
BER	Base Excision Repair
bFGF	Basic fibroblastic growth factor
BLB1	MHC class beta chain 1
BMP2	Bone morphogenic protein 2
BRCA1	Breast Cancer 1
BRCT –	BRCA c-terminus
BRD4	Bromodomain containing protein4
BrdU	Bromodeoxyuridine
BRG1	SWI/SNF related, matrix associated, actin dependent regulator of chromatin 1
Brm	Bromodomain
BUB3	Budding uninhibited by benzimidazole-3
BUBR1	Budding uninhibited by benzimidazole-related 1
CaKIId	Calcium dependent protein kinase
CAT	catalytic domain
CAV1	Caveolin
CBP	CREB binding protein
CBX5,-7	Chromobox 5,-7
CCL2	Chemokine ligand 2
CCNA	Cyclin A
CCNB	Cyclin B
CCR2+	Chemokine receptor 2
CD4+	Cluster differentiation 4
CDC25	Cell division cycle 25
CDH2	Cadherin 2
CDK-4,-6-,-8,-9	C*yclin-dependent kinase -4, -6, -8, -9*
CDKI	C*yclin-dependent kinase inhibitor*
CEBP/B	CCAAT Enhancer Binding Protein Beta
cGAS	*Cyclic GMP-AMP synthase*
ChIP	Chromatin immunoprecipitation

ChIP-Seq	Chromatin immunoprecipitation sequencing
CHK1/2	Checkpoint kinases 1,2
COPD	Chronic obstructive pulmonary disorder
CRAP	Chromatin ADP-ribosylation Affinity Purification
CREB	C-AMP response element-binding
Csf2	Granulocyte-macrophage colony-stimulating factor
CtBP	C-terminal binding protein
CTCF	CCCTC-binding factor
cTNT	Cardiac troponin T
CXCL1-3,5-6	CXC motif chemokine ligand 1-3,5-6
CXCR2	CXC motif chemokine Receptor 2
DAPI	4',6-Diamidino-2-Phenylindole
DBD	DNA binding domain
DDR	DNA damage response
DEGs	Differentially expressed genes
DNMT1	DNA methyltransferase 1
DSB	double strand break
ECM	extra cellular matrix
EdU	5-Ethynyl-2´-deoxyuridine
EGF	Epidermal growth factor
EGF-r	Epidermal growth factor receptor
ELKS	ETS-like protein 1
EMT	Epithelial-mesanchymal transition
ERK	Extracellular-signal-regulated Kinases
ESC	Embryonic stem cell
EZH2	Enhancer of zeste homologue 2
FGF4	Fibroblast growth factor 4
GATA4	GATA binding protein 4
GM-CSF	Granulocyte-macrophage colony-stimulating factor
GMP	Guanosine monophosphate
Gro-alpha	CXCL1
GSK3B	*Glycogen synthase kinase 3 beta*
H1	Histone 1
H2	Histone 2
H3	Histone 3
H4	Histone 4
HCC	Hepatocellular carcinoma
HDAC 1, -3	Histone de-acetylase 1,-3
HES1	hairy and enhancer of split-1
HGF	Human growth factor
HGPS	Hutchinson-gilfrod progeria syndrome
HMGA1/2	High mobility group protein 1/2
HMGN1	High Mobility Group Nucleosome-Binding Domain-Containing Protein 1
HOXB7	Homobox protein hox-B7
HP1	Histone protein 1
HPF1	Histone parylation factor 1
HS	Heat shock
HSP70	Heat shock protein 70
HUS1	HUS checkpoint clamp component
ICAM-1,-3	Intercellular Adhesion Molecule -1,-3
IGF-2,-3,-4,-6,-7	Insulin-like growth factor-1,-2,-3,-4,-6,-7
IGFBP	Insulin-like growth factor binding proteins

IGFBP-5/7	Insulin-link growth factor binding protein
IKKa,-b,-g	Inhibitor of nuclear factor kappa-B kinase subunit -a,-b,-g
IL-1a,-1b,-6,-7,-13,-15,-8,-12,-15	Interleukin-1a,-1b-6, 7,-13, -15,-8,-12,-15
IL6R	IL-6 Receptor
INF-B	Interferon beta
INK4A	Inhibitor of CDK4
iNOS	Inducible nitric oxide synthase
IPF	Idiopathic pulmonary fibrosis
IRF1,-3	Interferon regulatory factor-1,-3
JNK3	c-Jun N-terminal Kinase
K20me3	Lysine 20 tri-methylation
K27Ac	Lysine 27 acetylation
k4me1	Lysine 4 mono-methylation
K4me3	Lysine 4 tri-methylation
K9me2	Lysine 9 di-methylation
K9me3	Lysine 9 tri-methylation
KDM-4,-5	Lysine demethylase -4,-5
KGF	Keratinocyte growth factor
KLF4	Kruppel like factor 5
KO	Knock-out
LADS	Lamina associated domains
LIG3	DNA ligase 3
LPS	Lipopolysaccharides
LSD1	Lysine-specific histone demethylase 1A
Mash1	Mammalian Accaete –Scute Homolog-1
MCAT	Malonyl CoA-acyl carrier protein transacylase
MCP-2,4	Monocyte chemoattractant protein -2, -4
MDC1	Mediator of DNA damage checkpoint 1
MDM2	Murine double minute 2
MEK	Mitogen-activated protein kinase
MER11	meiotic recombination 11-like protein
mESCs	Mouse embryonic stem cells
MiDAS	Mitochondrial dysfunction-associated senescence
MIF	Macrophage Migration Inhibitory Factor
MIP-1a/3a	Major Intrinsic Protein Of Lens Fiber -1a,-3a
MMP-1,-3,-10,-12,-13,-14,	matrix metalloproteinases-1,-3,-10,-12,-13,-14,
MNASE	Micrococcal nuclease
MRN	Mre11, Rad50 and Nbs1
MTA1	metastisis protein 1
mTOR	mammalian target of rapamycin
mTORC1/2	mammalian target of rapamycin complex 1/2
Myc	Avian Myelocytomatosis Viral Oncogene Homolog
NAD+/NADH	Nicotinamide adenine dinucleotide
NBS1	Nibrin
NCoR	Nuclear Receptor Corepressor 1
NEIL1	Nei Like DNA Glycosylase *1*
NELF	negative elongation factor
NEMO	NF-kappa-B essential modulator
NER	Nucleotide excision repair
NF1	Nuclear factor 1
NFAT	Nuclear Factor of Activated T-Cells

NfkB	Nuclear factor kappa-light-chain-enhancer of activated B cells
NHEJ	Non-homologous end joining
NIS	Notch-mediated juxtracrine induced senescence
NK	Natural Killer
NKG2	Natural Killer group 2
NLS	nuclear locationzation signal
NO	Nitric Oxide
NOTCH1	NOTCH receptor 1
NOX4A	NADPH oxidase 4A
NuRD	Nucleosome remodelling deacetylase
OA	Osteoarthritis
OB-fold	Oligonucleotide/oligosaccharide-binding *fold*
Oct4	Octamer-binding transcription factor 4
OGG1	8-Oxoguanine DNA Glycosylase-1
OIS	Oncogene-induced senescence
OPG	Osteoprotegerin
P38MAPk	P38 mitogen-activated protein kinases
pADPr	Poly-ADP-ribose
PAI-1	Plasminogen activator inhibitor-1
PANADA	P21-associated noncoding *RNA* DNA damage-activated
PAR	Poly-ADP-ribose
PARG	*Poly (ADP-ribose) glycohydrolase*
PARK2	Parkin RBR E3 Ubiquitin-Protein Ligase
PARP1	Poly-ADP-ribose polymerase 1
PARPi	PARP inhibitor
PC-PPLC	Phosphatidylcholine-specific phospholipase C
PcG	Polycomb group proteins
PCNA	proliferating cell nuclear antigen 2
PGE2	Prostoglandin E2
PI3K	Phosphoinositide 3-kinase
PIASy	Protein inhibitor of activated STAT protein gamma
PIDD	p53-induced protein with a death domain
PIGF	Phosphatidylinositol Glycan Anchor Biosynthesis Class F
PIN	Peptidyl-prolyl cis-trans isomerase NIMA-interacting
PINK1	PTEN-induced putative kinase 1
PKB	Protein kinase B
PML	Promyelocytic Leukemia
Pot1	Protection of telomeres protein 1
pRB	Retinoblastoma protein (phosphorylated)
PRC1/2	Protein Regulator Of Cytokinesis 1
PTEFb	positive transcription elongation factor-b
PTEN	Phosphatase And Tensin Homolog
PTM	Post-translational modification
RAC1	Ras-Related C3 Botulinum Toxin Substrate 1
RAD-1,-9	*RAD1* Checkpoint DNA Exonuclease -1,-9
RAF	Rapidly Accelerated Fibrosarcoma
Rap1	RAS-related protein
RAR-A,-B	Tetinoic acid receptor-A,-B
RAS	Rat sarcoma
RBP2	Retinol Binding Protein 2
RECQ1	RecQ Like Helicase
REL-A,-B,-C	REL-associated protein-A,-B,-C

RIG1	Retinoic acid-inducible gene I
RIP-1	Receptor-interacting protein 1
RNA pol-II	RNA polymerase II
RNA-let7	RNA-the lethal 7
RNF168	Ring Finger Protein 168
ROS	Reactive oxygen species
RPA	Replication Protein A
RRM2	Ribonucleotide Reductase Regulatory Subunit M2
SA-B-gal	Senescence-associated beta galactosidase
SADS	Senescence-associated distention of satellites
SAFA	Scaffold-attachment-factor A
SAHF	Senescence-associated heterochromatin foci
Sam68	Src-associated in mitosis 68 kDa *protein*
SAPD	Senescence-associated protein degradation
SASP	Senescence-associated secretory phenotype
SCF	Stem cell factor
SDF –	Senescence DNA damage foci
SDF-1	Stromal cell derived factor 1
SEGs	Stably expressed genes
SET7/9	Histone H3-K4 methyltransferase
SGP130	Soluble gp130
shRNA	Short-hairpin RNA
Sin3	SIN3 Transcription Regulator Family Member
siRNA	Small-interfering RNA
SIRT-1,-3,-5	Sirtuin -1,-3,-5
SMAD-2,-3,-4	SMAD family member-2,-3,-4
SMARCA5	SWI/SNF related, matrix associated, actin dependent regulator of chromatin 5
SMRT	Silencing Mediator For Retinoid And Thyroid Hormone
SMS	Senescence messaging secretome
Sox2	SRY (sex determining region Y)-box 2
SP1	Specificity protein 1
SSB	Single strand break
SSBR	Single strand break repair
STAT3	Signal Transducer And Activator Of Transcription 3
STING	Stimulator of interferon *genes*
sTNFR1	Soluble tumor necrosis factor receptor 1
Suv39h1	Suppressor Of Variegation 3-9 Homolog 1
Suz12	Suppressor Of Zeste 12 Protein
SWI/SNF	SWItch/Sucrose Non-Fermentable
TAK1	TGF-b activated kinase 1
TARG1	Terminal ADP-ribose *protein* glycohydrolase
TEF-1	Translation elongation factor-1
TERT	Telomerase reverse transcriptase
TF	Transcription Factor
TGF-B	Transforming growth factor
TGS	Transcriptional gene silencing
TIF	Telomere-dysfunction-induced foci
TIMP-2	Tissue inhibitor of metalloproteinases -2
TIN2	TRF1 interacting nuclear factor 2
TIS	Therapy-induced senescence
TLE1	Groucho/Transducin-like Enhancer of Split 1 xv
TLR	Toll-like receptor

TMEM9B	Transmembrane protein 9-B
TNF-a	Tumor necrosis factor-a
TOPBP1	Topoisomerase II Binding Protein 1
TopoIIB –	Topoisomerase II-B
Tpp1 –	Tripeptidyl peptidase 1
TRAF6	TNF Receptor-Associated Factor 6
TRAIL-R3,	Tumor-necrosis-factor related apoptosis inducing ligand-receptor 3
Trf1/2	Telomeric repeat-binding factor 1 – TERF1 gene
UHRF1	Ubiquitin Like With PHD And Ring Finger Domains 1
uPAR	Urokinase *receptor*,
VEGF	Vascular endothelial growth factor
VHL	*Von Hippel-Lindau*
VSMC	Vascular smooth muscle cells
WIP1	Wild-type p53-induced phosphatase gene
XRCC1	X-ray repair cross-complementing protein 1
YB-1	Y box binding protein 1
YY1	Ying yang 1
ZFP36L1	ZFP36 Ring Finger Protein Like 1
ZnI, -II, -III	Zinc fingerI, -II, -III

Foreword

Cellular senescence is a cell fate triggered in response to a variety of non-lethal stressors acting as a safeguard of damaged or dysfunctional cells and playing important roles in aging, health, and disease. Senescent cells are characterized by their stable cell cycle arrest and important changes in chromatin architecture and gene expression, become resistant to cell death and secrete a bevy of inflammatory chemokines/cytokines and matrix remodeling metalloproteases, the so-called senescence-associate secretory phenotype (SASP). In line with its prominent role in aging and age-related diseases, elimination of senescent cells holds excellent therapeutic promise; however, a comprehensive understanding of the genetic and epigenetic mechanisms, which underlie the induction and maintenance of senescence, is still fragmentary and thus, prevents a deliberate manipulation of this cell fate.

PARP1 (Poly (ADP-ribose) polymerase 1), also referred to as ADP-ribosyltransferase Diphtheria toxin-like 1 (ARTD1), is an abundant nuclear protein, that catalyzes the transfer of ADP-ribose (ADPr) from NAD^+ onto target proteins, a process that is referred to as ADP-ribosylation. Historically the prime PARP1 function was associated with DNA damage repair; however, we know now that it is also implicated in many other nuclear processes, markedly in the transcriptional regulation of inflammatory genes, although many details are still missing.

Given its role in the transcriptional regulation of inflammatory genes, and chromatin structure we hypothesized that PARP1 plays a role in the regulation of the senescence gene expression program. To characterize the gene-regulatory role of PARP1 in the execution and maintenance of senescence we combined reverse genetics and pharmacological inhibitors with transcriptome, chromatin accessibility (ATAC-seq), genome-wide PARP1 (PARP1 ChIP-seq), and ADP-ribosylated chromatin profiling using a novel technique termed CRAP-seq (Chromatin-ribosylation affinity pull-down sequencing).

We discovered a novel and unexpected enzymatic and non-enzymatic function of PARP1 in senescence-associated gene regulation. Specifically, we unraveled that the

enzymatic function of PARP1-mediated ADP-ribosylation of chromatin was significantly enriched at enhancers of lowly expressed genes to fine-tune their transcription. PARP1's non-enzymatic function was particularly crucial at promoters, where it acts to maintain a stable and specific positioning to control transcription. Finally, we provided evidence that PARP inhibitors may be potent cell-death inducing agents of senescent cells by modulating the expression of apoptotic genes.

In conclusion, we uncovered novel gene-regulatory mechanisms of PARP1 function, thus expanding our understanding of how senescence is regulated epigenetically. Our long-term goal is to explore PARP1 inhibition as a therapeutic modality to manipulate the senescence phenotype.

General Introduction

Age is the most significant risk factor of disease and death in developed countries (Harman, 1991). Old age is accompanied by a striking increase in diseases that are rare in younger individuals, including cardiovascular disease, cancer, and neurodegeneration (López-otín et al., 2013). This correlation has led to the hypothesis that there are common underlying biological mechanisms of aging that drive disease. Hence, if we can target these underlying mechanisms of aging, we could ameliorate health-span and potentially extend life-span.

Aging is the progressive decline in functional integrity and homeostasis, culminating in death (Kennedy et al., 2014; López-otín et al., 2013; Mahmoudi and Brunet, 2012). Much of our understanding of the genetics of aging originates from short-lived non-vertebrate model organisms such as yeast, worms, and flies (Kennedy et al., 2014). Historically, aging was considered a stochastic process. We assumed that nature evolved mechanisms for protection and maximal fitness of an organism only until sexual maturity, and that beyond the age of reproductive capacity, absence of selective pressure leads to a gradual, decline of these systems (evolutionary theory of antagonistic pleiotropy as proposed by Paul Williams) (Williams and Day, 2003). However, as we advanced our molecular understanding of the aging process, it has become clear that aging is a much more organized and programmed process that can be manipulated (López-Otín et al., 2013; Mahmoudi and Brunet, 2012). Hence, we need to delineate the underlying mechanisms that drive age-related pathology, understand how systems that are protective in young organisms can become deleterious with age, and define how the progression of aging takes place across all organismal levels starting from the cell

passing through tissues, organs and of course the whole organism. Indeed, aging may, at one point in time, be qualified as a treatable disease.

Similar to the “Hallmarks of Cancer” (Weinberg and Hanahan), “Hallmarks of Aging” were stipulated (**Introduction Figure 1**) (López-Otín et al., 2013). The hallmarks of aging include: genomic instability, telomere attrition, epigenetic alterations, loss of proteostasis, deregulating nutrient-sensing, mitochondrial dysfunction, cellular senescence, stem cell exhaustion, and altered intercellular communication (López-Otín et al., 2013). These entities are not mutually exclusive, but maybe functionally interconnected and are meant to serve as primary entry points for scientific investigations and inroads for therapeutic interventions.

Introduction Figure 1. Hallmarks of Aging (Adapted from Lopez-Otin, 2013)

1.1. A Brief History of Cellular Senescence

One fundamental aging mechanism is cellular senescence (van Deursen, 2014). Leonard Hayflick and Paul Moorhead first described cellular senescence in 1961 (Hayflick, 1965; Hayflick and Moorhead, 1961). They observed that primary human cells grown in culture have a finite replicative lifespan, which refuted the long-standing dogma by Alexis Carrel that cells are inherently immortal (Carrel, 1912). Hayflick coined the term replicative senescence, and Olovnikov hypothesized that this cell culture phenomenon is related to organismal aging (Olovnikov, 1971). We now know that replicative senescence is a result of the progressive shortening of telomeres and only one example of many non-lethal stressors that can induce what we now more generally refer to as cellular senescence (Allsopp et al., 1992). Following this seminal discovery, an entire research field has developed, implicating cellular senescence in many physiological and pathophysiological conditions.

Cellular senescence is a cell fate and complex stress response characterized by a stable cell cycle arrest and inflammatory phenotype. Stressors include, replication-induced telomere shortening, hyper-active oncogenes, loss or derepression of tumor suppressor genes, cell fusion, wound-healing, mitochondrial dysfunction, DNA damage (chemotherapy, reactive oxygen species, irradiation), developmental signals, or cytokine signaling (Campisi and d'Adda di Fagagna, 2007; Kuilman et al., 2010; Martínez-Zamudio et al., 2017a; Muñoz-Espín and Serrano, 2014). To protect the organism from malignancy, and avoid the mass tissue loss through apoptosis, damaged cells are removed from the cell cycle and prevented from proliferating (Campisi and d'Adda di Fagagna, 2007; Kuilman et al., 2010; Martínez-Zamudio et al., 2017a; Muñoz-Espín and

Serrano, 2014). Yet, senescence is not only a potent tumor suppressor mechanism, but it also plays many other significant physiological and pathophysiological roles, for example, in tissue regeneration, maintenance of stem cell plasticity, age-related diseases, tissue degeneration and paradoxically tumor promotion (Kuilman et al., 2010; Martínez-Zamudio et al., 2017b).

1.2 Markers of Senescence

There is a diversity of senescence triggers, and all of these produce a panoply of senescence-associated biomarkers (**Introduction Figure 2**). However, not all biomarkers are present in each senescence context and none of them is specific for senescent cells. The faithful identification of senescent cells therefore requires a combination of a minimum two biomarkers (Campisi and d'Adda di Fagagna, 2007; Kuilman et al., 2010). Thus, it is critical to the field to identify specific, rather associated biomarkers, and ideally, a single biomarker to improve studies on the occurrence of senescence in health and disease.

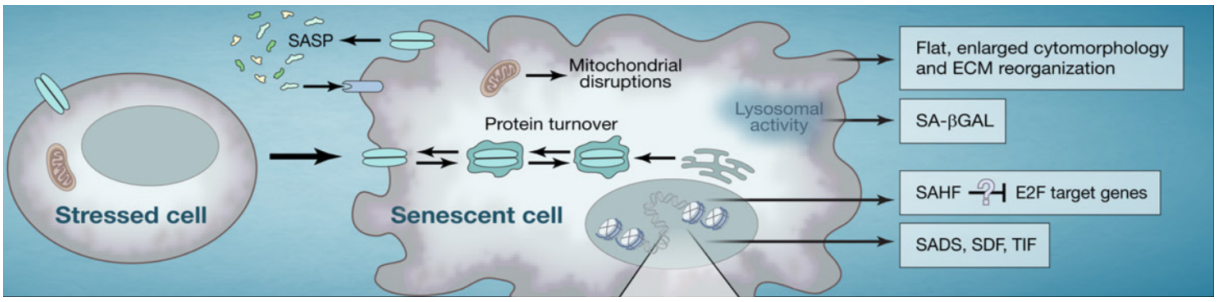

Introduction Figure 2. Markers of Senescence (Adapted from Zamudio-Martinez, 2017)

1.2.1. Senescence-Associated Growth Arrest (SAGA)

One of the most robust biomarkers of senescence is the stable cell cycle arrest. SAGA occurs typically in the G1 phase of the cell cycle and accordingly, cells stain negative for proliferation marker Ki67 and lack incorporation of nucleotide analogues like BrdU or Edu (Muñoz-Espín and Serrano, 2014). In certain instances of tumor senescence and OIS, the senescence arrest can also occur at the G2/S phase of the cell cycle (Bielak-

Zmijewska et al., 2014; Di Micco et al., 2006). Senescence can be identified through the upregulation of CDKis p16, p21, $p14^{ARF}$, p15, and the phosphorylation-status of Retinoblastoma Protein (pRB) (Serrano et al., 1997a; Sharpless and Sherr, 2015; Takahashi et al., 2007).

1.2.2. Apoptosis Resistance

Apoptosis and senescence are considered complementary mechanisms for controlling the outgrowth of abnormal or damaged cells. Apoptosis is a controlled and programmed cell death, while senescence maintains the cell in a metabolically active and are resistant to cellular death. Senescent cells downregulate pro-apoptotic genes, and upregulation of anti-apoptotic genes such as members of the BCL2 family of proteins (Piccolo and Crispi, 2012). Additionally, p21 can promote cell survival in the context of chronic DDR (Soto-Gamez et al., 2019). p21KD leads to upregulated JNK signaling and subsequent cell death (Soto-Gamez et al., 2019). Levels of autophagy during senescence also play an important role in survivability, as low levels of autophagy can lead to cell death through proteotoxic stress (Soto-Gamez et al., 2019).

1.2.3. Cytomorphological Changes

Senescent cells will often experience cytomorphological changes. In the context of DNA damage and replicative senescence, senescent cells become very enlarged, and flat

(Muñoz-Espín and Serrano, 2014). However, BRAF induced senescent cells, although they have striking morphological changes, they will often become elongated and exhibit a spindle-like shape (Michaloglou et al., 2005). Visually, there is a dramatic increase in the number of stress vacuoles and stress fibers (Kuilman et al., 2010; Muñoz-Espín and Serrano, 2014). It is also not uncommon to see an increased number of multi-nucleated cells (Kuilman et al., 2010).

1.2.4. Senescence-Associated Beta-Galactosidase (SAβG)

The most widely used and most readily applicable biomarker for identifying senescent cells in cell culture and tissues is senescence-associated beta-galactosidase (SAβG) activity (Debacq-Chainiaux et al., 2009; Sharpless and Sherr, 2015). β–Galactosidase activity in lysosomes is typically optimal at a pH of 10; however, in senescent cells, increased activity is achieved at an acidic pH of 2.0-6.0 (Dimri et al., 1995). During senescence, the expression of the gene encoding the lysosomal β-D-galactosidase GLB1 is increased but the gene is dispensable for senescence (Lee et al., 2006). Additionally, senescent cells have enlarged lysosomal compartment and activity, which corresponds with the increased autophagy in senescent cells (Criscione et al., 2016a; Wiley and Campisi, 2016).

1.2.5. Metabolism

Even though senescent cells cease proliferation, they are still metabolically active (**Introduction Figure 3**) (Rodier et al., 2009). Similar to the Warburg effect seen in cancer cells, senescent cells also display increased glycolysis, shifting to an increased AMP/ADP: ATP ratio (Baker et al., 2017; Wiley and Campisi, 2016; Wiley et al., 2016a). Energy sensing kinases, such as AMPK, are active components involved in senescence arrest (discussed in section 1.3.6) (Moiseeva et al., 2009; Wang et al., 2003). Along with increased glycolysis comes also a marked increase in pyruvate levels as well as an increased NADH/NAD^+ ratio (Kaplon et al., 2013; Ohanna et al., 2011a). This increased ratio can block senescence-inhibiting activities of SIRT3/5 and mitotic checkpoint kinase budding uninhibited by benzimidazole-related 1 (BUBR1) (Wiley and Campisi, 2016). Senescent cells also decrease the production of deoxyribonucleotides (dNTPs) through the downregulation of ribonucleotide reductase (RRM2), which impacts DNA replication and DNA damage – contributing to senescence promoting DDR signaling (Aird et al., 2015; Salama et al., 2014). Furthermore, cells shift autophagic and lysosomal activity and increase protein turn over to senescence-associated protein degradation (SAPD) (Salama et al., 2014). There is a decrease in autophagosome formation and fusion with the lysosome, even though the inhibition of autophagy can induce senescence (Galluzzi et al., 2016). That being said, there is increased autophagy and lysosome activity during OIS (Wiley and Campisi, 2016). Autophagy regulating protein mTOR is a significant driver for the expression of inflammatory components of the SASP (Herranz et al., 2015).

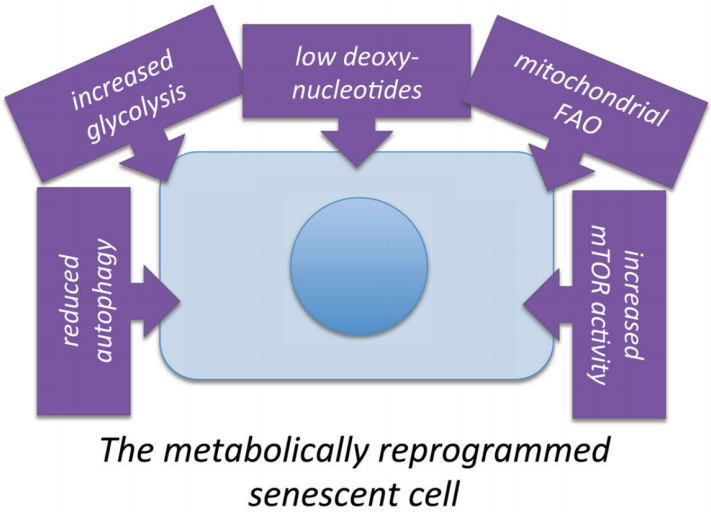

Introduction Figure 3. Metabolic characteristics of senescent cells (Adapted from Wiley, 2016).

1.2.6. Chromatin Conformation: SAHF/SAD/SDF/TIFS/LADS

Chromatin undergoes dramatic architectural changes in senescent cells epitomized by the appearance of senescence-associated heterochromatin foci (SAHF) (Narita et al., 2003). SAHF are regions of highly condensed heterochromatin that can be identified using DAPI DNA counterstaining. They are enriched for repressive histone marks H3K9me2/3, histone H4 hypoacetylation, histone variant macroH2A, and heterochromatin protein 1 (HP1), and are thought to stabilize the senescence arrest (Adams, 2007; Narita et al., 2003). Although these foci exhibit high condensation, there is also chromatin decondensation and 3-D architectural changes at pericentromeric satellite regions (senescence-associated distension of satellites (SADS) (Chandra et al., 2015a; Criscione et al., 2016a) that contribute to enforcing the senescence arrest (Swanson et al., 2013). Additional nuclear markers include senescence DNA damage foci (SDF) and telomere-dysfunction-induced foci (TIFs) (Criscione et al., 2016b; Rodier

et al., 2011; Takai et al., 2003). Sites of chronic DDR sites are called SCARS (DNA segments with chromatin alterations reinforcing senescence) and contain PML, ATM, TP53 binding protein (53BP1), γH2AX, and supporting DDR signaling proteins (Rodier et al., 2011). SCARS help to maintain a chronic DDR signaling which stimulates the SASP and reinforces arrest (Adams, 2007; Criscione et al., 2016b; Salama et al., 2014).

1.2.7. Senescence-Associated Secretory Phenotype (SASP)

Upon their arrest, senescent cells establish and maintain an extensive program to secrete factors, proteins, and vesicles into the surrounding microenvironment, which may act in an autocrine, paracrine or juxtacrine fashion to reinforce the senescence phenotype and spread it to the immediate cellular environment (**Table 1**) (Campisi and d'Adda di Fagagna, 2007; Coppé et al., 2008, 2010a; Kuilman and Peeper, 2009). SASP has pleiotropic functions in aging, age-related diseases, tissue homeostasis, and immune-surveillance (discussed in section 1.5) (Campisi and d'Adda di Fagagna, 2007; Kang et al., 2011; Sagiv and Krizhanovsky, 2013). SASP composition is heterogeneous and is dependent upon senescence context (Coppé et al., 2008, 2010a).

Introduction Table 1. Notable SASP Factors (Adapted from Coppé, 2008).

SASP factors
Soluble factors
Interleukins (IL) IL-6 IL-7 IL-1α, -1β IL-13 IL-15
Chemokines (CXCL, CCL)
IL-8 GRO-a,-b,-gc MCP-2 MCP-4 MIP-1a MIP-3a HCC-4 Eotaxin-3
Other inflammatory factors
GM-CSF MIF
Growth factors and regulators
Amphiregulin Epiregulin Heregulin EGF bFGF HGF KGF (FGF7) VEGF Angiogenin SCF SDF-1 PIGF IGFBP-2, -3, -4, -6, -7
Proteases and regulators
MMP-1, -3, -10, -12, -13, -14 TIMP-2 PAI-1, -2; tPA; uPA Cathepsin B
Soluble or shed receptors or ligands
ICAM-1, -3 OPG sTNFRI TRAIL-R3, Fas, sTNFRII Fas uPAR SGP130 EGF-R
Nonprotein soluble factors
PGE2 Nitric oxide Reactive oxygen species
Insoluble factors (ECM)
Fibronectin Collagens Laminin

1.3 Causes of Senescence

1.3.1. Replicative Senescence (RS)

Primary human cells have a finite replicative lifespan termed replicative senescence (RS). It is caused by the gradual shortening of telomeres during each replicational cycle, ultimately producing critically short telomeres (Allsopp et al., 1992). Telomeres consist of repetitive (TTAGGG) sequences, including a terminal 3' single-stranded over-hang that forms a t-loop. This DNA structure is protected by the "Shelterin" complex, which is composed of telomere binding proteins TRF1, TRF2, POT1, TPP1, TIN2 and RAP1 among others (Cech, 2004; Porro et al., 2014; Sharpless and DePinho, 2004). TRF1, TRF2, RAP1, TIN2 interact with the double-stranded DNA portion of the telomere while POT1 and TPP1 bind to the single-stranded over-hang as a dimer (Klement and Goodarzi, 2014). The Shelterin complex effectively protects the single-stranded t-loop from being sensed as a single-strand break, thus effectively blocking the activation of a DNA damage repair (DDR) response (Karlseder et al., 2004; Klement and Goodarzi, 2014; Schmutz and de Lange, 2016). When telomere integrity is compromised t-loops become undone and telomeres are sensed as DNA damage as the protective Shelterin complex is released (d'Adda di Fagagna et al., 2003; Fumagalli et al., 2012; Kuilman et al., 2010). The result is a chronic DDR including the recruitment of γ-H2AX, 53BP1, Mre11, NBS1, and MDC1 to unmasked telomeres (Takai et al., 2003). The DDR is relayed by ATR (Ataxia telangiectasia and Rad-3 related), ATM (Ataxia telangiectasia mutated gene) kinases, which phosphorylate checkpoint kinases CHK1/2 (D'Adda Di Fagagna, 2008; d'Adda di Fagagna et al., 2003). Furthermore, long-non coding RNA

TERRA directs the activity of histone demethylases LSD1 to facilitate the recruitment of the MRE11 complex (Porro et al., 2014). Ultimately, the DDR induces downstream stabilization of the tumor suppressor and guardian of the genome TP53 engaging the senescence arrest by transcriptional activation of cell-cycle-dependent kinase inhibitor CDKN1A (alias p21CIP) (d'Adda di Fagagna, 2008; Fumagalli et al., 2012; Herbig et al., 2004; Takai et al., 2003). RS further relies upon the activation of the INK4A locus, which encodes cell-cycle-dependent kinase inhibitors (CDKi) and tumor suppressor proteins CDKN2A and -B (*alias* p16 and $p14^{ARF}$). Together, these CDKi's activate the tumor suppressor protein pRB through hypophosphorylation enforcing senescence arrest by repressing cell cycle genes regulated by the E2F family of transcription factors (Dynlacht et al., 1994).

1.3.2. Stress-Induced Premature Senescence (SIPS)

Various other stressors, that I will discuss in the following sections, can also lead cells acutely into senescence (Muñoz-Espín and Serrano, 2014).

1.3.3. Oncogene-Induced Senescence (OIS)

Senescence is a tumor suppressor mechanism which arrests the proliferation of pre-cancerous cells. The initial discovery came from the observation that primary human and rodent cells over-expressing oncogenic RAS exhibited a senescent-like phenotype including loss of proliferative capacity, SABG activity, and enlarged, and flattened

cytomorphology (Serrano et al., 1997b). RAS-OIS depended both on functional TP53/p21 and p16/pRB activities (Ruiz et al., 2008; Serrano et al., 1997b). These results were validated *in vivo* in mice expressing oncogenic KRASG12D, where senescent cells were found in the pre-cancerous stages of the lung, liver or pancreas (Collado et al., 2007; Kang et al., 2011). In the case of RAS-OIS, senescence is induced through a chronic hyperactivation of the RAS-RAF-MEK-ERK pathway, replication stress, production of reactive oxygen species (ROS), DDR as well as activation of the JNK/p38MAPK stress kinase signaling pathway (Fumagalli et al., 2012; Gorgoulis and Halazonetis, 2010; Di Micco et al., 2006; Wang et al., 2002).

Similar to oncogenic RAS, overexpression of its direct downstream target kinase BRAFV600E also triggers OIS (Michaloglou et al., 2005). In vivo, BRAFV600E expression is the root cause for the development of benign melanocytic nevi that rarely progress to melanomas (Wang et al., 1996). Melanocytes in these nevi stain strongly positive for several senescence biomarkers (Wang et al., 1996). Although RAS and RAF function within the MAPK signaling pathway, senescence arrest kinetics, and genetic requirements are not identical. Other oncogenes inducing OIS are MYC, β-cadherin, PML, MOS, RAC1, MEK, AKT, E2F1, CCNE (Liu et al., 2018b).

In addition to oncogenic hyperactivation, disruption of tumor suppressor genes such as PTEN (Phosphatase And Tensin Homolog), NF1 (neurofibromin 1) or VHL (von Hippel Lindau) also induce a senescence arrest (Liu et al., 2018b). PTEN is the primary negative regulator of the PI3K-AKT-MDM2 pathway (Kuchay et al., 2017). However, in the absence of PTEN, mTORC1 and MTOC2 bind and phosphorylate Ser15 of TP53 and

out-compete the negative regulatory activities of MDM2 (Astle et al., 2012; Jung et al., 2019). The cells arrest with the upregulation of p21 and other downstream senescence targets (Astle et al., 2012; Jung et al., 2019). This TP53-mediated senescence arrest is DDR independent (Jung et al., 2019). In the absence of PTEN or RAS activation the loss of S-phase kinase-associated protein (SKP2) results in a senescence-arrest regulated by p21, p27 and ATF4 (Lin et al., 2010). Neurofibromin 1 (NF1) is a tumor suppressor gene which is a negative regulator of RAS, and upon disruption can lead to a senescence-arrest (Courtois-Cox et al., 2006). Senescence was demonstrated in human fibroblasts following treatment with RNA interference of NF1 which lead to a transient upregulation of the RAS/PI3k pathway followed by repression and subsequent growth arrest (Courtois-Cox et al., 2006). The RAS/PI3K pathway is repressed through negative-feedback signaling from RasGAPs and sprout proteins (Courtois-Cox et al., 2006). Lastly, VHL-loss induced senescence, is TP53 independent and is mediated through the upregulation of cyclin-dependent kinase inhibitor p27, which activates pRB (Young et al., 2008).

1.3.4. DNA Damage Induced Senescence (DDIS)

Senescence also acts as a stress response to genotoxic insults other than telomere damage (**Introduction Figure 4**) (d'Adda di Fagagna, 2008). Oxidative stress, sub-lethal H_2O_2 treatment, and the exposure to DNA damaging agents induce single (SSBs) or double strand breaks (DSBs) which can lead to an increase in mutagenic events and genomic instability (Chen et al., 1998; Pedro de Magalhães et al., 2004; te Poele et al.,

2002). An SSB is sensed by replication protein A (RPA) and ATR kinase (Falck et al., 2005) and the kinase signal is amplified by the heterotrimeric 9-1-1 complex (RAD9, RAD1, HUS1) and Topoisomerase II-binding protein 1 (TOPBP1) (Schmitt et al., 2007). DSBs recruit ATM kinase to the site of damage (Falck et al., 2005). ATM and ATR kinases activate DDR by phosphorylating γH2AX to reinforce the recruitment of ATM (**Introduction Figure 3**) (Falck et al., 2005). These kinases chronically act at the sites of DNA damage to create a positive feedback loop, and the formation DNA-SCARS. (d'Adda di Fagagna, 2008; Rodier et al., 2011; Schmitt et al., 2007). Additional mediators collaborating with ATM and ATR at the sight of damage are 53BP1, claspin/RAD1 and the mediator of DNA-damage checkpoint 1 (MDC1), which help in the activation of checkpoint kinases CHK1 and CHK2 (Armata et al., 2007; D'Amours and Jackson, 2002; Salama et al., 2014; Schmitt et al., 2007). The latter will phosphorylate and (in)activate cell cycle proteins, including TP53 and CDC25, enforcing a rapid cell cycle arrest that is stabilized by the activation of p21 and p16/pRB (Armata et al., 2007).

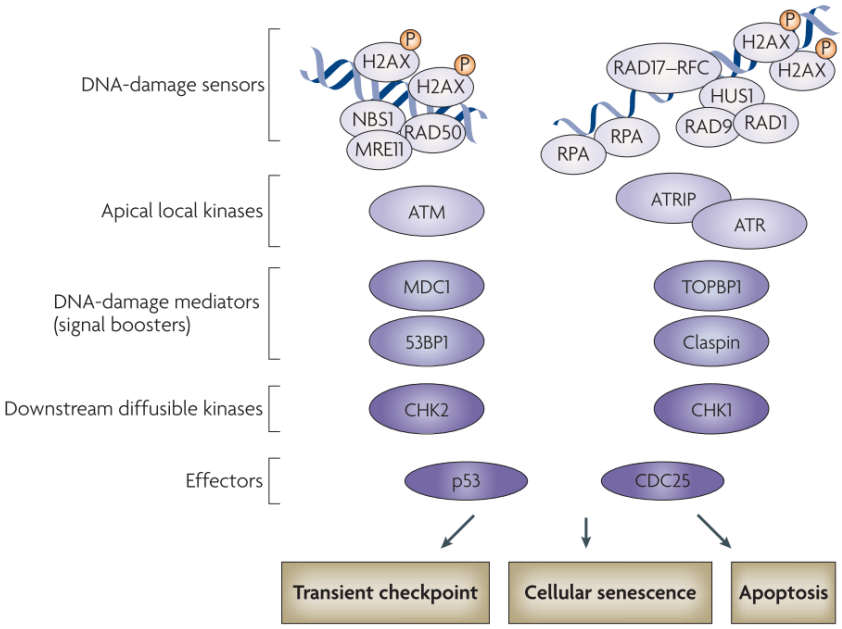

Introduction Figure 4. Characteristic DNA-damage response during senescence
(Adapted from d'Adda di Fagagna, 2007).

ROS signaling can also induce a senescence arrest. To arrest the cells ROS triggers DNA damage and initiate TP53-p21 as well as activation of ERK-p38MAPK signaling pathway (Freund et al., 2011). Additionally, ROS-induced p21 activation triggers downstream mitochondrial dysfunction, which in turn produces more ROS and creates a positive feed-forward loop which sustains the senescence arrest (Passos et al., 2010a). DNA damage from radiation (UV, gamma, X-ray) will form DNA breaks, which can arrest cells through DDR pathways described above (Mirzayans et al., 2012).

1.3.5. Therapy-induced senescence (TIS)

Tumor cells can still be driven into senescence through ionizing radiation, DNA damaging chemotherapy, or epigenomic damage (*e.g.,* HDAC inhibition) (Fan and Schmitt, 2017;

Gewirtz et al., 2008; Li et al., 2018). For example, a moderate dose of chemotherapeutic agents such as doxorubicin (20-100 nM) or etoposide (20μM), induces senescence rather than cell death in cancer cells (Bielak-Zmijewska et al., 2014; Roberson et al., 2005). Additionally, in BCL-2 null (a pro-apoptotic factor) context, Eu-MYC B-cell lymphoma in mice treated with chemotherapeutic agent cyclophosphamide experience a TP53-dependent cell cycle arrest (Schmitt et al., 2002). Finally, during cancer therapy, INK4A mutations negatively impact treatment outcome, which suggests that senescence induction is a definite indicator for treatment success, a failsafe mechanism for apoptosis (Schmitt et al., 2002). Radiation therapy induces large number of senescent cells in the regions outside of the direct target (non-lethal doses) (Li et al., 2018; Mirzayans et al., 2012). Ionizing radiation can push malignant tumors into apoptosis through direct DNA damage or secondary damage. Mitochondrial dysfunction from the radiation can produce large quantities of ROS through NOX4, which creates a perpetuating loop of damage and ROS production in the mitochondria itself, leading to senescence-arrest (Sakai et al., 2018; Shimura et al., 2017)

1.3.6. Mitochondrial Dysfunction-Associated Senescence (MiDAS)

Mitochondria dysfunction, which occurs with age, can induce a senescent phenotype markedly differing from that found in other senescence contexts and can occur also in post-mitotic cells (Wiley et al., 2016b). Cells that undergo MiDAS have lower NAD+/NADH ratios, which cause both the proliferative arrest and prevent the classical IL-1-associated senescence-associated phenotype (SASP) through AMPK (AMP-activated

protein kinase)-mediated TP53 activation. Furthermore, deregulation of anti-senescent mitochondrial proteins SIRT3 and SIRT5 can lead to MiDAS (Nacarelli et al., 2019; Wiley et al., 2016b).

1.3.7. Development

In recent years, senescence has been linked to embryonic development (Muñoz-Espín et al., 2013; Storer et al., 2013). Detailed studies of the mesonephros, the endolymphatic sac of the inner ear, apical ectodermal ridge, and neural roof plate show that senescence occurs naturally during embryonic development. Developmental cues evoke a senescence response through PI3K/SMAD and TGFβ/FOXO signaling, which induce p21 independent of TP53 activation and a canonical SASP, however, devoid of IL-6 and IL-8. During development, senescent cells are removed through apoptosis or the recruitment of macrophages (Muñoz-Espín et al., 2013; Storer et al., 2013). Together, these studies provided a first glance to the putative evolution of the senescence phenotype.

1.3.8. Tissue Regeneration, Repair and Maintenance of Plasticity and Stemness

Senescence plays a critical role in tissue regeneration, wound healing and the maintenance of cellular plasticity and stemness (Chiche et al., 2016; Milanovic et al., 2018; Mosteiro et al., 2016a; Ritschka et al., 2017a). In the context of cutaneous wound healing, senescent cells appear very early after injury, following CCN1 release, activating

integrin a6B1, heparan sulfate proteoglycans (HSPGs) as well as downstream RAC-1dependent NADPH oxidase 1 (Jun and Lau, 2010). Together, this upregulates ROS production, which induces senescence arrest via p38MAPK/ERK signaling and subsequent induction of p16/pRB and TP53 (Jeon et al., 2017; Jun and Lau, 2010). Wound-resident senescent cells release a SASP containing platelet-derived growth factor (PGDF-AA) (Jeon et al., 2017; Jun and Lau, 2010). PGDF-AA dependent tissue remodeling through the differentiation of myofibroblasts was found to be senescence-dependent, thus displaying the physiological benefits of senescence (Jeon et al., 2017; Jun and Lau, 2010). Additionally, in a mouse model expressing Yamanaka TFs (OCT4, SOX2, Klf4, and c-MYC), senescence was found to be a crucial component for cellular reprogramming and wound healing via SASP factor IL-6 in the context of muscle repair (Chiche et al., 2016; Mosteiro et al., 2016b). In the context of the liver, senescence induction and subsequent SASP expression leads to an increase in the presence of stem cell markers, as well as an increased capacity at regeneration, further emphasizing the role of senescence in facilitating stemness and plasticity (Ritschka et al., 2017b).

1.5. Mechanisms and Regulation of Cellular Senescence

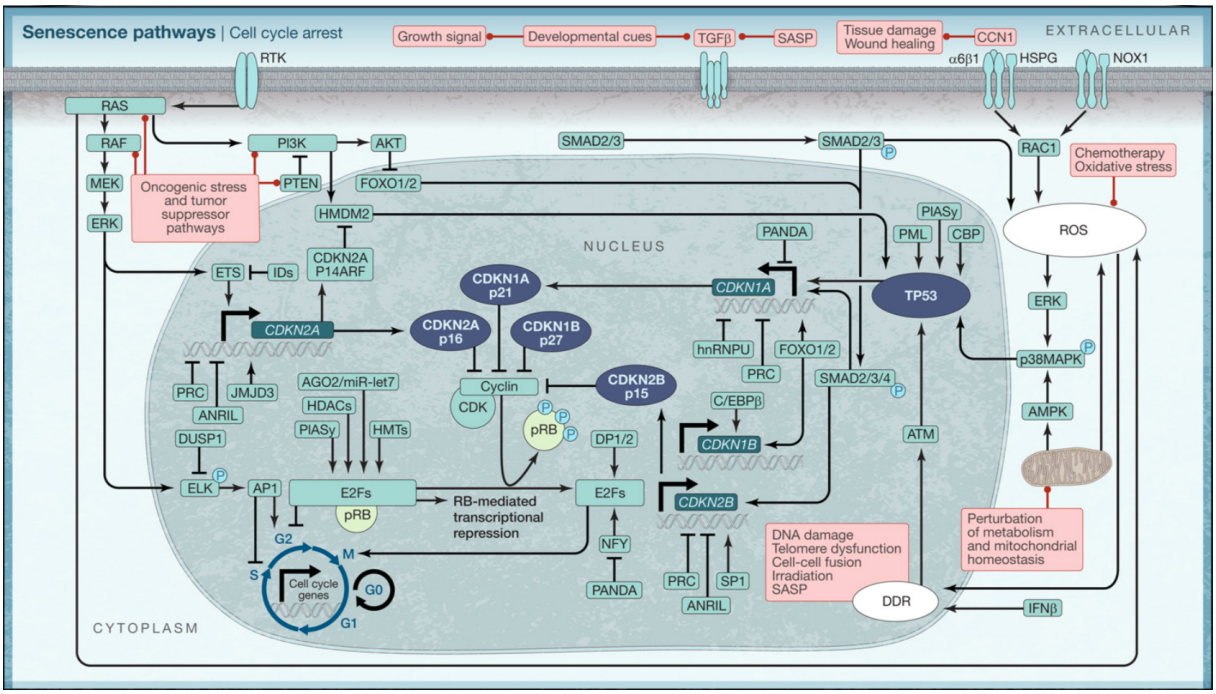

Introduction Figure 5. Pathways of Senescence (Adapted from Zamudio-Martinez, 2017).

1.5.1. Senescence arrest

Cell proliferation is under tight control, receiving a variety of signals from the environment or cell-autonomously to progress or not through replication of its genetic code, and finally division, known as the cell cycle (Smith and Martin, 1973). Cyclins and CDKs are contributory factors for cell cycle progression, facilitating the passing through various checkpoints in G1, S, G2, and M phase of the cell cycle to ensure proper proliferation (Johnson and Walker, 1999). During G1 phase, cyclin Ds receive signaling from the external environment, and depending on this messaging, will direct CDK4/6 to initiate the expression of cell cycle genes, pushing the cell through the next steps of the cell cycle

when other cyclins will take over (Johnson and Walker, 1999). CDKis p16INK4A, p15INK4B, p27Kip1, and p57Kip2, p18INK4C, p19INK4D, and p21Cip1 all negatively regulate CDKs, thus keeping pRB in a hypophosphorylated, active state. CDKis control check-points of the cell cycle and are instrumental in orchestrating the senescence arrest (Campisi, 1997; Itahana et al., 2003; Serrano, 1997).

Although various stressors trigger the senescence response, the arrest itself depends primarily on the activation of the tumor suppressor pathways pRB/p16 and TP53/p21 (Beauséjour et al., 2003; Shay et al., 1991). The mutation or disruption of the pRB/p16 and TP53/p21 pathways can facilitate senescence-bypass or senescence escape (Roberson et al., 2005). For example, expression of the SV40 large T antigen inhibits both TP53 and pRB, resulting in a senescence bypass (Shay et al., 1991).

1.4.2. TP53 and the Senescence Arrest

TP53 regulates a critical tumor suppressor pathway in senescence (Itahana et al., 2003; Serrano, 1997). TP53, a tetrameric transcription factor, is the most important tumor suppressive transcription factor, and as such is subject to complex regulation. Not surprisingly TP53 is mutated in more than 50% of all cancers (Harris, 1996). TP53 activation can halt cell proliferation and is implicated in the regulation of metabolism, apoptosis, and development (Bosari et al., 1995; Brady and Attardi, 2010).

In senescence, a bevy of factors such as DDR signaling, ROS, hyperactivated oncogenes, TGFβ, and cytokine signaling (including SASP from neighboring cells)

functionally activate TP53 (Lujambio et al., 2013). These stressors upregulate signaling pathways via AMPK, ATR, p38 mitogen-activated protein kinases, and ATM to post-translationally modify TP53 (Lujambio et al., 2013). In RAS-OIS, RAS signaling induces the formation of a trimeric complex, including acetyltransferase CBP, TP53, and PML (Pearson et al., 2000). In the absence of TP53 acetylation, senescence may be bypassed (Pearson et al., 2000). Furthermore, Protein Inhibitors of the of Activated STAT (PIASy), an E3 sumoylation ligase, sumoylates and activates TP53, and in concert with pRB induces a senescence arrest (Bischof et al., 2006). TP53 is strongly antagonized by MDM2, which facilitates its export from the nucleus and degradation via ubiquitylation; however, $p14^{ARF}$ acts as an inhibitor of MDM2, to stabilize TP53 (Brady and Attardi, 2010; Stott et al., 1998; Takemoto et al., 2000). Under normally proliferating conditions, the p21/CDKN1A gene locus is repressed by scaffold-attachment factor A (SAFA) and long-noncoding RNA PANDA, which recruit polycomb repressive complexes (PRC1 and PRC2), to produce the repressive chromatin mark H3K27me3 (Liu et al., 2018a; Puvvula et al., 2014a). Upon senescence induction, TP53 antagonizes these repressive complexes and strongly upregulate the expression of the p21/CDKN1A gene locus (Puvvula et al., 2014b). CDKN1A inhibits the kinase activity of CDK1, CDK2, CDK4/6, thereby inducing the hypophosphorylation and activation of pRB, thus, enforcing the senescence arrest (Datto et al., 2006; Yosef et al., 2017).

1.4.3. pRB and the Senescence Arrest

The second critical senescence arrest pathway is mediated by the gatekeeper of cell cycle progression, pRB (Serrano, 1997). Like TP53, pRB is tightly regulated by different posttranslational modifications, and upon hyperphosphorylation will allow for the G1/S transition to occur (Johnson and Walker, 1999). CDK 4/6 and CDK2 phosphorylate pRB to release its inhibitory effect on the E2F-DP1 TF dimer (Alexander et al., 2003). During senescence, pRB is maintained in a hypophosphorylated state, binding, and inhibiting E2F mediated cell cycle progression (Campisi, 1997; Haferkamp et al., 2009). pRB binds and represses the activity of E2F1-3 and recruit histone deacetylases (Brehm et al., 1998; Hara et al., 1996). The INK4a/ARF gene locus encodes both p16 and $p14^{ARF}$ (Stott et al., 1998). Under normal proliferating conditions, the CDKN2A locus is repressed by complexes including ANRIL (anti-sense ncRNA in the INK4 locus), CBX7, SUZ12 and polycomb repressive proteins, and is marked by inactive chromatin modifications such as H3K27me3 (DiMauro et al., 2015; Kotake et al., 2011). The depression of this locus is instrumental for the senescence arrest (Kotake et al., 2011). Identified factors involved in depressing the INK4A locus are p38MAPK stress kinase, transcription factor ETS, or SWI/SNF chromatin remodeling complexes leading to an increasingly active chromatin state (Childs et al., 2014; Hiroaki et al., 2003). p16, like other CDK inhibitors, acts to block CDKs from phosphorylating and inactivating pRB, thus facilitating the binding to and inhibition of E2F-regulated expression of genes important for cell cycle progression (for example, PCNA, CCNA2, or CCNB1/2) (Johnson and Walker, 1999). In a positive

loop, pRB prevents the down-regulation of the CDKN2A locus, maintaining the expression of p16 and $p14^{ARF}$ (Hara et al., 1996).

In addition to its interactions with E2F TFs, pRB facilitates a permanent cell cycle arrest during senescence through heterochromatin formation (Brehm et al., 1998; Narita et al., 2003). The most prominent heterochromatin structures are SAHF. The formation of SAHF is dependent upon activation of p16/pRB, and represses E2F cell cycle targets thus, forming a functional link between cell cycle arrest and the formation of heterochromatin foci during senescence (Corpet and Stucki, 2014; Narita et al., 2003). SAHF are enriched for macroH2A and HP1 (Zhang et al., 2005), which also facilitate the recruitment of PRC1 and PRC2 factors, which generate the repressive histone modification H3K27me3 (Narita et al., 2003, 2006; Zhang et al., 2005). In complex, PML bodies require the activity of high mobility group-A and B1 (HMGA2 and HMGB1) to bind E2F target areas and place repressive histone marks which alters the higher-order structure into foci (Narita et al., 2006). To form SAHF and repress cell cycle genes, pRB interacts with chromatin modifying proteins to shape the 3-D chromatin architecture and epigenomic landscape (Uchida, 2016). pRB drives specific SWI/SNF chromatin remodeling complexes during senescence (Uchida, 2016). SWI/SNF remodels chromatin through disrupting the nucleosome interaction with DNA, to increase, or in some cases, repress gene expression (Uchida, 2016). In the case of senescence, pRB recruits the SWI/SNF, BRM or BRG1 ATPases as part of a complex to remodel the chromatin into a repressed state in cooperation with histone deacetylases and histone methyltransferases (Adams, 2007; Tu et al., 2013b, 2013a).

As part of chromatin remodeling complexes, pRB, often acts in concert with PML nuclear bodies to facilitate the deacetylation of E2F target genes and promoters (Zhang et al., 2005). pRB recruits histone deacetylase 1 (HDAC1) to sites near the promoters of E2F target genes, in some cases in complex with SIN3B or COOH-terminal binding protein (CtBP) (DiMauro et al., 2015). Deacetylation of lysine on histones through complexes containing HDAC1 represses gene expression at these sites (Brehm et al., 1998; Narita et al., 2003). One study found that cyclin E could be re-expressed when pRB mediated repressive chromatin modifications were counteracted by HDAC inhibitors (Klement and Goodarzi, 2014; Zhang et al., 2005). pRB forms a complex with histone methyltransferase SUV39H1, which catalyzes di/trimethylation of histone three lysine 9 (H3K9me3/2) (Narita et al., 2003). These repressive marks are targeted to repress expression of cell cycle genes (E2F targets) and form the SAHF (Narita et al., 2003). H3K9me2/3 and macroH2A recruit heterochromatin protein 1 (HP1) (Rai et al., 2014). During the onset of senescence, the colocalization of histone chaperones HIRA and ASF1 into the PML nuclear bodies with HP1 is required for the formation of the SAHF (Zhang et al., 2005). These repressive complexes further compact chromatin through interactions with surrounding methylated histones (Chandra et al., 2012, 2015a).

1.4.4. Other Critical Players Regulating the Senescence Arrest

The senescence arrest and repression of E2F target genes also employ microRNA-mediated transcriptional gene silencing (TGS) (Benhamed et al., 2012). Micro-RNA (MiR)

molecules can disrupt gene expression through binding DNA, disrupting protein translocation, or degrading already transcribed mRNAs (Benhamed et al., 2012). In the context of senescence, AGO-2/MiR complexes are translocated to the nucleus (Benhamed et al., 2012; Rentschler et al., 2018). As part of the pRB repressor complex containing HDACs, AGO-2 is guided to E2F target genes MiR-let 7 (Benhamed et al., 2012). This gene silencing may also assist in the recruitment of additional chromatin repressive complexes to durably repress gene expression of E2F targets (Benhamed et al., 2012).

Nuclear lamina proteins regulate senescence. A shortened splice variant of Lamin A in Hutchinson-Gilford progeria syndrome (HGPS) leads to rapid aging (McClintock et al., 2007). Nuclear lamina proteins interact with DNA at lamina-associated domains (LADS) in a structural capacity, often interacting with vast stretches of heterochromatin and gene-poor areas, but as well to silence the expression of specific genes (Hänzelmann et al., 2015; Kind et al., 2015). In senescence, there is a downregulation of lamin B (LMNB1) (Shah et al., 2013). Loss of LMNB1 causes dissociation of the LADs and the delocalization of heterochromatin (Shah et al., 2013). These changes further stabilize the cell cycle arrest (Salama et al., 2014).

1.5. Mechanisms and Effects of the SASP

The SASP is one of the most important functional features of senescent cells. The SASP displays variability between different cell types and inducers, and is dynamic, which is to

say that not all components are expressed simultaneously and at all times (Acosta et al., 2013; Coppé et al., 2008).

The SASP plays a critical biological role in a cell-autonomous and cell non-autonomous fashion. Cell autonomously, senescent cells create a positive-feedback loop, to reinforce the senescent phenotype through the SASP (Chien et al., 2011; Orjalo et al., 2009). First, IL-6 and IL-8 SASP factors are essential to the maintenance of the senescence phenotype (Acosta et al., 2008). Silencing of CXCR2 (Receptor for IL-6 and IL-8) expression prevents the onset of OIS, with diminished activation of ATM and DDR (Acosta et al., 2008). The upregulation of CXCR2 and the accompanying chemokine production is largely regulated by NFκB (Nuclear Factor Kappa-light-chain-enhancer of activated B cells) and CEBPβ (CCAAAT/enhancer binding protein β) (Acosta et al., 2008). The mechanism by which CXCR2 can facilitate cell-autonomous maintenance of senescence involves ROS, DDR and continued activation of p21, which also helps their survival and avoidance of apoptosis through JNK (Yosef et al., 2017). Independently of CXCR2, IL-6 plays a significant role in autocrine maintenance and establishment of senescence (Kuilman et al., 2008). IL-6 production is significantly increased, as well as the IL-6 receptor (IL6R) (Kuilman et al., 2008). This cascade upregulates an entire inflammatory network in collaboration with CEBPβ (Kuilman et al., 2008). The IL-6/CEBPβ axis is involved in upregulating p15, contributing to the senescence arrest (Kuilman et al., 2008). Abrogation of this axis diminishes the formation of SAHF, SASP, and disrupts the senescence phenotype (Kuilman et al., 2008). Additionally, Plasminogen Activator Inhibitor 1 (PAI1), a known biomarker of senescence, plays an autocrine

functional role in senescence through the regulation of growth signaling pathways (Kortlever et al., 2006). PAI1, downstream of TP53 is upregulated during aging. PAI1 acts in an autocrine fashion to disrupt cell cycle progression through inhibiting PI3K-PKB-GSK3B and inhibiting the activity of cyclin D1. Ectopic expression of PAI1 is sufficient to induce senescence in TP53 positive cells. Additionally, secreted insulin-like growth factor binding proteins 5/7 (IGFBP-5/7 can also mediate senescence. Insulin-like growth factor pathways are critical in cell growth, as well as several other cell fate pathways (Kim et al., 2007). In the context of senescence, signaling from IGFBP-5/7 facilitates growth arrest through a DDR signaling pathway to induce a TP53/p21 cell cycle arrest (Kim et al., 2007).

1.5.1. Paracrine/Juxtracrine Effects of the SASP

In addition to the autocrine-maintenance of senescence, the SASP induces senescence in neighboring cells through paracrine-induced senescence (Young and Narita, 2009). Conditioned media from OIS, RS, or DDIS cells induce senescence in proliferating cells (Acosta et al., 2013) through ROS, an ensuing DDR and stimulation of the IL-6/STAT3, IL1β/ NFκB, and TGFβ/SMAD pathways. TGFβ family proteins (specifically TGFβ 1, Activin A, BMP2) are the primary modulators of paracrine induced senescence (Acosta et al., 2013). IL1α was found to induce DDR and ROS in bystander cells. TGFβ alone can induce a senescence arrest independently of TP53 through increased ROS and DDR signaling via Nox4 activation of p21 in the secondary senescent cell, as well as TGFβ

activated p27, and SMAD2/3 activation of p15 (Senturk et al., 2010). This response relies upon DDR signaling and the presence of ATM and macro H2A1.1 (Senturk et al., 2010).

Senescence can also be induced through cell-cell contacts and juxtacrine induced senescence (Hoare et al., 2016; Teo et al., 2019). The latter is a distinct form of senescence and is mediated through Notch signaling (Notch-mediated juxtracrine induced senescence, NIS) (Hoare et al., 2016; Teo et al., 2019). Notch signaling is mediated through JAG1 (Hoare et al., 2016; Teo et al., 2019). Although these cells are senescent, they express a modified SASP in comparison to OIS cells (Hoare et al., 2016). NIS is a TGFβ-driven primary SASP that is distinct from the late, secondary SASP in fully senescent cells and may have pro-tumorigenic potential (Hoare et al., 2016).

1.5.2. Immune Surveillance of Senescent Cells

To maintain tissue homeostasis, senescent cells are cleared by the adaptive and innate immune systems, a process that is called senescence immune surveillance (**Introduction Figure 6**) (Lujambio et al., 2013). Initially, innate immune cells were identified as the mediators of immune surveillance of senescent pre-cancerous cells (Xue et al., 2007). In a RAS-driven liver cancer model, induction of TP53 induces a SASP, that attracts the innate immune system (macrophages, natural killer cells, and neutrophils) (Xue et al., 2007). Furthermore, NK cells target senescence cells following the expression of NKG2 ligands and release of ICAM1 and IL-15 which is followed by NK cells initiating apoptosis in the target senescent cell (Burton et al., 2016). Additional studies also identified a role

for the adaptive immune system and specifically CD4+T cells (Kang et al., 2011). In this context, the clearance of the senescent cells required the recruitment of monocytes and freshly replenished macrophages (Kang et al., 2011). CCL2 signaling from the SASP brings CCR2+ myeloid cells to differentiate into macrophages (Eggert et al., 2016a). However, as liver carcinoma progresses, NK cells are blocked from infiltrating and clearing the tumors (Eggert et al., 2016a). Immune surveillance of senescent cells is critical for maintaining homeostasis, and the inhibition of this process can lead to the accumulation of senescent cells, tumor progression and age-related pathology (Burton and Faragher, 2015; Hoenicke and Zender, 2012).

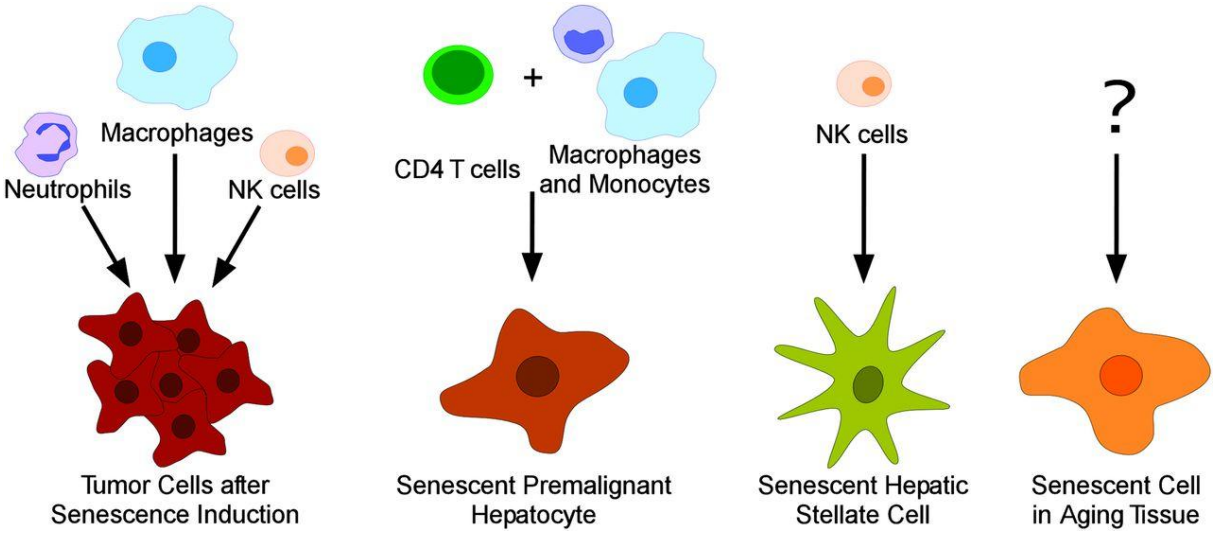

Introduction Figure 6. Immune surveillance of senescent cells (Adapted from Hoenicke, 2012). The immune system recognizes and eliminates senescent cells in through innate and adaptive immune responses, including CD4+ T-cells, NK cells, neutrophils and macrophages.

1.5.3. SASP and Tumor Promotion

The SASP can contribute to cancer progression (Coppé et al., 2010b; Gorgoulis and Halazonetis, 2010). Senescent cells both drive pre-neoplastic cells into hyperproliferation and accelerate the growth of neoplastic cells (Krtolica et al., 2001). Increased tumor outgrowth was attributed to SASP factors, including GROa and extracellular-matrix remodeling MMPs. Furthermore, the SASP has been implicated in endothelial-mesenchymal transition (EMT) via secretion of MMPs, uPAR, HGF, and modulating tumor angiogenesis via VEGF, CCL1, IL-8 (Balentien et al., 1991; Coppé et al., 2010b; Kim et al., 2007; Strieter et al., 2006; Wajapeyee et al.; Yang et al., 2005). In addition to cell proliferation, the SASP promotes cell motility, and cancer metastasis by remodeling the extracellular matrix (Coppé et al., 2010b; Liu and Hornsby, 2007).

1.6. Regulation of the SASP

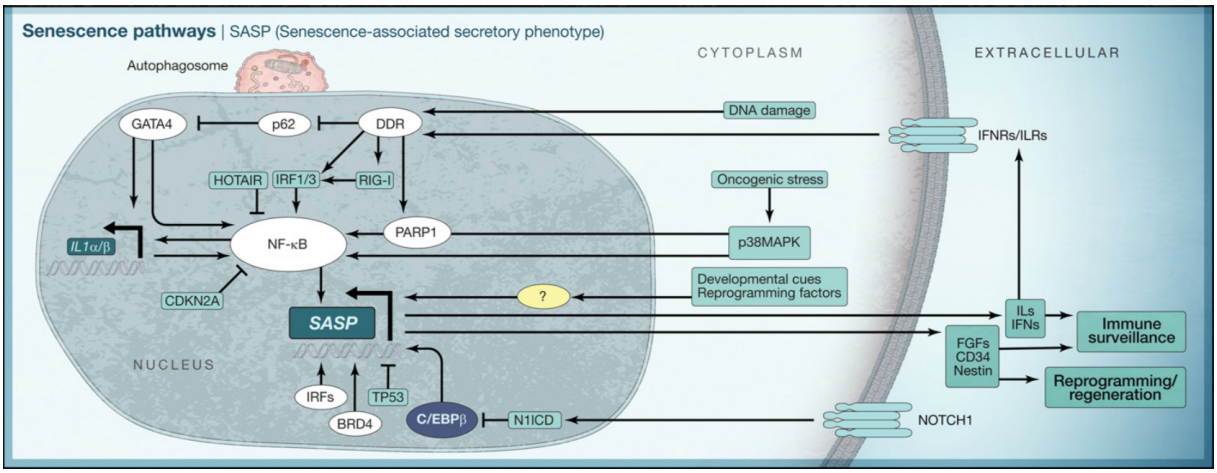

Introduction Figure 7. SASP Pathways. Outlining the pathways involved in regulating SASP expression (Adapted from Zamudio-Martinez, 2017).

The composition of the SASP is very diverse and dynamic, and its regulation is complex (Ito et al., 2017). Proteomics and transcriptomics studies showed that most of the regulation of the secretion occurs at the transcriptional level – i.e., there is a strong correlation between secreted protein and mRNA levels (Coppé et al., 2008). Secretion of inflammatory factors is often mediated by the TFs NFκB and CEBPβ, whose induction can be induced through several pathways, but not through SAGA alone (Rodier et al., 2009). Overexpression of p16 or pRB induces senescence growth arrest; however, these cells lack a SASP. NFκB and CEBPβ both act to upregulate the expression of inflammatory pathways including IL-6 and IL-8 though IL1α/β (Acosta et al., 2008; Chien et al., 2011; Kuilman et al., 2008). Positive feedback loops maintain their expression and facilitate a steady inflammatory signaling secretion (autocrine maintenance) (Acosta et al., 2008). Within this context, there is upregulation of a dampening signal from non-coding RNA miR146 a/b (Liu et al., 2012). miR146 a/b acts to restrict the secretion of IL-

6 and IL-8 but is not strong enough to completely diminish their expression (Liu et al., 2012). NFκB and CEBPβ are the primary executors of the SASP, and they are regulated extensively (**Introduction Figure 7**).

1.6.1. NF-κB and SASP Regulation

NF-κB is one of the primary regulators of SASP production. In addition to mediating inflammation, NFκB contributes to the establishment of senescence, localizes in the nuclei of senescent cells and one of its subunits p65 co-localizes with the SAHF (Chien et al., 2011). Pre-stimulation, NFκB subunits (RelA/B/C and NFκB1/2) are dimerized in the cytosol and repressed by NFκB inhibitor proteins (IKBs) (Shifera, 2010). Post-stimulation IKB kinase (IKK)s are phosphorylated by upstream kinases, which then phosphorylate IKB proteins and mediate their degradation (Shifera, 2010). Following IKB degradation, the components of NFκB are free to translocate from the cytosol to the nucleus.

NFκB is activated by DNA damage, inflammation, environmental cues, and the inflammasome (Shifera, 2010). As part of the DDR, ATM activates phosphorylation of p38MAPK and IKKg (NEMO), critical for the expression of the NFκB activation and SASP production (Ohanna et al., 2011b). NEMO forms a shuttle complex to activate and translocate NFκB and associated proteins to the nucleus (Shifera, 2010). Additionally, DNA damage can activate PARP1 and LUBAC which will induce ADP-ribosylation and ubiquitination of the IKK complex (Ohanna et al., 2011b). Together, this will free NFκB subunits and facilitate their nuclear translocation (Ohanna et al., 2011b).

Inflammasomes are cellular complexes that include cell surface receptors, and downstream signaling components which regulates expression of inflammatory cytokines, including IL6 and IL8 via NFκB and p38MAPk (Acosta et al., 2013).

NFκB is also activated through secreted proteins TGFβ, TNFα, TLR ligands, and IL1β (Salminen et al., 2012). TGFβ phosphorylates SMAD2/3 TFs, which can induce SASP expression.

Upon activation, NFκB interacts with TFs to facilitate inflammatory gene-expression. For example, SIRT6, which acetylates histones, cooperates with NFκB to enhance gene expression (Kawahara et al., 2009; Rovillain et al., 2011). High-mobility group protein B1 (HMGB1), which modifies chromatin structure around H1, is bound by NFκB to enhance DNA affinity for inflammatory targets (Agresti and Bianchi, 2003). NFκB driven inflammation is also stabilized through the activity of TF GATA4 in the presence of a DDR (Kang et al., 2015). GATA4 is activated independently of p16/TP53 and the cell cycle arrest by ATR, but its mRNA levels do not increase during senescence (Kang et al., 2015). GATA4 protein levels are stabilized during senescence due to the downregulation of p62, which targets GATA4 for degradation via lysosomal autophagy. GATA4 and NFκB collaborate to regulate the SASP (Kang et al., 2015).

1.6.2. CEBPβ and SASP Regulation

CEBPβ is another primary regulator of the SASP. CEBPβ is a TF that activates expression of inflammatory cytokines IL-6, IL-8, TNF-a, and other SASP components (Hardy et al., 2005). CEBPβ contributes to the senescence arrest in addition to mediating

inflammation and protease secretions (Chien et al., 2011). Unlike NFκB, the SASP driven by CEBPβ binding activity is dynamically regulated during senescence (Hoare et al., 2016; Ito et al., 2017; Teo et al., 2019). During the induction of senescence CEBPβ mRNA levels are repressed via NOTCH1. During senescence, NOTCH1 is upregulated, however, the cleavage of NOTCH1 is dynamic, and it peaks in activity only during the initial phases of senescence induction. This activity is reciprocally regulated with TGFβ, and coincides with the distinct shift between the TGFβ, mediated SASP and the pro-inflammatory SASP seen at the final stage of OIS. Initially, the SASP is driven by TGFβ, contributing to growth arrest (via p15), and producing a similar SASP to that seen during developmental senescence. NOTCH1 actively inhibits the inflammatory SASP via blockage of CEBPβ and downstream induction of IL1α, IL6, IL8. This inhibition is then lifted as NOTCH1 becomes deactivated, ushering in the full NFκB, and CEBPB driven SASP (Hoare et al., 2016).

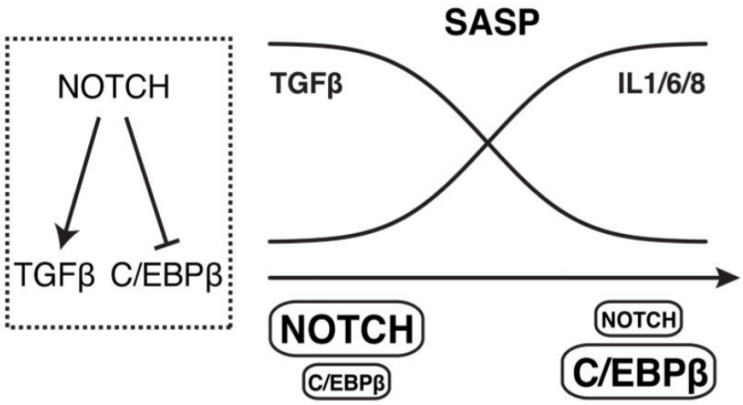

Introduction Figure 8. Two-phases of SASP governed by NOTCH signaling (Adapted from Hoare, 2016).

Other factors also have been implicated in regulating SASP expression. During senescence sensing of cytosolic DNA will also induce SASP gene expression through cyclic GMP/AMP (cGAS) and downstream inflammatory mediator Stimulator of interferon genes (STING) (Dou et al., 2017; Glück et al., 2017; Yang et al., 2017). DNA damage, reorganization of chromatin, and LADs leads to an increase in cytosolic DNA fragments (Dou et al., 2017; Glück et al., 2017). The sensing of cytoplasmic DNA reinforces inflammatory signaling in the SASP (Dou et al., 2017; Glück et al., 2017). mTOR is another regulatory component of the SASP production on a transcriptional and translational level (Herranz et al., 2015). Rapamycin inhibits mTOR which decreases IL6 and translation of IL1α, which negatively impacts NFκB activation. mTOR facilitates the translation MAPKAPK2, which phosphorylates and inhibits the activity of ZFP36L1 such that it can no longer bind and degrade SASP factor mRNAs. Additionally, histone variants like histone variant H2A.J can influence SASP expression during senescence (Contrepois et al., 2017).

1.7. Regulation of the Senescence-Associated Gene Expression Program

In addition to the dramatic chromatin architectural changes, *cis*-regulatory regions and enhancers govern the senescence gene expression program (Shlyueva et al., 2014). Enhancers are non-coding stretches of DNA often considered to be cis-acting (although they can act from very long distances) upstream or downstream of a target gene to enhance gene expression (Mercola et al., 1983). Enhancers can form activating complexes with TFs and chromatin modifiers to regulate transcription (Wang et al., 2009). Enhancers are marked by activating histone modifications H3K27ac and H3K4me1 as well as activating proteins p300 and CBP. The active-enhancer landscape and the TFs, which establish this landscape dictate cell identity and the gene-expression program that is executed by the cell (Hnisz et al., 2013; Ong and Corces, 2012). Specifically, a sub-type of TFs known as pioneers can access and bind to areas of heterochromatin and recruit other TFs to the previously inaccessible site (Hnisz et al., 2013; Ong and Corces, 2012).

In the context of senescence, the enhancer landscape is significantly remodeled and several enhancers were identified to control SASP gene expression (Tasdemir et al., 2016). Not surprisingly, SASP associated enhancers were enriched for bromodomain protein 4 (BRD4) binding, and accordingly, BRD4 inhibition disrupts part of the SASP gene expression program (Tasdemir et al., 2016). During replicative senescence, p300 histone acetyltransferase associated with enhancers that drive the senescence gene expression program (Sen et al., 2019). Depletion of p300, but not closely related CBP, impacted the senescence phenotype. Finally, recent studies revealed the underlying

transcription factor networks that drive the establishment of the senescence-associated enhancer landscape in OIS (Zamudio et al., 2019). The AP1 family of pioneer TFs orchestrates a hierarchical TF network. AP1 TFs pre-mark senescence-associated enhancers, which dynamically gain the activating histone marks H3K27ac and H3K4me1 during senescence establishment. Furthermore, AP1 facilitates the recruitment of other activating TFs to these senescence-driving enhancers. Disruption of the AP-1 network leads to a partial reversion of the senescence phenotype (Zamudio et al., 2019).

1.8. Clinical Relevance of Senescence

Senescence is a protective and health promoting mechanism enhancing wound-healing, mediating embryonic development, and acting as a durable tumor suppressive mechanism in the face of oncogenic stress, or DNA damage (Campisi and d'Adda di Fagagna, 2007; Kuilman et al., 2010). However, senescence has now also been linked to aging and age-related disease. Senescent cells accumulate in older organisms, as exemplified in baboons and human skin (Jeyapalan et al., 2007). When young mice are transplanted with senescent cells, or premature-senescence is induced, they express characteristics of aged mice: decreased movement speed, grip strength, and hanging endurance (Xu et al., 2018).

Although the elimination of senescent cells *in vivo* increases the lifespan of mice by approximately 17-35%, more importantly, it significantly increases their healthspan (**Introduction Figure 9**) (Baker et al., 2016; Xu et al., 2018). Specifically, senescence eliminator mouse models demonstrated a significant decrease in the onset of age-related pathologies and delayed aging. These seminal studies exemplify the potential of senescence-targeting therapies to treat age-related pathologies and delay aging.

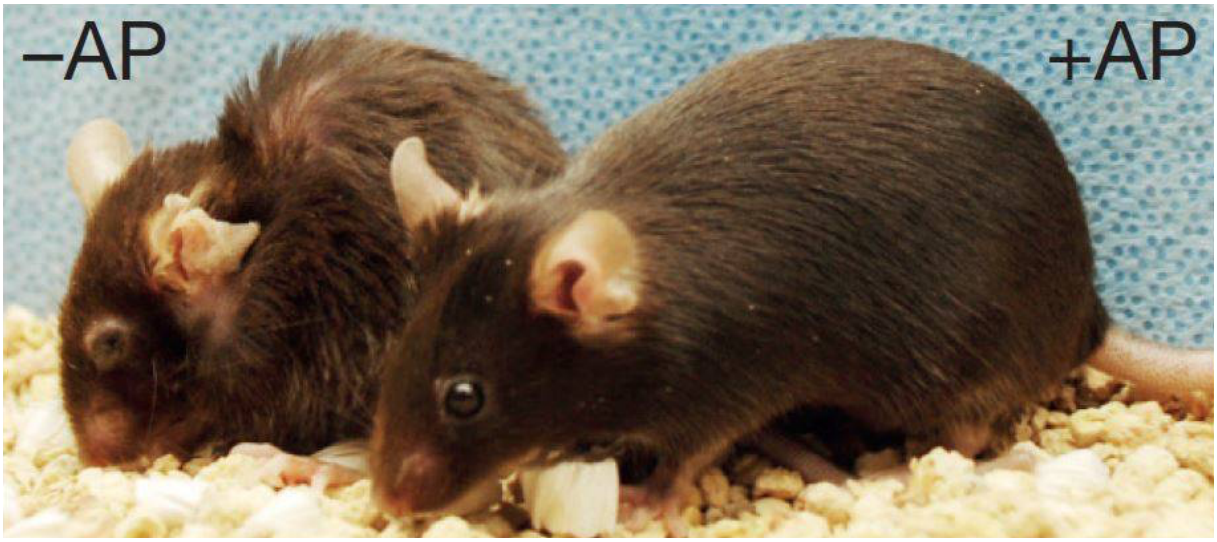

Introduction Figure 9. INK-ATTAC mice: Representative mice with (+AP, senescent cells are cleared) and without (-AP, senescent cells are not cleared). (Adapted from Baker, 2016).

Senescence therapies have also been introduced as an anti-cancer treatment modality (Therapy-induced senescence, TIS). A so-called one-two punch cancer therapy includes using senescence-inducing anti-cancer drugs followed by senolytics – drugs to eliminate senescent cells (Leite de Oliveira and Bernards, 2018; Wang and Bernards, 2018). Elimination of senescent cells following chemotherapy had a profound effect on the health of mice, decreasing chemotherapy-induced fatigue (Demaria et al., 2017).

However, a senescence arrest during anti-cancer therapy is a double-edged sword (Milanovic et al., 2018; Passos et al., 2010b). Senescent cells in the tumor microenvironment release pro-tumorigenic factors (discussed above). In pre-cancerous senescent hepatocytes, the release of CCL2 can trigger the differentiation of CCR2+ myeloid cells to mature macrophages and clear the senescent cells (Eggert et al., 2016; Kang et al., 2011). However, upon out-growth of hepatocellular carcinoma (HCC), the

micro-environmental changes from tumor-secreted factors block the maturation of the myeloid cells recruited by senescent cells, blocking NK cells from acting on the tumor, thus promoting the growth of the HCC (Eggert et al., 2016). Furthermore, in Eu-MYC B-cell lymphomas the stemness-promoting factors released by senescent cells can reprogram tumor cells into tumor stem cells, as well, upon senescence escape through the loss of TP53 or H3k9me3 from SUV39H1, these post-senescent cells grow more aggressively in a WNT-dependent manner (Milanovic et al., 2018). Senescence-induction is a viable target in cancer therapy.

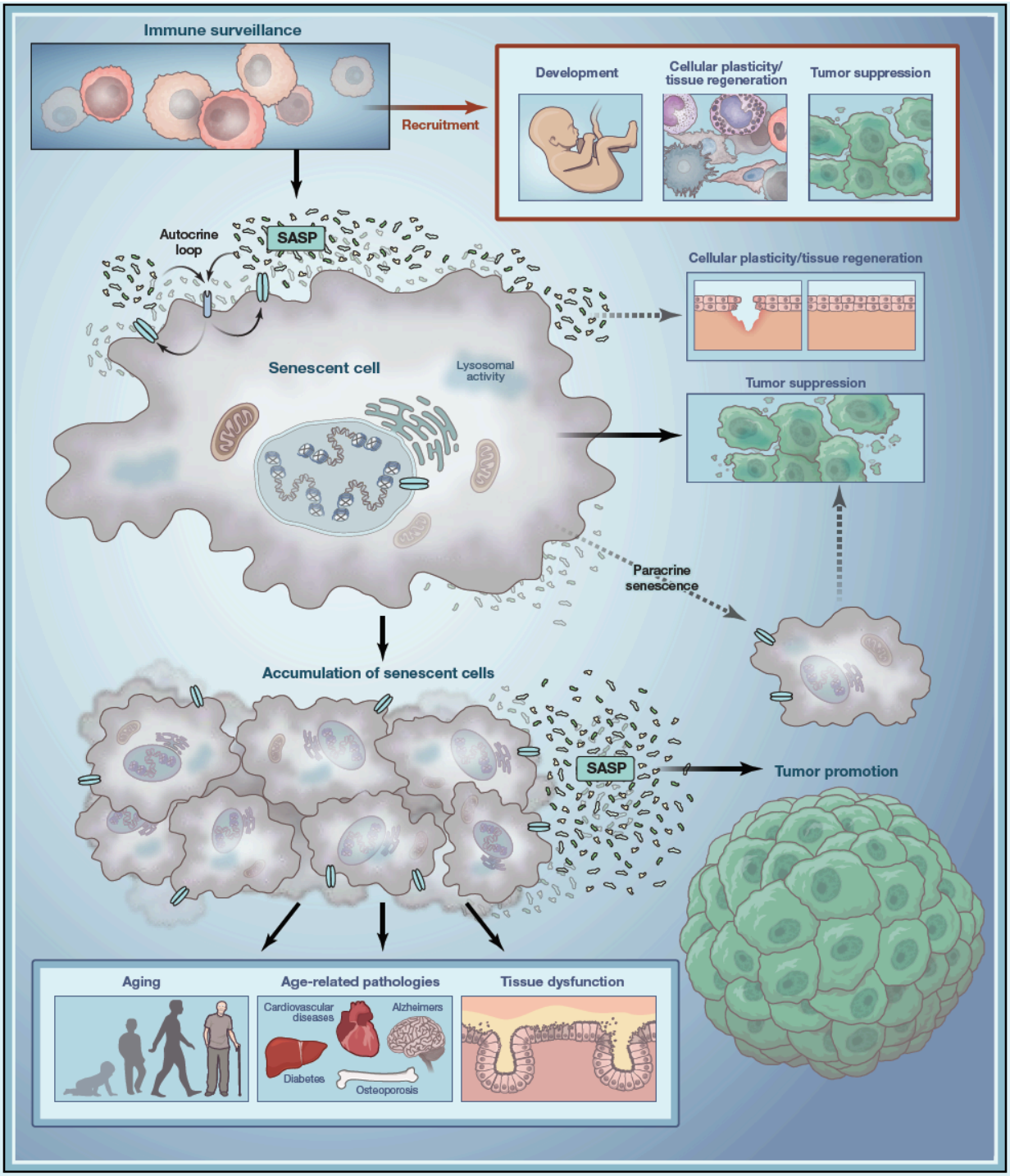

Introduction Figure 10. Cellular senescence in Pathophysiology (Adapted from Martinez, Zamudio 2017).

1.8.1 Senescence and Pathology

Senescence has been linked to many pathophysiological settings, where it can contribute functionally to age-related disease (**Introduction Figure 10**) (Martínez-Zamudio et al., 2017b). For example idiopathic pulmonary fibrosis (IPF) and smoking-induced chronic obstructive pulmonary disease (COPD) (Houssaini et al., 2018). Senescent cells accumulate during IPF in the mesenchymal, bronchial and alveolar layers of the lung as evidenced by the increased presence of senescence biomarkers including SABG, p16, p21, and TP53 (Schafer et al., 2017). In damaged IPF lungs, senescent cells secrete inflammatory cytokines, as well as NOX4 mediated ROS. The combination of inflammation and ROS contributes to the pathogenesis of IPF (Hecker et al., 2014). The knock-down of caveolin (CAV1) prevents senescence establishment in IPF conditions, and treatment with NOX4 inhibitors or anti-inflammatory agents improves the condition (Schafer et al., 2017). Furthermore, treatment with senescence eliminating drugs (Dasatinib and Quercetin) or using the INK-ATTAC senescence eliminator mouse model to eliminate p16 -expressing cells attenuates IPF dramatically (Schafer et al., 2017).

Cigarette smoking can induce COPD (Shivshankar et al., 2012). Similar to IPF, there is an increase in senescence biomarkers present in lungs, with an increase in inflammatory cytokines and ROS, which contribute to fibrosis (Rashid et al., 2018). However, in the context of COPD, the smoke damage to the mitochondria contributes to the disease (Rashid et al., 2018). Mitophagy mediating pathway PTEN-induced putative kinase 1 (PINK1)-PARK2 are involved in repairing mitochondrial damaging and dampening the production of ROS (Shivshankar et al., 2012). During COPD-senescence, there is an increase in ROS and a downregulation of this mitophagy pathway (Ito et al.,

2015). PARK2 is downregulated in COPD senescence, suggesting that the loss of this pathway contributes to senescence formation. COPD presents another potential target for senescence therapy (Rashid et al., 2018).

Senescence also contributes to neurodegenerative diseases. Although much of the brain cells are post-mitotic neurons, p16 expressing senescent astrocytes and microglia accumulate in a model of Alzheimer's disease (Bussian et al., 2018). Using the INK-ATTAC senescence eliminator mouse model showed a dramatic improvement of disease outcome including a reduction of neurofibrillary tangles of hyperphosphorylated TAO proteins, and prevention of degeneration of the hippocampus and cortical neurons (Bussian et al., 2018). These mice were able to maintain cognitive function compared to the control group. Besides, the use of senolytics ameliorated the neurodegeneration (Bussian et al., 2018).

Osteoarthritis (OA) is an age-related pathology of the joints that is characterized by an increase of inflammation, loss of cartilage tissue, and pain. Senescent cells accumulate in these damaged, inflamed tissues, contributing to inflammation as well as degradation of the extracellular matrix (Jeon et al., 2017; Marzetti et al., 2009) In a mouse model, the clearance of senescent cells ameliorates the OA and facilitates a regenerative microenvironment (Jeon et al., 2017). Treatment of osteoarthritis with senolytics is currently being explored in clinical trials. Furthermore, the muscle loss associated with aging, sarcopenia, is driven by senescence. Muscle satellite cells (muscle stem cells which renew lost muscle tissue) gain markers of senescence with age, corresponding to a decline of muscular function. Clearance of senescence, as well as a calorie-restricted

nutritious diet restores these stem cells to regenerate lost muscle tissue (Marzetti et al., 2009).

Obesity and type II diabetes are also associated with senescence. Adipocyte accumulation is associated with senescence and increased inflammation, contributing to detrimental health, and diabetes type II is intimately linked with senescence (Minamino et al., 2009). Pancreatic B-islet cells produce insulin in response to uptake of glucose. In the case of obesity and over-eating, B cells produce a large amount of insulin and multiply to meet the need. However, these cells can reach proliferative exhaustion and replicative senescence. Furthermore, mutations found in these cells to induced type-2 diabetes are also found to be associated with an upregulation of senescence biomarkers (Palmer et al., 2015; Tacutu et al., 2011).

Senescent cells can also contribute to cardiac disease, atherosclerosis, and hypertension in the cellular context of vascular smooth muscle and vascular endothelial cells (Fyhrquist et al., 2013; Katsuumi et al., 2018). Initial findings showed that there was an association between telomere shortening and cardiovascular disease, even in patients under the age of 50 (Fyhrquist et al., 2013; Katsuumi et al., 2018). Moreover, other senescence biomarkers including increased TP53, p16, p21, inflammatory cytokines, and ROS were also present (Fyhrquist et al., 2013). Senescent cells accumulate in patients with hypertension, which contributed to increased inflammation and stiffness of the vascular smooth muscle, and further exacerbating the condition in a feed-forward loop. Senescent cells can be causative and detrimental in atherosclerotic plaques (Chen et al., 1995). The presence of senescence increases TNFα, INFβ, IL8, IL1β, MCP-1, which

further drive pathology (Campisi et al., 2011; Katsuumi et al., 2018). In mouse models, elimination of senescent cells, and overexpression of SIRT1 (found to suppress senescence in VSMC) have strong promise in treating cardiac and vascular disease associated with aging individuals (Visel et al., 2010).

There are more and more pathologies linked causatively with senescence, which further underscores the need for the developing of senescence-targeting therapies to increase health- and lifespan.

2.1 Poly (ADP-ribose) Polymerase 1 (PARP1)

Poly (ADP-ribose) polymerase 1 (PARP1) is the predominant member of a large family of enzymes, catalyzing the transfer of nicotinamide adenine dinucleotide (NAD^+) to target proteins as ADP-ribose (ADPr) (Gupte et al., 2017). ADPr is covalently attached to target proteins as a single unit of ADPr as mono-ADPr and in a branched or linear post-translational modification composed of ADPr units linked by glycosidic bonds - poly-(ADP-ribose) (pADPr) (Kiehlbauch et al., 1993). This protein and its post-translational modification have a rich history of research starting nearly 60 years ago, and the understanding of its biological significance continues to expand. PARP1 is implicated in DNA sensing and repair, modulation of transcription, chromatin structure, mediation of inflammation, and replication. PARP1 is omnipresent in the nucleus with $5x10^5$ -$1x10^6$ molecules per cell, accounting for 80-90% of the pADPr activity of the cell and is the primary target of pADPr automodification (Ludwig et al., 1988; Yamanaka et al., 1988a). Despite years of research, delineating its mechanisms of action and regulatory roles is still incomplete.

2.2 PARP1 Protein Structure

PARP1 is a 1014 amino acid 116 kD protein that is divided into three domains: N-terminal DNA binding domain (DBD), auto-modification domain (AD), and the C-terminal catalytic domain that contains the NAD^+ binding site and PARP homology site (CAT) (**Introduction Figure 11**) (Kameshita et al., 1984, 1986).

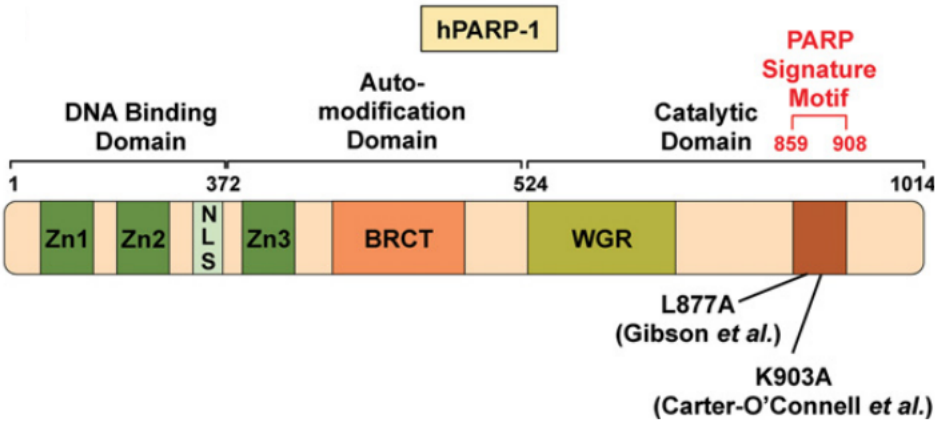

Introduction Figure 11. Structure of PARP1: Outline of features (DNA-Binding Domain, Auto-modification Domain and Catalytic domain) in PARP1 protein. (Adapted from Kraus, 2005).

The N-terminal DNA binding domain (DBD) is 372 amino acids long (42 kDa) and contains the nuclear localization signal (NLS) (Kameshita et al., 1984, 1986). The DNA binding domain contains three zinc fingers, which are critical for the DNA binding (binding to DNA breaks and damage), as well as inducing catalytic activity on the C-terminus (D'Amours et al., 1999). ZnI, ZnII, and ZnIII are all zinc fingers; however, they exhibit functional differences. Single strand breaks are identified explicitly by the ZnII zinc finger (Malanga and Althauss, 1994). *In vitro* studies showed that PARP1 can form a dimer with its DBD when binding to a 5'-recessed DNA break, and binds a monomer to a 3'-recessed and double-stranded DNA (Pion et al., 2005). The third zinc finger, ZnIII (located further from the N-terminal than ZnI and ZnII) of PARP1 was not identified until recently (Langelier et al., 2008). ZnIII is not critical for DNA binding activity; instead, ZnIII acts to activate PARP1 enzymatic activity by interacting with the C-terminal. PARP1 also binds directly to intact DNA, junctions, looped DNA, and nuclear matrix DNA (Galande and Kohwi-Shigematsu, 1999; Gradwohl et al., 1987; Lonskaya et al., 2005).

The AD is an important site for PARP1 automodification in addition to other PTMs (D'Amours et al., 1999). AD is enriched for glutamic acid, lysine, and aspartate residues, which are the prime acceptors of ADPr (Kraus and Lis, 2003; Naegelis and Althaust, 1991). Recent proteomics studies have found several different ADPr-modified residues, including serine, and asparagine (Bai, 2015). The mechanism of PARP1 automodification can occur through the formation of trans modification in a PARP1 dimer, as well as through cis modification through a monomer of PARP1 (Alemasova and Lavrik, 2019; Bauer et al., 1990). However, PARP1 is also modified outside of the AD (Alemasova et al., 2019). The AD contains the BRCA c-terminus (BCRT) domain which was first characterized in the BRCA1 DNA damage repair protein (Bai, 2015). Initially, this domain was found to function in recruitment of other proteins to sites of DNA damage (i.e., XRCC1); however, many other proteins, DNA binding proteins, and protein complexes have been identified (Kim et al., 2005).

The C-terminus of PARP1 (aa 525-1014) contains the catalytic domain (CAT) as well as the PARP protein family PARP signature motif (D'Amours et al., 1999). The CAT of PARP1 is capable catalyzing each step of ADP-ribosylation: initiation (first ADPr moiety), elongation (additional glycosidic bonds between moieties of ADPr) and branching of the pADPr chains (Kim et al., 2005). The donor site contains an NAD^+ binding pocket of histidine, tyrosine, and glutamic acid (Barkauskaite et al., 2015). The histidine binds the 2'-OH of NAD^+, and any substitutions of this amino acid result in a catalytically inactive PARP1 (Barkauskaite et al., 2015; Vyas et al., 2014). The glutamic acid is necessary for

the elongation step of the reaction, and an amino acid substitution at this location precludes elongation (Barkauskaite et al., 2015).

2.3. ADP-ribose

Individual units of ADPr are linked through a 1”-2’ ribose-ribose glycosidic bonds, and each ADPr has a strong negative charge (**Introduction Figure 12**) (Kiehlbauch et al., 1993). The addition of ADPr from NAD^+ creates the by-product of nicotinamide (NAA). PADPr can reach up to 200 units long with branches every 20-50 units(Kawaichi et al., 1981; Miwa et al., 1981). These long chains can form secondary structures, including helices and larger matrix structures (Minaga and Kun, 2011; Miwa et al., 1981). Other PARP family members contribute to ADP-ribosylation events in the cell, including PARP2 (the second most abundant and active member of the family) and the tankyrases, which are known to modify the telomeres (Smith et al., 1998).

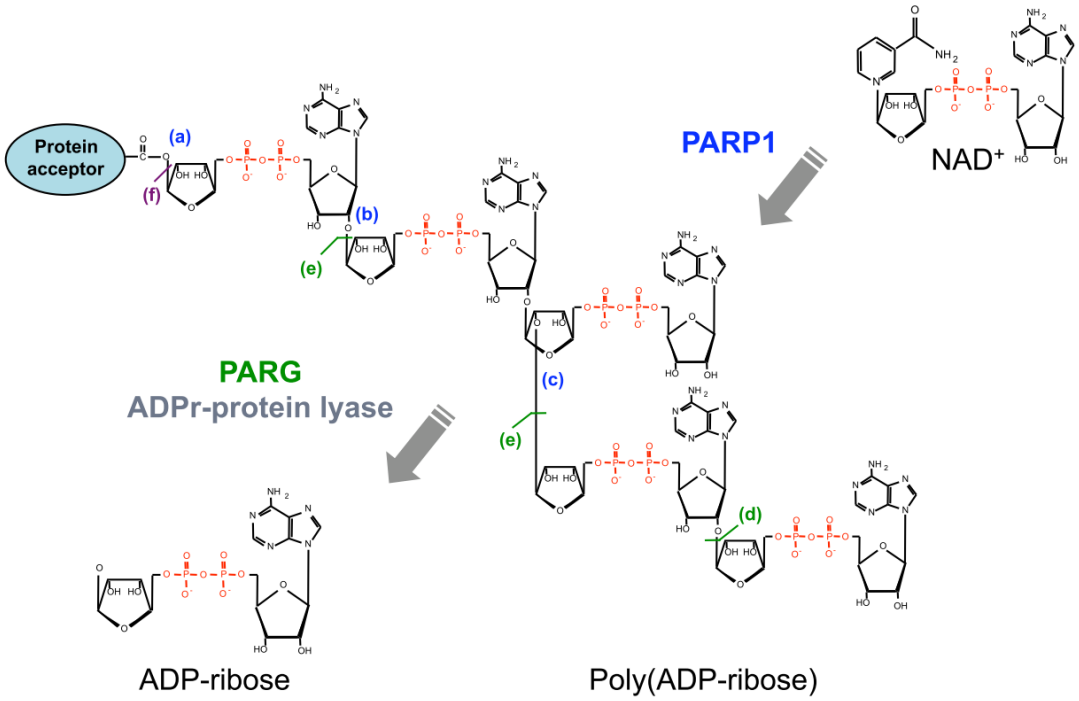

Introduction Figure 12. ADP-ribosylation metabolism: Displaying the initiation (a), elongation (b), and branching (c) steps of pADPr synthesis as catalyzed by PARP1. The degradation of pADPr by exoglycosidase (d) endoglycosidase (e) activities of PARG. Protein-proximal ADPr monomers are cleaved by ADPr-protein lyase (f). (Adapted from Zamudio-Martinez, 2012).

ADPr is a dynamic PTM that once added is removed rapidly by poly-ADP-ribose glycohydrolase (PARG), endoglycosidase to remove pADPr, ADP-ribose protein lyase and the recently discovered terminal ADP-ribose glycohydrolase 1 (TARG1) to remove the final ADPr unit (Gibson and Kraus, 2012). During stress and DNA damage, the half-life of ADPr can be as low as 1 minute, while under normal conditions it may last several 7 hours (Alvarez-Gonzalez and Althaus, 1989).

2.4. Modes of PARP1 Regulation

Many different signaling pathways, protein-protein interactions, and PTMs including ADP-ribosylation, phosphorylation, methylation, or acetylation regulate PARP1 activity (Hottiger, 2015). For example, SET7/9 can methylate PARP1 at K508 for recruitment purposes during DNA damage (Kassner et al., 2013). Methylation of PARP1 can stabilize the AD which enhances enzymatic activity. DDR signaling kinases JNK and ERKs phosphorylate and activate PARP1 (Kauppinen et al., 2006). ERK2 phosphorylates PARP1 at S732 and T373 to stimulate its enzymatic activity via increasing affinity for NAD^+ (Cohen-armon et al., 2007; Kauppinen et al., 2006). In the context of DNA damage, maximal ADP-ribosylation activity depends upon ERK1/2 kinase activity, and inhibition of this phosphorylation decreases PARP1 enzymatic activity (Cohen-Armon, 2007). However, phosphorylation by protein kinase C decreases PARP1 activity, which acts to protect the cell from necrotic death through over-activated PARP1 (El-Hamoly and Hegedűs, 2014). Acetylation of PARP1 by CBP/p300 and PCAF stimulates ADP-ribosylation activity and is essential in the full activation of the PARP1-NFκB signaling axis (Hassa et al., 2005). However, this acetylation can be reversed by deacetylases such as SIRT1 and HDACs (Kolthur-Seetharam et al., 2006). Another PTM, sumoylation acts to specify gene targets for PARP1 action as exemplified for the localization of PARP1 to the heatshock protein 70 (HSP70) gene locus after heat stress (Martin et al., 2009).

Protein-protein interactions also dictate PARP1 enzymatic activity. The first PARP interaction discovered was with histones (Wong et al., 1982). Histone 1 (H1) and Histone 3 (H3) were found to be potent stimulators of ADP-ribosylation activity (Ernest Kun et al., 2005). Acetylation of PARP1 prevents PARP-histone associations (Ernest Kun et al.,

2005). Furthermore, H4 and H2B binding activates PARP1 at promoters, while H2A can repress ADP-ribosylation activity (Hurtado-Bagès et al., 2018; Pinnola et al., 2007). The interactions with histones and histone variants are important mediators of chromatin remodeling, DNA damage, and gene-expression regulatory roles of PARP1 discussed in further sections. Proteins involved in DNA damage repair can stimulate PARP1 through protein-protein interactions, including HMGN1, NEIL1, OGG1, HPF1, SAM68 (Gibbs-Seymour et al., 2016; Masaoka et al., 2012; Noren Hooten et al., 2012; Sun et al., 2016). These interactions are not all of the same quality; for instance, histone ADR-r factor 1 (HPF1) primes the PARP1 catalytic domain by increasing its affinity for serine (Leung, 2017). YB-1 is an RNA-binding protein that can bind and disrupt PARP activity (Alemasova and Lavrik, 2019). Interestingly, ADP-ribosylation of YB-1 can prevent binding to PARP1, and thus loses its inhibitory effects. Furthermore, TP53 is found to interact with PARP1, modulating its activity (Fischbach et al., 2018). Although TP53 can be ADP-ribosylated, non-covalent protein-protein interactions can still stimulate PARP 1 activity (Fischbach et al., 2018). LPS challenge or stimulation of toll-like receptor 4 (TLR-4), which signals bacterial infections, induces a signaling cascade through MEK1/2, which phosphorylates ERK2, leading to the activation of PARP1 (Martinez-Zamudio and Ha, 2012). Furthermore, PARP activation through ERK is also possible through TNFα signaling (Vuong et al., 2015).

2.5. Functions and mechanisms of PARP1 and ADP-ribosylation

To understand PARP1 function in vivo, various labs have generated PARP1 knock-out (KO) mouse models. These mouse models were instrumental for defining a role for PARP1 in DNA damage repair, gene expression, replication, transcription, inflammatory signaling, and iNOS production (Shall and de Murcia, 2000a). Despite the involvement of PARP1 in many cellular processes, and its high abundance in cells, PARP1 knock-out is not lethal in mice; however, a double KO of PARP1 and PARP2 is lethal (Shall and de Murcia, 2000a). The latter indicates that PARP2 may compensate for the loss of PARP1 (Ménissier de Murcia et al., 2003). PARP1 deficient mice are significantly impaired in maintaining genomic instability. Sister chromatid exchanges are increased by 5-fold, and formation of micronuclei, sensitivity to gamma irradiation and DNA alkylating reagent N-Nitroso-N-methyl urea are equally increased. A surprising feature of these mice is their resistance to stress. PARP1 deficient mice are more resistant to the streptozotocin (STZ) induced diabetes, myocardial and cerebral ischemia, and inflammatory stressors such as LPS-induced septic shock (Shall and de Murcia, 2000a). Increased resistance to inflammatory stress results from defective induction of NFκB in these mice (Boulares et al., 2003). PAPR1 KO mice are also particularly sensitive to carcinogenesis and display a shortened life-span (Piskunova et al., 2008).

2.6. PARP1 binding and catalytic activity play a multi-facetted role in the nucleus

2.6.2. PARP1 is a key player in DNA damage repair

PARP1 was historically recognized for its involvement in DNA damage repair. PARP1 rapidly binds to sites of DNA damage and activates ADP-ribosylation activity, which recruits DDR proteins through ADPr recognition domains: PAR binding motif (PBM), PAR binding zinc fingers, macrodomains, WWE domains, BRC, PIN domains, and an OB-fold (Teloni and Altmeyer, 2016). The different readers of ADPr can form complexes and begin the repair process (Teloni and Altmeyer, 2016). PARP1 sensing and subsequent hyper-ADP-ribosylation is involved in double-strand breaks, single-strand breaks, base-pair excision repair (BER), nucleotide excision repair (NER), non-homologous end joining (NEJ), replication fork stability, and homologous recombination. Double-strand breaks are quickly recognized by PARP1, leading to enzymatic activity (Schuhwerk et al., 2017). ADP-ribosylation recruits DDR signaling kinase ATM to recruit and phosphorylate H2AX, TP53, PARP2, the MRN complex (Mre11/RAD50/NBS1), and SMC1 (Aguilar-Quesada et al., 2007; D'Amours and Jackson, 2002; Haince et al., 2007, 2008). In this context, PARP1 binds DDR-ATM-yH2AX foci and mediates damage signaling (Aguilar-Quesada et al., 2007; D'Amours and Jackson, 2002; Haince et al., 2007, 2008). The DNA DSBs repair pathway regulated by the PARP1-ATM axis includes both homologous recombination (HR) and non-homologous end-joining (NHEJ) (Aguilar-Quesada et al., 2007). For HR, PARP1 recognizes the DSB and recruits the MRN complex, facilitating the co-binding of Mre11 onto DNA with replication protein A (RPA) and BRCA1 (D'Amours and Jackson, 2002; Haince et al., 2008), thus, limiting the extent of DNA end resection

through ADP-ribosylation of BRCA1 (Hochegger et al., 2006). PARP1 can also initiate NHEJ and the alternative NHEJ at sites of DSBs through ADP-ribosylation of DNA-dependent protein kinase catalytic subunit (DNA-PKcs) and Cadherin 2 (CDH2) in a Ku-70/Ku-80 dependent fashion (Luijsterburg et al., 2016; Ruscetti et al., 1998).

During replication stress, ADP-riobsylation activity inhibits ATP-dependent DNA helicase Q1 (RECQ1), preventing damaging actions by prematurely restarting the replication machinery (Berti et al., 2013).

Single-strand breaks (SSBs), which are repaired through single-strand break repair (SSBR), nucleotide excision repair (NER) rely upon PARP1 catalytic activity (El-khamisy et al., 2003; Marintchev et al., 2000). During SSBR, ADP-ribosylation recruits X-ray repair cross-complimenting protein 1 (XRCC1), which forms a complex including DNA polymerase β, DNA ligase 3 (LIG3), and bifunctional polynucleotide kinase 3′-phosphatase (PNKP) (El-khamisy et al., 2003; Marintchev et al., 2000). In the context of NER, DNA damage-binding protein 2 (DDB2) will binds and activates PARP1 to recruit and ADP-ribosylate chromatin-remodeling helicase amplified in liver cancer protein 1 (ALC1) (Luijsterburg et al., 2012; Robu et al., 2013).

2.6.3. Chromatin remodeling during DNA damage

PARP1 binding and catalytic activity influence chromatin accessibility to facilitate safe DNA damage repair (Ray Chaudhuri and Nussenzweig, 2017). During DNA repair, ADP-ribosylation drives ALC1 nucleosome sliding away from the site of damage and relaxation of chromatin, to facilitate the recruitment of protein complexes for repair (Ahel et al., 2012;

Gottschalk et al., 2009). ALC1 binds to ADPr via its C-terminal macrodomain, which stimulates nucleosome sliding while maintaining the histone octamer, through an N-terminal ATPase. Under normal conditions, ALC1 is maintained in an auto-repressed state, and not until PARP1 activation when it binds to ADPr through its macrodomain is it released (Singh et al., 2017). Chromatin remodeling at the periphery of DNA damage is facilitated through ADP-ribosylation of SWI/SNF related, matrix associated, actin-dependent regulator of chromatin, subfamily A 5 (SMARCA5), which binds to ADPr through an E3 ubiquitin ligase ring finger protein 168 (RNF168) (Smeenk et al., 2013). Additionally, to further relax the chromatin during DDR, ADP-ribosylation activates chromatin remodeling protein CHD2, which deposits histone variant H3.3, known to be a chromatin-relaxing histone variant (Luijsterburg et al., 2016).

Faithful DNA damage repair requires the repression of transcription in the flanking regions as a protective mechanism until the repair is completed (Ray Chaudhuri and Nussenzweig, 2017). Activated PARP1 recruits polycomb repressor complex (PRC) proteins, nucleosome remodelers, and members of the deacetylase complex (NuRD), CHD4 and metastasis protein 1 (MTA1) (Chou et al., 2010). As such, RNA pol II transcription is disrupted, and transcription can be repressed. The recruitment of PRC proteins leads to chromatin compaction, deacetylation and PRC-EZH2 driven methylation of H3K27 (Chou et al., 2010). Following UV laser micro-irradiation, PARG inhibition (i.e., increased ADP-ribosylation activity) leads to enhanced repression of transcription and removal of nascent RNA. Additionally, during DNA damage repair, the macrodomain of MacroH2A1.1 can bind to ADPr chains on PARP1 leading to chromatin compaction which

can be abrogated using PARP1 inhibition (Timinszky et al., 2009). The chromatin compaction driven by the binding of ADPr and MacroH2A1.1 alters the binding of DDR signaling gH2Ax as well as repair machinery Ku70 and Ku68. MacroH2A1.1 is immobile, and it is thought that chromatin containing this histone variant may be binding PARP1 though a looping mechanism, although this still needs to be confirmed (Timinszky et al., 2009).

2.6.4 PARP1 and ADP-ribosylation and the Regulation of Gene Expression

PARP1 regulates transcription via distinct and non-mutually exclusive mechanisms including chromatin accessibility, histone modifications, chromatin insulation, DNA methylation, serving as a co-regulator of TF function and other chromatin associated proteins, and binding to and functioning at gene regulatory loci such as promoters and enhancers.

2.6.5 PARP1-Driven Chromatin Decondensation at *D. melanogaster* heat-shock protein 70 (HSP70) loci

One of the best-characterized examples of PARP1 mediated chromatin decondensation is demonstrated at the *D. melanogaster* heat-shock protein 70 (HSP70) loci. On the polytene chromosome, heat-shock very rapidly induces massive chromatin loosening and formation of a puff, seen through microscopy and sensitivity to micrococcal nuclease (MNase) digestion (Petesch and Lis, 2008). This functions increase accessibility of the

locus to transcription factors and the transcriptional machinery to rapidly induce transcription of HSP70 (Boehm et al., 2003). Rapid loosening of chromatin includes the release of nucleosomes from the chromatin (Petesch and Lis, 2008). PARP1 is a critical regulator of this process through ADP-ribosylation of histones, auto-modification resulting in release from the chromatin, and rapid recruitment of the transcriptional machinery to the gene locus (Petesch and Lis, 2008). Upon inhibition of PARP1, the heat shock puff is disrupted, and the expression of HSP70 is diminished (Tulin and Spradling, 2003a).

Additionally, the rapid recruitment of Positive-Transcription Elongation Factor b (pTEFb) and RNA-polymerase II (RNA pol-II) is dependent on PARP1 through a mechanism called the cage effect of pADP-PARP1 (Zobeck et al., 2010). Newly released auto-modified PARP1 can recruit and keep the transcriptional machinery close to the HS puff, facilitating transcription (Zobeck et al., 2010). Furthermore, these mechanisms work in concert with chromatin remodeling protein MI-2 (Murawska et al., 2011). Mi-2 binds to ADPr through a K/R rich domain and is attracted to the heat shock puff, where it enhances transcription through interactions with nascent RNA transcripts (Murawska et al., 2011). The HS puff is a robust model for its potential mediation of relaxation of chromatin.

2.6.6. PARP1 and the Regulation of Histones and DNA Modification

Histone methylation

PARP1 binding at promoters strongly correlates with H3K4me3, a hallmark of active transcription (Krishnakumar and Kraus, 2010a). These promoters are protected from the

demethylase KDM5B, which becomes ADP-ribosylated, thus, preventing the removal of methyl groups from H3K4 (Krishnakumar and Kraus, 2010a). However, PARP1, through its binding activity, has been also found to repress H3K4me3 through binding to histone methyltransferase MLL (Minotti et al., 2015). Furthermore, in a similar fashion to KDM5B inhibition, ADP-ribosylation of KDM4 disrupts the demethylation of repressive heterochromatin methylation marks K3K9me2/3 (Khoury-haddad et al., 2014).

Histone acetylation

Histone acetylation is associated with actively transcribed genes and active chromatin states (Wang et al., 2009). Early *in vitro* studies suggested a positive link between acetylated histones H3/H4 and ADP-ribosylation through binding of acetylated chromatin in an ADPr antibody column (Wong and Smulson, 1984). Furthermore, in human cells, transcriptomic studies observed that macroH2A driven gene expression requires PARP1 and CBP to facilitate acetylation and promote gene expression (Chen et al., 2014). PARP can maintain acetylation levels through its antagonistic relationship with SIRT1 deacetylase (Bai et al., 2011; Mendelsohn and Larrick, 2017). Sirtuins compete with PARP enzymes for intracellular NAD^+ pools, and while deacetylation of PARP1 by SIRT1 can decrease activation, so to can ADPr of SIRT 1 reduce deacetylation activity (Bai et al., 2011a; Canto et al., 2011; Cantó et al., 2013).

DNA methylation

DNA methylation is an extensive and repressive epigenetic modification and is characterized by the addition of 5-methylcytosine (5mc) at CpG islands (repetitive CG dinucleotides) via DNA-methyl transferase (DNMT 1, 3A, 3B) (Li et al., 1992). Global DNA methylation levels decrease with age; however, there is upregulation at specific loci (Horvath, 2013). PARP1 inhibition results in a global increase in 5mc, which is mediated through an ADPr-mediated binding and inhibition of DNMT1 (Caiafa et al., 2009). Therefore, PARP is antagonistic of DNA methylation (Caiafa et al., 2009). ADP-ribosylation drives CTCF translocation into the nucleus where it protects the genome from DNA methylation (Ohanna et al., 2011b; Zampieri et al., 2012). PARP1 forms a complex with CTFC, ChIP-seq analysis revealed co-localization of PARP1 with CTCF binding sites and low DNA-methylation areas was observed through a ChIP-seq of PARP1 (Nalabothula et al., 2015).

2.6.6. PARP1 and Chromatin insulation

Insulators are cis-regulatory elements, which control gene expression by blocking the interaction of enhancers with promoters or prevent repression through disrupting heterochromatinization (Phillips-Cremins and Corces, 2013). PARP1 is implicated in insulation through interactions with one of the most essential proteins driving this process, CTCF (Yu et al., 2004). CTCF and other insulators are involved in maternal imprinting and maintaining repression of H19 imprinting control region, which regulates the expression of insulin-like growth factor 2 (IGF2) (Yu et al., 2004). A study in mouse cells demonstrated that ADP-ribosylation of CTCF at the H19 locus is required to maintain repression, and PARP inhibitors disrupt chromatin insulation, leading to increased

expression. Currently, the exact mechanism by which ADP-ribosylation of CTCF can repress chromatin is unclear.

2.6.7 PARP1 and Heterochromatin

PARP1 is now also recognized as a critical factor for the stability and formation of heterochromatin (e.g. at telomeres and pericentromeric regions), repressed chromatin states, and X chromosome inactivation (Dantzer and Santoro, 2013). PARP1 co-localizes and ADP-ribosylates chromobox homolog 5 (CBX5), also known as heterochromatin protein 1 – involved in heterochromatin complexes, and interactions with repressive histone methylation (Quénet et al., 2008). Compelling evidence displays PARP1 activity at the inactive X chromosome in females, wherein heterochromatinization of one of the X-chromosomes represses gene expression (Pollex and Heard, 2012). PARP1 -/+; PARP2 -/- mice display lethality only in females, and this was due to the improper silencing of the second X-chromosome (Pollex and Heard, 2012). The silent X-chromosome accumulates histone variant macro-H2A1.2, which binds PARP1 and inhibits its enzymatic activity, contributing to the formation of heterochromatin and silencing (Dantzer and Santoro, 2013; Pollex and Heard, 2012). PARP1 KO decreases global levels of heterochromatin marks H3K27me3, H3K9me2/3, H4K20me3, and methylated DNA (Ciccarone et al., 2017). Through ADPr of UHRF1, PARP1 mediates the stability of H4K20me3, preventing the ubiquitylation of DNMT1 by UHRF1 (De Vos et al., 2014). At centromeres, PARP1 colocalizes with centromere protein A and B (CENPA/B) and budding uninhibited by benzimidazoles 3 (BUB3), which upon DNA damage activates

ADPr activity and dissociation from centromeres (Saxena et al., 2002). The above suggests that unmodified PARP1 is involved in maintaining the condensed chromatin found typically at centromeres. In the absence of PARP1 enzymatic activity chromatin accessibly is decreased, which can be reversed through its activation; however, ADPr is found to recruit heterochromatin forming proteins and complexes during DNA damage (as discussed earlier).

2.6.8 Interactions with Histones

Early *In vitro* studies observed that ADP-ribosylation of histones lead to relaxed chromatin structure through histone modifications. Using purified chromatin, exogenous PARP1 and NAD^+ reduced chromatin compaction, and higher-order chromatin structure in an NAD^+ concentration-dependent manner via modification of histones, which was reversible through PARG addition (Huletsky et al., 1985, 1989; De murcia et al., 1986; Poirier et al., 1982). This argues that the highly negative charge of ADPr is a disruptive and repulsive force to DNA. Accordingly, in the absence of NAD^+, PARP1 binding to histones compacts DNA structure; however, in the presence of NAD^+, PARP1 activity relaxes chromatin structure to "a beads on string" conformation, and eventually release nucleosomes from chromatin (Kim et al., 2004).

PARP1, core histones, and linker histone H1 are the most abundant interaction partners on chromatin (Wong and Smulson, 1984). H1 and PARP1 dynamics are instructive, and their interplay is a critical component of gene expression (Nalabothula et al., 2015). Linker histone H1 binds to the linker DNA exiting from the core nucleosome

and can influence local chromatin structure around promoters. ChIP-seq of PARP1 displayed that genomic binding is primarily at actively transcribed genes, in a mutually exclusive relationship with H1 (Khoury-haddad et al., 2014; Krishnakumar and Kraus, 2010a; Nalabothula et al., 2015). Using purified chromatin, PARP1, and H1 compete for the same linker DNA, wherein H1 can exclude PARP1 binding to the nucleosome at this position (Kim et al., 2004). The mechanism by which PARP1 binds to linker DNA competes with H1 binding *in vivo* is still unclear.

2.6.10 PARP1 Binding and Enzymatic Interactions with Transcription Factors

PARP1 co-binding and enzymatic activity functionally impact transcription factors in both activating and repressive functions and biological outcomes depending on the context. There is also still no unifying mechanism or role for PARP1 in terms of its effects on chromatin structure, gene-expression regulation, and so far, it remains at the whimsy of its local context and interacting partners. This section will outline some of the known PARP1 interactions with transcription factors.

PARP1 interactions, independent of its catalytic function can be instrumental in activating TF functions. PARP1 regulates Retinoic acid receptor (RAR) dependent determination of site-specificity and composition of the Mediator complex located at the RARβ promoter (Pavri et al., 2005). In the inactive state, the RARβ promoter is bound by repressive complexes, including HDACs, NCoR, SMRT, and the Mediator complex, including repressive TF CDK8 (Pavri et al., 2005). Upon stimulation with retinoic acid (RA), PARP1, through BRCT binding to the Mediator complex facilitates the exchange of

the repressive TF CDK8 with activating TF ERCC3/TFIIH (Pavri et al., 2005). The release of CDK8 and the activation of the Mediator complex drives expression of the RARβ gene in a PARP1 catalytic-independent fashion (Pavri et al., 2005). In mouse embryonic stem cells, PARP1 interacts with SOX2, a TF that is critical for maintaining pluripotency (Liu et al., 2017). PARP1 localizes at SOX2 binding sites, as shown through a ChIP-seq study (Liu et al., 2017). The DNA binding motifs of PARP1, DBD, and BRCT, together are required to bind to nucleosomes containing SOX2 DNA sequence motifs. Co-binding with PARP1 is required to overcome the barriers of binding at nucleosomal DNA and is independent of ADPr activity. PARP1 knock-down and inhibition of ADPr decreases the efficiency of Yamanaka-factors (KLF4/SOX2/OCT4/c-MYC) to induce pluripotent stem cells (Chiou et al., 2013). Additionally, PARP1, independent of its enzymatic activity, can act as a co-activating transcription factor with E2F1, B-MYB and Tax progression and growth (Anderson et al., 2000; Cervellera and Sala, 2000; Simbulan-Rosenthal et al., 2003).

PARP1 catalytic activity can be instrumental for its specific binding to DNA. NFAT is the master regulator of IL-2 expression upon stimulation (Olabisi et al., 2008). Nuclear factor of activated T-cells (NFAT) is recruited to the nucleus where it forms an activating complex with CEBPs, FOS-JUN, FOX3p, CREB/p300 as well as histone acetylases to upregulate IL-2 expression (Olabisi et al., 2008). In this scenario, binding of PARP1 and ADP-ribosylation of NFAT acts as a molecular switch to activate expression. During ERK2 signaling of mouse cardiomyocytes and cortical brain neurons treated with growth factors, PARP1 is activated and assists in the downstream activation of ELK1 (Cohen-Armon,

2007). Phosphorylation of ERK2 is found to activate the enzymatic activity of PARP1 in a phosphorylation-independent and DNA-independent mechanism (Cohen-Armon, 2007). PARP1 binds and ADP-ribosylates pERK2, which functions as a complex to increase the phosphorylation of ELK1. In the transcriptional control of muscle-specific genes, PARP1 and its enzymatic activity drive TEF-1 transcription factor binding to promoters and enhancers in MCAT elements (Butler and Ordahl, 1999). Cardiac troponin T (cTNT) expression is driven by TEF-1 binding at an MCAT1 element, where PARP1 can be co-immunoprecipitated with TEF1, and inhibiting PARP activity decreased gene expression (Butler and Ordahl, 1999).

PARP1 catalytic activity also drives the transition from a repressed to a transcriptionally active chromatin state through Mammalian Accaete –Scute Homolog-1 (MASH1) in rat neural stem cells (Ju et al., 2004). Under normal conditions, MASH1 is repressed by a repressive complex containing PARP1, Hairy/Enhancer of split (HES1 transcription factor), Groucho (GRO)/like enhancer of split 1 (TLE1) (Ju et al., 2004). This repressor complex recruits HDAC1 and repressive SIN3 components (Ju et al., 2004). Upon stimulation of PDGF, calcium-dependent protein kinase CaKIId becomes activated, and MASH1 is expressed by through the transition of this repressive complex into an activating complex. CaKIId phosphorylates PARP1, leading to its subsequent enzymatic activation, which in concert with phosphorylated HES1 (now in a transcriptionally promoting conformation) facilitates the site-specific recruitment of activating transcription factors. This transformation is disrupted during PARP1 inhibition (Ju et al., 2004).

PARP1 enzymatic activity can also lead to decreased function of TFs. TGFβ is an important cytokine that induces phosphorylation of SMAD transcription factors and formation of a SMAD2:3:4 TF complex in the nucleus (Feng and Derynck, 2005). PARP1 binds to the SMAD complex as shown in co-immunoprecipitation studies of SMAD4 and PARP1 (Lönn et al., 2010). However, upon PARP1 activation, ADP-ribosylation of SMAD3 and SMAD4 inhibits gene expression of SMAD2:3:4 bound promoters (Lönn et al., 2010). ADP-ribosylation-mediated disruption of expression is a potent barrier to EMT, which can occur after the extended exposure to TGFβ and in line with these findings, PARP inhibitors accelerate EMT (Lönn et al., 2010).

During differentiation, PARP1 has an antagonistic relationship with SOX-2, contrary to the relationship during stem cell maintenance (Gao et al., 2009; Liu et al., 2017) PARP1 acts as a decisive transcription factor, binding to the FGF4 enhancer to facilitate its expression as well as ADP-ribosylating SOX-2, leading to its detachment from the chromatin (Gao et al., 2009). In a similar fashion, ADP-ribosylation of CEBPβ, HOXB7, CREB, YY1, Sp1, or TP53 results in reduced affinity for DNA binding, thus inhibiting part of their binding activity (Oei et al., 1997; Simbulan-rosenthal et al., 1999; Simbulan-Rosenthal et al., 2000; Wu et al., 2012; Zaniolo et al., 2007). Interestingly, PARP1 catalyzed ADP-ribosylation of TP53 disrupts its binding to the consensus sequence, but this may act to stabilize the protein during its upregulation in the early stages of apoptosis (Kumari et al., 1998; Simbulan et al., 2001). Furthermore, one of the critical transcriptional programs of adipocyte differentiation driven by CEBPβ relies upon the enzymatic activity of PARP1 (Erener et al., 2012; Luo et al., 2017). ADP-ribosylation

of amino acids K133, E135, E139 in pre-adipocytes prevents gene-expression driven by CEBPβ (Erener et al., 2012; Luo et al., 2017). Only during the differentiation process ADPr is removed, and DNA binding activity can start unimpeded (Erener et al., 2012; Luo et al., 2017).

2.6.9 PARP1 Regulation of Inflammatory Gene Expression

PARP1 is instrumental in the inflammatory gene expression program. PARP1 KO mice are highly resistant to LPS-induced endotoxic-shock (Shall and de Murcia, 2000b). In response to LPS treatment, PARP1 null mice do not accumulate TNF-a, VCAM, ICAM, INF-g, P-selectin, iNOS, which is attributed to a complete failure to activate the NFκB signaling pathway (Oliver et al., 1999). Furthermore, mice treated with PARP inhibitors and challenged with zymosan (a glucan found on the surface of fungi to induce sterile inflammation) display diminished recruitment of neutrophils alongside a global and local reduction in inflammation, iNOS signaling, and inflammatory cytokine release (Szabó et al., 1997a). The latter is in part due to defective NFκB signaling. In a glial cell model, PARP inhibitors disrupt the expression of IL1β, INOS2, TNF, INFγ, which is linked to defective p38MAPk downstream phosphorylation of ATF-2, cAMP signaling and p65 NFκB (Ha, 2004). Several inflammatory genes are thus affected by the loss of PARP1 function.

The primary pathway highlighted in these functional studies is the PARP1-NFκB signaling axis. NFκB commonly refers to the classical and most common heterodimer

containing p65 (RELA) and p50 (NFκB1). Early studies found that PARP1 interacts with p50 and p65 in an enzymatic and DNA-independent fashion to facilitate NFκB binding shown through induction of a constructed NFκB reporter gene (Hassa et al., 2001). Furthermore, this study showed NFκB signaling using a PARP1 -/- complementation with a mutated PARP1 that is enzymatically inactive and mutated DNA-binding domain (Hassa et al., 2001). This PARP1-NFκB co-binding is stabilized through acetylation of PARP1 by CBP/p300 and facilitates the formation of PARP1- NFκB with activating Mediator complex (Hassa et al., 2005). However, contradictory to this, early in vitro studies found that ADP-ribosylation strengthened the PARP1-NFκB protein-protein interaction, and this interaction was weaker in the presence of a PARP1 inhibitor (Chang and Alvarez-Gonzalez, 2001). Besides, auto-modification, PARP1 can facilitate the gene-regulatory activities by increasing the DNA binding capacity of NFκB (Nakajima et al., 2004). PARP inhibition reduces the expression of LPS induced TNFα in a dose-dependent manner (Nakajima et al., 2004). Furthermore, a study in macrophage during LPS challenge found that PARP1 ADP-ribosylates histones at the promoters of IL1β, MIP-2, and csf2, to recruit NFκB, as well as maintain an open chromatin structure for the increase expression (Martinez-Zamudio and Ha, 2012). They found that LPS stimulation induces upregulation of ADP-ribosylation of histones, with H3 being the most favored (Martinez-Zamudio and Ha, 2012). This ADP-ribosylation activity is driven through toll-like receptor 4 signaling (TLR-4), which activates the phosphorylation of MEK1/2 and downstream ERK, which is a known activator of PARP1 (Martinez-Zamudio and Ha, 2012). In the LPS challenge,

treatment with a MEK1/2 inhibitor blocks PARP1 activation and ADP-ribosylation of histones (Martinez-Zamudio and Ha, 2012).

Additionally, the regulation of CXCL-1 expression present further insight into the mechanisms by which PARP1 controls expression in collaboration with NFκB (Amiri et al., 2006). In normal melanocytes, enzymatically-inactive PARP1 binds to the CXCL1 promoter, represses expression, and prevents NFκB binding (Amiri et al., 2006). However, in the malignant melanoma setting, PARP1 becomes active at this promoter, which results in NFκB binding (Amiri et al., 2006). PARP1 auto-modification leads its release from the promoter, facilitating NFκB binding (Amiri et al., 2006). PARP1 inhibition leads to the downregulation of CXCL1 expression, while PARP1 depletion leads to an increase in its expression (Amiri et al., 2006). It may also be possible that this catalytic activity plays a role in recruiting NFκB to the CXCL1 promoter site.

Together, these findings exemplify the complexity of PARP1 in gene-regulation.

2.7 Role of PARP1 Binding and Catalytic Activity in Physiology and Pathophysiology

PARP1 displays a wide range of nuclear, metabolic, and regulatory functions. Thus, it stands to reason that PARP1 dysfunction is a significant contributor to human pathologies. Human pathologies, especially those in which oxidative stress or inflammation plays a vital role, are accompanied by an elevated level of ADPr; however, a causative role for ADPr is still in question for many pathologies (Pacher and Szabo, 2008). Over-activated PARP can lead to a dangerous level of inflammation, ROS, iNOS, as well as NAD+ depletion-driven necrosis (Ha and Snyder, 1999). In the context of cardiovascular disease, PARP1 activity exacerbates injury by generating iNOS and increased inflammation in vascular endothelial cells, which can lead to rigidity of the vasculature (Szabó et al., 1997b). During hypertension, angiotensin II signaling increases cellular levels of NADPH and peroxynitrate, which drive DNA strand breaks and subsequent PARP1 overactivation (Szabó et al., 1997b). PARP1-mediated injury can be attenuated through the use of PARP inhibitors (Szabó et al., 1997b). In diabetes, PARP1 can worsen vascular conditions through similar mechanisms, wherein mitochondrial dysfunction causes superoxide from mitochondrial complex III, which leads to peroxynitrate production and DNA damage. Besides, PARP1 overactivation disrupts GAPDH function further exacerbating metabolic distress (Du et al., 2003). PARP1 levels and ADP-ribosylation are also elevated in asthma, wherein PARP inhibition facilitated recruitment of CD4+ T-cells through IL-17 signaling ameliorating the condition (Ghonim et al., 2015).

2.7.1 Role of PARP1 in Cancer

PARP1 KO mice are significantly impaired in their ability to repair damaged DNA, which contributes to their increased rate of carcinogenesis, especially after exposure to DNA damaging agents such as cigarette smoke, asbestos, *Helicobacter pylori* infection, increases the rate of carcinogenesis when PARP1 is depleted (Masutani and Fujimori, 2013; Tsutsumi et al., 2001). PARP1 controls epigenetic stability and plasticity through, for example, maintenance of DNA methylation and chromatin insulation through CTCF interactions as mentioned earlier (Caiafa et al., 2009). Changes in DNA demethylation and chromatin accessibility, working in concert with PARP1, are an essential step in the reprogramming of cells to pluripotent stem cells and are involved in malignant transformation (Masutani and Fujimori, 2013; Yu et al., 2004). Although PARP1 can block EMT through attenuating TGFβ–SMAD2:3:4 signaling, malignant transformation can be exacerbated through increased PARP1-mediated inflammatory signaling and secretion of matrix remodeling metalloproteases (MMPs) (Mabley et al., 2002).

2.7.2. PARP1 Inhibitors in Cancer Therapy

Many PARP inhibitors are to-date employed in cancer therapy based on the hypothesis that PARP1 inhibition leads to increased DNA damage, and therefore PARP inhibitors are used extensively in BRCA1/2 mutated breast and ovarian cancers (D'Andrea, 2018). For example, Olaparib shows synthetic lethality in mutated BRAC1/2 cancers and is already approved as a first line treatment in the clinic (Tutt et al., 2010). With the

impairment of DNA damage repair in BRCA1/2 mutant cancer cells, PARP1 inhibition further increases genomic instability, eventually inducing cell death (Tutt et al., 2010). Besides, combination therapies using genotoxic agents, such as topoisomerase inhibitors or doxorubicin together with PARP1i, exacerbate genotoxicity (Muñoz-Gámez et al., 2005). The exploration of PARP1 inhibition in cancer therapy has immense potential, especially, as we know now that the roles of PARP1 go beyond DNA damage repair.

2.7.3. PARP1 and Aging

PARP1 is also an exciting target for other age-related pathologies other than cancer. Indeed, using a classical hyperglycemic C. elegans aging model Olaparib was able to rescue the shortened life-span of these worms (Xia et al., 2017). PARP1 is an essential contributor to the cellular NAD+/NADH ratio, and NAD^+ has been implicated for many years as a life-extending agent initially from the work of David Sinclair and Leo Guarente (Anderson et al., 2003). NAD^+ decreases with age, and supplementation has been found to increase life-span in mice (Imai and Guarente, 2016). In aging cells, PARP1 has a decreased accessibility to NAD^+ as it becomes sequestered by DBC1 (Deleted in breast cancer 1 protein) (Li et al., 2017). These studies usually link the decrease in NAD^+ with decreased sirtuin activity; however, there is also decreased PARP1 activity with age, and an inability to maintain genomic stability as a result (Mendelsohn and Larrick, 2017). Despite early indications that PARP1 activity plays a role in aging through SIRT interactions, there are still many unknowns (Bai et al., 2011b; Mouchiroud et al., 2013). On the one hand, there is the upside in inhibiting PARP1 to ablate associated

inflammaging; on the other hand, there is the downside in the potential increase of genetic instability and carcinogenesis.

3. Thesis Rationale, Aims and Hypothesis

Cellular senescence is a durable cell cycle arrest induced by diverse forms of cellular stress. It is characterized by cell death resistance as well as an inflammatory gene expression. This complex pro-inflammatory response is known as the senescence-associated secretory phenotype (SASP), which can modulate senescence status, tissue microenvironment, and interactions with immune cells. The execution of the senescence program goes hand-in-hand with a large-scale restructuring of the epigenetic landscape. While select genetic and epigenetic elements crucial for senescence induction have been identified, the dynamics, underlying mechanisms, and regulatory networks defining senescence competence, induction and maintenance remain poorly understood, precluding a deliberate therapeutic manipulation of these dynamic processes.

Mounting evidence supports a role of PARP1, as a chromatin-based transcriptional co-regulator of genes involved in inflammation and cancer, in addition to its canonical role in DNA damage repair. The moonlighting functions of PARP1 as a chromatin-based transcriptional co-regulator are underexplored, and clinical focus has remained mainly on its role in DNA repair for its efficacy in cancer therapies.

As a nuclear protein, PARP1 binding and catalytic activity directly affects higher-order chromatin structure through binding to DNA, binding and modifying histones, regulating histone modifications (acetylation, methylation), DNA-methylation, chromatin insulation through CTCF interactions, as well as modulation of gene expression through promoter and enhancer-binding and interactions with transcription factors. PARP1 is a driver of inflammatory gene expression through interactions with NFκB. Given the

parallels between the SASP and inflammatory responses, and the chromatin-based regulation of inflammatory gene expression by PARP1 enzymatic activity, it is of interest to establish the function of PARP1 in the transcriptional control in senescent cells.

3.1. Thesis Aims

My PhD thesis aims at closing these critical gaps in our knowledge by characterizing the gene-regulatory role of PARP1 in the execution and maintenance of senescence by combining reverse genetics and pharmacological inhibitors with transcriptome, chromatin accessibility (ATAC-seq), genome-wide PARP1 (by ChIP-seq) and ADP-ribosylated chromatin profiling (using a novel technique termed CRAP-seq). Specifically, I proposed to:

Aim 1: Delineate the individual contributions of PARP1 chromatin-binding and enzymatic activity in regulation of senescence gene-expression.

Aim 2: Determine the impact of PARP1 chromatin binding and ADP-ribosylation of chromatin associated proteins on the epigenetic landscape and structural changes that occur during senescence.

Aim 3: Establish the functional partners by which PARP1 binding and enzymatic functions regulate the senescence gene expression program.

Aim 4: Evaluate the potential of PARP1 inhibitors as senescence-eliminating drugs (seonlytics), and a new treatment paradigm for PARP inhibitors in cancer therapy.

3.2. Hypothesis:

Together, my Ph.D. thesis will define a novel and global role for PARP1 in the regulation senescence-associated gene regulation and chromatin structure both through its prevalent and direct interaction with chromatin and its enzymatic modification of chromatin components. An expanded understanding of how PARP1 function contributes to senescence will therefore open new therapeutic in-roads aimed at establishing PARP inhibitors in a new senescence treatment paradigm.

4. Results

4.1 PARP1 enzymatic activity and ADP-ribosylation are increased in OIS

PARP1 is the most abundant nuclear PARP family member catalyzing the majority of ADP-ribosylation from NAD+ onto target proteins and playing an essential role in gene regulation (Bai, 2015; D'Amours et al., 1999; Kraus and Lis, 2003). Genome-wide chromatin ADP-ribosylation analysis of chromatin still poses a significant challenge due to the lack of robust experimental methodologies. To overcome this limitation, we developed a novel "Chromatin ADP-ribosylation Affinity Purification Sequencing (CRAP-seq)" method to detect and track genome-wide PARP1-mediated changes in chromatin-associated ADP-ribosylation in senescence (**Figure 1A**). This method relies on metabolic pulse labeling with biotinylated NAD^+ as previously introduced by (Zhang and Snyder, 1992), followed by nuclear fractionation and micrococcal nuclease (MNase) digestion of the isolated chromatin fraction. ADP-ribosylated chromatin fragments are then affinity-purified with streptavidin (SA)-coupled beads, and bound proteins are analyzed by Western blotting (CRAP-WB) (see figures 1 and 2) or DNA is analyzed by high-throughput sequencing (CRAP-seq) (see Figure 4).

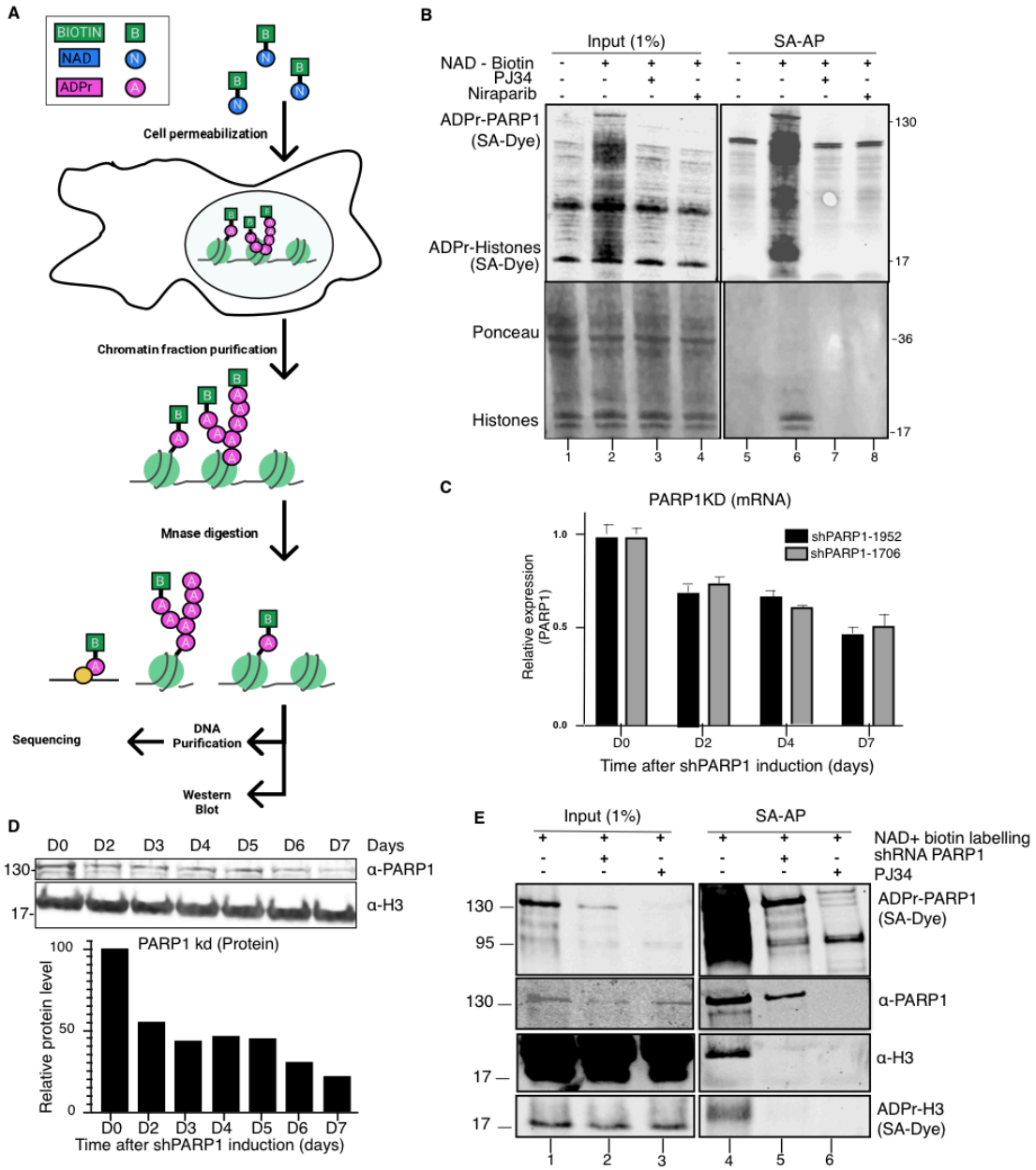

Figure 1: Outline and validation of Chromatin ADP-ribosylation Affinity Purification (CRAP) method **A.** Digitonin-permeabilized cells are metabolically labelled with biotinylated-NAD+. Chromatin is isolated and digested with Micrococcal nuclease (MNase). ADP-ribosylated chromatin is affinity-purified by streptavidin-coupled beads (SA-AP) coupled beads and analysed by high-throughput sequencing (CRAP-seq) or Western Blot (CRAP-WB). **B.** Cells were labelled with biotinylated-NAD+ (20 μM) and treated with H2O2 (500 μM) for 15 minutes either alone or together with PARPi PJ34 (50μM), or niraparib (30μM) for 2 hours prior to H2O2 treatment. Equal loading was controlled with Ponceau staining, and blots were stained with IRDye 800CW Streptavidin (Licor). 1% input is shown in the left blot. ADP-ribosylation levels (primarily automodification of PARP1 and histones) represent the enzymatic activity of PARP1. **C.** Cells expressing two independent doxycycline-inducible shPARP1 retroviral vectors (1952 and 1706). PARP1 silencing was induced for seven days with doxycycline (10μg/mL). Relative mRNA levels were measured by RT-qPCR. Values represent mean relative expression (n=3) +/- s.e.m. **D.** Cells were infected with doxycycline-inducible retroviral vector expressing shPARP1-1952. PARP1 silencing was induced for seven days with doxycycline (10μg/mL). Western blot analysis with antibodies to PARP1 and histone-H3 for loading control. Densitometric quantification of PARP1 signal is shown in the bar plot as a function of time in days (D) after PARP1 silencing. **E.** CRAP-WB analysis with antibodies to PARP1, histone H3 and IRDye-800CW Streptavidin (SA-Dye) of H2O2 treated cells following PARP1 silencing or PARP enzymatic inhibition.

To validate our method, we first treated cells with a sub-lethal dose of hydrogen peroxide (H_2O_2) to hyper-induce PARP1 enzymatic activity (Ba and Garg, 2011). We observed a substantial and global increase in ADP-ribosylated proteins only in the chromatin fraction of cells labeled with biotinylated-NAD^+, affecting primarily automodification of PARP1 (ADPr-PARP1) (Bartolomei et al., 2016), representing PARP1 enzymatic activity, and ADP-ribosylation of histones, known PARP1 targets (**Figure 1B**, compare lanes 1-2 and 5-6). Importantly, ADP-ribosylation of target proteins was markedly diminished by pre-treatment of cells with two selective PARP1/2 inhibitors (PARPi's), PJ34 and niraparib (Hopkins et al., 2018) (**Figure 1B,** compare lanes 3-4 and 7-8).

To study the relative contribution of PARP1-mediated ADP-ribosylation of target proteins more directly and compare it with PARPi treatment, we depleted PARP1 in cells using doxycycline-inducible retroviral shRNA vectors (shPARP1-1952 and -1706). Both shRNAs effectively reduced PARP1 transcript levels by approximately two-fold (**Figure 1C**) and PARP1 protein levels decreased approximately two-fold as soon as two days after shRNA-induced PARP1 silencing, reaching a maximum five-fold reduction at day seven (D7) (**Figure 1D**). Overall PARP1-depleted cells showed a less prominent, but still robust reduction in ADPr-PARP1 and -H3 levels, when compared to PARPi PJ34-treated cells (**Figure 1E, compare lanes 4-6**).

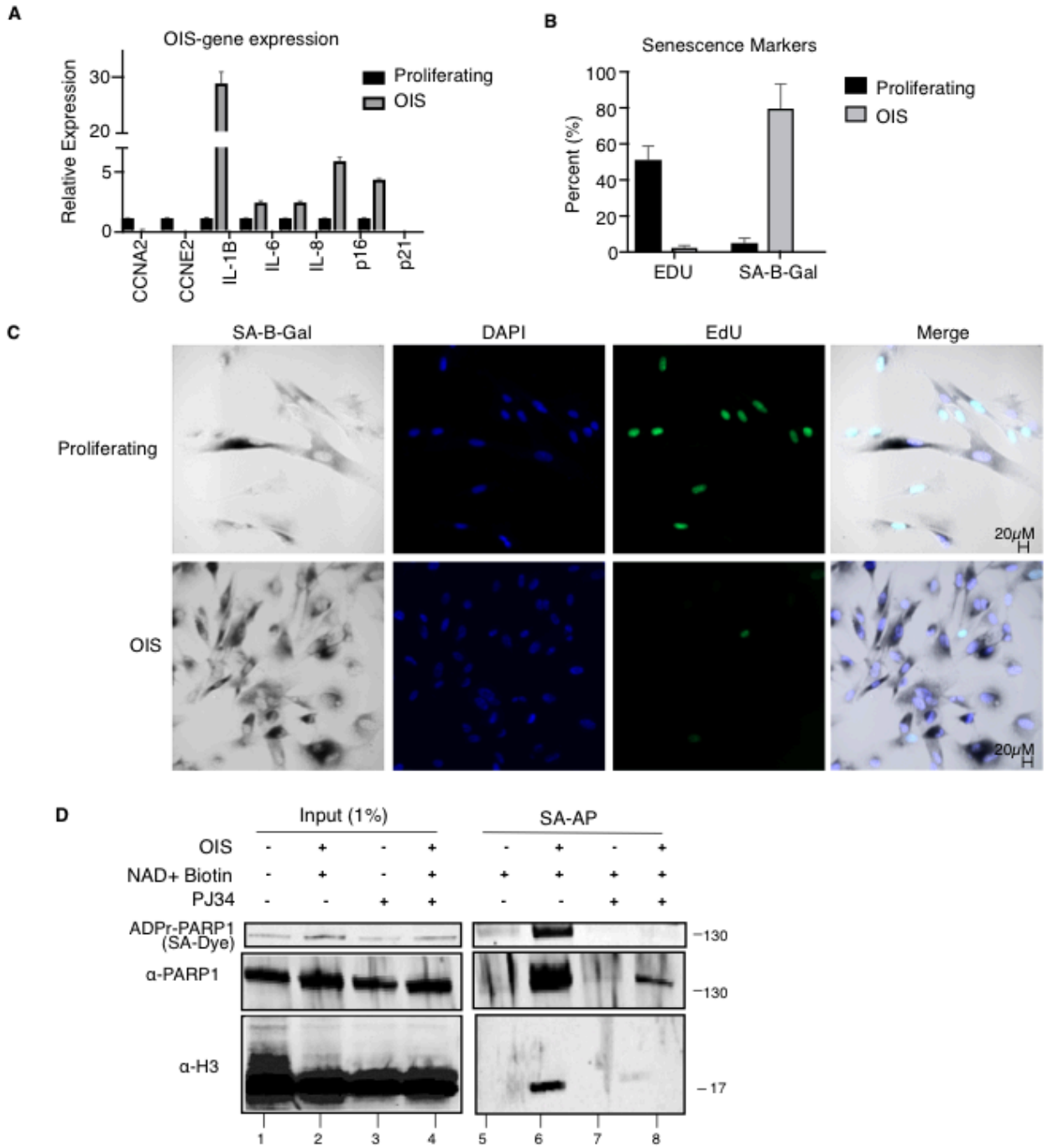

Figure 2: PARP1 enzymatic activity and ADP-ribosylation levels are increased in OIS cells. **A.** Gene expression profiling of select genes in proliferating and OIS cells. **B.** Quantification of EdU incorporation and senescence-associated beta galactosidase (SABG) staining in proliferating and OIS cells. **C.** Representative microscopy images of OIS and proliferating cells stained for EdU, SABG and DAPI. Scale bar, 20mM. **D.** Proliferating and 4OHT-induced ER:RasV12 OIS cells (at day seven after induction) were treated with biotinylated-NAD+ (20 μM) alone or together with PARPi PJ34 (50 μM) for 2 hours. ADP-ribosylated chromatin was purified as outlined in Figure 1A. Western Blot was performed with antibodies directed against PARP1, histone-H3 and IRDye 800CW streptavidin (SA-Dye). PARP1 automodification signal (ADPr-PARP1) corresponding to size of PARP1 is also shown.

Having established the validity of our CRAP method, we then asked whether chromatin-associated PARP1 enzymatic activity and ADP-ribosylation levels are altered in cells undergoing RAS-OIS when compared to proliferating cells (**Figure 2A-C**). While PARP1 protein levels remained unchanged in proliferating and RAS-OIS cells (**Figure 2D**, lanes 1-4), RAS-OIS cells had largely increased PARP1 enzymatic activity as evidenced by their much higher PARP1 automodification (ADPr-PARP1) and histone H3 ADP-ribosylation (ADPr-histone H3) levels (**Figure 2D**, compare lanes 5 and 6). Importantly, treatment of RAS-OIS cells with PARPi PJ34 substantially decreased ADPr-PARP1 and -H3 levels (**Figure 2D**, lanes 7-8) underscoring further the prime role of PARP1 in chromatin-associated ADP-ribosylation in RAS-OIS cells.

Altogether, our results establish CRAP as a methodology to accurately monitor chromatin-associated PARP1 enzymatic activity and -ADP-ribosylation levels and demonstrate that RAS-OIS cells have substantially increased PARP1 enzymatic activity and -ADP-ribosylation levels.

4.2 Experimental outline to measure the differential impact of PARP1 depletion and enzymatic inhibition on the RAS-OIS gene expression program

If and how PARP1 regulates gene expression during senescence and whether or not PARP1 chromatin binding and chromatin-associated ADP-ribosylation play distinct roles in this process are open questions.

To address these questions, we employed time-series experiments on WI38 fibroblasts undergoing oncogene-induced senescence (OIS) using a tamoxifen-inducible

ER:RASV12 expression system as previously described (**Figure 3A**) (Puvvula et al., 2014b) (Zamudio et al., 2019). We determined global gene expression profiles by microarrays and mapped the full set of accessible chromatin sites by ATAC-seq at indicated points and different treatment regimen (green spheres PARP1 depletion; red spheres, PARPi PJ34 treatment). From accessible chromatin regions determined by ATAC-seq, we deduced TF binding dynamics. Cells intended for PARP1-seq and CRAP-seq (blue spheres) were obtained at three and two time-points, respectively, as indicated.

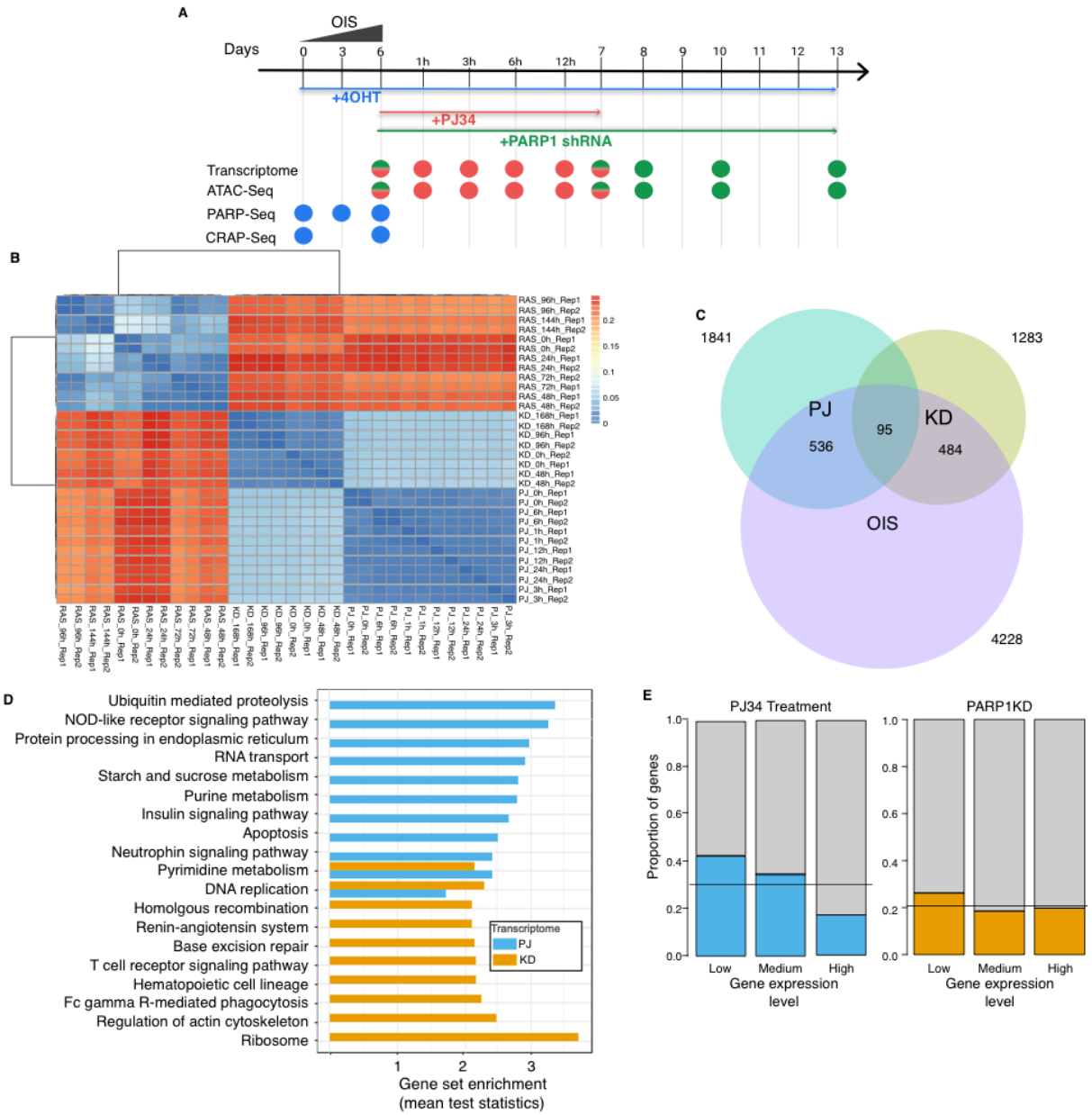

Figure 3: Differential impact of PARP1 depletion and enzymatic inhibition on the senescence gene expression program. A. Experimental outline. Time-resolved study of RAS-OIS WI-38 Fibroblasts (transcriptome, ATAC-seq, PARP1-seq, and CRAP-seq), treatments with PARP1i PJ34, and PARP1KD with shRNA. **B.** Transcriptome data quality heatmap as determined by sample clustering. Heatmap of the sample-to-sample distances estimated using Pearson correlation of time-resolved transcriptome data sets for biological replicates of: RAS-OIS (RAS_Rep 1 and -2), RAS-OIS PARP1 depletion (KD) (shPARP1-1952 (KD_Rep 1) and -1706 (KD_Rep 2), and RAS-OIS PJ34-treatment (PJ). **C.** Venn diagram of differentially expressed genes (DEGs) in RAS-OIS (RAS), PJ34-treated RAS-OIS (PJ_Rep 1 and -2), and the PARP1 knock-down (KD) RAS-OIS cells. Numbers outside the circles correspond to total DEGs per treatment, while those inside indicate the number of overlapping DEGs between treatments. **D.** GAGE-based gene set enrichment statistic for the 10 top gene sets of significantly enriched (adjusted p-value < 0.075) RAS-OIS DEGs affected by PJ34 and PARP1 KD treatment. **E.** Proportion of RAS-OIS DEGs affected by PJ34 and PARP1 KD treatment grouped as a function of their expression level. Genes were grouped into quantiles according to their expression decile in low (Q1 - Q3), medium (Q4 - Q7), and high (Q8 - Q10). For each category the proportion of PJ and KD DEGs is represented using the total number of DEGs. Lines represent the expected proportion of DEGs calculated over the 6204 genes that are differentially expressed in at least one of the time course transcriptomes.

4.3 Differential impact of PARP1 depletion and enzymatic inhibition on the RA-OIS gene expression program

To determine the impact of PARP1 enzymatic inhibition and PARP1 depletion have on the senescence transcriptional program we treated RAS-OIS cells either with PARPi PJ34 for 24 hrs or stably silenced PARP1 expression with our two validated shRNAs for PARP1 for seven days (**Figure 3A**). Time-resolved transcriptomic analysis revealed that PJ34 treatment and PARP1 depletion differentially impacted the senescence transcriptional program (**Figures 3B and -C**). PJ34 treatment caused the differential expression of 1841 genes in total, 536 of which were differentially expressed and 1305 stably expressed in RAS-OIS cells. PARP1 silencing affected 1283 genes in total, 484 of which were differentially expressed, and 799 stably expressed in RAS-OIS cells (**Figure 3C**). Remarkably, PARPi PJ34 treatment and PARP1 silencing communally affected only 95 genes strongly arguing in favor of separable enzymatic and non-enzymatic roles for PARP1 in gene regulation. Functional overrepresentation analyses of differentially regulated genes (DEGs) in RAS-OIS affected by PJ34 treatment or PARP1 depletion highlighted distinct biological pathways for each treatment (**Figure 3D**). For example, PJ34 treatment had significant effects on genes involved in ubiquitin-mediated proteolysis, NOD-like receptor signaling, and apoptosis, while PARP1 depletion affected strongly the expression of genes involved in ribosome biology and regulation of actin cytoskeleton. To further refine PARP1 function in the transcriptional regulation of RAS-OIS, we divided RAS-OIS DEGs affected by PARPi PJ34 treatment or PARP1 depletion into three quantiles representing lowly (L), medium (M) and highly (H) expressed genes. This analysis revealed that PJ34 treatment predominantly affected the expression level

of lowly differentially expressed genes in RAS-OIS, while medium expressed genes were only marginally affected and highly expressed not at all (**Figure 3E,** left panel). By contrast, the effect of PARP1 depletion on lowly expressed genes in RAS-OIS was only moderate (**Figure 3E,** right panel).

We conclude that PARP1 exercises a hither-to underappreciated global gene-regulatory role in RAS-OIS, with functionally disparate enzymatic and non-enzymatic roles in the transcriptional regulation of lowly expressed genes.

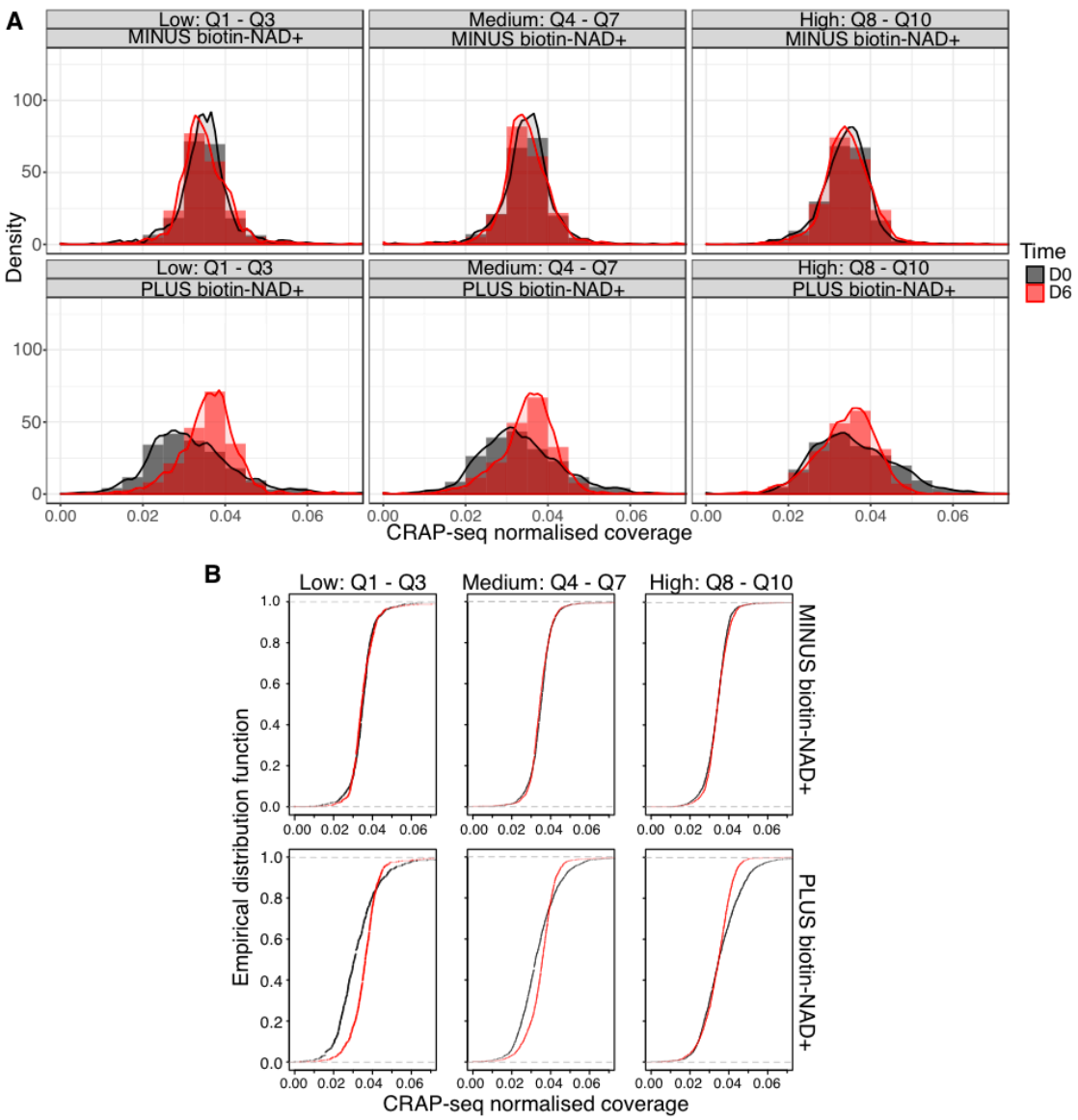

Figure 4: Validation of K/S metric to measure changes in ADP-ribosylation in RAS-OIS. A. Average CRAP-seq read coverage is shown for active enhancers associated to differentially expressed genes according to their expression level at day 6 of RAS OIS induction: low (Q1 - Q3), medium (Q4 - Q7) and high (Q8 - Q10). The distribution was calculated for the MINUS (above) and PLUS (below) biotin-NAD+ conditions and for day zero (black) and day six (red) after RAS-OIS induction time points. Kolmogorov-Smirnov statistic was used, which quantifies the distance between the empirical distribution function of the signal between any two samples, which we called K/S metric. This test can be applied to the distribution of the CRAP-seq signal calculated over any set of annotations, e.g. TSSs, enhancers, as the average read coverage normalized by size. To quantify the gain in ADP-ribosylation between day zero and six, the alternative hypothesis will be that the empirical distribution function of day zero is not greater than that of day six 6. When applied to the comparison of the CRAP-seq signal between day zero and six, the K/S metric reproduces the global increase in ADP-ribosylation measured by CRAP-WB (Figure 2D). The K/S metric detects a significant increase only for the PLUS biotin-NAD+ condition and not for the MINUS biotin-NAD+, indicating that it efficiently distinguishes biologically relevant differences. **B.** Empirical distribution function of CRAP-seq signal at active enhancers at days zero and six of RAS OIS induction. Cumulative distributions of the CRAP-seq signal as plotted in panel 4A.

4.4 PARP1 regulates chromatin-associated ADP-ribosylation at enhancers to fine-tune the transcription of lowly expressed genes

Given that inhibiting the enzymatic activity of PARP1 affected mainly the expression of lowly expressed genes in RAS-OIS, we focused our attention on the gene-regulatory role of ADP-ribosylation at these genes. To this effect, we first mapped genome-wide ADP-ribosylation changes using CRAP-seq between day zero (D0) and six (D6) after RAS-OIS induction (see **Figure 1A**) and correlated chromatin-associated ADP-ribosylation profiles (**Figure 4A and -B**) with our previously published RAS-OIS chromatin states (**Figure 5A**) (Zamudio et al., 2019). Our analysis revealed that ADP-ribosylation is strongly enriched (approximately 10-100-fold) at enhancers as well as unmarked chromatin, and particularly at active enhancers at day six post OIS induction, when compared to transcriptional start sites (TSS) and polycomb-repressed chromatin, which is in line with previous findings (Bartolomei et al., 2016). These data imply that ADP-ribosylation plays a critical role at active enhancers. To further define the role of enhancer-associated ADP-ribosylation, we investigated whether ADP-ribosylation at active enhancers correlated with any of the three gene expression quantiles as defined in Figure 3. We previously published that there is a tight correlation between OIS enhancer activation and the expression of their nearest genes (Zamudio et al., 2019). As shown in Figure 5B, we found that gains in ADP-ribosylation levels at day six post-RAS-OIS induction were highest at active enhancers of lowly differentially expressed genes progressively declining at active enhancers of medium and highly expressed genes. Interestingly, we observed this correlation also in stably expressed genes (SEGs) in RAS-OIS (**Figure 5B**, left panels). By contrast, the loss of enhancer ADP-ribosylation did not correlate significantly with gene expression

quantiles in RAS-OIS (**Figure 5B**, right panels). These data indicate that a gain of ADP-ribosylation at active enhancers plays a regulatory role of lowly expressed genes in RAS-OIS. We then asked whether changes in ADP-ribosylation occurred preferentially at active enhancers of RAS-OIS-specific genes sensitive to PARP1 enzymatic inhibition by PARPi PJ34 (**Figure 5C**). Indeed, gains in ADP-ribosylation were highest at active enhancers of RAS-OIS-specific genes sensitive to PJ34 (OIS-PJ) when compared to RAS-OIS-specific genes insensitive to PJ34 (OIS only) and stably expressed RAS-OIS genes sensitive to PJ34 treatment (PJ only) (**Figure 5C**). To investigate how ADP-ribosylation at active enhancers impacts transcriptional outcomes, we then plotted gene expression changes upon PJ34 treatment against quantiles of ADP-ribosylation gain in RAS-OIS (**Figure 5D**). This analysis revealed that PJ34 treatment of RAS-OIS cells preferentially dysregulates (*i.e.* genes become up- or down-regulated) the transcription of lowly expressed genes whose enhancers have the greatest gains in ADP-ribosylation (Q9 and -10), irrespective of whether these genes are stably (SEGs) (**Figure 5D,** left panels) or differentially (**Figure 5D,** right panels) expressed (DEGs) in RAS-OIS.

Altogether, our analysis uncovers a new layer of complexity to ADP-ribosylation-mediated gene regulation by demonstrating that PARP1-mediated ADP-ribosylation of enhancers fine-tunes the transcription of lowly expressed genes.

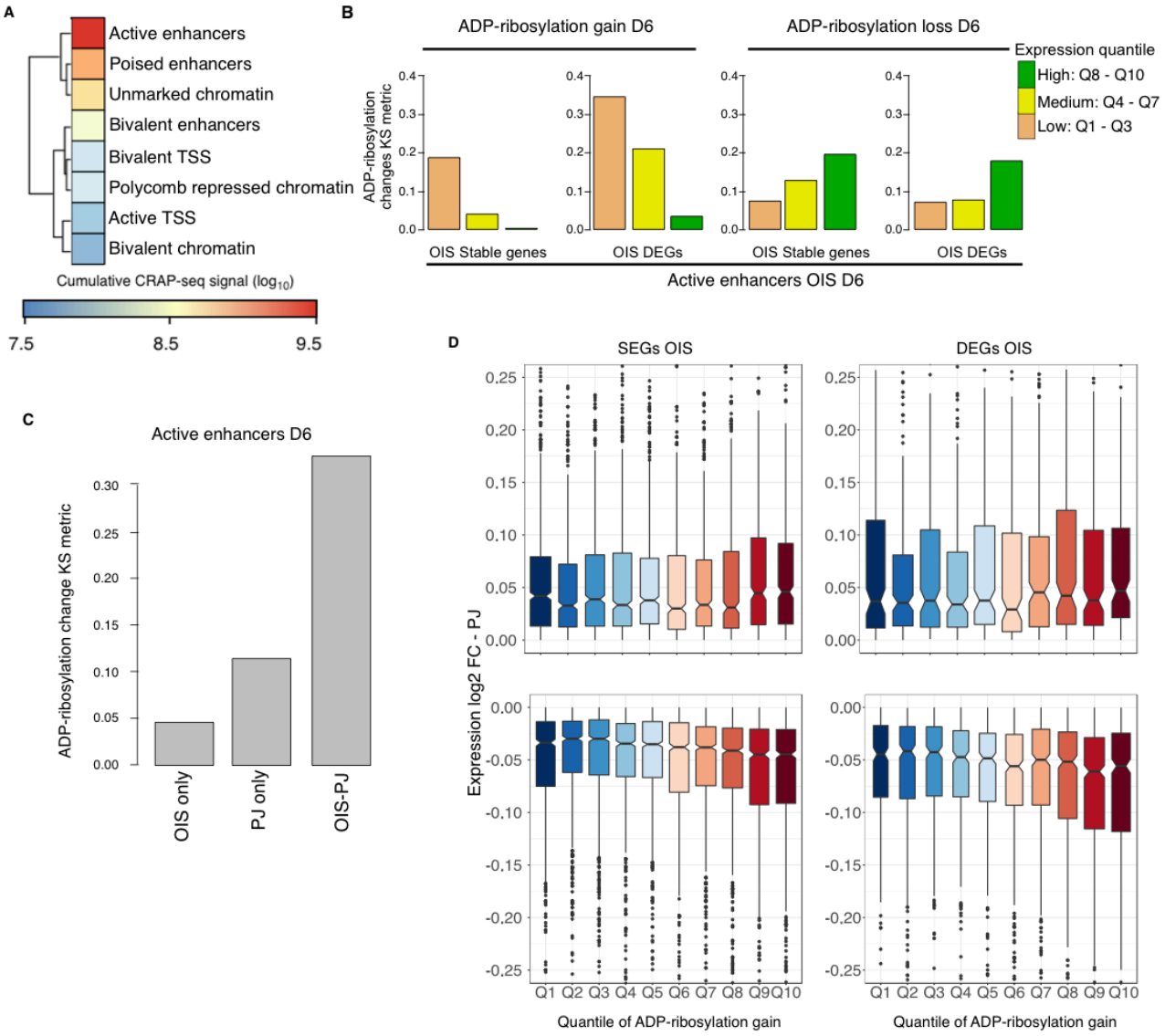

Figure 5. PARP1 regulates chromatin-associated ADP-ribosylation at enhancers to fine-tune the transcription of lowly expressed genes. A. ADP-ribosylation was determined by CRAP-seq in cells undergoing RAS-OIS at day six after OIS induction. Log10-fold changes in ADP-ribosylation using the K/S metric were plotted against indicated chromatin states as described previously (Zamudio et al., 2019). **B.** Gain (left) and loss (right) in ADP-ribosylation were measured using the K/S metric in active enhancers at day six and associated to stably (SEGs) and differentially expressed genes (DEGs) as a function of expression quantiles (see Figure 3) at day six. **C**. Bar plot depicting changes in ADP-ribosylation at active enhancers of genes at day six of RAS-OIS the expression of which is affected by OIS only, PJ34-treatment only, or OIS-PJ34-treatment. **D.** Log2-fold changes of OIS DEGs and -SEGs after 24 hrs of PJ 34 treatment of RAS-OIS cells at day six after OIS induction is plotted as a function of log2-fold changes in ADP-ribosylation quantiles at associated active enhancers.

4.5 PARP1-mediated ADP-ribosylation modulates chromatin accessibility of active RAS-OIS enhancers

Chromatin accessibility is determined by the degree of nucleosomes, as well as TFs and other chromatin-binding factors, to contact chromatinized DNA physically (Klemm et al., 2019). Whether chromatin-associated ADP-ribosylation effects chromatin accessibility genome-wide is currently not known.

To determine how ADP-ribosylation affects chromatin accessibility at ADP-ribosylated active enhancers first, we overlaid ADP-ribosylation profiles, as determined by CRAP-seq, with accessible chromatin regions as determined by ATAC-seq in RAS-OIS cells. While gains in chromatin accessibility were independent of enhancer-associated increases of ADP-ribosylation (**Figure 6A,** left panel), loss of chromatin accessibility was positively correlated to enhancer-associated increases of ADP-ribosylation (**Figure 6A**, right panel). Next, we determined the effect of PARPi PJ34 on chromatin accessibility of these active enhancers. Remarkably, we found that inhibition of PARP1 enzymatic activity resulted both in gains (**Figure 6B,** top panels) and losses (**Figure 6B,** bottom panels) of chromatin accessibility as a function of ADP-ribosylation levels at active enhancers that either gain or lose chromatin accessibility in RAS-OIS. We conclude that PARP-mediated ADP-ribosylation of active enhancers fine-tunes chromatin accessibility.

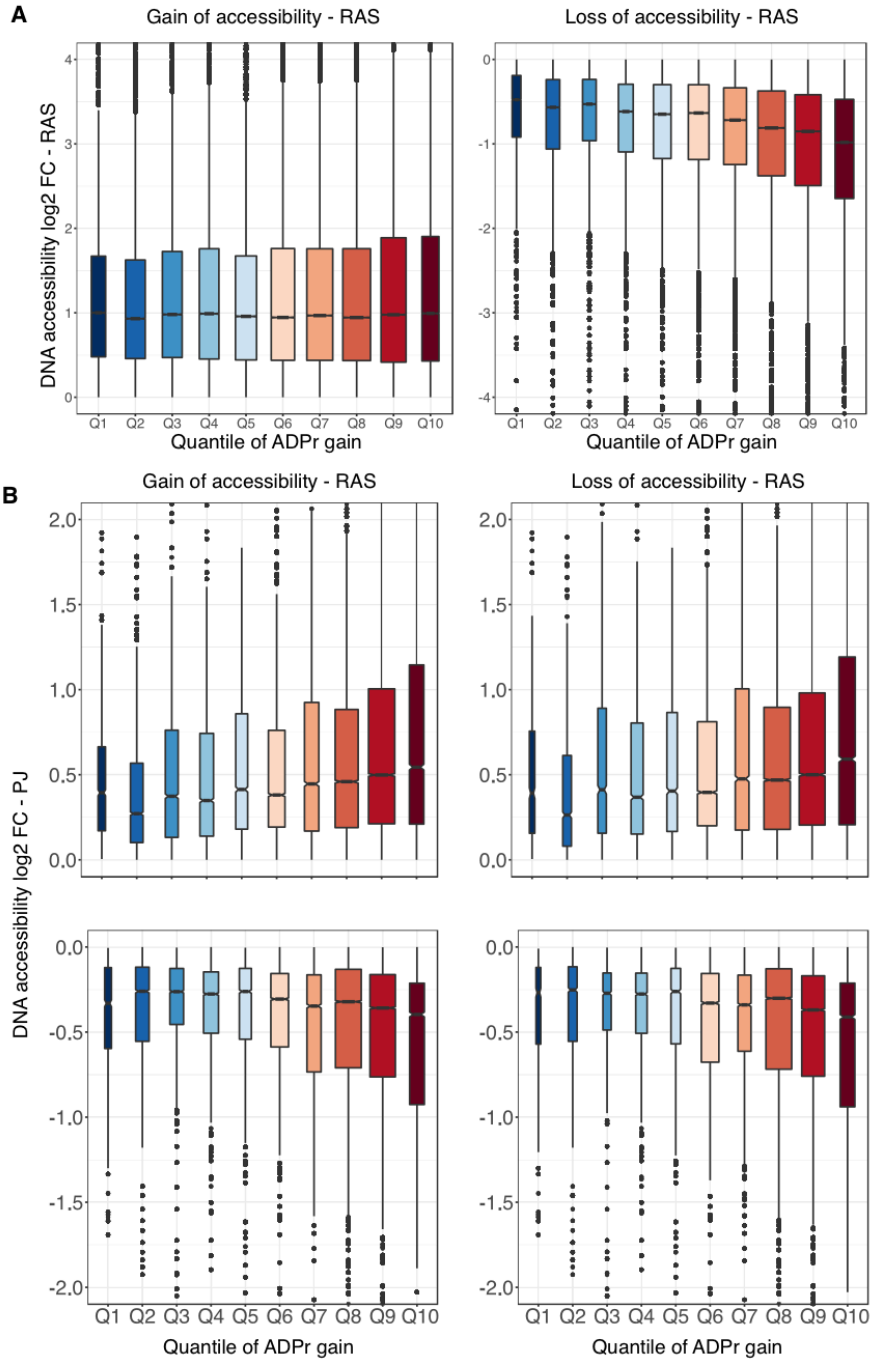

Figure 6: ADP-ribosylation modulates chromatin accessibility of active RAS-OIS enhancers. A. Gain and loss of in DNA accessibility is measured as the normalized ATAC-seq coverage. Log2 fold change of DNA accessibility at active enhancers in RAS-OIS cells between day zero and six after OIS induction is plotted against log2 fold changes in ADP-ribosylation quantiles (Q1-10). **B**. Log2 fold change of DNA accessibility at active enhancers at day six 24 hrs after PARPi PJ34 treatment is plotted according to the corresponding log2 fold change in ADP-ribosylation quantiles. Distributions are shown for active enhancers gaining accessibility (left) and those losing (right) accessibility during RAS OIS induction at day six.

4.6 Active ADP-ribosylated RAS-OIS enhancers are enriched for select TF binding sites

The mechanism of enhancer-associated ADP-ribosylation to fine-tune chromatin accessibility and the RAS-OIS gene expression program likely include the differential recruitment of TFs (Hassa and Hottiger, 1999; Liu et al., 2017; Olabisi et al., 2008). Our ATAC- and CRAP-seq data sets allow us to quantify TF binding sites in ADP-ribosylated active RAS-OIS enhancers. We previously established that ATAC-seq is a reliable method to deduct TF-binding sites (TFBSs) *in silico* (Zamudio et al., 2019). Plotting the ADP-ribosylation signal of active RAS-OIS enhancers against TFBSs showed significant enrichment for select TFs, notably SREBF2, TBX1, RARB, PAX5, and SMAD2:3:4 (**Figure 7**). Interestingly, PARP1 functionally and physically interacts with SMAD2:3:4 and RARB and SMADs are ADP-ribosylated by PARP1 (Dahl et al., 2014; Izhar et al., 2015). These data suggest that enhancer-associated ADP-ribosylation is involved in the recruitment of select TFs to active RAS-OIS enhancers to fine-tune the transcription of associated genes.

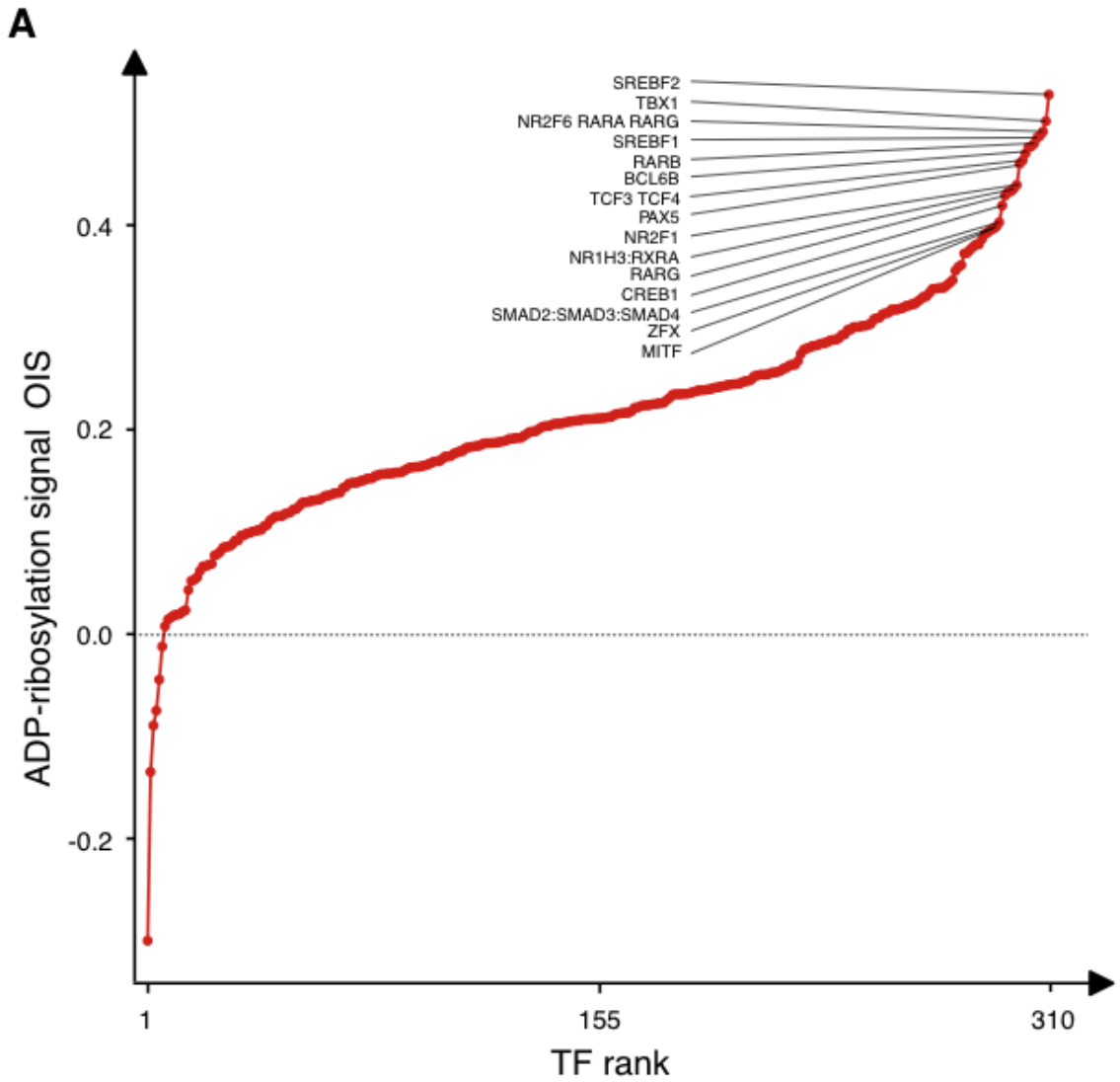

Figure 7: Active ADP-ribosylated RAS-OIS enhancers are enriched for select TF binding sites. A. Transcription factor (TF) ranking at ADP-ribosylated enhancers in RAS-OIS. TF-footprinting was performed as described previously (Zamudio et al., 2019), Highest coincidence between ADP-ribosylated enhancers and TFBSs is seen on the right side of the plot. Top TFs are indicated.

4.7 PARP1 binding is enriched at transcription start-sites to regulate the RAS-OIS transcriptional program

We have shown that PARP1 depletion and the enzymatic inhibition of PARP1 differentially impact the RAS-OIS gene expression program (Figure 3C) and that the enzymatic function of PARP1 and ADP-ribosylation are predominantly linked to RAS-OIS enhancer activation (Figures 5 and 6). Together, these results strongly suggest that PARP1 also regulates transcription in a manner independent of enhancer-associated ADP-ribosylation, most likely through direct binding to other *cis*-regulatory elements. We, therefore, mapped PARP1 binding genome-wide during RAS-OIS. Previous PARP1-seq analysis failed to define the genome-wide PARP1 binding profile because only a chromatin-feature centric approach was applied (Liu et al., 2017; Nalabothula et al., 2015) and because of PARP's inherent nucleosomal binding activity (Martínez-Zamudio, 2012) and potentially non-optimal PARP1-seq conditions. To overcome this technical impasse, we optimized a new crosslinking ChIP-seq protocol (X-ChIP-seq) pioneered by Henikoff and co-workers (Orsi et al., 2015) and used a "spike-in" ChIP-seq approach comparing PARP1 binding in control OIS and PARP1-depleted cells using our validated shRNAs against PARP1. Applying these two modifications allowed us to separate real PARP1 binding events from background binding unequivocally, and thus to faithfully identify genome-wide PARP1 binding sites (**Figure 8A**). We found that PARP1 binds extensively throughout the genome behaving essentially like a histone, which was corroborated by its interaction with histone H3 in co-immunoprecipitation experiments (**Figure 8B**).

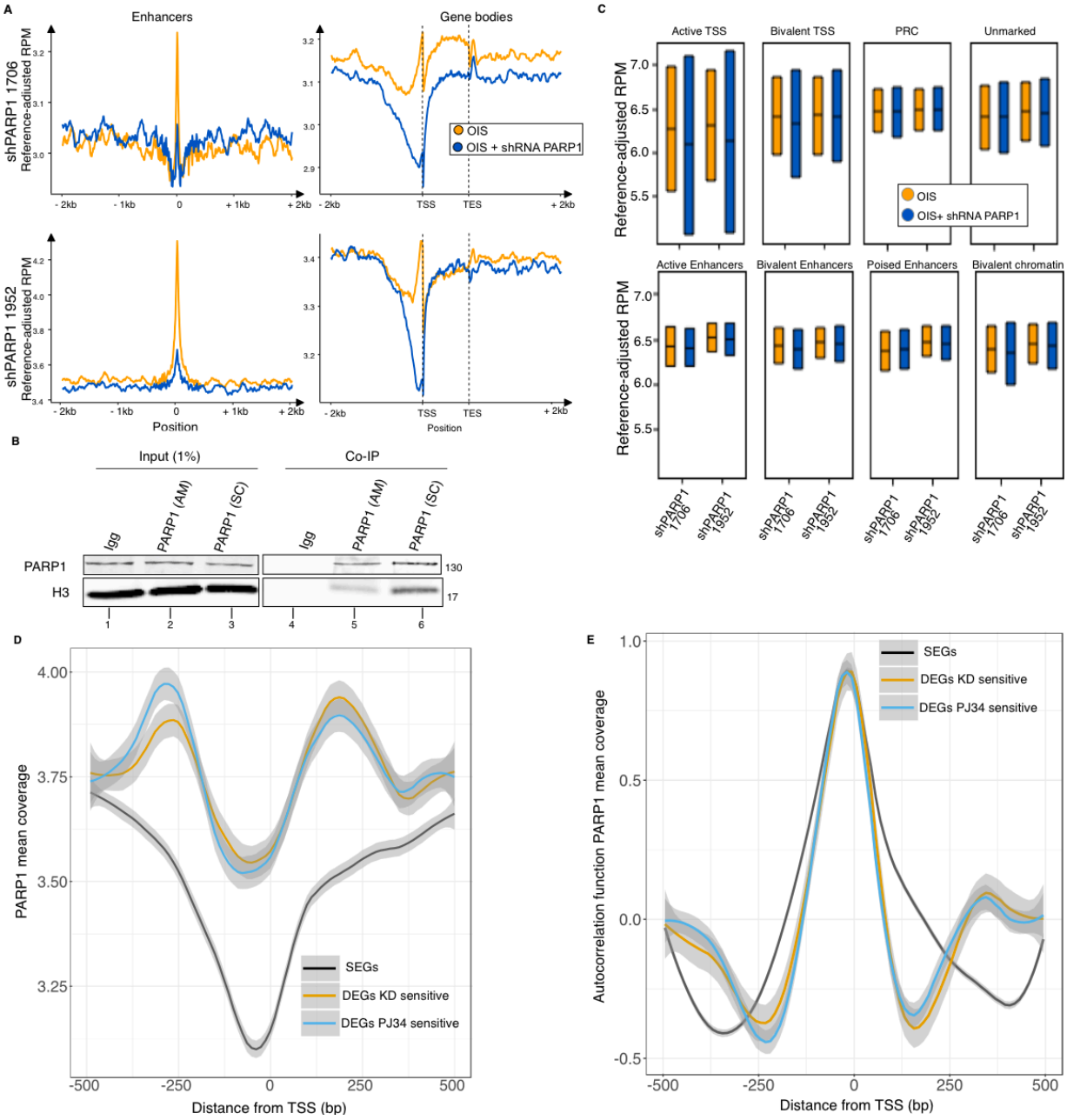

Figure 8: PARP1 binding is enriched at transcription start-sites to regulate the RAS-OIS transcriptional program. A. PARP1 meta-profiles in control and PARP1-depleted (shPARP1-1952 and -1706) RAS-OIS cells at enhancers and gene bodies. RAS-OIS cells were treated for three days with doxycycline to reduce PARP1 protein levels to 50% (see Figure 1E). **B.** Co-immunoprecipitation using WI-38 fibroblasts of histone H3 with PARP1, conducted with two independent PARP1 antibodies AM (Active Motif Cat#39561) and SC (Santa-Cruz, Cat#sc-7150), with Igg as an immunoprecipitation control **C.** PARP1 binding instances in control and PARP1-depleted (shPARP1-1952 and -1706) RAS-OIS cells as a function of chromatin state (Zamudio et al., 2019). PRC, polycomb-repressed chromatin. **D.** PARP1 binding profiles 500 bp up- and downstream of TSSs in RAS OIS cells for SEGs and DEGs sensitive to PARPi PJ34 treatment and PARP1 depletion. **E.** Spatial phasing of PARP1 binding proximal to TSSs in control and PARP1-depleted (shPARP1-1952 and -1706) RAS-OIS cells. Autocorrelation function of PARP1 binding for SEGs and DEGs genes sensitive to PARPi PJ34 treatment and PARP1 depletion. Up- and down-stream minima are located at -360, 420 (SEGs, black line) -240, 185 (DEGs KD sensitive, orange line) -235, 170 (DEGs PJ34 sensitive, blue line) bps relative to TSS.

A gene-centered analysis revealed global binding of PARP1 both at enhancers (**Figure 8A,** left panels) and gene bodies, with a prominent peak at TSSs (Krishnakumar and Kraus, 2010a; Nalabothula et al., 2015), which was significantly reduced upon PARP1 depletion. This result was corroborated with a chromatin-state centered analysis demonstrating that PARP1 depletion led to a sharp reduction of binding at active TSSs, while this reduction was moderate at enhancers and mostly absent at other chromatin states (**Figure 8C**).

Given the preference of PARP1 binding for TSSs, we asked how PARP1 binding at TSSs regulates the RAS-OIS transcriptional program. Mapping PARP1 TSS binding to RAS-OIS SEGs and DEGs sensitive to PJ34 treatment or PARP1 silencing showed that PARP1 preferentially bound in a well-defined fashion up- and downstream of TSS of genes sensitive to PARPi PJ34 treatment and PARP1 depletion (**Figure 8D**) (Valouev et al., 2011). These data suggested that PARP1 is involved in chromatin structuring of TSSs. To support this finding, we performed an autocorrelation analysis of PARP1 binding at these TSSs, which confirmed the strong phasing of PARP1 binding with minima at positions -240, -235, 170, and 185 bp relative to TSSs. By contrast, TSSs of SEGs displayed a more relaxed phasing with minima at positions -360 and 420 base-pairs (bps) relative to TSSs.

In conclusion, our analysis demonstrates that PARP1 binds extensively across the genome, pointing at a gene-regulatory role of PARP1 phasing through well-defined binding at TSSs of promoters that is distinct from its ADP-ribosylation-mediated transcriptional regulation at enhancers.

4.8 Repositioning PARP1-inhibitors as potential senolytics

PARP inhibitors are currently employed in the treatment of breast cancers harboring BRCA1/2 mutations (Lord et al., 2015). Considering that PARP1 has many other nuclear functions outside of DDR, we asked if these other functions are actionable therapeutic targets. Our transcriptome analysis revealed that PARP1 enzymatic activity is an important regulator of apoptotic genes in RAS-OIS, raising the possibility PARP inhibitors could function as senescence-eliminating drugs (senolytics). Exposing proliferating, quiescent and senescent WI38 fibroblasts to 10 μM niraparib for seven days induced the death of 95% of senescent cells but only 30% of quiescent and no death of proliferating fibroblasts (**Figure 10A**). These data suggest that senescent cells are preferentially sensitive to PARP inhibitors. A “one-two punch” consecutive therapy for cancer treatment involves senescence induction of cancer cells therapy-induced senescence, TIS), followed by the elimination of these cancerous senescent cells by senolytics (Wang and Bernards, 2018). To test the efficacy of PARPis in this approach, we induced or not TIS in MCF-7 breast cancer cells by doxorubicin (1μM) treatment for six days followed by a niraparib (5μM) treatment for three consecutive days (**Figure 10B**). Strikingly, 75% of MCF-7 TIS cells underwent cell death within three days, while proliferating cells continued to grow unimpeded. These preliminary data highlight the potential of PARP inhibitors as clinically relevant senolytics.

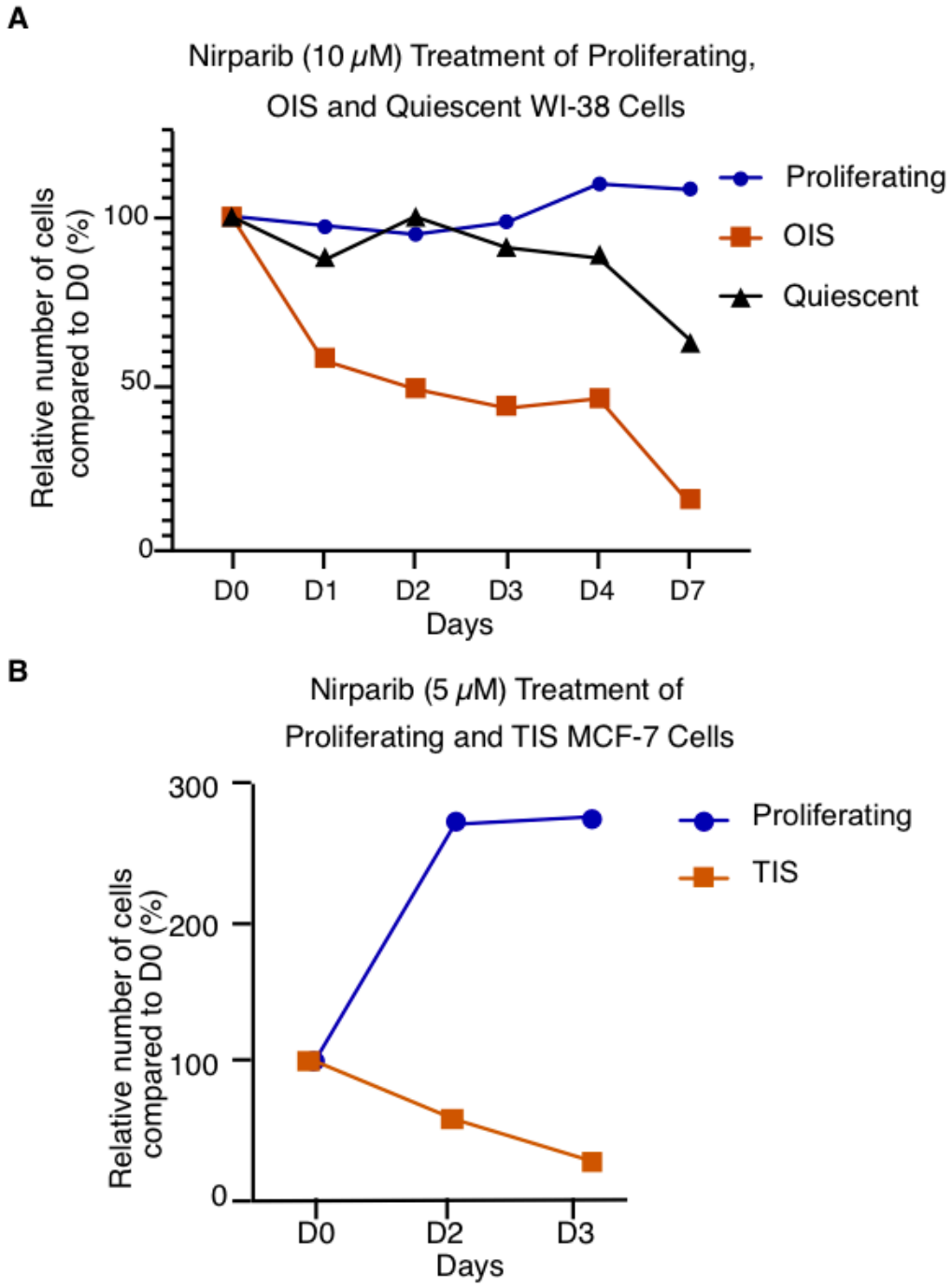

Figure 9: Repositioning PARP1-inhibitors as potential senolytics. A. Proliferation curves of proliferating and RAS-OIS cells treated with PARPi niraparib. Growth curves display percentage of cells compared to day zero (D0) following treatment of RAS-OIS and proliferating WI-38 fibroblasts with 10μM niraparib over seven days. **B.** Proliferation curves of proliferating and therapy-induced (1 μM doxorubicin treatment for six days) senescent (TIS) MCF-7 breast cancer cells treated with niraparib (5μM) for three days.

5. Discussion and Future Directions

Cellular senescence has long been considered a pure cell culture artifact (Sherr et al., 2000). However, we now know that this cell fate has significant implications for human physiology, pathophysiology and longevity. Senescence is a double edged-sword - on the one hand, senescence promotes health through suppression of tumorigenesis, aiding in development, maintaining cellular plasticity, and tissue homeostasis, on the other side, the chronic accumulation of senescent cells contributes to aging, age-related disease, tissue dysfunction, and tumor growth through its inflammatory phenotype, the SASP (Martínez-Zamudio et al., 2017a). As such, senescence is an attractive target for clinical interventions and therapies to promote healthspan.

Senescent cells undergo a significant reorganization of their chromatin structure, epigenomic landscape and transcriptional program. Recent studies have started to describe the significance of the epigenetic landscape and transcription factors which govern the senescence gene expression program (described in detail in section 1.5-1.7). This expanding area of research has yet to entirely define the underlying framework and agents, which drive and maintain the senescence phenotype. My thesis aimed to further define the gene-regulatory mechanisms regulating the senescence gene expression program.

PARP1, after histones, is one of the most abundant nuclear proteins (5×10^5 – 1×10^6 copies per nucleus) (Ludwig et al., 1988; Yamanaka et al., 1988b). It is integral to a wide host of nuclear functions including transcriptional and chromatin structure control as well as DNA damage repair (described in detail in section 2.4-2.6) (Kraus and Hottiger, 2013). For example, during DNA damage, PARP1 binding and catalytic activity are induced to sense DNA breaks, recruiting proteins and modulating chromatin structure and transcription to facilitate error-free DNA repair (Ray Chaudhuri

and Nussenzweig, 2017). Furthermore, PARP1 displays context-dependent interactions with TF SOX2 to maintain the pluripotency gene expression program of embryonic stem (ES) cells (Liu et al., 2017). PARP1 is also a major player in the expression of inflammatory genes functionally interacting with NFκB though the precise underlying mechanism is currently not known (Amiri et al., 2006; Hassa et al., 2005; Martinez-Zamudio and Ha, 2012; Nakajima et al., 2004). Given its roles in regulation of chromatin structure and gene expression, especially in inflammation, we hypothesized that PARP1 regulates the senescence gene expression program. Using time-resolved integrative profiling, we elucidated how PARP1 regulates the transcriptional senescence program, thus, expanding our understanding of the underlying framework controlling the senescence phenotype.

Our results show that PARP1 plays a global regulatory role in the senescence gene expression program rather than only contributing specifically to the regulation of NFκB-dependent gene expression, a process PARP1 has been historically tightly associated to (Hassa and Hottiger, 1999; Hassa et al., 2003; Martínez-Zamudio, 2012). Furthermore, we demonstrate that PARP1chromatin-binding and catalytic activities play largely distinct gene-regulatory roles. PARP1 enzymatic activity increases dramatically during RAS-OIS, leading to a prominent ADP-ribosylation especially of active enhancers driving the expression of lowly expressed genes. In particular, ADP-ribosylation of active enhancers resulted in both gains and losses in chromatin accessibility. We suggest a model by which ADP-ribosylation at active enhancers of lowly expressed genes fine-tunes chromatin accessibility and gene expression through context-dependent TF recruitment as well as the electrostatic repulsion of chromatin-associated proteins driven by the negative charge of ADPr chains.

Apart from this enzymatic role, PARP1 plays a more chromatin structural role. Indeed, our data indicate that PARP1 stabilizes nucleosome positioning specifically at the –1 and +1 nucleosomes of TSSs for a subset of senescence-associated genes. Thus, we uncovered that PARP1 modulates the RAS-OIS transcription program in a previously underappreciated and novel dichotomous fashion.

5.1. PARP1 is enzymatically activated during OIS

By exploiting our newly developed CRAP approach, we revealed a sharp global increase of ADP-ribosylation in RAS-OIS when compared to proliferating cells that was mostly linked to PARP1 automodification and ADP-ribosylation of histones and could be reduced by PARP1 inhibitors (**Figure 2E**). These findings highlight that PARP1 is the major ADP-poly-ribosylase responsible for ADP-ribosylation of target proteins in RAS-OIS.

How is PARP1 activity induced in RAS-OIS? PARP1 and its enzymatic activity play significant role in the context of DNA damage sensing and repair, and it is a possible mechanism by which ADP-ribosylation levels increase during RAS-OIS because a strong DDR accompanies RAS-OIS (Gorgoulis and Halazonetis, 2010). In addition to the activation through DNA binding, PARP1 can be activated by SET 7/9 at the sites of DNA damage.

Alternatively, PARP1 catalytic activity may increase during senescence through a DNA-damage independent mechanism. For example, PARP1 catalytic activity is induced through acetylation by CBP/p300 or sumoylation via PIASy, kinase phosphorylation, direct histone interactions, and transcription factors (as described in section 1.11) (Hassa et al., 2005; Kolthur-Seetharam et al., 2006; Martin et al., 2009).

One potential candidate activation pathway of PARP1 in a non-DNA damage dependent mechanism may be facilitated through ERK2. It was shown that ERK2 activation through Toll-like receptor 4, independent of a p38MAPK response, can activate PARP1 (Cohen-Armon, 2007; Martinez-Zamudio and Ha, 2012). This mechanism is similar to the signal transduction cascade that is engaged upon oncogenic RAS activation, which leads to the downstream activation of ERK1/2 (Vasudevan et al., 2007). Therefore, it is possible that activated ERK2, as a result of oncogenic RAS hyper-activation, activates PARP1 enzymatic activity. Additional experiments are needed to elucidate the exact mechanism by which PARP1 is activated during RAS-OIS.

5.2. Distinct PARP1 catalytic and chromatin-binding activities control the RAS-OIS gene expression program.

A previous study identified PARP1 as a critical factor of SASP regulation by inducing the transcriptional activity of NFκB (Ohanna et al., 2011a). However, the precise mechanisms underlying this activation are still unknown. To begin to dissect the gene-regulatory role of PARP1 during senescence, we first performed time resolved transcriptome analysis on cells undergoing RAS-OIS following PARP1 enzymatic inhibition and PARP1 depletion. Although we saw effects on SASP gene expression, our transcriptome analysis revealed a much broader role of PARP1 catalytic activity in the regulation of the senescence gene expression program (**Figure 3C**). Remarkably, we found that PARP1 enzymatic inhibition and depletion differentially impacted the RAS-OIS gene expression program and there was only a small overlap in genes affected by both treatments.

Inhibition of ADP-ribosylation led to changes in expression of genes related to NFκB, inflammation, RNA, metabolism of proteins and nucleic acids, growth signaling as well as Apoptosis. PARP1 protein depletion led to the dysregulation of genes involved in DNA damage repair, cytoskeleton, metabolism of proteins, as well as growth signaling. The overlapping gene sets related to nucleic acid metabolism, DNA replication and growth. Our results suggest a much more global role of PARP1 in the regulation of gene expression during OIS through distinct catalytic and catalytic-independent mechanisms. Indeed, PARP1 is functionally linked to a number of biological functions through transcriptional regulation in other cellular contexts, including the regulation of inflammation, differentiation, growth, metabolism and circadian rhythm genes (Kraus and Lis, 2003).

5.3. Genome-wide mapping of ADP-ribosylation

A major obstacle in the study of PARP1 and ADP-ribosylation has been the generation of high-quality genomic profiles due to the lack of specific, ChIP-seq quality antibodies against both for PARP1 and ADPr. Consequently, alternative methods have been explored to map ADP-ribosylated proteins along the genome. For instance, the Hottiger laboratory developed a chromatin-affinity precipitation (ChAP) technique, which relied on the affinity of RNF146 WWE domain to poly-ADPr (Bartolomei et al., 2016). The second technique developed to identify ADP-ribosylated proteins comes from the Kraus laboratory, and uses a mutated PARP proteins with a “click” chemistry-compatible NAD^+ analog (8-Bu(3-yne)T-NAD^+) (Gibson et al., 2016). Utilization of 8-Bu(3-yne)T-NAD^+ required the development of PARPs 1, 2, and 3 mutants which can use the NAD^+-analog as a substrate. Both methodologies have their own limitations

and therefore, we developed our own methodology to map ADP-ribosylation genome-wide, that we termed CRAP-seq for “Chromatin-Ribosylation-Affinity-Purification Sequencing” (**Figure 1A**). We validated the technique extensively, but we are aware of its short-comings: exogenously added biotinylated-NAD^+ may vary from *in vivo* levels and cells are permeabilized by detergents, and the length of the ADPr chains is unknown.

5.4. PARP1 catalytic activity localizes to active enhancers of lowly expressed genes

Using CRAP-seq, we mapped ADP-ribosylation genome-wide and evaluated the chromatin states ADP-ribosylation coincided with. We found that ADP-ribosylation was most enriched at active enhancers. We then wanted to understand how ADP-ribosylation at enhancers was related to transcriptional outcomes. During the transcriptome analysis we revealed that PARP1 inhibition had a more pronounced effect on lowly expressed genes differentially regulated during OIS. This prompted us to determine ADP-ribosylation levels of active enhancers of genes in the three quantiles of expression: low, medium and high (**Figure 5B**). We observed that the highest accumulation of ADP-ribosylation during OIS was at active enhancers associated to lowly expressed, senescence-associated genes. In order to evaluate the functionality of these ADP-ribosylated enhancers with regards to PJ34 treatment, we observed that genes sensitive to PJ34 treatment accumulated the highest ADPr levels at their respective active enhancers (**Figure 5D**). Interestingly, this included genes which were stable during RAS induction but changed their expression upon PJ34 treatment also shared a correlation with ADP-ribosylation accumulation. This

argues that ADP-ribosylation is involved in the basal expression of these genes during RAS-OIS, which was only observable during PJ34 treatment. Together, these data indicate a regulatory mechanism by which ADP-ribosylation fine-tunes gene expression at active enhancers specific to lowly expressed genes.

5.5. PARP1 catalytic activity influences chromatin accessibility at active enhancers of senescence-associated genes through a context-dependent mechanism

To understand the mechanisms by which ADP-ribosylation at enhancers fine-tunes transcription of lowly expressed genes, we evaluated how chromatin accessibility is affected by PARP1 enzymatic activity. We saw that active enhancers, which lose accessibility during RAS-OIS correlated with accumulating ADP-ribosylation, while accumulation of ADP-ribosylation did not lead to an obvious increase in chromatin accessibility during OIS. In response to PJ34 treatment, these enhancers both increased and decreased chromatin accessibility as a function of increasing ADP-ribosylation levels (**Figure 7B**). These data suggest that ADP-ribosylation functions in both maintenance of open chromatin and the restricting of chromatin accessibility of enhancers during OIS. However, the mechanism by which this dualistic function is exerted is presently unclear.

Previous studies have shown that PARP1 catalytic activity impacts chromatin structure and accessibility through chromatin insulation, histone-ADP-ribosylation, and modification of transcription factors (Krishnakumar and Kraus, 2010b). One hypothesis is therefore that ADP-ribosylation is mediating 3-D chromatin structures at enhancers to modulate chromatin accessibility and subsequent gene expression during RAS-OIS.

ADP-ribosylation is implicated in chromatin insulation through interactions with CTCF (Yu et al., 2004). 3-D chromatin structures are important features which halt the expansion of heterochromatin, and regulate interactions between promoters and enhancers (Phillips-Cremins and Corces, 2013; Wallace and Felsenfeld, 2008). ADP-ribosylation of CTCF can facilitate the formation of chromatin loops between enhancers and promoters to augment expression (Yu et al., 2004).

Furthermore, we propose that ADP-ribosylation may contribute to open chromatin at active enhancers during OIS through its negative electrostatic charge. ADPr is a negatively charged modification, which can influence chromatin accessibility (Poirier et al., 1982). ADP-ribosylation is implicated in transcriptional activation and chromatin remodeling in *D. melanogaster* at the HSP70 locus (Tulin and Spradling, 2003b). Heat shock leads to a rapid increase in chromatin accessibility at the HSP70 locus in an ADP-ribosylation dependent fashion (Collesano et al., 2008; Tulin and Spradling, 2003b). ADP-ribosylation also impacts chromatin structure during NFκB driven inflammatory gene expression following LPS challenge (Martinez-Zamudio and Ha, 2012). ADP-ribosylation of histones increases accessibility of chromatin at NFκB target sites through disruption of nucleosomes (Martinez-Zamudio and Ha, 2012). Oppositely, PARP1 catalytic activity also recruits the formation of repressive chromatin (Guetg et al., 2012; Timinszky et al., 2009). PARP1 modifies histone variant H2A1.1 which forms repressive structures, potentially through chromatin loops (Timinszky et al., 2009).

We further hypothesize that PARP1 enzymatic activity acts to recruit transcription factors to active enhancers of lowly expressed genes during OIS, rendering the chromatin less accessible. ADP-ribosylation is an important post-

translational modification (PTM) for transcription factor function in activating and repressive chromatin contexts (Gibson and Kraus, 2012; Kraus and Lis, 2003; Ryu et al., 2015). ADP-ribosylation can facilitate site-specificity of TF binding (Olabisi et al., 2008). ADP-ribosylation of NFAT dictates the binding of transcription factors (C/EBP, FOS-JUN, CREB/p300) which increases the expression of IL-2 (Olabisi et al., 2008). In the context of rDNA repression, ADP-ribosylation activity forms repressive chromatin complex with NoRC through interactions with TIP5 (Guetg et al., 2012). Disruption of ADP-ribosylation results in the abrogation of this NoRC repressive complex (Guetg et al., 2012).

Considering the current knowledge of ADP-ribosylation described above, and our results demonstrating its dualistic role in changes of chromatin accessibility during RAS- OIS, we propose that PARP1 and ADP-ribosylation is present at active enhancers of lowly expressed genes to recruit and modify transcription factors and other chromatin factors rendering chromatin less accessible. Additionally, ADP-ribosylation physically maintains open chromatin through electrostatic disruption of nucleosomes. The combination and balance of these antagonistic forces contributes to fine-tuning of chromatin accessibility and subsequent transcription of lowly expressed, senescence-associated genes.

5.6. ADP-ribosylation co-localizes with TFs at enhancers during OIS

We found TF binding sites (TFBSs) (*e.g.,* NR2F, RARB, FOXD3, TBX1, NR2F1,TCF3:TFC4, DDIT3:CEBPA, PAX5, SREBF1/2 and SMAD2:3:4) at enhancers enriched for ADP-ribosylation, which included TFBSs. Past research has linked SMAD 2:3:4, RARB and FOXD3 to PARP1 and ADP-ribosylation (Izhar et al., 2015; Lönn et

al., 2010; Zhao et al., 2018). ADP-ribosylation of SMAD TFs decreases affinity for genes induced by TGF-β (Lönn et al., 2010). FOXD3 interacts with PARP1 during Neuroblastoma to disrupt CTCF ADP-ribosylation, which leads to the upregulation of tumor-promoting gene expression (Zhao et al., 2018). It would be valuable to explore further the context-dependent function of these TFs during RAS-OIS and how TF-ADP-ribosylation regulates gene expression during OIS.

5.7. PARP1 binds globally across the genome, but exerts a regulatory role at the TSS by maintaining stable nucleosome positioning at TSSs through its chromatin-binding activity

We optimized PARP1-seq to faithfully map PARP1 to the genome. We detected global binding with enrichment at the TSS of promoters and PARP1 depletion studies unraveled that PARP1 is preferentially lost at these sites with more moderate loss across the genome (**Figure 9A**). These data suggest a differential regulatory role between global PARP1 binding and its presence at TSSs. Upon evaluation of PARP1 binding at the TSS we found higher signals at genes, which were transcriptionally sensitive to PARP1 silencing or PARP inhibition. Interestingly, the binding pattern of PARP1 appeared to be more stable and phased at these sites. A more detailed analysis indicated that PARP1 may facilitate the positioning of TSS-proximal nucleosomes, which correlates with the presence of RNA-pol-II at genes that are poised or actively transcribed (Schones et al., 2008). Well phased nucleosomes are seen more often at the TSS of house-keeping genes and is more variable throughout the rest of the genome (**Discussion Figure 1**) (Radman-Livaja and Rando, 2010a). The nucleosome positioning in the human genome is less reliant upon sequence

composition, and rather regulated through transcription factors, chromatin remodelers and RNA polymerases (Lascaris et al., 2000; Radman-Livaja and Rando, 2010b). As such, we propose that PARP1 binding stabilizes nucleosome positioning at the TSS to facilitate transcription during OIS.

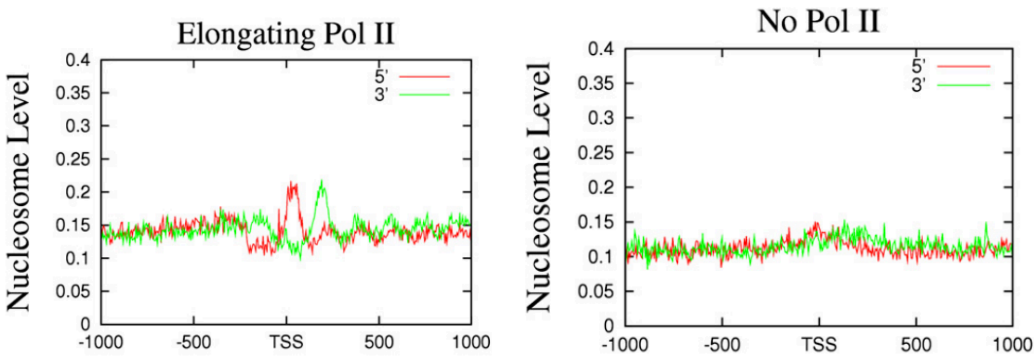

Discussion Figure 1: Well-positioned nucleosomes at TSS facilitate transcription. Nucleosome positioning near the TSS with or without Pol II generated from sequencing data on the 5' and 3' DNA strands. This figure shows the stability of nucleosomes at transcriptionally active TSSs. (Adapted from Schones, 2008).

5.8. PARP inhibitors selectively eliminate senescent cells from cell culture through prolonged exposure

We found that extended treatment of senescent cells with PARP inhibitors resulted in their selective cell death when compared to quiescent and proliferating controls. OIS fibroblasts and chemotherapy-induced senescent cancer cells treated with clinically approved PARP inhibitors induced cell death within five to seven days. Although the mechanisms underlying synthetic lethality of PARP inhibitors used in the clinic remain hotly disputed, the current tenet holds that synthetic lethality is mainly a result of the disruption of PARP1 in DNA repair pathways (Lord et al., 2015). In contrast, whether PARP inhibitors exert their effects through other mechanisms such

as the gene expression programs remains to be explored (Frizzell and Kraus, 2009). Indeed, we found that PARP inhibition effects the expression of genes related to anti-apoptotic functions, and perhaps this is one such mechanism of synthetic lethality. However, we have yet to elucidate in detail the mechanism by which inhibition of ADP-ribosylation leads to the selective death of senescent cells and have to test the efficacy of PARPi's as senolytics in animal models.

5.9. Future Directions:

To deepen our understanding of the context-dependent mechanisms by which PARP1 regulates gene expression and chromatin structure in RAS-OIS, we would like to specifically identify the binding partners of PARP1 and ADP-ribosylated transcription factors. ADP-ribosylation at enhancers involves both the maintenance of open chromatin and restricted chromatin accessibility. Thus, specifying the ADP-ribosylated proteins in these enhancer contexts is critical. We can exploit further *in silico* approaches using TF-footprinting to predict potential interactions between ADPr signal and TFs at these enhancers. Direct targets of ADP-ribosylation may also be identified by expanding the CRAP technology to include proteomics studies. One such study applied the technology developed from the WWE ADPr-ChAP technique with proteomics (Hendriks et al., 2019). Applying proteomics with CRAP technology in the context of OIS would allow us to see the entire spectrum of ADP-ribosylated proteins, and further understand the role TFs.

Additionally, we would like to define the relevance of auto-modified PARP1 on the genome. Currently, we are unable to distinguish unmodified and modified PARP1. We would like to identify the genomic locations of auto-modified PARP1 compared to unmodified PARP1. In order to accomplish this, we can perform sequential CRAP-PARP1-ChIP-Seq.

There are a number of large-scale chromatin reorganizations that occur during the establishment of the senescent cell-fate discussed above: pericentromeric regions become dissociated, hypomethylation, down-regulation of Lamin B and the reorganization of lamina associated domains and the formation of SAHFs (Chandra et al., 2015b; Ito et al., 2017). Hi-C has been performed on senescent cells, however,

further investigation to the functional mechanisms controlling these 3-D reorganizations is warranted (Criscione et al., 2016c, 2016a). We found that PARP1 stabilizes chromatin structure around promoters of senescence-associated genes, and structural potential across the genome, however, we did not consider 3-D chromatin structures that may be regulated by PARP1 chromatin binding and catalytic activity. We would like to compare our ADP-ribosylation and PARP1 positioning data with CTCF ChIP-seq or Hi-C data in OIS cells to make predictions regarding PARP1's impact on 3-D structures in the genome. Additionally, we can employ Hi-ChIP, a technique which combines the power of ChIP-Seq and chromatin capture technologies, to evaluate the looping structures which may be regulated by PARP1 and ADP-ribosylation (Mumbach et al., 2016). It is possible that PARP1 catalytic and binding functions are involved in the formation of the 3-D chromatin conformation in OIS.

PARP inhibition is an exciting avenue we would like to further explore in the context of cancer and age-related pathology. We found that PARP inhibitors selectively eliminate OIS and TIS cells compared to proliferating and quiescent cells. We would like to further explore the potentiality of PARP inhibitors and to define the mechanism by which senescent cells are selectively eliminated. To this end, we will begin by discriminating the type of cell death senescent cells succumb to upon PARP inhibition: apoptosis, necrosis or necroptosis. We suspect that the mechanism may include disruption of DDR signaling, or disrupt the anti-apoptosis transcriptional program.

We also plan to explore the potential of PARP1 inhibition in the context of cancer therapy *in vivo*. Precancerous senescent hepatocytes via the SASP evoke very

efficient immune responses resulting in clearance of these cells and suppression of liver tumorigenesis (Kang et al., 2011). However, the SASP of the same precancerous hepatocytes can accelerate the growth of fully transformed liver carcinomas (Eggert et al., 2016c). The latter finding is of high relevance for patients with advanced liver cancer, as liver carcinomas develop in chronically damaged livers, eventually resulting in a situation where full-blown cancer cells and precancerous senescent cells co-exist. Based on our data PARP1 can impact senescence gene expression programs including the SASP and may be a viable senolytic. It is possible that transcriptional disruption from PARP inhibition allows immune surveillance of pre-cancerous senescent cells but abolish the pro-tumorigenic effect of SASP. *In vivo*, it would be important to evaluate whether sustained exposure to PARP inhibition or depletion exerts senolytic activity.

Together, our study and prospective studies to follow provide exciting possibilities in the fields of ageing and cancer research as well as deepening the understanding of PARP1.

6. Materials and Methods

Cell culture

WI-38 fibroblasts (purchased from ECCAC) were cultured in high glucose Dulbecco's Modified Eagle medium GlutaMAX (Gibco) supplemented with 10% FBS, 1X primocin antibiotic cocktail (Invivogen) at 37ºC in 3% oxygen. Tamoxifen inducible WI-ER:H-RASV12 (puromycin or neomycin resistant) and doxycycline-inducible retrovirus vector containing GFP, puromycin selection cassette and shRNA-PARP1 (1952 or 1706) cells were generated through retroviral transfection and infection as previously described (Puvvula et al., 2014a). Oncogene-induced senescence was induced with 400nM tamoxifen (4-hydroxytamoxifen, Sigma) with the culture media. PARP1 inhibition was performed through the addition of PJ34 20-50μM (PJ34 hydrochloride – Abcam) or 20μM Niraparib (MF-4827-tosylate – Selleck Chem) to the culture media. ShRNA PARP1 expression was induced with 10 μg/mL doxycycline added to the culture media. Mycoplasma testing was conducted routinely throughout the experiments using the MycoAlert (Lonza) according to manufacturer's instructions.

shRNA Sequences

shRNA PARP1 1952

TGCTGTTGACAGTGAGCGCACGGTGATCGGTAGCAACAAATAGTGAAGCCACA
GATGTATTTGTTGCTACCGATCACCGTATGCCTACTGCCTCGGA

shRNA PARP1 1706

TGCTGTTGACAGTGAGCGAAAGGAGGAAGGTATCAACAAATAGTGAAGCCACA
GATGTATTTGTTGATACCTTCCTCCTTGTGCCTACTGCCTCGGA

Edu/SAβGal

A representative sampling from proliferating and OIS cells, 6 days post-4OHT tamoxifen induction, were seeded in LabTek chamber slides (Nunc). Senescence-

associated beta-galactosidase was performed using the previously described protocol (Itahana et al., 2007). To measure EdU incorporation, Click-iT EdU Alexa Fluor Imaging Kit (Thermo fisher) was used as per manufacturer's instructions. Images were collected using the Zeiss confocal fluorescence microscope and analyzed using the Zen software.

Western Blot

Standard western blotting analysis was carried out using whole-cell lysate, generated using Lämely buffer, and boiled at 100ºC for 5 minutes. Protein was measured using qbit protein (Thermo) and equalized to 30μg. After membrane transfer, blots were analyzed via Ponceau staining for equal loading of wells. Blots were probed with the following antibodies: PARP1 ((H-250)– Santa Cruz – SC- 7150 – lot K1815), H3 (Histone 3 ab 1791 – Abcam – lot: GR265017-2), PARP1 (Active Motif, 39561) and Streptavidin IRDye 800cw (1:2000, Licor, 925-32230).

RNA extraction and quality control

Total RNA from each time point, specified above was collected from the cells using QIAGEN RNeasy Plus kit according to the manufacturers provided protocol. Quality of RNA (RIN metric) was measured using Agilent Technologies 4200 Tapestation (G2991-90001).

Quantitative RT-PCR

RNA extracted, as described above, was reverse transcribed into cDNA using High-Capacity Reverse-Transcriptase Kit following manufacturer's instructions (Applied biosystems, Thermo Fisher). qRT-PCR was performed using SYBR green qPCR Universal super mix (Bio-rad), with 500 ng cDNA using primers listed below:

QPCR Primer list

IL-1B	Hs_IL1B_1_SG QuantiTect Primer Assay – QT00021385
IL-6	Hs_IL6_1_SG QuantiTect Primer Assay – QT00083720
IL-8	Hs_CXCL8_1_SG QuantiTect Primer Assay – QT00000322
CCNA2	Hs_CCNA2_1_SG QuantiTect Primer Assay – QT00014798
CCNE2	Hs_CCNE2_1_SG QuantiTect Primer Assay – QT00063511
p16	Hs_CDKN2A_1_SG QuantiTect Primer Assay – QT00089964
GAPDH	Hs_GAPDH_1_SG QuantiTect Primer Assay – QT00079247
PARP1	Hs_PARP1_1_SG QuantiTect Primer Assay – QT00032690

Affymetrix RNA microarrays

Collection of RNA and QC was performed as described above. Whole transcriptome profiling was performed using Clariom™ D and GeneChip™ WT PLUS Reagent Kit (Affymetrix/Thermo Fisher) according to the manufacturer's instructions.

ATAC-seq

Proliferating and senescent WI-38 fibroblasts were treated with 4OHT for 6 days, followed by treatment (PJ34) or induction of shRNA over time course described. Method for ATAC-seq was described previously (Zamudio et al., 2019).

Chromatin ADP-ribosylation Affinity Purification (CRAP)

Proliferating and senescent WI-38 fibroblasts treated with 4OHT for 6 days were washed with PBS and 20 million cells were collected per condition. Cells were spun down at 2500 rpm for 5 min, 4ºC. The cell pellet was transferred to a1.5 mL Eppendorf tube. Pellet was resuspended in 300 μL of freshly PARP-assay buffer (50mM Tris-Cl pH8.0, 28mM KCl, 10mM $MgCl_2$, 0.01% digitonin, 1mM DTT, 20μM biotinylated NAD^+ (6-biotin-17NAD^+ – Trevigin), 500nM ADP-HPD (Merck Chemicals). Cells were incubated at room temperature for 30 minutes, agitating the tube every 10 minutes. The labelling reaction was quenched by adding PJ34 to a concentration of 10μM and immediately transferred to ice for 5 min. Mixture was spun down for 5 min, 2500 RPM,

4ºC and the supernatant discarded. The cell pellet was resuspended in 1 mL cold PBS, spin down for 5 min at 2500 RPM, 4ºC. Supernatant was discarded, and wash was repeated. 15 mL of 1x PBS was added and transferred to a 50 mL falcon tube. Cells were cross-linked with 1% formaldehyde (1mL of 16% formaldehyde) and rocked for 10 min at room temperature.

Cross-linking was quenched with 1mL of 2M glycine and rocked for 5 min. Cells were spun down at 2500 RPM for 5 min, 4ºC. Discard supernatant. Cells were washed with 1 mL of cold 1xPBS and transferred to a 1.5 mL Eppendorf tube. Nuclei were isolated and chromatin was digested with 1.2 μL of Micrococcal Nuclease for 20 minutes at 37ºC using the SimpleChIP kit (Cell Signalling). The MNase digestion was validated through DNA gel electrophoresis to reach a level of 70% mononucleosome fragments with up to 5 nucleosome fragments visible. Final volume was brought up to 1mL with ChIP dilution buffer. 10μL of diluted chromatin was reserved for input (1% input).

70μL of streptavidin beads coupled magnetic beads (Dynabeads™ M-280 Streptavidin – Invitrogen) were washed with ChIP dilution buffer three times. Labelled, MNase digested chromatin with was incubated with 70μL of washed streptavidin beads over night at 4ºC rotating.

Following incubation, tubes were transferred to magnetic rack and let the beads separate from the solution for 2 min. Supernatant was removed and samples were beads were washed with 1mL low-salt buffer (150mM NaCl, 0.1% SDS, 1% Triton X100, 20mM EDTA, 20mM Tris-Cl PH 8, 10mM Tris-Cl PH 8, 5mM EDTA, 150mM NaCl, 0.5% SDS). Wash was repeated two times with 1mL high-salt buffer (150 mM NaCl, 0.1% SDS, 1% Triton X100, 20mM EDTA, 20mM Tris-Cl PH 8, 10mM Tris-Cl

PH 8, 5mM EDTA, 300mM NaCl, 0.5% SDS), and twice with EDTA Buffer (10mM Tris-Cl PH 8, 1mM EDTA). For Western blots, beads were resuspended in 1x protein loading buffer and incubated at 95ºC for 5 minutes, and Western blot was performed as described above.

CRAP-Sequencing

For sequencing of CRAP isolated chromatin, beads were resuspended in 50 μL of ChIP elution buffer (10 mM Tris-Cl pH 8.0, 5 mM EDTA, 300 mM NaCl, 0.5% SDS) and treated with 2 μL of RNase A for 30 minutes at 37ºC followed by 2 hours incubated with 1 μL of glycogen (20 mg/mL) and 2.5 μL of Proteinase K. These samples were de-crosslinked at 65ºC over-night. Supernatant was removed from beads and DNA was extracted with the addition of 1:1 25:24:1 phenol:chloroform:isoamyl alcohol and subsequent precipitation with ethanol over-night at -20ºC with a 1/10 volume of 3M sodium acetate, $MgCl_2$ to a final concentration of 0.01M, 1μL glycogen (20mg/ml). The DNA pellet was washed 2 times with 70% ethanol and resuspended in 20 μL of low-EDTA TE buffer. The DNA subsequently underwent library preparation.

DNA preparation for ChIP-Seq and CRAP-seq libraries:

DNA was eluted by phenol/chloroform extraction (2X) followed by ethanol precipitation overnight at -20ºC. The DNA pellet was washed with 70% ethanol, allowed to dry, and DNA was resuspended in 35 μL 10 mM Tris-Cl pH 8.0. CRAP/ChIP-Seq libraries were produced following the Accel-NGS 2S Plus DNA Library Kit (#21024), with a modified protocol where we used 25:24:1 phenol:chloroform:isoamyl alcohol extractions followed by overnight ethanol precipitation of DNA with 1/10 volume of 3M sodium acetate, $MgCl_2$ to a final concentration of 0.01M, 1μL glycogen (20mg/ml) following each step of the protocol up to the PCR amplification. Before PCR amplification, we

performed an enrichment for small DNA fragments using Ampure XP (Beckman coulter) SPRI beads outlined previously in the X-ChIP protocol (Skene and Henikoff, 2015). We performed 9 cycles of PCR amplification, followed by a clean-up as per the Accel-NGS 2S Plus DNA Library Kit instructions. CRAP/ChIP-Seq libraries underwent quality control using the 4200 Tape-station (Agilent Technologies, G2991-90001) and quantified using the Invitrogen Qbit DS DNA HS Assay kit (Q32854). Libraries were sequenced using an Illumina High-Seq 2500 to a depth of 100 million reads per library.

Chromatin preparation and ChIP-seq

15 million cells were harvested in 10 million cell aliquots in 15 mL media. Each aliquot was cross-linked in 1% paraformaldehyde for 10 minutes at room temp. The cross-linking was quenched with the addition of 1mL of 2 M glycine and incubated at room temperature for 5 minutes. Nuclei were isolated and chromatin was digested with 1.2 μL of Micrococcal Nuclease for 20 minutes at 37ºC using the Simple-ChIP kit (Cell Signaling, #9002). The MNase digestion was validated through DNA gel electrophoresis to reach a level of 70% mononucleosome fragments with up to 5 nucleosome fragments. 15 million cell equivalents of chromatin were pre-cleared incubating 12.5 μL of Protein A/G Ultralink resin beads (Thermo Fisher). Chromatin volume was brought up to 1 mL with ChIP-buffer (Cell Signaling) and inputs were derived from 500 000 cell equivalents of chromatin. The immunoprecipitation was performed overnight at 4ºC with rotation using 4μg PARP1 antibody (H-250– Santa Cruz – SC- 7150 – lot K1815). Following immunoprecipitation, 30 μL of Ultralink resin beads were added and incubated for 4 hours rotating at 4ºC. The beads were pelleted by centrifugation (1000 RPM) and washed three times in low salt buffer (150 mM NaCl, 0.1% SDS, 1% Triton X-100, 20 mM EDTA, 20 mM Tris-HCl pH 8.0), once in high salt

buffer (500 mM NaCl, 0.1% SDS, 1% Triton X-100, 20 mM EDTA, 20 mM Tris-HCl pH 8.0), twice in lithium chloride buffer (250 mM LiCl, 1% IGEPAL CA-630, 15 sodium deoxycholate, 1 mM EDTA, 10 mM Tris- HCl pH 8.0) and twice in TE buffer (10 mM Tris-HCl, 1 mM EDTA). Washed beads were resuspended in 50 μL elution buffer (10 mM Tris-Cl pH 8.0, 5 mM EDTA, 300 mM NaCl, 0.5% SDS) and treated with 2 μL of RNase A for 30 minutes at 37ºC followed by 2 hours incubated with 1 μL of glycogen (20 mg/mL) and 2.5 μL of Proteinase K. These samples were de-crosslinked at 65ºC over-night. DNA was purified with the addition of 1:1 25:24:1 phenol:chloroform:isoamyl alcohol and subsequent precipitation with ethanol over-night at -20ºC with a 1/10 volume of 3M sodium acetate, $MgCl_2$ to a final concentration of 0.01M, 1μL glycogen (20mg/ml). The DNA pellet was washed 2 times with 70% ethanol and resuspended in 20 μL of low-EDTA TE buffer. The DNA subsequently underwent library preparation.

Spike-in ChIP-seq

Standard ChIP-seq protocol was performed, with the addition of 1:20 ratio of drosophila chromatin (Active Motif, 53083) following manufacturer's instructions. The immuno-precipitation was performed using the standard PARP1 antibody with an addition of the *drosophila*-specific histone variant H2Av spike-in antibody (Active Motif, 61686). The following ChIP and library preparation were performed as described above.

Quality control of sequencing data

The quality of every library was determined using the fastqc tool (http://www.bioinformatics.babraham.ac.uk/projects/fastqc/). Reads were subsequently trimmed and adapters clipped using the fastq-mcf

(https://github.com/ExpressionAnalysis/ea-utils/blob/wiki/FastqMcf.md). Only reads with none of the known high-throughput sequencing adapters, longer than 25 base pairs, with a mean quality score above 30 and maximum 1 N-call were kept.

ChIP-seq, ATAC-seq and CRAP-seq mapping

High quality single end reads were mapped to the *Homo sapiens* reference genome (hg19) using the end-to-end mode and the very-sensitive parametrization of bowtie2 (https://www.ncbi.nlm.nih.gov/pubmed/22388286) and keeping the read matches reported by default. For ATAC-seq only concordant pairs even if they dovetail and with a maximum fragment size of 2 Kbp were kept. In order to avoid PCR amplification biases in read quantification, duplicated reads were removed using the MarkDuplicates tool of Picard v1.94 (https://broadinstitute.github.io/picard/). Following the ENCODE guidelines for the analysis of ChIP-seq datasets (https://www.ncbi.nlm.nih.gov/pubmed/22955991) blacklisted regions were removed with bedtools v2.19.1 (http://bedtools.readthedocs.io/en/latest/)

Quantification and visualization of sequence data

The quality of the ChIP-seq, ATAC-seq and CRAP-seq libraries was checked by clustering and principal component analysis. Outlying replicates were thus identified and discarded. Genome browser visualizations were obtained by calculating the read coverage over non-overlapping windows of 50 bp genome wide. This tiled coverage was then quantile normalized to allow comparisons between different samples. For the quantification of ChIP-seq, ATAC-seq and CRAP-seq at specific regions, the corresponding read coverage was calculated and normalized over 1 Kbp windows around all the annotated transcription start sites (TTSs) and over active enhancers at day 6 of RAS OIS induction, as defined by chromatin state analysis of histone

modifications (ref). The obtained values were normalized using the DESeq2 size normalization approach (https://www.ncbi.nlm.nih.gov/pmc/articles/PMC4302049/) and by the size of the annotation when necessary. The average coverage profiles around the TSS were obtained by calculating the read coverage over non-overlapping windows of 10 bp spanning 1 Kbp around the TTS and normalized by using the DESeq2 approach. This normalized coverage was then averaged over the gene categories of interest according to the specific analysis.

Comparative transcriptome analysis

Cell files transcriptome were RMA normalized using the affy R package (https://doi.org/10.1093/bioinformatics/btg405); they were subsequently annotated using the pd.clariom.d.human R annotation package (https://bioconductor.org/packages/release/data/annotation/html/pd.clariom.d.human.html). To maximize the detection power for the time course analysis, control probe sets as well as lowly expressed probes were removed. Additionally, batch effects were identified and removed using the sva package (DOI: 10.18129/B9.bioc.sva).

The normalized and batch corrected expression time courses for PJ and KD treatments were analyzed with the Transcript time course analysis (TTCA) R package (https://bmcbioinformatics.biomedcentral.com/articles/10.1186/s12859-016-1440-8) using default parameters for the lambda smoothing factor and the p-value threshold for significance tests. The first time point was used as the control proliferative state for the time course comparison. All genes identified as significantly dynamic by any of the metrics of the TTCA method were defined as the PJ and KD sensitive genes.

The differential analysis for the RAS time course was performed as described in (Zamudio et al., 2019)

Functional analysis of PJ and KD time-course transcriptomes

The functional analysis of the pathways affected by the PJ and KD treatments was done using GAGE (https://bmcbioinformatics.biomedcentral.com/articles/10.1186/1471-2105-10-161), a generalized version of the gene set analysis (GSA) method and the kegg.gs data collection of up-to-date gene sets from the KEGG. All time points were compared to the initial one (0h for PJ and day 0 for KD) and gene sets significantly enriched (adjusted p-value < .075) with up or down regulated genes were identified for each transcriptome.

ADP-ribosylation quantification and comparison

A metric had to be developed to translate the sequencing information of the CRAP-seq technique into a quantification of ADP-ribosylation changes during OIS RAS induction. The broad distribution and the high variability of this signal prevented the application of peak-calling or differential analysis-based approaches. As an alternative, the non-parametric Kolmogorov-Smirnov statistic was used, which quantifies the distance between the empirical distribution function of the signal between any two samples, which we called KS metric. This test can be applied to the distribution of the CRAP-seq signal calculated over any set of annotations, e.g. TSSs, enhancers, as the average read coverage normalised by size (Figure S1 A and B). Moreover, it is possible to test both the gain and loss of ADP-ribosylation by setting the alternative hypothesis of the Kolmogorov-Smirnov test. For example, to quantify the gain in ADP-ribosylation between day 6 and 0, the alternative hypothesis will be that the empirical distribution function of day 0 is not greater than that of day 6. When applied to the comparison of the CRAP-seq signal between day 6 and 0, the KS metric reproduces the global

increase in ADP-ribosylation. Additionally, the KS metric detects a significant increase only for the PLUS NAD^+ condition and not for the MINUS NAD^+, indicating that it efficiently distinguishes biologically relevant differences from the technical variation intrinsic to the CRAP-seq technique.

PARP1 binding analysis

PARP1 binding was explored by quantifying and plotting the average ChIP-seq coverage up and downstream from the TSS of various gene categories. In order to study the differential phasing of the PARP1 signal around the TSS and autocorrelation analysis of this average signal was performed. For each coverage profile 2 calculations were done: from the TSS downstream and from the TSS upstream. The resulting autocorrelation vectors were then merged at the TSS, which corresponds to lag 0 and thus the autocorrelation maxima. The function shows up and down stream minima for the distances at which there is a maximum average enrichment of PARP1 ChIP-seq coverage around the nucleus. These distances are subsequently compared to the nucleosome positioning.

Transcription factor footprinting

In silico foot-printing was performed as described previously (Zamudio et al., 2019).

Chromatin state differential analysis

Chromatin state analysis was performed as described previously (Zamudio et al., 2019).

7. Bibliography

Acosta, J.C., O'Loghlen, A., Banito, A., Guijarro, M. V, Augert, A., Raguz, S., Fumagalli, M., Da Costa, M., Brown, C., Popov, N., et al. (2008). Chemokine signaling via the CXCR2 receptor reinforces senescence. Cell *133*, 1006–1018.

Acosta, J.C., Banito, A., Wuestefeld, T., Georgilis, A., Janich, P., Morton, J.P., Athineos, D., Kang, T.-W., Lasitschka, F., Andrulis, M., et al. (2013). A complex secretory program orchestrated by the inflammasome controls paracrine senescence. Nat. Cell Biol. *15*, 978–990.

Adams, P.D. (2007). Remodeling of chromatin structure in senescent cells and its potential impact on tumor suppression and aging. Gene *397*, 84–93.

Agresti, A., and Bianchi, M.E. (2003). HMGB proteins and gene expression. Curr. Opin. Genet. Dev. *13*, 170–178.

Aguilar-Quesada, R., Muñoz-Gámez, J., Martín-Oliva, D., Peralta, A., Valenzuela, M.T., Matínez-Romero, R., Quiles-Pérez, R., Murcia, J., de Murcia, G., de Almodóvar, M., et al. (2007). Interaction between ATM and PARP-1 in response to DNA damage and sensitization of ATM deficient cells through PARP inhibition. BMC Mol. Biol. *8*, 29.

Ahel, D., Ho, Z., Wiechens, N., Polo, S.E., Garcia-, E., Owen-hughes, T., and Boulton, S.J. (2012). MEU AGRADECIMENTO AOS CRIACIONISTAS (comentado) . *325*, 1240–1243.

Aird, K.M., Worth, A.J., Snyder, N.W., Lee, J. V., Sivanand, S., Liu, Q., Blair, I.A., Wellen, K.E., and Zhang, R. (2015). ATM Couples Replication Stress and Metabolic Reprogramming during Cellular Senescence. Cell Rep. *11*, 893–901.

Alemasova, E.E., and Lavrik, O.I. (2019). Poly(ADP-ribosyl)ation by PARP1: reaction mechanism and regulatory proteins. Nucleic Acids Res. 1–17.

Alexander, K., Yang, H.-S., and Hinds, P.W. (2003). pRb inactivation in senescent cells leads to an E2F-dependent apoptosis requiring p73. Mol. Cancer Res. *1*, 716–728.

Allsopp, R.C., Vaziri, H., Pattersont, C., Goldsteint, S., Younglai, E. V, Futcher, A.B., Greidert, C.W., and Harley, C.B. (1992). Telomere length predicts replicative capacity of human fibroblasts. Biochemistry *89*, 10114–10118.

Alvarez-Gonzalez, R., and Althaus, F.R. (1989). Poly(ADP-ribose) catabolism in mammalian cells exposed to DNA-damaging agents. Mutat. Res. *218*, 67–74.

Amiri, K.I., Ha, H.C., Smulson, M.E., and Richmond, A. (2006). Differential regulation of CXC ligand 1 transcription in melanoma cell lines by poly(ADP-ribose) polymerase-1. Oncogene *25*, 7714–7722.

Anderson, M.G., Scoggin, K.E.S., and Simbulan-rosenthal, C.M. (2000). Identification of Poly (ADP-Ribose) Polymerase as a Transcriptional Coactivator of the Human T-Cell Leukemia Virus Type 1 Tax Protein. *74*, 2169–2177.

Anderson, R.M., Bitterman, K.J., Wood, J.G., Medvedik, O., and Sinclair, D.A. (2003). Nicotinamide and PNC1 govern lifespan extension by calorie restriction in Saccharomyces cerevisiae. Nature *423*, 181–185.

Armata, H.L., Garlick, D.S., and Sluss, H.K. (2007). The ataxia telangiectasia-mutated target site Ser18 is required for p53-mediated tumor suppression. Cancer Res. *67*, 11696–11703.

Astle, M. V., Hannan, K.M., Ng, P.Y., Lee, R.S., George, A.J., Hsu, A.K., Haupt, Y., Hannan, R.D., and Pearson, R.B. (2012). AKT induces senescence in human cells via mTORC1 and p53 in the absence of DNA damage: Implications for targeting mTOR during malignancy. Oncogene *31*, 1949–1962.

Ba, X., and Garg, N.J. (2011). Signaling mechanism of poly(ADP-ribose) polymerase-1 (PARP-1) in inflammatory diseases. Am. J. Pathol. *178*, 946–955.

Bai, P. (2015). Biology of Poly(ADP-Ribose) Polymerases: The Factotums of Cell Maintenance. Mol. Cell *58*, 947–958.

Bai, P., Cantó, C., Oudart, H., Brunyánszki, A., Cen, Y., Thomas, C., Yamamoto, H., Huber, A., Kiss, B., Houtkooper, R.H., et al. (2011a). PARP-1 Inhibition Increases Mitochondrial Metabolism through SIRT1 Activation. Cell Metab. *13*, 461–468.

Bai, P., Cantó, C., Oudart, H., Brunyánszki, A., Cen, Y., Thomas, C., Yamamoto, H., Huber, A., Kiss, B., Houtkooper, R.H., et al. (2011b). PARP-1 Inhibition Increases Mitochondrial Metabolism through SIRT1 Activation. Cell Metab. *13*, 461–468.

Baker, D.J., Childs, B.G., Durik, M., Wijers, M.E., Sieben, C.J., Zhong, J., Saltness, R.A., Jeganathan, K.B., Casaclang Verzosa, G., Pezeshki, A., et al. (2016). Naturally occurring p16 Ink4a -positive cells shorten healthy lifespan. Nature *530*, 1–5.

Baker, D.J., Alimirah, F., van Deursen, J.M., Campisi, J., and Hildesheim, J. (2017). Oncogenic senescence: a multi-functional perspective. Oncotarget *8*, 27661–27672.

Balentien, E., Mufson, B.E., Shattuck, R.L., Derynck, R., and Richmond, A. (1991). Effects of MGSA/GRO alpha on melanocyte transformation. Oncogene *6*, 1115–1124.

Barkauskaite, E., Jankevicius, G., and Ahel, I. (2015). Structures and Mechanisms of Enzymes Employed in the Synthesis and Degradation of PARP-Dependent Protein ADP-Ribosylation. Mol. Cell *58*, 935–946.

Bartolomei, G., Leutert, M., Manzo, M., Baubec, T., and Hottiger, M.O. (2016). Analysis of Chromatin ADP-Ribosylation at the Genome-wide Level and at Specific Loci by ADPr-ChAP. Mol. Cell *61*, 474–485.

Bauer, P.I., Buki, K.G., Hakam, A., and Kun, E. (1990). Macromolecular association of ADP-ribosyltransferase and its correlation with enzymic activity. Biochem. J. *270*, 17–26.

Beauséjour, C.M., Krtolica, A., Galimi, F., Narita, M., Lowe, S.W., Yaswen, P., and Campisi, J. (2003). Reversal of human cellular senescence: roles of the p53 and p16 pathways. EMBO J. *22*, 4212–4222.

Benhamed, M., Herbig, U., Ye, T., Dejean, A., and Bischof, O. (2012). Senescence is an endogenous trigger for microRNA-directed transcriptional gene silencing in human cells. Nat. Cell Biol. *14*, 266–275.

Berti, M., Ray Chaudhuri, A., Thangavel, S., Gomathinayagam, S., Kenig, S., Vujanovic, M.,

Odreman, F., Glatter, T., Graziano, S., Mendoza-Maldonado, R., et al. (2013). Human RECQ1 promotes restart of replication forks reversed by DNA topoisomerase I inhibition. Nat. Struct. Mol. Biol. *20*, 347–354.

Bielak-Zmijewska, A., Wnuk, M., Przybylska, D., Grabowska, W., Lewinska, A., Alster, O., Korwek, Z., Cmoch, A., Myszka, A., Pikula, S., et al. (2014). A comparison of replicative senescence and doxorubicin-induced premature senescence of vascular smooth muscle cells isolated from human aorta. Biogerontology *15*, 47–64.

Bischof, O., Schwamborn, K., Martin, N., Werner, A., Sustmann, C., Grosschedl, R., and Dejean, A. (2006). The E3 SUMO Ligase PIASy Is a Regulator of Cellular Senescence and Apoptosis. Mol. Cell *22*, 783–794.

Boehm, A.K., Saunders, A., Werner, J., and Lis, J.T. (2003). Transcription factor and polymerase recruitment, modification, and movement on dhsp70 in vivo in the minutes following heat shock. Mol. Cell. Biol. *23*, 7628–7637.

Bosari, S., Marchetti, A., Buttitta, F., Graziani, D., Borsani, G., Loda, M., Bevilacqua, G., and Coggi, G. (1995). Detection of p53 mutations by single-strand conformation polymorphisms (SSCP) gel electrophoresis. A comparative study of radioactive and nonradioactive silver-stained SSCP analysis. Diagn. Mol. Pathol. *4*, 249–255.

Boulares, A.H., Zoltoski, A.J., Sherif, Z.A., Jolly, P., Massaro, D., and Smulson, M.E. (2003). Gene knockout or pharmacological inhibition of poly(ADP-ribose) polymerase-1 prevents lung inflammation in a murine model of asthma. Am. J. Respir. Cell Mol. Biol. *28*, 322–329.

Brady, C.A., and Attardi, L.D. (2010). p53 at a glance. J. Cell Sci. *123*, 2527–2532.

Brehm, A., Miska, E.A., McCance, D.J., Reid, J.L., Bannister, A.J., and Kouzarides, T. (1998). Retinoblastoma protein recruits histone deacetylase to repress transcription. Nature *391*, 597–601.

Burton, D.G. a., and Faragher, R.G. a. (2015). Cellular senescence: from growth arrest to immunogenic conversion. Age (Omaha). *37*.

Burton, D.G.A., Moshayev, Z., Vadai, E., Wensveen, F., Golani, O., Polic, B., and Krizhanovsky, V. (2016). NKG2D ligands mediate immunosurveillance of senescent cells. *8*, 328–344.

Bussian, T.J., Aziz, A., Meyer, C.F., Swenson, B.L., van Deursen, J.M., and Baker, D.J. (2018). Clearance of senescent glial cells prevents tau-dependent pathology and cognitive decline. Nature *562*, 578–582.

Butler, A.J., and Ordahl, C.P. (1999). Poly (ADP-Ribose) Polymerase Binds with Transcription Enhancer Factor 1 to MCAT1 Elements To Regulate Muscle-Specific Transcription. *19*, 296–306.

Caiafa, P., Guastafierro, T., and Zampieri, M. (2009). Epigenetics: poly(ADP-ribosyl)ation of PARP-1 regulates genomic methylation patterns. FASEB J. *23*, 672–678.

Campisi, J. (1997). The biology of replicative senescence. Eur. J. Cancer *33*, 703–709.

Campisi, J., and d'Adda di Fagagna, F. (2007). Cellular senescence: when bad things happen to good cells. Nat. Rev. Mol. Cell Biol. *8*, 729–740.

Campisi, J., Andersen, J.K., Kapahi, P., and Melov, S. (2011). Cellular senescence: A link between cancer and age-related degenerative disease? Semin. Cancer Biol. *21*, 354–359.

Canto, C., Oudart, H., Brunya, A., Cen, Y., Thomas, C., Yamamoto, H., Houtkooper, R.H., Schoonjans, K., Sauve, A.A., and Huber, A. (2011). Short Article PARP-1 Inhibition Increases Mitochondrial Metabolism through SIRT1 Activation. *1720*.

Cantó, C., Sauve, A.A., and Bai, P. (2013). Crosstalk between poly(ADP-ribose) polymerase and sirtuin enzymes. Mol. Aspects Med. *34*, 1168–1201.

Carrel, A. (1912). On the permanent life of tissues outside of the organism. J. Exp. Med. *15*, 75 and 76.

Cech, T.R. (2004). Beginning to understand the end of the chromosome. Cell *116*, 273–279.

Cervellera, M.N., and Sala, A. (2000). Poly (ADP-ribose) Polymerase Is a B-MYB Coactivator . *275*, 10692–10696.

Chandra, T., Kirschner, K., Thuret, J.Y., Pope, B.D., Ryba, T., Newman, S., Ahmed, K., Samarajiwa, S.A., Salama, R., Carroll, T., et al. (2012). Independence of Repressive Histone Marks and Chromatin Compaction during Senescent Heterochromatic Layer Formation. Mol. Cell *47*, 203–214.

Chandra, T., Ewels, P.A., Schoenfelder, S., Furlan-Magaril, M., Wingett, S.W., Kirschner, K., Thuret, J.-Y., Andrews, S., Fraser, P., and Reik, W. (2015a). Global Reorganization of the Nuclear Landscape in Senescent Cells. Cell Rep. *10*, 471–483.

Chandra, T., Ewels, P.A., Schoenfelder, S., Furlan-Magaril, M., Wingett, S.W., Kirschner, K., Thuret, J.-Y., Andrews, S., Fraser, P., and Reik, W. (2015b). Global Reorganization of the Nuclear Landscape in Senescent Cells. Cell Rep. *10*, 471–483.

Chang, W., and Alvarez-Gonzalez, R. (2001). The Sequence-specific DNA Binding of NF-κB Is Reversibly Regulated by the Automodification Reaction of Poly (ADP-ribose) Polymerase 1. J. Biol. Chem. *276*, 47664–47670.

Chen, H., Ruiz, P.D., Novikov, L., Casill, A.D., Park, J.W., and Gamble, M.J. (2014). MacroH2A1.1 and PARP-1 cooperate to regulate transcription by promoting CBP-mediated H2B acetylation. Nat. Struct. Mol. Biol. *21*, 981–989.

Chen, Q., Fischer, A., Reagan, J.D., Yan, L.J., and Ames, B.N. (1995). Oxidative DNA damage and senescence of human diploid fibroblast cells. Proc. Natl. Acad. Sci. U. S. A. *92*, 4337–4341.

Chen, Q.M., Bartholomew, J.C., Campisi, J., Acosta, M., Reagan, J.D., and Ames, B.N. (1998). Molecular analysis of H2O2-induced senescent-like growth arrest in normal human fibroblasts: p53 and Rb control G1 arrest but not cell replication. Biochem. J. *332*, 43.

Chiche, A., Le Roux, I., von Joest, M., Sakai, H., Aguín, S.B., Cazin, C., Salam, R., Fiette, L., Alegria, O., Flamant, P., et al. (2016). Injury-Induced Senescence Enables In Vivo

Reprogramming in Skeletal Muscle. Cell Stem Cell 1–8.

Chien, Y., Scuoppo, C., Wang, X., Fang, X., Balgley, B., Bolden, J.E., Premsrirut, P., Luo, W., Chicas, A., Lee, C.S., et al. (2011). Control of the senescence-associated secretory phenotype by NF-κB promotes senescence and enhances chemosensitivity. Genes Dev. *25*, 2125–2136.

Childs, B.G., Baker, D.J., Kirkland, J.L., Campisi, J., and Deursen, J.M. Van (2014). Senescence and apoptosis : dueling or complementary cell fates ? *15*, 1139–1154.

Chiou, S.-H., Jiang, B.-H., Yu, Y.-L., Chou, S.-J., Tsai, P.-H., Chang, W.-C., Chen, L.-K., Chen, L.-H., Chien, Y., and Chiou, G.-Y. (2013). Poly(ADP-ribose) polymerase 1 regulates nuclear reprogramming and promotes iPSC generation without c-Myc. J. Exp. Med. *210*, 85–98.

Chou, D.M., Adamson, B., Dephoure, N.E., Tan, X., Nottke, A.C., and Hurov, K.E. (2010). A chromatin localization screen reveals poly (ADP ribose) -regulated recruitment of the repressive polycomb and NuRD complexes to sites of DNA damage. *107*, 18475–18480.

Ciccarone, F., Zampieri, M., and Caiafa, P. (2017). PARP1 orchestrates epigenetic events setting up chromatin domains. Semin. Cell Dev. Biol. *63*, 123–134.

Cohen-armon, M., Visochek, L., Rozensal, D., Kalal, A., and Geistrikh, I. (2007). Article by Phosphorylated ERK2 Increases Elk1 Activity : A Link to Histone Acetylation. 297–308.

Cohen-Armon, M. (2007). PARP-1 activation in the ERK signaling pathway. Trends Pharmacol. Sci. *28*, 556–560.

Collado, M., Blasco, M.A., and Serrano, M. (2007). Cellular Senescence in Cancer and Aging. Cell *130*, 223–233.

Collesano, M., Sala, A., Rocca, G. La, Burgio, G., Kotova, E., Gesu, D. Di, Ingrassia, A.M.R., Tulin, A. V, and Corona, D.F. V (2008). The Nucleosome-Remodeling ATPase ISWI Is Regulated by Poly-ADP-Ribosylation. *6*.

Contrepois, K., Coudereau, C., Benayoun, B.A., Schuler, N., Roux, P.F., Bischof, O., Courbeyrette, R., Carvalho, C., Thuret, J.Y., Ma, Z., et al. (2017). Histone variant H2A.J accumulates in senescent cells and promotes inflammatory gene expression. Nat. Commun. *8*.

Coppé, J.-P., Patil, C.K., Rodier, F., Sun, Y., Muñoz, D.P., Goldstein, J., Nelson, P.S., Desprez, P.-Y., and Campisi, J. (2008). Senescence-associated secretory phenotypes reveal cell-nonautonomous functions of oncogenic RAS and the p53 tumor suppressor. PLoS Biol. *6*, 2853–2868.

Coppé, J.-P., Patil, C.K., Rodier, F., Krtolica, A., Beauséjour, C.M., Parrinello, S., Hodgson, J.G., Chin, K., Desprez, P.-Y., and Campisi, J. (2010a). A human-like senescence-associated secretory phenotype is conserved in mouse cells dependent on physiological oxygen. PLoS One *5*, e9188.

Coppé, J.-P., Desprez, P., Krtolica, A., and Campisi, J. (2010b). The Senescence-Associated Secretory Phenotype: The Dark Side of Tumor Suppression. Annu. Rev. Pathol. Mech. Dis. *5*, 99–118.

Corpet, A., and Stucki, M. (2014). Chromatin maintenance and dynamics in senescence: a spotlight on SAHF formation and the epigenome of senescent cells. Chromosoma *123*, 423–436.

Courtois-Cox, S., Genther Williams, S.M., Reczek, E.E., Johnson, B.W., McGillicuddy, L.T., Johannessen, C.M., Hollstein, P.E., MacCollin, M., and Cichowski, K. (2006). A negative feedback signaling network underlies oncogene-induced senescence. Cancer Cell *10*, 459–472.

Criscione, S.W., Teo, Y.V., and Neretti, N. (2016a). The Chromatin Landscape of Cellular Senescence. Trends Genet. *32*, 751–761.

Criscione, S.W., De Cecco, M., Siranosian, B., Zhang, Y., Kreiling, J.A., Sedivy, J.M., and Neretti, N. (2016b). Reorganization of chromosome architecture in replicative cellular senescence. Sci. Adv. *2*, e1500882.

Criscione, S.W., De Cecco, M., Siranosian, B., Zhang, Y., Kreiling, J.A., Sedivy, J.M., and Neretti, N. (2016c). Reorganization of chromosome architecture in replicative cellular senescence. Sci. Adv. *2*, e1500882.

D'Adda di Fagagna, F. (2008). Living on a break: cellular senescence as a DNA-damage response. Nat. Rev. Cancer *8*, 512–522.

D'Adda di Fagagna, F., Reaper, P.M., Clay-Farrace, L., Fiegler, H., Carr, P., von Zglinicki, T., Saretzki, G., Carter, N.P., and Jackson, S.P. (2003). A DNA damage checkpoint response in telomere-initiated senescence. Nature *426*, 194–198.

D'Adda Di Fagagna, F. (2008). Living on a break: Cellular senescence as a DNA-damage response. Nat. Rev. Cancer *8*, 512–522.

D'Amours, D., and Jackson, S.P. (2002). The MRE11 complex: at the crossroads of DNA repair and checkpoint signalling. Nat. Rev. Mol. Cell Biol. *3*, 317–327.

D'Amours, D., Desnoyers, S., D'Silva, I., and Poirier, G.G. (1999). Poly(ADP-ribosyl)ation reactions in the regulation of nuclear functions. Biochem. J. *342 (Pt 2*, 249–268.

D'Andrea, A.D. (2018). Mechanisms of PARP inhibitor sensitivity and resistance. DNA Repair (Amst). *71*.

Dahl, M., Maturi, V., Lönn, P., Papoutsoglou, P., Zieba, A., Vanlandewijck, M., Van Der Heide, L.P., Watanabe, Y., Söderberg, O., Hottiger, M.O., et al. (2014). Fine-tuning of smad protein function by poly(ADP-ribose) polymerases and poly(ADP-ribose) glycohydrolase during transforming growth factor β signaling. PLoS One *9*.

Dantzer, F., and Santoro, R. (2013). The expanding role of PARPs in the establishment and maintenance of heterochromatin. FEBS J.

Datto, M.B., Li, Y., Panus, J.F., Howe, D.J., Xiong, Y., and Wang, X.F. (2006). Transforming growth factor beta induces the cyclin-dependent kinase inhibitor p21 through a p53-independent mechanism. Proc. Natl. Acad. Sci. *92*, 5545–5549.

Debacq-Chainiaux, F., Erusalimsky, J.D., Campisi, J., and Toussaint, O. (2009). Protocols to

detect senescence-associated beta-galactosidase (SA-betagal) activity, a biomarker of senescent cells in culture and in vivo. Nat. Protoc. *4*, 1798–1806.

Demaria, M., O'leary, M.N., Chang, J., Shao, L., Liu, S., Alimirah, F., Koenig, K., Le, C., Mitin, N., Deal, A.M., et al. (2017). Cellular senescence promotes adverse effects of chemotherapy and cancer relapse. Cancer Discov *7*, 165–176.

Van Deursen, J.M. (2014). The role of senescent cells in ageing. Nature *509*, 439–446.

DiMauro, T., Cantor, D.J., Bainor, A.J., and David, G. (2015). Transcriptional repression of Sin3B by Bmi-1 prevents cellular senescence and is relieved by oncogene activation. Oncogene *34*, 4011–4017.

Dimri, G.P., Lee, X., Basile, G., Acosta, M., Scott, G., Roskelley, C., Medrano, E.E., Linskens, M., Rubelj, I., and Pereira-Smith, O. (1995). A biomarker that identifies senescent human cells in culture and in aging skin in vivo. Proc. Natl. Acad. Sci. U. S. A. *92*, 9363–9367.

Dou, Z., Ghosh, K., Vizioli, M.G., Zhu, J., Sen, P., Wangensteen, K.J., Simithy, J., Lan, Y., Lin, Y., Zhou, Z., et al. (2017). Cytoplasmic chromatin triggers inflammation in senescence and cancer. Nature *550*, 402–406.

Du, X., Matsumura, T., Edelstein, D., Rossetti, L., and Brownlee, M. (2003). Inhibition of GAPDH activity. J. Clin. Invest. *112*, 1049–1057.

Dynlacht, B.D., Lees, J.A., and Harlow, E. (1994). Differential regulation of E2F trans-activation by cyclin / cdk2 complexes. *130*, 1772–1786.

Eggert, T., Wolter, K., Ji, J., Ma, C., Yevsa, T., Klotz, S., Medina-Echeverz, J., Longerich, T., Forgues, M., Reisinger, F., et al. (2016a). Distinct Functions of Senescence-Associated Immune Responses in Liver Tumor Surveillance and Tumor Progression. Cancer Cell *30*, 533–547.

Eggert, T., Wolter, K., Ji, J., Ma, C., Yevsa, T., Klotz, S., Medina-Echeverz, J., Longerich, T., Forgues, M., Reisinger, F., et al. (2016b). Distinct Functions of Senescence-Associated Immune Responses in Liver Tumor Surveillance and Tumor Progression. Cancer Cell *30*, 533–547.

Eggert, T., Wolter, K., Ji, J., Ma, C., Yevsa, T., Klotz, S., Medina-Echeverz, J., Longerich, T., Forgues, M., Reisinger, F., et al. (2016c). Distinct Functions of Senescence-Associated Immune Responses in Liver Tumor Surveillance and Tumor Progression. Cancer Cell *30*, 533–547.

El-Hamoly, T., and Hegedűs, C, Lakatos, P., Kovacs, K., Bai, P., El-Ghazaly, M., El-Denshary, E., Szabo, E., Virag, L. (2014). Activation of Poly (ADP-Ribose) Polymerase 1 delays wound healing by regulating keratinocyte migration and production of inflammatory medators. Mol. Med. *20*, 1.

El-khamisy, S.F., Masutani, M., Suzuki, H., and Caldecott, K.W. (2003). A requirement for PARP-1 for the assembly or stability of XRCC1 nuclear foci at sites of oxidative DNA damage. *31*, 5526–5533.

Erener, S., Hesse, M., Kostadinova, R., and Hottiger, M.O. (2012). Poly(ADP-

Ribose)Polymerase-1 (PARP1) Controls Adipogenic Gene Expression and Adipocyte Function. Mol. Endocrinol. *26*, 79–86.

Ernest Kun, *, Eva Kirsten, Jerome Mendeleyev, and, and Charles P. Ordahl, * (2005). Regulation of the Enzymatic Catalysis of Poly(ADP-ribose) Polymerase by dsDNA, Polyamines, Mg2+, Ca2+, Histones H1 and H3, and ATP, by.

Falck, J., Coates, J., and Jackson, S.P. (2005). Conserved modes of recruitment of ATM, ATR and DNA-PKcs to sites of DNA damage. Nature *434*, 605–611.

Fan, D.N.Y., and Schmitt, C.A. (2017). Detecting Markers of Therapy-Induced Senescence in Cancer Cells. pp. 41–52.

Feng, X.-H., and Derynck, R. (2005). SPECIFICITY AND VERSATILITY IN TGF-β SIGNALING THROUGH SMADS. Annu. Rev. Cell Dev. Biol. *21*, 659–693.

Fischbach, A., Kr, A., Hampp, S., Assmann, G., Rank, L., Fischer, J.M.F., Veith, S., Hufnagel, M., St, M.T., Rossatti, P., et al. (2018). The C-terminal domain of p53 orchestrates the interplay between non-covalent and covalent poly (ADP-ribosyl) ation of p53 by PARP1. *46*, 804–822.

Freund, A., Patil, C.K., and Campisi, J. (2011). P38MAPK is a novel DNA damage response-independent regulator of the senescence-associated secretory phenotype. EMBO J. *30*, 1536–1548.

Frizzell, K.M., and Kraus, W.L. (2009). PARP inhibitors and the treatment of breast cancer: Beyond BRCA1/2? Breast Cancer Res. *11*, 11–12.

Fumagalli, M., Rossiello, F., Clerici, M., Barozzi, S., Cittaro, D., Kaplunov, J.M., Bucci, G., Dobreva, M., Matti, V., Beausejour, C.M., et al. (2012). Telomeric DNA damage is irreparable and causes persistent DNA-damage-response activation. Nat. Cell Biol. *14*, 355–365.

Fyhrquist, F., Saijonmaa, O., and Strandberg, T. (2013). The roles of senescence and telomere shortening in cardiovascular disease. Nat. Rev. Cardiol. *10*, 274–283.

Galande, S., and Kohwi-Shigematsu, T. (1999). Poly(ADP-ribose) Polymerase and Ku Autoantigen Form a Complex and Synergistically Bind to Matrix Attachment Sequences. J. Biol. Chem. *274*, 20521–20528.

Galluzzi, L., Bravo-San Pedro, J.M., and Kroemer, G. (2016). Autophagy Mediates Tumor Suppression via Cellular Senescence. Trends Cell Biol. *26*, 1–3.

Gao, F., Kwon, S.W., Zhao, Y., and Jin, Y. (2009). PARP1 Poly(ADP-ribosyl)ates Sox2 to Control Sox2 Protein Levels and FGF4 Expression during Embryonic Stem Cell Differentiation. J. Biol. Chem. *284*, 22263–22273.

Gewirtz, D.A., Holt, S.E., and Elmore, L.W. (2008). Accelerated senescence: An emerging role in tumor cell response to chemotherapy and radiation. Biochem. Pharmacol. *76*, 947–957.

Ghonim, M.A., Pyakurel, K., Ibba, S. V, Wang, J., Rodriguez, P., Al-khami, A.A., Lammi, M.R., Kim, H., Zea, A.H., Davis, C., et al. (2015). PARP is activated in human asthma and its inhibition by olaparib blocks house dust mite-induced disease in mice. 951–962.

Gibbs-Seymour, I., Fontana, P., Rack, J.G.M., and Ahel, I. (2016). HPF1/C4orf27 Is a PARP-1-Interacting Protein that Regulates PARP-1 ADP-Ribosylation Activity. Mol. Cell *62*, 432–442.

Gibson, B.A., and Kraus, W.L. (2012). New insights into the molecular and cellular functions of poly(ADP-ribose) and PARPs. Nat. Rev. Mol. Cell Biol. *13*, 411–424.

Gibson, B.A., Zhang, Y., Jiang, H., Hussey, K.M., Shrimp, J.H., Lin, H., Schwede, F., Yu, Y., and Kraus, W.L. (2016). Chemical genetic discovery of PARP targets reveals a role for PARP-1 in transcription elongation. Science (80-.). *353*, 45–50.

Glück, S., Guey, B., Gulen, M.F., Wolter, K., Kang, T.-W., Schmacke, N.A., Bridgeman, A., Rehwinkel, J., Zender, L., and Ablasser, A. (2017). Innate immune sensing of cytosolic chromatin fragments through cGAS promotes senescence. Nat. Cell Biol. *19*.

Gorgoulis, V.G., and Halazonetis, T.D. (2010). Oncogene-induced senescence: the bright and dark side of the response. Curr. Opin. Cell Biol. *22*, 816–827.

Gottschalk, A.J., Timinszky, G., Kong, S.E., Jin, J., Cai, Y., Swanson, S.K., Washburn, M.P., Florens, L., Ladurner, A.G., Conaway, J.W., et al. (2009). Poly(ADP-ribosyl)ation directs recruitment and activation of an ATP-dependent chromatin remodeler. Proc. Natl. Acad. Sci. *106*, 13770–13774.

Gradwohl, G., Mazen, A., and Murcia, G. de (1987). Poly(ADP-ribose) polymerase forms loops with DNA. Biochem. Biophys. Res. Commun. *148*, 913–919.

Guetg, C., Scheifele, F., Rosenthal, F., Hottiger, M.O., and Santoro, R. (2012). Inheritance of Silent rDNA Chromatin Is Mediated by PARP1 via Noncoding RNA. Mol. Cell *45*, 790–800.

Gupte, R., Liu, Z., and Kraus, W.L. (2017). PARPs and ADP-ribosylation: recent advances linking molecular functions to biological outcomes. Genes Dev. *31*, 101–126.

Ha, H.C. (2004). Defective transcription factor activation for proinflammatory gene expression in poly(ADP-ribose) polymerase 1-deficient glia. Proc. Natl. Acad. Sci. U. S. A. *101*, 5087–5092.

Ha, H.C., and Snyder, S.H. (1999). Poly(ADP-ribose) polymerase is a mediator of necrotic cell death by ATP depletion. Proc. Natl. Acad. Sci. U. S. A. *96*, 13978–13982.

Haferkamp, S., Tran, S.L., Becker, T.M., Scurr, L.L., Kefford, R.F., and Rizos, H. (2009). The relative contributions of the p53 and pRb pathways in oncogene-induced melanocyte senescence. Aging (Albany. NY). *1*, 542–556.

Haince, J.-F., Kozlov, S., Dawson, V.L., Dawson, T.M., Hendzel, M.J., Lavin, M.F., and Poirier, G.G. (2007). Ataxia Telangiectasia Mutated (ATM) Signaling Network Is Modulated by a Novel Poly (ADP-ribose) -dependent Pathway in the Early Response to DNA-damaging Agents * □. *282*, 16441–16453.

Haince, J.F., McDonald, D., Rodrigue, A., Déry, U., Masson, J.Y., Hendzel, M.J., and Poirier, G.G. (2008). PARP1-dependent kinetics of recruitment of MRE11 and NBS1 proteins to multiple DNA damage sites. J. Biol. Chem. *283*, 1197–1208.

Hänzelmann, S., Beier, F., Gusmao, E.G., Koch, C.M., Hummel, S., Charapitsa, I., Joussen,

S., Benes, V., Brümmendorf, T.H., Reid, G., Wagner, W. (2015). Replicative senescence is associated with nuclear reorganization and with DNA methylation at specific transcription factor binding sites. Clin. Epigenetics *7*, 19.

Hara, E., Smith, R., Parry, D., Tahara, H., Stone, S., and Peters, G. (1996). Regulation of p16CDKN2 expression and its implications for cell immortalization and senescence. Mol. Cell. Biol. *16*, 859–867.

Hardy, K., Mansfield, L., Mackay, a, Benvenuti, S., Ismail, S., Arora, P., O'Hare, M.J., and Jat, P.S. (2005). Transcriptional networks and cellular senescence in human mammary fibroblasts. Mol. Biol. Cell *16*, 943–953.

Harman, D. (1991). The aging process: major risk factor for disease and death. Proc. Natl. Acad. Sci. U. S. A. *88*, 5360–5363.

Harris, C.C. (1996). Structure and Function of the p53 Tumor Suppressor Gene: Clues for Rational Cancer Therapeutic Strategies. *88*.

Hassa, P.O., and Hottiger, M.O. (1999). A Role of Poly (ADP-Ribose) Polymerase in NF- B Transcriptional Activation. Biol. Chem. *380*, 953–959.

Hassa, P.O., Covic, M., Hasan, S., Imhof, R., and Hottiger, M.O. (2001). The Enzymatic and DNA Binding Activity of PARP-1 Are Not Required for NF-??B Coactivator Function. J. Biol. Chem. *276*, 45588–45597.

Hassa, P.O., Buerki, C., Lombardi, C., Imhof, R., and Hottiger, M.O. (2003). Transcriptional Coactivation of Nuclear Factor- B-dependent Gene Expression by p300 Is Regulated by Poly (ADP) -ribose Polymerase-1 *. *278*, 45145–45153.

Hassa, P.O., Haenni, S.S., Buerki, C., Meier, N.I., Lane, W.S., Owen, H., Gersbach, M., Imhof, R., and Hottiger, M.O. (2005). Acetylation of Poly (ADP-ribose) Polymerase-1 by p300 / CREB-binding Protein Regulates Coactivation. *280*, 40450–40464.

Hayflick, L. (1965). The limited *in vitro* lifetime of human diploid cell strains. Exp. Cell Res. *37*, 614–636.

Hayflick, L., and Moorhead, P.S. (1961). The serial cultivation of human diploid cell strains. Exp. Cell Res. *25*, 585–621.

Hendriks, I.A., Larsen, S.C., and Nielsen, M.L. (2019). An Advanced Strategy for Comprehensive Profiling of ADP-ribosylation Sites Using Mass Spectrometry-based Proteomics. Mol. Cell. Proteomics *18*, 1010–1026.

Herbig, U., Jobling, W.A., Chen, B.P.C., Chen, D.J., and Sedivy, J.M. (2004). Telomere shortening triggers senescence of human cells through a pathway involving ATM, p53, and p21(CIP1), but not p16(INK4a). Mol. Cell *14*, 501–513.

Herranz, N., Gallage, S., Mellone, M., Wuestefeld, T., Klotz, S., Hanley, C.J., Raguz, S., Acosta, J.C., Innes, A.J., Banito, A., et al. (2015). mTOR regulates MAPKAPK2 translation to control the senescence-associated secretory phenotype. Nat. Cell Biol. *17*, 1205–1217.

Hiroaki, I., Jiahuai, H., and Huyuki, I. (2003). Mitogen-activated protein kinase p38 defines the

common senescence-signalling pathway. Genes to Cells *8*, 131–134.

Hnisz, D., Abraham, B.J., Lee, T.I., Lau, A., Saint-André, V., Sigova, A.A., Hoke, H.A., and Young, R.A. (2013). XSuper-enhancers in the control of cell identity and disease. Cell *155*.

Hoare, M., Ito, Y., Kang, T.-W., Weekes, M.P., Matheson, N.J., Patten, D.A., Shetty, S., Parry, A.J., Menon, S., Salama, R., et al. (2016). NOTCH1 mediates a switch between two distinct secretomes during senescence. Nat. Cell Biol. *18*.

Hochegger, H., Fukushima, T., Morrison, C., Sonoda, E., Zhao, G.Y., Saberi, A., Masutani, M., Adachi, N., Koyama, H., Murcia, G. De, et al. (2006). Parp-1 protects homologous recombination from interference by Ku and Ligase IV in vertebrate cells. *25*, 1305–1314.

Hoenicke, L., and Zender, L. (2012). Immune surveillance of senescent cells-biological significance in cancer-and non-cancer pathologies. Carcinogenesis *33*, 1123–1126.

Hopkins, T.A., Ainsworth, W.B., Ellis, P.A., Donawho, C.K., DiGiammarino, E.L., Panchal, S.C., Abraham, V.C., Algire, M.A., Shi, Y., Olson, A.M., et al. (2018). PARP1 trapping by PARP inhibitors drives cytotoxicity both in cancer cells and healthy bone marrow. Mol. Cancer Res. *12*, molcanres.0138.2018.

Hottiger, M.O. (2015). Nuclear ADP-Ribosylation and Its Role in Chromatin Plasticity, Cell Differentiation, and Epigenetics. Annu Rev Biochem *84*, 227–263.

Houssaini, A., Breau, M., Kebe, K., Abid, S., Marcos, E., Lipskaia, L., Rideau, D., Parpaleix, A., Huang, J., Amsellem, V., et al. (2018). mTOR pathway activation drives lung cell senescence and emphysema. JCI Insight *3*, 1–20.

Huletsky, A., Niedergang, C., Fréchette, A., Aubin, R., Gaudreau, A., and Poirier, G.G. (1985). Sequential ADP-ribosylation pattern of nucleosomal histones. ADP-ribosylation of nucleosomal histones. Eur. J. Biochem. *146*, 277–285.

Huletsky, A., de Murcia, G., Muller, S., Hengartner, M., Menard, L., Lamarre, D., and Poirier, G.G. (1989). The Effect of Poly(ADP-ribosyl)ation on Native and H1-depleted Chromatin. J. Biol. Chem. *264*, 8878–8886.

Hurtado-Bagès, S., Guberovic, I., and Buschbeck, M. (2018). The MacroH2A1.1 – PARP1 Axis at the Intersection Between Stress Response and Metabolism. Front. Genet. *9*, 417.

Imai, S., and Guarente, L. (2016). It takes two to tango: NAD+ and sirtuins in aging/longevity control. Npj Aging Mech. Dis. *2*, 16017.

Itahana, K., Zou, Y., Itahana, Y., Martinez, J.-L., Beausejour, C., Jacobs, J.J.L., van Lohuizen, M., Band, V., Campisi, J., and Dimri, G.P. (2003). Control of the Replicative Life Span of Human Fibroblasts by p16 and the Polycomb Protein Bmi-1. Mol. Cell. Biol. *23*, 389–401.

Itahana, K., Campisi, J., and Dimri, G.P. (2007). Methods to detect biomarkers of cellular senescence: the senescence-associated beta-galactosidase assay. Methods Mol. Biol. *371*, 21–31.

Ito, S., Araya, J., Kurita, Y., Kobayashi, K., Takasaka, N., Yoshida, M., Hara, H., Minagawa, S., Wakui, H., Fujii, S., et al. (2015). PARK2-mediated mitophagy is involved in regulation of

HBEC senescence in COPD pathogenesis. Autophagy *11*, 547–559.

Ito, Y., Hoare, M., and Narita, M. (2017). Spatial and Temporal Control of Senescence. Trends Cell Biol *27*, 820–832.

Izhar, L., Adamson, B., Ciccia, A., Lewis, J., Pontano-Vaites, L., Leng, Y., Liang, A.C., Westbrook, T.F., Harper, J.W., and Elledge, S.J. (2015). A Systematic Analysis of Factors Localized to Damaged Chromatin Reveals PARP-Dependent Recruitment of Transcription Factors. Cell Rep. *11*, 1486–1500.

Jeon, O.H., Kim, C., Laberge, R.-M., Demaria, M., Rathod, S., Vasserot, A.P., Chung, J.W., Kim, D.H., Poon, Y., David, N., et al. (2017). Local clearance of senescent cells attenuates the development of post-traumatic osteoarthritis and creates a pro-regenerative environment. Nat. Med. 1–9.

Jeyapalan, J.C., Ferreira, M., Sedivy, J.M., and Herbig, U. (2007). Accumulation of senescent cells in mitotic tissue of aging primates. Mech. Ageing Dev. *128*, 36–44.

Johnson, D.G., and Walker, C.L. (1999). CYCLINS AND CELL CYCLE CHECKPOINTS. Annu. Rev. Pharmacol. Toxicol. *39*, 295–312.

Ju, B., Solum, D., Song, E.J., Lee, K., Rose, D.W., Glass, C.K., and Rosenfeld, M.G. (2004). TLE1 Corepressor Complex Mediates a CaMKinase II ʕ -Dependent Neurogenic Gene Activation Pathway. *119*, 815–829.

Jun, J. Il, and Lau, L.F. (2010). Cellular senescence controls fibrosis in wound healing. Aging (Albany. NY). *2*, 627–631.

Jung, S.H., Hwang, H.J., Kang, D., Park, H.A., Lee, H.C., Jeong, D., Lee, K., Park, H.J., Ko, Y.G., and Lee, J.S. (2019). mTOR kinase leads to PTEN-loss-induced cellular senescence by phosphorylating p53. Oncogene *38*, 1639–1650.

Kameshita, I., Matsuda, Z., Taniguchi, T., and Shizuta, Y. (1984). Poly (ADP-Ribose) Synthetase. *259*, 4770–4777.

Kameshita, I., Matsuda, M., Nishikimis, M., Ushiro, H., and Shizuta, Y. (1986). Reconstitution and Poly(ADP-ribosy1)ation of Proteolytically Fragmented Poly(ADP-Ribose) Synthetase*. *261*, 3863–3868.

Kang, C., Xu, Q., Martin, T.D., Li, M.Z., Demaria, M., Aron, L., Lu, T., Yankner, B.A., Campisi, J., and Elledge, S.J. (2015). The DNA damage response induces inflammation and senescence by inhibiting autophagy of GATA4. Science (80-.). *349*, aaa5612–aaa5612.

Kang, T.-W., Yevsa, T., Woller, N., Hoenicke, L., Wuestefeld, T., Dauch, D., Hohmeyer, A., Gereke, M., Rudalska, R., Potapova, A., et al. (2011). Senescence surveillance of pre-malignant hepatocytes limits liver cancer development. Nature *479*, 547–551.

Kaplon, J., Zheng, L., Meissl, K., Chaneton, B., Selivanov, V. a, Mackay, G., van der Burg, S.H., Verdegaal, E.M.E., Cascante, M., Shlomi, T., et al. (2013). A key role for mitochondrial gatekeeper pyruvate dehydrogenase in oncogene-induced senescence. Nature *498*, 109–112.

Karlseder, J., Hoke, K., Mirzoeva, O.K., Bakkenist, C., Kastan, M.B., Petrini, J.H.J., and Lange,

T. de (2004). The Telomeric Protein TRF2 Binds the ATM Kinase and Can Inhibit the ATM-Dependent DNA Damage Response. PLoS Biol. *2*, e240.

Kassner, I., Andersson, A., Fey, M., Tomas, M., Ferrando-May, E., and Hottiger, M.O. (2013). SET7/9-dependent methylation of ARTD1 at K508 stimulates poly-ADP-ribose formation after oxidative stress. Open Biol. *3*, 120173.

Katsuumi, G., Shimizu, I., Yoshida, Y., and Minamino, T. (2018). Vascular Senescence in Cardiovascular and Metabolic Diseases. Front. Cardiovasc. Med. *5*, 1–13.

Kauppinen, T.M., Chan, W.Y., Suh, S.W., Wiggins, A.K., Huang, E.J., and Swanson, R.A. (2006). Direct phosphorylation and regulation of poly (ADP-ribose) polymerase-1 by extracellular signal-regulated kinases 1 2. *6*.

Kawahara, T.L.A., Michishita, E., Adler, A.S., Damian, M., Berber, E., Lin, M., McCord, R.A., Ongaigui, K.C.L., Boxer, L.D., Chang, H.Y., et al. (2009). SIRT6 Links Histone H3 Lysine 9 Deacetylation to NF-κB-Dependent Gene Expression and Organismal Life Span. Cell *136*, 62–74.

Kawaichi, M., Ueda, K., and Hayaishi, O. (1981). Multiple autopoly(ADP-ribosyl)ation of rat liver poly(ADP-ribose) synthetase. Mode of modification and properties of automodified synthetase. J. Biol. Chem. *256*, 9483–9489.

Kennedy, B.K., Berger, S.L., Brunet, A., Campisi, J., Cuervo, A.M., Epel, E.S., Franceschi, C., Lithgow, G.J., Morimoto, R.I., Pessin, J.E., et al. (2014). Geroscience: Linking Aging to Chronic Disease. Cell *159*, 709–713.

Khoury-haddad, H., Guttmann-raviv, N., Ipenberg, I., Huggins, D., and Jeyasekharan, A.D. (2014). PARP1-dependent recruitment of KDM4D histone demethylase to DNA damage sites promotes double-strand break repair.

Kiehlbauch, C.C., Aboul-Ela, N., Jacobson, E.L., Ringer, D.P., and Jacobson, M.K. (1993). High resolution fractionation and characterization of ADP-ribose polymers. Anal. Biochem. *208*, 26–34.

Kim, K.S., Kim, M.-S., Seu, Y.B., Chung, H.Y., Kim, J.H., and Kim, J.-R. (2007). Regulation of replicative senescence by insulin-like growth factor-binding protein 3 in human umbilical vein endothelial cells. Aging Cell *6*, 535–545.

Kim, M.Y., Mauro, S., Gévry, N., Lis, J.T., and Kraus, W.L. (2004). NAD+-Dependent Modulation of Chromatin Structure and Transcription by Nucleosome Binding Properties of PARP-1. Cell *119*, 803–814.

Kim, M.Y., Zhang, T., and Kraus, W.L. (2005). Poly (ADP-ribosyl) ation by PARP-1 : ‘ PAR-laying ’ NAD + into a nuclear signal. 1951–1967.

Kind, J., Pagie, L., De Vries, S.S., Nahidiazar, L., Dey, S.S., Bienko, M., Zhan, Y., Lajoie, B., De Graaf, C.A., Amendola, M., et al. (2015). Genome-wide Maps of Nuclear Lamina Interactions in Single Human Cells. Cell *163*, 134–147.

Klement, K., and Goodarzi, A.A. (2014). DNA double strand break responses and chromatin alterations within the aging cell. Exp. Cell Res. *329*, 42–52.

Klemm, S.L., Shipony, Z., and Greenleaf, W.J. (2019). Chromatin accessibility and the regulatory epigenome. Nat. Rev. Genet. *20*, 207–220.

Kolthur-Seetharam, U., Dantzer, F., McBurney, M.W., Murcia1, G. de, and Sassone-Corsi, P. (2006). Control of AIF-mediated Cell Death by the Functional Interplay of SIRT1 and PARP-1 in Response to DNA Damage. Cell Cycle *5*, 873–877.

Kortlever, R.M., Higgins, P.J., and Bernards, R. (2006). Plasminogen activator inhibitor-1 is a critical downstream target of p53 in the induction of replicative senescence. Nat. Cell Biol. *8*, 877–884.

Kotake, Y., Nakagawa, T., Kitagawa, K., Suzuki, S., Liu, N., Kitagawa, M., and Xiong, Y. (2011). Long non-coding RNA ANRIL is required for the PRC2 recruitment to and silencing of p15(INK4B) tumor suppressor gene. Oncogene *30*, 1956–1962.

Kraus, W.L., and Hottiger, M.O. (2013). PARP-1 and gene regulation: Progress and puzzles. Mol. Aspects Med. *34*, 1109–1123.

Kraus, W.L., and Lis, J.T. (2003). PARP goes transcription. Cell *113*, 677–683.

Krishnakumar, R., and Kraus, W.L. (2010a). PARP-1 Regulates Chromatin Structure and Transcription through a KDM5B-Dependent Pathway. Mol. Cell *39*, 736–749.

Krishnakumar, R., and Kraus, W.L. (2010b). The PARP Side of the Nucleus: Molecular Actions, Physiological Outcomes, and Clinical Targets. Mol. Cell *39*, 8–24.

Krtolica, A., Parrinello, S., Lockett, S., Desprez, P.-Y., and Campisi, J. (2001). Senescent fibroblasts promote epithelial cell growth and tumorigenesis: A link between cancer and aging. Proc. Natl. Acad. Sci. *98*, 12072–12077.

Kuchay, S., Giorgi, C., Simoneschi, D., Pagan, J., Missiroli, S., Saraf, A., Florens, L., Washburn, M.P., Collazo-Lorduy, A., Castillo-Martin, M., et al. (2017). PTEN counteracts FBXL2 to promote IP3R3- and Ca2+-mediated apoptosis limiting tumour growth. Nature *546*, 554–558.

Kuilman, T., and Peeper, D.S. (2009). Senescence-messaging secretome: SMS-ing cellular stress. Nat. Rev. Cancer *9*, 81–94.

Kuilman, T., Michaloglou, C., Vredeveld, L.C.W., Douma, S., van Doorn, R., Desmet, C.J., Aarden, L.A., Mooi, W.J., and Peeper, D.S. (2008). Oncogene-induced senescence relayed by an interleukin-dependent inflammatory network. Cell *133*, 1019–1031.

Kuilman, T., Michaloglou, C., Mooi, W.J., and Peeper, D.S. (2010). The essence of senescence. Genes Dev. *24*, 2463–2479.

Kumari, S.R., Mendoza-alvarez, H., and Alvarez-gonzalez, R. (1998). Apoptosis following DNA Damage : Covalent Poly (ADP-ribosyl) ation of p53 by Exogenous PARP and Noncovalent Binding of p53 to the Mr 85 , 000. 5075–5078.

Langelier, M.F., Servent, K.M., Rogers, E.E., and Pascal, J.M. (2008). A third zinc-binding domain of human poly(ADP-ribose) polymerase-1 coordinates DNA-dependent enzyme activation. J. Biol. Chem. *283*, 4105–4114.

Lascaris, R.F., Groot, E., Hoen, P.B., Mager, W.H., and Planta, R.J. (2000). Different roles for Abf1p and a T-rich promoter element in nucleosome organization of the yeast RPS28A gene. Nucleic Acids Res. *28*, 1390–1396.

Lee, B.Y., Han, J.A., Im, J.S., Morrone, A., Johung, K., Goodwin, E.C., Kleijer, W.J., DiMaio, D., and Hwang, E.S. (2006). Senescence-associated β-galactosidase is lysosomal β-galactosidase. Aging Cell *5*, 187–195.

Leite de Oliveira, R., and Bernards, R. (2018). Anti-cancer therapy: senescence is the new black. EMBO J. *37*, e99386.

Leung, A.K.L. (2017). SERious Surprises for ADP-Ribosylation Specificity: HPF1 Switches PARP1 Specificity to Ser Residues. Mol. Cell *65*, 777–778.

Li, E., Bestor, T.H., and Jaenisch, R. (1992). Targeted mutation of the DNA methyltransferase gene results in embryonic lethality. Cell *69*, 915–926.

Li, J., Bonkowski, M.S., Moniot, S., Zhang, D., Hubbard, B.P., Ling, A.J.Y., Rajman, L.A., Qin, B., Lou, Z., Gorbunova, V., et al. (2017). A conserved NAD + binding pocket that regulates protein-protein interactions during aging. Science (80-.). *355*.

Li, M., You, L., Xue, J., and Lu, Y. (2018). Ionizing Radiation-Induced Cellular Senescence in Normal, Non-transformed Cells and the Involved DNA Damage Response: A Mini Review. Front. Pharmacol. *9*, 522.

Lin, H.-K., Chen, Z., Wang, G., Nardella, C., Lee, S.-W., Chan, C.-H., Yang, W.-L., Wang, J., Egia, A., Nakayama, K.I., et al. (2010). Skp2 targeting suppresses tumorigenesis by Arf-p53-independent cellular senescence. Nature *464*, 374–379.

Liu, D., and Hornsby, P.J. (2007). Senescent Human Fibroblasts Increase the Early Growth of Xenograft Tumors via Matrix Metalloproteinase Secretion. Cancer Res. *67*, 3117–3126.

Liu, F.-J., Wen, T., and Liu, L. (2012). MicroRNAs as a novel cellular senescence regulator. Ageing Res. Rev. *11*, 41–50.

Liu, J., Ben, Q., Lu, E., He, X., Yang, X., Ma, J., Zhang, W., Wang, Z., Liu, T., Zhang, J., et al. (2018a). Long noncoding RNA PANDAR blocks CDKN1A gene transcription by competitive interaction with p53 protein in gastric cancer. Cell Death Dis. *9*, 168.

Liu, X., Ding, J., and Meng, L. (2018b). Oncogene-induced senescence: a double edged sword in cancer. Acta Pharmacol. Sin. *39*, 1553–1558.

Liu, Z., Kraus, W.L., Liu, Z., and Kraus, W.L. (2017). Catalytic-Independent Functions of PARP-1 Determine Sox2 Pioneer Activity at Intractable Genomic Loci Article Catalytic-Independent Functions of PARP-1 Determine Sox2 Pioneer Activity at Intractable Genomic Loci. Mol. Cell *65*, 589-603.e9.

Lönn, P., van der Heide, L.P., Dahl, M., Hellman, U., Heldin, C.H., and Moustakas, A. (2010). PARP-1 attenuates smad-mediated transcription. Mol. Cell *40*, 521–532.

Lonskaya, I., Potaman, V.N., Shlyakhtenko, L.S., Oussatcheva, E.A., Lyubchenko, Y.L., and Soldatenkov, V.A. (2005). Regulation of Poly (ADP-ribose) Polymerase-1 by DNA Structure-

specific Binding * □. *280*, 17076–17083.

López-otín, C., Blasco, M.A., Partridge, L., and Serrano, M. (2013). The Hallmarks of Aging (copy without figures, can't seem to remove). *153*, 1194–1217.

López-Otín, C., Blasco, M.A., Partridge, L., Serrano, M., and Kroemer, G. (2013). The Hallmarks of Aging. Cell *153*, 1194–1217.

Lord, C.J., Tutt, A.N.J., and Ashworth, A. (2015). Synthetic lethality and cancer therapy: lessons learned from the development of PARP inhibitors. Annu. Rev. Med. *66*, 455–470.

Ludwig, A., Behnke, B., Holtlund, J., and Hilz, H. (1988). Immunoquantitation and size determination of intrinsic poly(ADP-ribose) polymerase from acid precipitates. An analysis of the in vivo status in mammalian species and in lower eukaryotes. J. Biol. Chem. *263*, 6993–6999.

Luijsterburg, M.S., Lindh, M., Acs, K., Vrouwe, M.G., Pines, A., van Attikum, H., Mullenders, L.H., and Dantuma, N.P. (2012). DDB2 promotes chromatin decondensation at UV-induced DNA damage. J. Cell Biol. *197*, 267–281.

Luijsterburg, M.S., de Krijger, I., Wiegant, W.W., Shah, R.G., Smeenk, G., de Groot, A.J.L., Pines, A., Vertegaal, A.C.O., Jacobs, J.J.L., Shah, G.M., et al. (2016). PARP1 Links CHD2-Mediated Chromatin Expansion and H3.3 Deposition to DNA Repair by Non-homologous End-Joining. Mol. Cell *61*, 547–562.

Lujambio, A., Akkari, L., Simon, J., Grace, D., Tschaharganeh, D.F., Bolden, J.E., Zhao, Z., Thapar, V., Joyce, J.A., Krizhanovsky, V., et al. (2013). Non-cell-autonomous tumor suppression by p53. Cell *153*, 449–460.

Luo, X., Ryu, K.W., Kim, D.S., Nandu, T., Medina, C.J., Gupte, R., Gibson, B.A., Soccio, R.E., Yu, Y., Gupta, R.K., et al. (2017). PARP-1 Controls the Adipogenic Transcriptional Program by PARylating C/EBPβ and Modulating Its Transcriptional Activity. Mol. Cell *65*, 260–271.

Mabley, J.G., Németh, Z.H., Pacher, P., Deitch, E.A., and Szabó, C. (2002). Poly (ADP-ribose) Polymerase is a Regulator of Chemokine Production : Relevance for the Pathogenesis of Shock and Inflammation. *8*, 283–289.

Mahmoudi, S., and Brunet, A. (2012). Aging and reprogramming: a two-way street. Curr. Opin. Cell Biol. *24*, 744–756.

Malanga, M., and Althauss, F.R. (1994). THE JOURNAL OF BIOUICICAL CHEMISTRY Poly(ADP-ribose) Molecules Formed during DNA Repair in Vivo*. *269*, 17691–17696.

Marintchev, A., Robertson, A., Dimitriadis, E.K., Prasad, R., Wilson, S.H., and Mullen, G.P. (2000). Domain specific interaction in the XRCC1 – DNA polymerase β complex. *28*, 2049–2059.

Martin, N., Schwamborn, K., Schreiber, V., Werner, A., Guillier, C., Zhang, X.-D., Bischof, O., Seeler, J.-S., and Dejean, A. (2009). PARP-1 transcriptional activity is regulated by sumoylation upon heat shock. EMBO J. *28*, 3534–3548.

Martinez-Zamudio, R., and Ha, H.C. (2012). Histone ADP-Ribosylation Facilitates Gene

Transcription by Directly Remodeling Nucleosomes. Mol. Cell. Biol. *32*, 2490–2502.

Martínez-Zamudio, R.I. (2012). Histone ADP-ribosylation by Poly(ADP-ribose) Polymerase 1 (PARP1) Facilitates Inflammatory Gene Transcription by Directly Altering Nucleosome Structure.

Martínez-Zamudio, R.I., Robinson, L., Roux, P.F., and Bischof, O. (2017a). SnapShot: Cellular Senescence Pathways. Cell *170*, 816-816.e1.

Martínez-Zamudio, R.I., Robinson, L., Roux, P.F., and Bischof, O. (2017b). SnapShot: Cellular Senescence in Pathophysiology. Cell *170*, 1044-1044.e1.

Marzetti, E., Lees, H.A., Wohlgemuth, S.E., and Leeuwenburgh, C. (2009). Sarcopenia of aging: Underlying cellular mechanisms and protection by calorie restriction. BioFactors *35*, 28–35.

Masaoka, A., Gassman, N.R., Kedar, P.S., Prasad, R., Hou, E.W., Horton, J.K., Bustin, M., and Wilson, S.H. (2012). HMGN1 Protein Regulates Poly (ADP-ribose) Polymerase-1 (PARP-1) Self-PARylation in Mouse Fibroblasts *. *287*, 27648–27658.

Masutani, M., and Fujimori, H. (2013). Molecular Aspects of Medicine Poly (ADP-ribosyl) ation in carcinogenesis. Mol. Aspects Med. *34*, 1202–1216.

McClintock, D., Ratner, D., Lokuge, M., Owens, D.M., Gordon, L.B., Collins, F.S., and Djabali, K. (2007). The Mutant Form of Lamin A that Causes Hutchinson-Gilford Progeria Is a Biomarker of Cellular Aging in Human Skin. PLoS One *2*, e1269.

Mendelsohn, A.R., and Larrick, J. (2017). A NAD+/PARP1/SIRT1 axis in Aging. Rejuvenation Res. *20*, rej.2017.1980.

Ménissier de Murcia, J., Ricoul, M., Tartier, L., Niedergang, C., Huber, A., Dantzer, F., Schreiber, V., Amé, J.C., Dierich, A., LeMeur, M., et al. (2003). Functional interaction between PARP-1 and PARP-2 in chromosome stability and embryonic development in mouse. EMBO J. *22*, 2255–2263.

Mercola, M., Wang, X.F., Olsen, J., and Calame, K. (1983). Transcriptional enhancer elements in the mouse immunoglobulin heavy chain locus. Science *221*, 663–665.

Di Micco, R., Fumagalli, M., Cicalese, A., Piccinin, S., Gasparini, P., Luise, C., Schurra, C., Garre', M., Nuciforo, P.G., Bensimon, A., et al. (2006). Oncogene-induced senescence is a DNA damage response triggered by DNA hyper-replication. Nature *444*, 638–642.

Michaloglou, C., Vredeveld, L.C.W., Soengas, M.S., Denoyelle, C., Kuilman, T., Van Der Horst, C.M.A.M., Majoor, D.M., Shay, J.W., Mooi, W.J., and Peeper, D.S. (2005). BRAFE600-associated senescence-like cell cycle arrest of human naevi. Nature *436*, 720–724.

Milanovic, M., Fan, D.N.Y., Belenki, D., Däbritz, J.H.M., Zhao, Z., Yu, Y., Dörr, J.R., Dimitrova, L., Lenze, D., Monteiro Barbosa, I.A., et al. (2018). Senescence-associated reprogramming promotes cancer stemness. Nature *553*, 96–100.

Minaga, T., and Kun, E. (2011). Probable Helical Conformation of Poly(ADP-Ribose). *25*, 41–46.

Minamino, T., Orimo, M., Shimizu, I., Kunieda, T., Yokoyama, M., Ito, T., Nojima, A., Nabetani, A., Oike, Y., Matsubara, H., et al. (2009). A crucial role for adipose tissue p53 in the regulation of insulin resistance. Nat. Med. *15*, 1082–1087.

Minotti, R., Andersson, A., and Hottiger, M.O. (2015). ARTD1 suppresses interleukin 6 expression by repressing MLL1-dependent histone H3 trimethylation. Mol. Cell. Biol. *35*, MCB.00196-15.

Mirzayans, R., Andrais, B., Hansen, G., and Murray, D. (2012). Role of p16 INK4A in replicative senescence and DNA damage-induced premature senescence in p53-deficient human cells. Biochem. Res. Int. *2012*.

Miwa, M., Ishihara, M., Takishima, S., Takasuka, N., Maeda, M., Yamaizumi, Z., Sugimura, T., Yokoyama, S., and Miyazawa, T. (1981). The branching and linear portions of poly(adenosine diphosphate ribose) have the same alpha(1 leads to 2) ribose-ribose linkage. J. Biol. Chem. *256*, 2916–2921.

Moiseeva, O., Bourdeau, V., Roux, A., Deschenes-Simard, X., and Ferbeyre, G. (2009). Mitochondrial Dysfunction Contributes to Oncogene-Induced Senescence. Mol. Cell. Biol. *29*, 4495–4507.

Mosteiro, L., Pantoja, C., Alcazar, N., Marión, R.M., Chondronasiou, D., Rovira, M., Fernández-Marcos, P., Muñoz-Martin, M., Blanco-Aparicio, C., Pastor, J., et al. (2016a). Tissue damage and senescence provide critical signals for cellular reprogramming in vivo. Science (80-.). *354*.

Mosteiro, L., Pantoja, C., Alcazar, N., Marión, R.M., Chondronasiou, D., Rovira, M., Fernandez-Marcos, P.J., Muñoz-Martin, M., Blanco-Aparicio, C., Pastor, J., et al. (2016b). Tissue damage and senescence provide critical signals for cellular reprogramming in vivo. Science (80-.). *354*, aaf4445.

Mouchiroud, L., Houtkooper, R.H., Moullan, N., Katsyuba, E., Ryu, D., Canto, C., Mottis, A., Jo, Y., Viswanathan, M., Schoonjans, K., et al. (2013). The NAD + / Sirtuin Pathway Modulates Longevity through Activation of Mitochondrial UPR and FOXO Signaling.

Mumbach, M.R., Rubin, A.J., Flynn, R.A., Dai, C., Khavari, P.A., Greenleaf, W.J., and Chang, H.Y. (2016). HiChIP: Efficient and sensitive analysis of protein-directed genome architecture. BioRxiv 073619.

Muñoz-Espín, D., and Serrano, M. (2014). Cellular senescence: from physiology to pathology. Nat. Rev. Mol. Cell Biol. *15*, 482–496.

Muñoz-Espín, D., Cañamero, M., Maraver, A., Gómez-López, G., Contreras, J., Murillo-Cuesta, S., Rodríguez-Baeza, A., Varela-Nieto, I., Ruberte, J., Collado, M., et al. (2013). Programmed cell senescence during mammalian embryonic development. Cell *155*, 1104–1118.

Muñoz-Gámez, J.A., Martín-Oliva, D., Aguilar-Quesada, R., Cañuelo, A., Nuñez, M.I., Valenzuela, M.T., Ruiz De Almodóvar, J.M., De Murcia, G., and Oliver, F.J. (2005). PARP inhibition sensitizes p53-deficient breast cancer cells to doxorubicin-induced apoptosis. Biochem. J. *386*, 119–125.

Murawska, M., Hassler, M., Renkawitz-Pohl, R., Ladurner, A., and Brehm, A. (2011). Stress-Induced PARP Activation Mediates Recruitment of Drosophila Mi-2 to Promote Heat Shock Gene Expression. PLoS Genet. *7*, e1002206.

De murcia, G., Huletskyst, A., Lamarregli, D., Gaudreaugff, A., Pouyets, J., and Poirier, G.G. (1986). Modulation of Chromatin Superstructure Induced by Poly (ADP-ribose) Synthesis and Degradation *. *261*, 7011–7017.

Nacarelli, T., Lau, L., Fukumoto, T., Zundell, J., Fatkhutdinov, N., Wu, S., Aird, K.M., Iwasaki, O., Kossenkov, A. V, Schultz, D., et al. (2019). NAD+ metabolism governs the proinflammatory senescence-associated secretome. Nat. Cell Biol. *21*, 397–407.

Naegelis, H., and Althaust, F.R. (1991). Regulation of Poly(ADP-ribose) Polymerase. 10596–10601.

Nakajima, H., Nagaso, H., Kakui, N., Ishikawa, M., Hiranuma, T., and Hoshiko, S. (2004). Critical Role of the Automodification of Poly(ADP-ribose) Polymerase-1 in Nuclear Factor-κB-dependent Gene Expression in Primary Cultured Mouse Glial Cells. J. Biol. Chem. *279*, 42774–42786.

Nalabothula, N., Al-jumaily, T., Eteleeb, A.M., Flight, R.M., Xiaorong, S., Moseley, H., Rouchka, E.C., and Fondufe-Mittendorf, Y.N. (2015). Genome-Wide Profiling of PARP1 Reveals an Interplay with Gene Regulatory Regions and DNA Methylation. PLoS One *10*, e0135410.

Narita, M., Nũnez, S., Heard, E., Narita, M., Lin, A.W., Hearn, S.A., Spector, D.L., Hannon, G.J., and Lowe, S.W. (2003). Rb-mediated heterochromatin formation and silencing of E2F target genes during cellular senescence. Cell *113*, 703–716.

Narita, M., Narita, M., Krizhanovsky, V., Nuñez, S., Chicas, A., Hearn, S.A., Myers, M.P., and Lowe, S.W. (2006). A Novel Role for High-Mobility Group A Proteins in Cellular Senescence and Heterochromatin Formation. Cell *126*, 503–514.

Noren Hooten, N., Fitzpatrick, M., Kompaniez, K., Jacob, K.D., Moore, B.R., Nagle, J., Barnes, J., Lohani, A., and Evans, M.K. (2012). Coordination of DNA repair by NEIL1 and PARP-1: A possible link to aging. Aging (Albany. NY). *4*, 674–685.

Oei, S.L., Griesenbeck, J., Schweiger, M., Babich, V., Kropotov, A., and Tomilin, N. (1997). Interaction of the Transcription Factor YY1 with Human Poly(ADP-Ribosyl) Transferase. Biochem. Biophys. Res. Commun. *240*, 108–111.

Ohanna, M., Giuliano, S., Bonet, C., Imbert, V., Hofman, V., Zangari, J., Bille, K., Robert, C., Bressac-de Paillerets, B., Hofman, P., et al. (2011a). Senescent cells develop a PARP-1 and nuclear factor-{kappa}B-associated secretome (PNAS). Genes Dev. *25*, 1245–1261.

Ohanna, M., Giuliano, S., Bonet, C., Imbert, V., Hofman, V., Zangari, J., Bille, K., Robert, C., Bressac-de Paillerets, B., Hofman, P., et al. (2011b). Senescent cells develop a PARP-1 and nuclear factor- B-associated secretome (PNAS). Genes Dev. *25*, 1245–1261.

Olabisi, O.A., Soto-Nieves, N., Nieves, E., Yang, T.T.C., Yang, X., Yu, R.Y.L., Suk, H.Y., Macian, F., and Chow, C.-W. (2008). Regulation of Transcription Factor NFAT by ADP-Ribosylation. Mol. Cell. Biol. *28*, 2860–2871.

Oliver, F.J., Ménissier-de Murcia, J., Nacci, C., Decker, P., Andriantsitohaina, R., Muller, S., De La Rubia, G., Stoclet, J.C., and De Murcia, G. (1999). Resistance to endotoxic shock as a consequence of defective NF-κB activation in poly (ADP-ribose) polymerase-1 deficient mice. EMBO J. *18*, 4446–4454.

Olovnikov, A.M. (1971). [Principle of marginotomy in template synthesis of polynucleotides]. Dokl. Akad. Nauk SSSR *201*, 1496–1499.

Ong, C.-T., and Corces, V.G. (2012). Enhancers: emerging roles in cell fate specification. EMBO Rep. *13*, 423.

Orjalo, A. V., Bhaumik, D., Gengler, B.K., Scott, G.K., and Campisi, J. (2009). Cell surface-bound IL-1 is an upstream regulator of the senescence-associated IL-6/IL-8 cytokine network. Proc. Natl. Acad. Sci. *106*, 17031–17036.

Orsi, G.A., Kasinathan, S., Zentner, G.E., Henikoff, S., and Ahmad, K. (2015). Mapping regulatory factors by immunoprecipitation from native chromatin. Curr. Protoc. Mol. Biol. *2015*, 21.31.1-21.31.25.

Pacher, P., and Szabo, C. (2008). Role of the peroxynitrite-poly(ADP-ribose) polymerase pathway in human disease. Am. J. Pathol. *173*, 2–13.

Palmer, A.K., Tchkonia, T., LeBrasseur, N.K., Chini, E.N., Xu, M., and Kirkland, J.L. (2015). Cellular senescence in type 2 diabetes: A therapeutic opportunity. Diabetes *64*, 2289–2298.

Passos, J.F., Nelson, G., Wang, C., Richter, T., Simillion, C., Proctor, C.J., Miwa, S., Olijslagers, S., Hallinan, J., Wipat, A., et al. (2010a). Feedback between p21 and reactive oxygen production is necessary for cell senescence. Mol. Syst. Biol. *6*, 347.

Passos, J.F., Nelson, G., Wang, C., Richter, T., Simillion, C., Proctor, C.J., Miwa, S., Olijslagers, S., Hallinan, J., Wipat, A., et al. (2010b). Feedback between p21 and reactive oxygen production is necessary for cell senescence. Mol. Syst. Biol. *6*, 347.

Pavri, R., Lewis, B., Kim, T., Dilworth, F.J., Erdjument-bromage, H., Tempst, P., Murcia, G. De, Evans, R., Chambon, P., Reinberg, D., et al. (2005). PARP-1 Determines Specificity in a Retinoid Signaling Pathway via Direct Modulation of Mediator. *18*, 83–96.

Pearson, M., Carbone, R., Sebastiani, C., Cioce, M., Fagioli, M., Saito, S., Higashimoto, Y., Appella, E., Minucci, S., Pandolfi, P.P., et al. (2000). PML regulates p53 acetylation and premature senescence induced by oncogenic Ras. Nature *406*, 207–210.

Pedro de Magalhães, J., Chainiaux, F., de Longueville, F., Mainfroid, V., Migeot, V., Marcq, L., Remacle, J., Salmon, M., and Toussaint, O. (2004). Gene expression and regulation in H2O2-induced premature senescence of human foreskin fibroblasts expressing or not telomerase. Exp. Gerontol. *39*, 1379–1389.

Petesch, S.J., and Lis, J.T. (2008). Rapid, Transcription-Independent Loss of Nucleosomes over a Large Chromatin Domain at Hsp70 Loci. Cell *134*, 74–84.

Phillips-Cremins, J.E., and Corces, V.G. (2013). Chromatin insulators: linking genome organization to cellular function. Mol. Cell *50*, 461–474.

Piccolo, M.T., and Crispi, S. (2012). The Dual Role Played by p21 May Influence the Apoptotic or Anti-Apoptotic Fate in Cancer. 189–202.

Pinnola, A., Naumova, N., Shah, M., and Tulin, A. V (2007). Nucleosomal Core Histones Mediate Dynamic Regulation of Poly (ADP-ribose) Polymerase 1 Protein Binding to Chromatin and Induction of Its Enzymatic Activity * □. *282*, 32511–32519.

Pion, E., Ullmann, G.M., Amé, J.-C., Gérard, D., de Murcia, G., and Bombarda, E. (2005). DNA-Induced Dimerization of Poly(ADP-ribose) Polymerase-1 Triggers Its Activation †. Biochemistry *44*, 14670–14681.

Piskunova, T.S., Yurova, M.N., Ovsyannikov, A.I., Semenchenko, A. V, Zabezhinski, M.A., Popovich, I.G., Wang, Z., and Anisimov, V.N. (2008). Accelerates Aging and Spontaneous Carcinogenesis in Mice. *2008*.

Te Poele, R.H., Okorokov, A.L., Jardine, L., Cummings, J., and Joel, S.P. (2002). DNA damage is able to induce senescence in tumor cells in vitro and in vivo. Cancer Res. *62*, 1876–1883.

Poirier, G.G., de Murcia, G., Jongstra-Bilen, J., Niedergang, C., and Mandel, P. (1982). Poly(ADP-ribosyl)ation of polynucleosomes causes relaxation of chromatin structure. Proc. Natl. Acad. Sci. U. S. A. *79*, 3423–3427.

Pollex, T., and Heard, E. (2012). Recent advances in X-chromosome inactivation research. Curr. Opin. Cell Biol. *24*, 825–832.

Porro, A., Feuerhahn, S., Delafontaine, J., Riethman, H., Rougemont, J., and Lingner, J. (2014). Functional characterization of the TERRA transcriptome at damaged telomeres. Nat. Commun. *5*, 5379.

Puvvula, P.K., Desetty, R.D., Pineau, P., Marchio, A., Moon, A., Dejean, A., and Bischof, O. (2014a). Long noncoding RNA PANDA and scaffold-attachment-factor SAFA control senescence entry and exit. Nat. Commun. *5*, 5323.

Puvvula, P.K., Desetty, R.D., Pineau, P., Marchio, A., Moon, A., Dejean, A., and Bischof, O. (2014b). Long noncoding RNA PANDA and scaffold-attachment-factor SAFA control senescence entry and exit. Nat. Commun. *5*.

Quénet, D., Gasser, V., Fouillen, L., Cammas, F., Sanglier-Cianferani, S., Losson, R., and Dantzer, F. (2008). The histone subcode: poly(ADP-ribose) polymerase-1 (Parp-1) and Parp-2 control cell differentiation by regulating the transcriptional intermediary factor TIF1beta and the heterochromatin protein HP1alpha. FASEB J. *22*, 3853–3865.

Radman-Livaja, M., and Rando, O.J. (2010a). Nucleosome positioning: How is it established, and why does it matter? Dev. Biol. *339*, 258–266.

Rai, T.S., Cole, J.J., Nelson, D.M., Dikovskaya, D., Faller, W.J., Vizioli, M.G., Hewitt, R.N., Anannya, O., McBryan, T., Manoharan, I., et al. (2014). HIRA orchestrates a dynamic chromatin landscape in senescence and is required for suppression of neoplasia. Genes Dev. *28*, 2712–2725.

Rashid, K., Sundar, I.K., Gerloff, J., Li, D., and Rahman, I. (2018). Lung cellular senescence is independent of aging in a mouse model of COPD/emphysema. Sci. Rep. *8*, 1–14.

Ray Chaudhuri, A., and Nussenzweig, A. (2017). The multifaceted roles of PARP1 in DNA repair and chromatin remodelling. Nat. Rev. Mol. Cell Biol. *18*, 610–621.

Rentschler, M., Chen, Y., Pahl, J., Soria-Martinez, L., Braumüller, H., Brenner, E., Bischof, O., Röcken, M., and Wieder, T. (2018). Nuclear Translocation of Argonaute 2 in Cytokine-Induced Senescence. Cell. Physiol. Biochem. *51*, 1103–1118.

Ritschka, B., Storer, M., Mas, A., Heinzmann, F., Ortells, M.C., Morton, J.P., Sansom, O.J., Zender, L., and Keyes, W.M. (2017a). The senescence-associated secretory phenotype induces cellular plasticity and tissue regeneration. Genes Dev. *31*, 172–183.

Roberson, R.S., Kussick, S.J., Vallieres, E., Chen, S.-Y.J., and Wu, D.Y. (2005). Escape from Therapy-Induced Accelerated Cellular Senescence in p53-Null Lung Cancer Cells and in Human Lung Cancers. Cancer Res. *65*, 2795–2803.

Robu, M., Shah, R.G., Petitclerc, N., Brind'Amour, J., Kandan-Kulangara, F., and Shah, G.M. (2013). Role of poly(ADP-ribose) polymerase-1 in the removal of UV-induced DNA lesions by nucleotide excision repair. Proc. Natl. Acad. Sci. *110*, 1658–1663.

Rodier, F., Coppé, J.-P., Patil, C.K., Hoeijmakers, W.A.M., Muñoz, D.P., Raza, S.R., Freund, A., Campeau, E., Davalos, A.R., and Campisi, J. (2009). Persistent DNA damage signalling triggers senescence-associated inflammatory cytokine secretion. Nat. Cell Biol. *11*, 973–979.

Rodier, F., Muñoz, D.P., Teachenor, R., Chu, V., Le, O., Bhaumik, D., Coppé, J.-P., Campeau, E., Beauséjour, C.M., Kim, S.-H., et al. (2011). DNA-SCARS: distinct nuclear structures that sustain damage-induced senescence growth arrest and inflammatory cytokine secretion. J. Cell Sci. *124*, 68–81.

Rovillain, E., Mansfield, L., Lord, C.J., Ashworth, A., and Jat, P.S. (2011). An RNA interference screen for identifying downstream effectors of the p53 and pRB tumour suppressor pathways involved in senescence. BMC Genomics *12*, 355.

Ruiz, L., Traskine, M., Ferrer, I., Castro, E., Leal, J.F.M., Kaufman, M., and Carnero, A. (2008). Characterization of the p53 response to oncogene-induced senescene. PLoS One *3*.

Ruscetti, T., Lehnert, B.E., Halbrook, J., Trong, H. Le, Hoekstra, M.F., Chen, D.J., and Peterson, S.R. (1998). Stimulation of the DNA-dependent Protein Kinase by Poly (ADP-Ribose) Polymerase *. *273*, 14461–14467.

Ryu, K.W., Kim, D.S., and Kraus, W.L. (2015). New facets in the regulation of gene expression by ADP-ribosylation and poly(ADP-ribose) polymerases. Chem. Rev. *115*, 2453–2481.

Sagiv, A., and Krizhanovsky, V. (2013). Immunosurveillance of senescent cells: the bright side of the senescence program. Biogerontology.

Sakai, Y., Yamamori, T., Yoshikawa, Y., Bo, T., Suzuki, M., Yamamoto, K., Ago, T., and Inanami, O. (2018). NADPH oxidase 4 mediates ROS production in radiation-induced senescent cells and promotes migration of inflammatory cells. Free Radic. Res. *52*, 92–102.

Salama, R., Sadaie, M., Hoare, M., and Narita, M. (2014). Cellular senescence and its effector programs. 99–114.

Salminen, A., Kauppinen, A., and Kaarniranta, K. (2012). Emerging role of NF-κB signaling in the induction of senescence-associated secretory phenotype (SASP). Cell. Signal. *24*, 835–845.

Saxena, A., Wong, L.H., Kalitsis, P., Earle, E., Shaffer, L.G., and Choo, K.H.A. (2002). Poly(ADP-ribose) polymerase 2 localizes to mammalian active centromeres and interacts with PARP-1, Cenpa, Cenpb and Bub3, but not Cenpc. Hum. Mol. Genet. *11*, 2319–2329.

Schafer, M.J., White, T.A., Iijima, K., Haak, A.J., Ligresti, G., Atkinson, E.J., Oberg, A.L., Birch, J., Salmonowicz, H., Zhu, Y., et al. (2017). Cellular senescence mediates fibrotic pulmonary disease. Nat. Commun. *8*.

Schmitt, C.A., Fridman, J.S., Yang, M., Lee, S., Baranov, E., Hoffman, R.M., Lowe, S.W., and Diego, S. (2002). A Senescence Program Controlled by p53 and p16 INK4a Contributes to the Outcome of Cancer Therapy. *109*, 335–346.

Schmitt, E., Paquet, C., Beauchemin, M., and Bertrand, R. (2007). DNA-damage response network at the crossroads of cell-cycle checkpoints, cellular senescence and apoptosis. J. Zhejiang Univ. Sci. B *8*, 377–397.

Schmutz, I., and de Lange, T. (2016). Shelterin. Curr. Biol. *26*, R397–R399.

Schones, D.E., Cui, K., Cuddapah, S., Roh, T.Y., Barski, A., Wang, Z., Wei, G., and Zhao, K. (2008). Dynamic Regulation of Nucleosome Positioning in the Human Genome. Cell *132*, 887–898.

Schuhwerk, H., Bruhn, C., Siniuk, K., Min, W., Erener, S., Grigaravicius, P., Krüger, A., Ferrari, E., Zubel, T., Lazaro, D., et al. (2017). Kinetics of poly(ADP-ribosyl)ation, but not PARP1 itself, determines the cell fate in response to DNA damage in vitro and in vivo. Nucleic Acids Res. *45*.

Sen, P., Lan, Y., Li, C.Y., Sidoli, S., Donahue, G., Dou, Z., Frederick, B., Chen, Q., Luense, L.J., Garcia, B.A., et al. (2019). Histone Acetyltransferase p300 Induces De Novo Super-Enhancers to Drive Cellular Senescence. Mol. Cell *73*, 684-698.e8.

Senturk, S., Mumcuoglu, M., Gursoy-Yuzugullu, O., Cingoz, B., Akcali, K.C., and Ozturk, M. (2010). Transforming growth factor-beta induces senescence in hepatocellular carcinoma cells and inhibits tumor growth. Hepatology *52*, 966–974.

Serrano, M. (1997). MINIREVIEW The Tumor Suppressor Protein p16 INK4a. Exp. Cell Res. *13*, 7–13.

Serrano, M., Lin, A.W., McCurrach, M.E., Beach, D., and Lowe, S.W. (1997a). Oncogenic ras provokes premature cell senescence associated with accumulation of p53 and p16INK4a. Cell *88*, 593–602.

Serrano, M., Lin, A.W., McCurrach, M.E., Beach, D., and Lowe, S.W. (1997b). Oncogenic ras provokes premature cell senescence associated with accumulation of p53 and p16(INK4a). Cell *88*, 593–602.

Shah, P.P., Donahue, G., Otte, G.L., Capell, B.C., Nelson, D.M., Cao, K., Aggarwala, V., Cruickshanks, H. a, Rai, T.S., McBryan, T., et al. (2013). Lamin B1 depletion in senescent cells

triggers large-scale changes in gene expression and the chromatin landscape. Genes Dev. 1787–1799.

Shall, S., and de Murcia, G. (2000a). Poly(ADP-ribose) polymerase-1: what have we learned from the deficient mouse model? Mutat. Res. Repair *460*, 1–15.

Shall, S., and de Murcia, G. (2000b). Poly(ADP-ribose) polymerase-1: What have we learned from the deficient mouse model? Mutat. Res. - DNA Repair *460*, 1–15.

Sharpless, N.E., and DePinho, R.A. (2004). Telomeres, stem cells, senescence, and cancer. J. Clin. Invest. *113*, 160–168.

Sharpless, N.E., and Sherr, C.J. (2015). Forging a signature of in vivo senescence. Nat. Rev. Cancer *15*, 397–408.

Shay, J.W., Pereira-Smith, O.M., and Wright, W.E. (1991). A role for both RB and p53 in the regulation of human cellular senescence. Exp. Cell Res. *196*, 33–39.

Sherr, C.J., Depinho, R.A., and Hughes, H. (2000). Cellular Senescence: Mitotic Clock or Culture Shock? *102*, 407–410.

Shifera, A.S. (2010). The zinc finger domain of IKKγ (NEMO) protein in health and disease. J. Cell. Mol. Med. *14*, 2404–2414.

Shimura, T., Sasatani, M., Kawai, H., Kamiya, K., Kobayashi, J., Komatsu, K., and Kunugita, N. (2017). A comparison of radiation-induced mitochondrial damage between neural progenitor stem cells and differentiated cells. Cell Cycle *16*, 565–573.

Shivshankar, P., Brampton, C., Miyasato, S., Kasper, M., Thannickal, V.J., and Le Saux, C.J. (2012). Caveolin-1 Deficiency Protects from Pulmonary Fibrosis by Modulating Epithelial Cell Senescence in Mice. Am. J. Respir. Cell Mol. Biol. *47*, 28–36.

Shlyueva, D., Stampfel, G., and Stark, A. (2014). Transcriptional enhancers: from properties to genome-wide predictions. Nat. Rev. Genet. *15*, 272–286.

Simbulan-rosenthal, C.M., Rosenthal, D.S., Luo, R., and Smulson, M.E. (1999). Poly (ADP-ribosyl) ation of p53 during Apoptosis in Human Osteosarcoma Cells 1. 2190–2194.

Simbulan-Rosenthal, C.M., Ly, D.H., Rosenthal, D.S., Konopka, G., Luo, R., Wang, Z.Q., Schultz, P.G., and Smulson, M.E. (2000). Misregulation of gene expression in primary fibroblasts lacking poly(ADP-ribose) polymerase. Proc. Natl. Acad. Sci. U. S. A. *97*, 11274–11279.

Simbulan-Rosenthal, C.M., Rosenthal, D.S., Luo, R., Samara, R., Espinoza, L. a, Hassa, P.O., Hottiger, M.O., and Smulson, M.E. (2003). PARP-1 binds E2F-1 independently of its DNA binding and catalytic domains, and acts as a novel coactivator of E2F-1-mediated transcription during re-entry of quiescent cells into S phase. Oncogene *22*, 8460–8471.

Simbulan, C.M., Rosenthal, D.S., Luo, R., Samara, R., Jung, M., Dritschilo, A., Spoonde, A., and Smulson, M.E. (2001). Poly (ADP-ribosyl) ation of p53 In Vitro and In Vivo Modulates Binding to its DNA Consensus Sequence 1. *3*, 179–188.

Singh, H.R., Nardozza, A.P., Möller, I.R., Knobloch, G., Kistemaker, H.A.V., Hassler, M., Harrer, N., Blessing, C., Eustermann, S., Kotthoff, C., et al. (2017). A Poly-ADP-Ribose Trigger Releases the Auto-Inhibition of a Chromatin Remodeling Oncogene. Mol. Cell *68*, 860-871.e7.

Skene, P.J., and Henikoff, S. (2015). A simple method for generating highresolution maps of genome-wide protein binding. Elife *4*, 1–9.

Smeenk, G., Wiegant, W.W., Marteijn, J.A., Luijsterburg, M.S., Sroczynski, N., Costelloe, T., Romeijn, R.J., Pastink, A., Mailand, N., Vermeulen, W., et al. (2013). Poly(ADP-ribosyl)ation links the chromatin remodeler SMARCA5/SNF2H to RNF168-dependent DNA damage signaling. J. Cell Sci. *126*, 889–903.

Smith, J.A., and Martin, L. (1973). Do cells cycle? Proc. Natl. Acad. Sci. U. S. A. *70*, 1263–1267.

Smith, S., Giriat, I., Schmitt, A., and de Lange, T. (1998). Tankyrase, a Poly(ADP-Ribose) Polymerase at Human Telomeres. Science (80-.). *282*, 1484–1487.

Soto-Gamez, A., Quax, W.J., and Demaria, M. (2019). Regulation of Survival Networks in Senescent Cells: From Mechanisms to Interventions. J. Mol. Biol. *431*, 2629–2643.

Storer, M., Mas, A., Robert-Moreno, A., Pecoraro, M., Ortells, M.C., Di Giacomo, V., Yosef, R., Pilpel, N., Krizhanovsky, V., Sharpe, J., et al. (2013). XSenescence is a developmental mechanism that contributes to embryonic growth and patterning. Cell *155*, 1119–1130.

Stott, F.J., Bates, S., James, M.C., McConnell, B.B., Starborg, M., Brookes, S., Palmero, I., Ryan, K., Hara, E., Vousden, K.H., et al. (1998). The alternative product from the human CDKN2A locus, p14(ARF), participates in a regulatory feedback loop with p53 and MDM2. EMBO J. *17*, 5001–5014.

Strieter, R.M., Burdick, M.D., Mestas, J., Gomperts, B., Keane, M.P., and Belperio, J.A. (2006). Cancer CXC chemokine networks and tumour angiogenesis. Eur. J. Cancer *42*, 768–778.

Sun, X., Fu, K., Hodgson, A., Wier, E.M., and Wen, M.G. (2016). Sam68 Is Required for DNA Damage Responses via Regulating Poly (ADP-ribosyl) ation. 1–28.

Swanson, E.C., Manning, B., Zhang, H., and Lawrence, J.B. (2013). Higher-order unfolding of satellite heterochromatin is a consistent and early event in cell senescence. J. Cell Biol. *203*, 929–942.

Szabó, C., Lim, L.H.K., Cuzzocrea, S., Getting, S.J., Zingarelli, B., Flower, R.J., Salzman, A.L., and Perretti, M. (1997a). Inhibition of poly (ADP-ribose) Synthetase Attenuates Neutrophil Recruitment and Exerts Antiinflammatory Effects. *186*.

Szabó, C., Cuzzocrea, S., Zingarelli, B., Connor, M.O., and Salzman, A.L. (1997b). Endothelial Dysfunction in a Rat Model of Endotoxic Shock Importance of the Activation of Poly (ADP-ribose) Synthetase by Peroxynitrite. 723–735.

Tacutu, R., Budovsky, A., Yanai, H., and Fraifeld, V.E. (2011). Molecular links between cellular senescence, longevity and age-related diseases - a systems biology perspective. Aging (Albany. NY). *3*, 1178–1191.

Takahashi, A., Ohtani, N., and Hara, E. (2007). Irreversibility of cellular senescence: Dual roles of p16INK4a/Rb-pathway in cell cycle control. Cell Div. *2*, 1–5.

Takai, H., Smogorzewska, A., and de Lange, T. (2003). DNA damage foci at dysfunctional telomeres. Curr. Biol. *13*, 1549–1556.

Takemoto, S., Trovato, R., Cereseto, A., Nicot, C., Kislyakova, T., Casareto, L., Waldmann, T., Torelli, G., and Franchini, G. (2000). p53 stabilization and functional impairment in the absence of genetic mutation or the alteration of the p14(ARF)-MDM2 loop in ex vivo and cultured adult T-cell leukemia/lymphoma cells. Blood *95*, 3939–3944.

Tasdemir, N., Banito, A., Roe, J.-S., Alonso-Curbelo, D., Camiolo, M., Tschaharganeh, D.F., Huang, C.-H., Aksoy, O., Bolden, J.E., Chen, C.-C., et al. (2016). BRD4 Connects Enhancer Remodeling to Senescence Immune Surveillance. Cancer Discov. *6*, 612–629.

Teloni, F., and Altmeyer, M. (2016). Readers of poly (ADP-ribose): designed to be fit for purpose. *44*, 993–1006.

Teo, Y.V., Rattanavirotkul, N., Olova, N., Salzano, A., Quintanilla, A., Tarrats, N., Kiourtis, C., Müller, M., Green, A.R., Adams, P.D., et al. (2019). Notch Signaling Mediates Secondary Senescence. Cell Rep. *27*, 997-1007.e5.

Timinszky, G., Till, S., Hassa, P.O., Hothorn, M., Kustatscher, G., Nijmeijer, B., Colombelli, J., Altmeyer, M., Stelzer, E.H.K., Scheffzek, K., et al. (2009). A macrodomain-containing histone rearranges chromatin upon sensing PARP1 activation. Nat. Struct. Mol. Biol. *16*, 923–929.

Tsutsumi, M., Masutani, M., Nozaki, T., Kusuoka, O., Tsujiuchi, T., Nakagama, H., Suzuki, H., Konishi, Y., and Sugimura, T. (2001). Increased susceptibility of poly(ADP-ribose) polymerase-1 knockout mice to nitrosamine carcinogenicity. Carcinogenesis *22*, 1–3.

Tu, Z., Aird, K.M., and Zhang, R. (2013a). Chromatin remodeling, BRCA1, SAHF and cellular senescence. Cell Cycle *12*, 1653–1654.

Tu, Z., Zhuang, X., Yao, Y.-G., and Zhang, R. (2013b). BRG1 Is Required for Formation of Senescence-Associated Heterochromatin Foci Induced by Oncogenic RAS or BRCA1 Loss. Mol. Cell. Biol. *33*, 1819–1829.

Tulin, A., and Spradling, A. (2003a). Chromatin Loosening by Poly (ADP) -Ribose Polymerase (PARP) at Drosophila Puff Loci. *299*, 560–563.

Tutt, A., Robson, M., Garber, J.E., Domchek, S.M., Audeh, M.W., Weitzel, J.N., Friedlander, M., Arun, B., Loman, N., Schmutzler, R.K., et al. (2010). Oral poly(ADP-ribose) polymerase inhibitor olaparib in patients with BRCA1 or BRCA2 mutations and advanced breast cancer: a proof-of-concept trial. Lancet *376*, 235–244.

Uchida, C. (2016). Roles of pRB in the Regulation of Nucleosome and Chromatin Structures. Biomed Res. Int. *2016*, 1–11.

Valouev, A., Johnson, S.M., Boyd, S.D., Smith, C.L., Fire, A.Z., and Sidow, A. (2011). Determinants of nucleosome organization in primary human cells. Nature *474*, 516–520.

Vasudevan, K.M., Burikhanov, R., Goswami, A., and Rangnekar, V.M. (2007). Suppression of

PTEN Expression Is Essential for Antiapoptosis and Cellular Transformation by Oncogenic Ras. Cancer Res. *67*, 10343–10350.

Visel, A., Zhu, Y., May, D., Afzal, V., Gong, E., Attanasio, C., Blow, M.J., Cohen, J.C., Rubin, E.M., and Pennacchio, L.A. (2010). Targeted deletion of the 9p21 non-coding coronary artery disease risk interval in mice. Nature *464*, 409–412.

De Vos, M., El Ramy, R., Quénet, D., Wolf, P., Spada, F., Magroun, N., Babbio, F., Schreiber, V., Leonhardt, H., Bonapace, I.M., et al. (2014). Poly(ADP-ribose) polymerase 1 (parp1) associates with E3 ubiquitin-protein ligase UHRF1 and modulates UHRF1 biological functions. J. Biol. Chem. *289*, 16223–16238.

Vuong, B., Hogan-Cann, A.D.J., Alano, C.C., Stevenson, M., Chan, W.Y., Anderson, C.M., Swanson, R.A., and Kauppinen, T.M. (2015). NF-κB transcriptional activation by TNFα requires phospholipase C, extracellular signal-regulated kinase 2 and poly(ADP-ribose) polymerase-1. J. Neuroinflammation *12*, 229.

Vyas, S., Matic, I., Uchima, L., Rood, J., Zaja, R., Hay, R.T., Ahel, I., and Chang, P. (2014). Family-wide analysis of poly(ADP-ribose) polymerase activity. Nat. Commun. *5*, 4426.

Wajapeyee, N., Malonia, S.K., Palakurthy, R.K., and Green, M.R. Oncogenic RAS directs silencing of tumor suppressor genes through ordered recruitment of transcriptional repressors. 2221–2226.

Wallace, J.A., and Felsenfeld, G. (2008). NIH Public Access. *17*, 400–407.

Wang, L., and Bernards, R. (2018). Taking advantage of drug resistance, a new approach in the war on cancer. Front. Med. *12*, 490–495.

Wang, W., Chen, J.X., Liao, R., Deng, Q., Zhou, J.J., Huang, S., and Sun, P. (2002). Sequential Activation of the MEK-Extracellular Signal-Regulated Kinase and MKK3/6-p38 Mitogen-Activated Protein Kinase Pathways Mediates Oncogenic ras-Induced Premature Senescence. Mol. Cell. Biol. *22*, 3389–3403.

Wang, W., Yang, X., De Silanes, I.L., Carling, D., and Gorospe, M. (2003). Increased AMP:ATP ratio and AMP-activated protein kinase activity during cellular senescence linked to reduced HuR function. J. Biol. Chem. *278*, 27016–27023.

Wang, Y.L., Uhara, H., Yamazaki, Y., Nikaido, T., and Saida, T. (1996). Immunohistochemical detection of CDK4 and p16INK4 proteins in cutaneous malignant melanoma. Br. J. Dermatol. *134*, 269–275.

Wang, Z., Zang, C., Cui, K., Schones, D.E., Barski, A., Peng, W., and Zhao, K. (2009). Genome-wide mapping of HATs and HDACs reveals distinct functions in active and inactive genes. Cell *138*, 1019.

Wiley, C.D., and Campisi, J. (2016). From Ancient Pathways to Aging Cells—Connecting Metabolism and Cellular Senescence. Cell Metab. *23*, 1013–1021.

Wiley, C.D., Velarde, M.C., Lecot, P., Liu, S., Sarnoski, E.A., Freund, A., Shirakawa, K., Lim, H.W., Davis, S.S., Ramanathan, A., et al. (2016a). Mitochondrial dysfunction induces senescence with a distinct secretory phenotype. Cell Metab. *23*, 303–314.

Wiley, C.D., Velarde, M.C., Lecot, P., Liu, S., Sarnoski, E.A., Freund, A., Shirakawa, K., Lim, H.W., Davis, S.S., Ramanathan, A., et al. (2016b). Mitochondrial dysfunction induces senescence with a distinct secretory phenotype. Cell Metab. *23*, 303–314.

Williams, P.D., and Day, T. (2003). Antagonistic pleiotropy, mortality source interactions, and the evolutionary theory of senescence. Evolution (N. Y). *57*, 1478–1488.

Wong, M., and Smulson, M. (1984). A relationship between nuclear poly(adenosine diphosphate ribosylation) and acetylation posttranslational modifications. 2. Histone studies. Biochemistry *23*, 3726–3730.

Wong, M., Malik, N., and Smulson, M. (1982). The participation of poly(ADP-ribosyl)ated histone H1 in oligonucleosomal condensation. Eur. J. Biochem. *128*, 209–213.

Wu, X., Ellmann, S., Rubin, E., Gil, M., Jin, K., Han, L., Chen, H., Kwon, E.M., Guo, J., Ha, H.C., et al. (2012). ADP ribosylation by PARP-1 suppresses HOXB7 transcriptional activity. PLoS One *7*, 1–14.

Xia, Q., Lu, S., Ostrovsky, J., McCormack, S.E., Falk, M.J., Grant, S.F.A., Xia, Q., Lu, S., Ostrovsky, J., McCormack, S.E., et al. (2017). PARP-1 Inhibition Rescues Short Lifespan in Hyperglycemic C. Elegans And Improves GLP-1 Secretion in Human Cells. Aging Dis. *8*, 0.

Xu, M., Pirtskhalava, T., Farr, J.N., Weigand, B.M., Allyson, K., Weivoda, M.M., Inman, C.L., Ogrodnik, M.B., Christine, M., Fraser, D.G., et al. (2018). Senolytics Improve Physical Function and Increase Lifespan in Old Age. Nat. Med. *24*, 1246–1256.

Xue, W., Zender, L., Miething, C., Dickins, R.A., Hernando, E., Krizhanovsky, V., Cordon-Cardo, C., and Lowe, S.W. (2007). Senescence and tumour clearance is triggered by p53 restoration in murine liver carcinomas. Nature *445*, 656–660.

Yamanaka, H., Penning, C.A., Willis, E.H., Wasson, D.B., and Carson, D.A. (1988a). Characterization of human poly(ADP-ribose) polymerase with autoantibodies. J. Biol. Chem. *263*, 3879–3883.

Yamanaka, H., Penning, C.A., Willis, E.H., Wasson, D.B., and Carson, D.A. (1988b). Characterization of human poly(ADP-ribose) polymerase with autoantibodies. J. Biol. Chem. *263*, 3879–3883.

Yang, F., Tuxhorn, J.A., Ressler, S.J., McAlhany, S.J., Dang, T.D., and Rowley, D.R. (2005). Stromal Expression of Connective Tissue Growth Factor Promotes Angiogenesis and Prostate Cancer Tumorigenesis. Cancer Res. *65*, 8887–8895.

Yang, H., Wang, H., Ren, J., Chen, Q., and Chen, Z.J. (2017). cGAS is essential for cellular senescence. Proc. Natl. Acad. Sci. *114*, E4612–E4620.

Yosef, R., Pilpel, N., Papismadov, N., Gal, H., Ovadya, Y., Vadai, E., Miller, S., Porat, Z., Ben-Dor, S., and Krizhanovsky, V. (2017). p21 maintains senescent cell viability under persistent DNA damage response by restraining JNK and caspase signaling. EMBO J. *36*, 2280–2295.

Young, A.R.J., and Narita, M. (2009). SASP reflects senescence. EMBO Rep. *10*, 228–230.

Young, A.P., Schlisio, S., Minamishima, Y.A., Zhang, Q., Li, L., Grisanzio, C., Signoretti, S., and Kaelin, W.G. (2008). VHL loss actuates a HIF-independent senescence programme mediated by Rb and p400. Nat. Cell Biol. *10*, 361–369.

Yu, W., Ginjala, V., Pant, V., Chernukhin, I., Whitehead, J., Docquier, F., Farrar, D., Tavoosidana, G., Mukhopadhyay, R., Kanduri, C., et al. (2004). Poly (ADP-ribosyl) ation regulates CTCF-dependent chromatin insulation. *36*, 1105–1110.

Zampieri, M., Guastafierro, T., Calabrese, R., Ciccarone, F., Bacalini, M.G., Reale, A., Perilli, M., Passananti, C., and Caiafa, P. (2012). methylation of Ctcf target sites. *652*, 645–652.

Zamudio, R.I.M., Roux, P.-F., Freitas, J.A., Robinson, L., Dore, G., Sun, B., Gil, J., Herbig, U., and Bischof, O. (2019). AP-1 Imprints a Reversible Transcriptional Program of Senescent Cells. BioRxiv 633594.

Zaniolo, K., Desnoyers, S., Leclerc, S., and Guérin, S.L. (2007). Regulation of poly(ADP-ribose) polymerase-1 (PARP-1) gene expression through the post-translational modification of Sp1: A nuclear target protein of PARP-1. BMC Mol. Biol. *8*, 1–18.

Zhang, J., and Snyder, S.H. (1992). Nitric oxide stimulates auto-ADP-ribosylation of glyceraldehyde-3-phosphate dehydrogenase. Proc. Natl. Acad. Sci. *89*, 9382–9385.

Zhang, R., Poustovoitov, M. V., Ye, X., Santos, H.A., Chen, W., Daganzo, S.M., Erzberger, J.P., Serebriiskii, I.G., Canutescu, A.A., Dunbrack, R.L., et al. (2005). Formation of macroH2A-containing senescence-associated heterochromatin foci and senescence driven by ASF1a and HIRA. Dev. Cell *8*, 19–30.

Zhao, X., Li, D., Huang, D., Song, H., Mei, H., Fang, E., Wang, X., Yang, F., Zheng, L., Huang, K., et al. (2018). Risk-Associated Long Noncoding RNA FOXD3-AS1 Inhibits Neuroblastoma Progression by Repressing PARP1-Mediated Activation of CTCF. Mol. Ther. *26*, 755–773.

Zobeck, K.L., Buckley, M.S., Zipfel, W.R., and Lis, J.T. (2010). Recruitment Timing and Dynamics of Transcription Factors at the Hsp70 Loci in Living Cells. Mol. Cell *40*, 965–975.

8. Appendix

8.1 Contributions to Publications:

8.1.1 AP-1 Imprints a Reversible Transcriptional Program of Senescent Cells

bioRxiv preprint first posted online May. 9, 2019; doi: http://dx.doi.org/10.1101/633594. The copyright holder for this preprint (which was not peer-reviewed) is the author/funder, who has granted bioRxiv a license to display the preprint in perpetuity. All rights reserved. No reuse allowed without permission.

AP-1 Imprints a Reversible Transcriptional Program of Senescent Cells

Ricardo Iván Martínez-Zamudio[1,5,8], Pierre-François Roux[1,5], José Américo N L F de Freitas[1,4], Lucas Robinson[1,4], Gregory Doré[1], Bin Sun[6,7], Jesús Gil[6,7], Utz Herbig[8] and Oliver Bischof[1,2,3,9*]

[1] Institut Pasteur, Laboratory of Nuclear Organization and Oncogenesis, Department of Cell Biology and Infection, 75015 Paris, France

[2] INSERM, U993, 75015 Paris, France

[3] Equipe Labellisée Fondation ARC pour la recherche sur le cancer, Paris, France

[4] Université de Paris, Sorbonne Paris Cité, Paris, France

[5] These authors contributed equally to this work

[6] MRC London Institute of Medical Sciences (LMS), Du Cane Road, London, W12 0NN, UK.

[7] Institute of Clinical Sciences (ICS), Faculty of Medicine, Imperial College London, Du Cane Road, London W12 0NN, UK.

[8] Department of Microbiology, Biochemistry & Molecular Genetics, Rutgers Biomedical & Health Sciences, Rutgers University, 205 South Orange Avenue, Newark, NJ 07103, USA

[9] Lead contact

*Correspondence: oliver.bischof@pasteur.fr

bioRxiv preprint first posted online May. 9, 2019; doi: http://dx.doi.org/10.1101/633594. The copyright holder for this preprint (which was not peer-reviewed) is the author/funder, who has granted bioRxiv a license to display the preprint in perpetuity. All rights reserved. No reuse allowed without permission.

SUMMARY

Senescent cells play important physiological- and pathophysiological roles in tumor suppression, tissue regeneration, and aging. While select genetic and epigenetic elements crucial for senescence induction were identified, the dynamics, underlying epigenetic mechanisms, and regulatory networks defining senescence competence, induction and maintenance remain poorly understood, precluding a deliberate therapeutic manipulation of these dynamic processes. Here, we show, using dynamic analyses of transcriptome and epigenome profiles, that the epigenetic state of enhancers predetermines their sequential activation during senescence. We demonstrate that activator protein 1 (AP-1) 'imprints' the senescence enhancer landscape effectively regulating transcriptional activities pertinent to the timely execution of the senescence program. We define and validate a hierarchical transcription factor (TF) network model and demonstrate its effectiveness for the design of senescence reprogramming experiments. Together, our findings define the dynamic nature and organizational principles of gene-regulatory elements driving the senescence program and reveal promising inroads for therapeutic manipulation of senescent cells.

bioRxiv preprint first posted online May. 9, 2019; doi: http://dx.doi.org/10.1101/633594. The copyright holder for this preprint (which was not peer-reviewed) is the author/funder, who has granted bioRxiv a license to display the preprint in perpetuity. All rights reserved. No reuse allowed without permission.

INTRODUCTION

Cellular senescence plays beneficial roles during embryonic development, wound healing, and tumor suppression. Paradoxically, it is also considered a significant contributor to aging and age-related diseases including cancer and degenerative pathologies[1]. As such, research on therapeutic strategies exploiting senescence targeting (*e.g.*, senolytics, senomorphics or pro-senescence cancer therapies) to improve healthspan has gained enormous momentum in recent years[2].

Cellular senescence is a cell fate that stably arrests proliferation of damaged and dysfunctional cells as a complex stress response. The most prominent inducers of senescence are hyper-activated oncogenes (oncogene-induced senescence, OIS)[3]. The senescence arrest is accompanied by widespread changes in gene expression, including a senescence-associated secretory phenotype (SASP) – the expression and secretion of inflammatory cytokines, growth factors, proteases, and other molecules, which exert pleiotropic effects on senescent cells themselves as well as the surrounding tissue[4]. Importantly, although activation of the senescence program can pre-empt the initiation of cancer, the long-term effects of the SASP make the local tissue environment more vulnerable to the spread of cancer and other age-related diseases. Therefore, therapeutic interventions aimed at limiting SASP production are of relevance for cancer and many age-related diseases[4-6].

The knowledge on epigenetic mechanisms underlying senescence has only recently increased revealing significant contributions of select transcription factors (TFs), chromatin modifiers and structural components, as well as non-coding RNAs to the senescent phenotype[7-12]. A major limitation of such studies, however, was their restriction to start-end-point comparisons, ignoring the dynamic nature of the

bioRxiv preprint first posted online May. 9, 2019; doi: http://dx.doi.org/10.1101/633594. The copyright holder for this preprint (which was not peer-reviewed) is the author/funder, who has granted bioRxiv a license to display the preprint in perpetuity. All rights reserved. No reuse allowed without permission.

senescence fate transition. Consequently, critical gene-regulatory aspects of the execution and maintenance of the senescence state remain poorly understood. Therefore, an integrative, temporally resolved, multidimensional profiling approach is required to establish essential regulatory principles that govern this key biological decision-making process. Such knowledge would be instrumental both for identifying stage-specific senescence regulators and urgently needed specific biomarkers as well as control points in TF and gene regulatory networks, which would pave the way for a deliberate therapeutic manipulation of the senescence cell fate.

Enhancers are key genomic regions that drive cell fate transitions. The enhancer landscape is established during development by the concerted action of TF networks and chromatin modifiers[13]. The details on how this information converges in *cis* remain unclear, and we still lack valid organizational principles that explain the function of mammalian TF networks. In mammalian cells, enhancer elements are broadly divided into two major categories -active and poised. While active enhancers are characterized by the simultaneous presence of H3K4me1 together with H3K27ac and are associated with actively transcribed genes, only H3K4me1 marks poised enhancers, and their target genes are generally not expressed[14]. A subset of enhancers may also be activated *de novo* from genomic areas devoid of any TF binding and histone modifications. These latent or nascent enhancers serve an adaptive role in mediating stronger and faster gene expression upon cycles of repeated stimulation[15,16]. Recent evidence showed a role for enhancer remodeling in driving senescence-associated gene expression[11,12,17]. However, it is currently unknown which enhancer elements, epigenetic marks or TFs render cells competent to respond to senescence-inducing signals with precise timing and output. A thorough understanding of how senescence competence is

bioRxiv preprint first posted online May. 9, 2019; doi: http://dx.doi.org/10.1101/633594. The copyright holder for this preprint (which was not peer-reviewed) is the author/funder, who has granted bioRxiv a license to display the preprint in perpetuity. All rights reserved. No reuse allowed without permission.

established, realized and what defines it would allow for the prediction of a positive senescence engagement for example in pro-senescence cancer therapies[18].

Pioneer TFs are critical in establishing new cell fate competence by granting long-term chromatin access to non-pioneer factors and are also crucial determinants of cell identity through their opening and licensing of the enhancer landscape[19,20]. We can now reliably deduce pioneer and non-pioneer TF activity from chromatin accessibility data allowing for the hierarchization of TF function whereby pioneer TFs sit atop a TF binding hierarchy, recruiting non-pioneers such as settler and migrant TFs to gene-regulatory regions for optimal transcriptional output[21]. The pioneer TFs bestowing senescence potential have not been identified to date. However, their identification might be a pre-requisite for reprogramming or manipulation of senescent cells for future therapeutic benefit as was shown successfully for the reprogramming to adopt full stem cell identity[22].

In this study, we examined the possibility that the epigenetic state of enhancers could determine senescence cell fate. We explored this question by generating time-resolved transcriptomes and comprehensive epigenome profiles during oncogenic RAS-induced senescence. Through integrative analysis and further functional validation, we revealed novel and unexpected links between enhancer chromatin, TF recruitment, and senescence potential and defined the organizational principles of the TF network that drive the senescence program. Together, this allowed us to precisely manipulate the senescence phenotype with important therapeutic implications. Specifically, we show that the senescence program is predominantly encoded at the enhancer level and that the enhancer landscape is dynamically reshaped at each step of the senescence transition. Remarkably, we find that this process is pre-determined before senescence

bioRxiv preprint first posted online May. 9, 2019; doi: http://dx.doi.org/10.1101/633594. The copyright holder for this preprint (which was not peer-reviewed) is the author/funder, who has granted bioRxiv a license to display the preprint in perpetuity. All rights reserved. No reuse allowed without permission.

induction and AP-1 acts as a pioneer TF that 'premarks' prospective senescence enhancers to direct and localize the recruitment of other transcription factors into a hierarchical TF network that drives the senescence transcriptional program after induction. We also uncover a class of enhancers that retain an epigenomic memory after their inactivation during the senescence transition. These "remnant" enhancers lack traditional enhancer histone-modification marks but are instead "remembered" by AP-1 TF bookmarking for eventual future re-activation. Finally, functional perturbation of prospective senescence enhancers and AP-1 validated and underscored the importance of these entities for the timely execution of the senescence gene expression program and allowed for the precise reprogramming and reversal of the senescence cell fate.

bioRxiv preprint first posted online May. 9, 2019; doi: http://dx.doi.org/10.1101/633594. The copyright holder for this preprint (which was not peer-reviewed) is the author/funder, who has granted bioRxiv a license to display the preprint in perpetuity. All rights reserved. No reuse allowed without permission.

RESULTS

We employed time-series experiments on WI38 fibroblasts undergoing oncogene-induced senescence (OIS) using a tamoxifen-inducible ER: RASV12 expression system[23]. We determined global gene expression profiles by microarrays and mapped the full set of accessible chromatin sites by ATAC-seq[24] at 6-time points (0, 24, 48, 72, 96 and 144 h). Cells intended for ChIP-seq were crosslinked at 3-time-points (0, 72 and 144h) and used for profiling histone modifications including H3K4me1 (putative enhancers), H3K4me3 (promoters), H3K27ac (active enhancers and promoters) and H3K27me3 (polycomb repressed chromatin). From accessible chromatin regions determined by ATAC-seq we deduced TF binding dynamics and hierarchies (Figure 1A). For comparison, we included cells undergoing quiescence (Q) by serum withdrawal for up to 96h. Unlike senescence arrested cells, quiescence arrested cells can be triggered to re-enter the cell cycle upon serum addition. Q and OIS cells were validated using classical markers (Supplementary Figures 1A-B).

Multi-state establishment of the senescence transcriptional program

To identify and visualize dynamic gene expression patterns across the entire Q and RAS-OIS time-courses, we employed an unsupervised, self-organizing map (SOM) machine learning technique[25] (Figure 1B) and multidimensional scaling (MDS) (Figure 1C) to our transcriptome data sets. Remarkably, serum-deprived fibroblasts rapidly established a Q-specific gene expression program within 24 h after serum deprivation, which changed only marginally within the remainder of the time-course (Figure 1B, left column and Figure 1C), and mainly involves only up-regulated (Figure 1B, top right corner, red) and down-regulated (Figure 1B, bottom left corner, blue) genes. By

bioRxiv preprint first posted online May. 9, 2019; doi: http://dx.doi.org/10.1101/633594. The copyright holder for this preprint (which was not peer-reviewed) is the author/funder, who has granted bioRxiv a license to display the preprint in perpetuity. All rights reserved. No reuse allowed without permission.

contrast, fibroblasts undergoing RAS-OIS displayed dynamic gene expression trajectories that evolved steadily, both for up- (red) and down-regulated metagenes (blue) (Figures 1B, right column and Figure 1C). Thus, RAS-OIS, unlike Q, is highly dynamic and does not gyrate towards a stable transcriptome end state. To substantiate this further we calculated the diversity and specialization of transcriptomes and gene specificity[26] (Figure 1D) and performed a kernel density estimation analysis (Supplementary Figure 1C). These analyses demonstrated that RAS-OIS cells exhibit a temporally evolving increase in transcriptional diversity, whereas Q cells exhibit a temporally evolving, specific gene expression program. We conclude that the RAS-OIS cell fate is an open-ended succession of cell states rather than a fixed cell fate with a defined end-point, which is the current tenet. The apparent open-endedness and transcriptional diversity may provide a fertile soil for the eventual escape of pre-cancerous senescent cells as previously shown[27,28].

To further delineate the evolution of the RAS-OIS gene expression program, we next performed dynamic differential gene expression analysis on the Q and OIS datasets[29]. A total of 4,986 genes (corresponding to 2,931 up-regulated and 2,055 down-regulated genes) were differentially regulated in at least one-time point (with a minimal leading log2 fold-change of 1.2; $q=5*10^{-4}$) and partitioned into seven (I-VII) gene expression modules with distinct functional overrepresentation profiles in line with the senescence phenotype (Figures 1E-F and Figure S1D). The highly reproducible dynamics of gene expression during RAS-OIS transition suggest a high degree of preprogramming of this succession of cell states.

Cell-fate decisions are typically associated with stable changes in gene expression that shift the regulatory system from one steady state to the next[30]. In line

bioRxiv preprint first posted online May. 9, 2019; doi: http://dx.doi.org/10.1101/633594. The copyright holder for this preprint (which was not peer-reviewed) is the author/funder, who has granted bioRxiv a license to display the preprint in perpetuity. All rights reserved. No reuse allowed without permission.

with this, we found that proliferation-promoting genes of modules II and IV (E2F targets and G2M checkpoint) became increasingly repressed (*i.e.* senescence arrest), while pro-senescent SASP genes of modules VI and VII (*e.g.*, inflammatory and interferon response genes) became persistently induced (Figure 1F and Supplementary Figure 1E). Apoptosis-related genes of module III were repressed very early on in the time-course (within the first 24-48 hours during RAS-OIS induction), which is surprising given that apoptosis-resistance is considered a very late event in senescence (Figure 1F and Supplementary Figure 1E). This indicates that the commitment to senescence is a very early event made at the expense of apoptosis. Finally, we identified a set of genes in modules I and V that would have gone unnoticed in a traditional start-end-point analysis because they follow an "impulse"-like pattern. In these modules, transcript levels spiked-up (module V) or down (module I) following RAS-OIS induction, then sustained a new level, before transitioning to a new steady state, similar to the original levels (Figures 1E and Supplementary Figure 1E). These expression patterns support the notion that genes of module V play an active and vital role early in the transition to RAS-OIS, while genes in module I hold key regulators to maintain the proliferative fibroblast state.

Altogether, our investigation of transcriptome dynamics defined a modular organization and transcriptional diversity of the RAS-OIS gene expression program, providing a framework to unravel the gene-regulatory code underlying the senescence process.

bioRxiv preprint first posted online May. 9, 2019; doi: http://dx.doi.org/10.1101/633594. The copyright holder for this preprint (which was not peer-reviewed) is the author/funder, who has granted bioRxiv a license to display the preprint in perpetuity. All rights reserved. No reuse allowed without permission.

A dynamic enhancer program shapes the senescence transcriptome

Senescence cell fate involves a global remodeling of chromatin and specifically, the enhancer landscape[11,12]. An unanswered question, however, is how TFs and epigenetic modifications cooperatively shape a transcriptionally permissive enhancer landscape prior to gene activation to endow the cell with senescence potential.

To provide mechanistic insight into this question, we first comprehensively mapped genomic regulatory elements (*i.e.* putative enhancers, promoters and polycomb-repressed chromatin) during the transition of proliferating cells to RAS-OIS, profiling genome-wide histone modifications by ChIP-seq and transposon-accessible chromatin by ATAC-seq. To capture and quantify chromatin state dynamics we used ChromstaR (see Materials and Methods), which identified a total of sixteen chromatin states (Supplementary Figure 2A). The majority of the genome (≈80%) was, irrespective of the time-point, either devoid of any of the histone modifications analyzed (≈62%) or polycomb-repressed (≈18%). The fraction of the genome represented by active and accessible chromatin states (*i.e.*, enhancers and promoters) was comparably lower (≈20% combined). Chromatin state transitions occurred most prominently at enhancers, while promoters were only mildly affected (Figures 2A-B and Supplementary Figure 2A, arrows) congruent with previous results[11]. Unexpectedly, we found, however, that most of the enhancer activation, *i.e.* acquisition of H3K4me1 and H3K27ac, occurred *de novo* from unmarked chromatin at the T0-72 h and 72 h-144 h intervals, followed by the more stereotypical enhancer activation from a poised state (H3K4me1^{+} plus H3K27ac acquisition) and enhancer poising from the unmarked and polycomb-repressed state at the T0-72 h interval (acquisition of H3K4me1) (Figures 2A and -B). Thus, the regulatory

bioRxiv preprint first posted online May. 9, 2019; doi: http://dx.doi.org/10.1101/633594. The copyright holder for this preprint (which was not peer-reviewed) is the author/funder, who has granted bioRxiv a license to display the preprint in perpetuity. All rights reserved. No reuse allowed without permission.

landscape of senescence is largely predetermined by sequential enhancer activation from *de novo* and poised enhancers implying the existence of a prior imprint of past cell fate decisions.

The (in)activation chronology of enhancers was highly concordant with the temporal expression pattern of the nearest genes, indicating that most of these elements indeed function as *bona fide* enhancers (Supplementary Figure 2B). In line with this, correspondence analysis (CA) (Supplementary Figure 2C) revealed a strong correlation between gene expression modules (Figure 1E) and chromatin state transitions (Figure 2A). For example, globally up-regulated transcriptomic modules V, VI, VII projected proximally to chromatin state transitions involving enhancer activation congruent with the installation of the SASP. By contrast, dynamic enhancer inactivation associated with repressed transcriptomic modules (II, III, IV) congruent with installation of the senescence arrest. Finally, the oscillatory expression of genes in the module I associated with an equally oscillatory activation of its closest enhancers. Therefore, dynamic remodeling of the enhancer landscape reflects and defines the modular and dynamic nature of the RAS-OIS gene expression program.

We next addressed the question of which TFs are key drivers for the dynamic enhancer remodeling driving the senescence transcriptome. To this end, we first intersected ATAC-seq peaks with the identified enhancer coordinates (Figure 2A-B) and performed a motif over-representation test. This analysis identified AP-1 super-family members (cJUN, FOS, FOSL1, FOSL2, BATF) as well as AP-1-associated TFs ATF3 and ETS1 as the most enriched motifs at any given time-point, thus, hinting at a putative chromatin priming and pioneer function for these TFs (Supplementary Figure 2D). Because AP-1 TFs are essential and inducible downstream effectors for the RAS

bioRxiv preprint first posted online May. 9, 2019; doi: http://dx.doi.org/10.1101/633594. The copyright holder for this preprint (which was not peer-reviewed) is the author/funder, who has granted bioRxiv a license to display the preprint in perpetuity. All rights reserved. No reuse allowed without permission.

signaling pathway in cellular transformation[31] the possibility remains that the observed enrichment of AP-1 TFs at enhancers is strictly dependent on oncogenic RAS signaling *per se* and not a reflection of a specific pioneering role in the enhancer landscape independent of RAS signaling. We therefore performed the same analysis in cells undergoing replicative senescence (which is driven by loss of telomere integrity) and also in growth factor-deprived (and thus RAS signaling-muted) quiescent cells (Supplementary Figures 2E-F). In both cases, the AP-1 motif ascended as the predominant motif enriched at enhancers, thus, corroborating the notion that AP-1 TFs act as the universal pioneers imprinting the global as well as senescence-associated enhancer landscape.

To elaborate this further, we analyzed our time-resolved ATAC-seq data sets by adapting the "Protein Interaction Quantitation (PIQ)" algorithm, which was developed initially for DNAse-seq-based digital TF footprinting[21]. Importantly, PIQ allows for the functional hierarchization of TFs into pioneers, settlers, and migrants - whereby pioneer TFs bind nucleosome-compacted chromatin to initiate chromatin remodeling and to enable subsequent binding of non-pioneers (*i.e.*, settler and migrant TFs). PIQ segregated TFs into pioneers (*e.g.*, AP-1 TF family members), settlers (*e.g.*, NFY and RELA subunit of NF-κB) and migrants (*e.g.*, TF RAR family members and SREBF1) (Figure 2C). We confirmed this TF hierarchization by inspecting a selection of individual TF footprints for their adjacent nucleosomal positioning (Supplementary Figure 2G-I). AP-1 family member FOSL1, for example, bound to its cognate binding site despite the presence of strongly positioned flanking nucleosomes, as would be expected from a pioneer TF (Supplementary Figure 2G), while RELA binding required partial nucleosome

bioRxiv preprint first posted online May. 9, 2019; doi: http://dx.doi.org/10.1101/633594. The copyright holder for this preprint (which was not peer-reviewed) is the author/funder, who has granted bioRxiv a license to display the preprint in perpetuity. All rights reserved. No reuse allowed without permission.

displacement/chromatin opening, as would be expected for a settler TF (Supplementary Figure 2H), and SREBF1 bound to its cognate site in a near-nucleosome free context, as would be expected for a migrant TF (Supplementary Figure 2I). Importantly, there was a high correspondence between PIQ predictions and TF ChIP-seq profiling as exemplified for AP-1-members FOSL2 and cJUN, which we used as surrogate marks for bound AP-1 (which is typically a complex of JUN-JUN or JUN-FOS family member dimers), and RELA (Supplementary Figure 2J).

To decode additional TF properties critical for shaping the dynamic RAS-OIS enhancer landscape, we applied a principal component analysis (PCA) considering several metrics describing TF binding characteristics (Figure 2D). This analysis revealed two key features: First, pioneer TFs bind statically, extensively, and most importantly before RAS-OIS induction (*i.e.*, pre-stimulation) along the genome, while settler and migrant TFs bind more dynamically ("Dynamicity" in Figure 2D), far less frequently ("Windows" in Figure 2D), and on average less often before OIS induction (*i.e.* pre-stimulation) along the genome. Second, and in line with the proposed pioneering activity of AP-1 TFs, the latter clearly stand out amongst other pioneer TFs (highlighted by black circle in Figure 2D) because they bind exclusively and extensively to enhancers prior to RAS-OIS induction whereas most of the remaining pioneer TFs tend to accumulate away from them.

In summary, we identify *de novo* enhancer activation and AP-1 as novel and key elements that pioneer and shape a transcriptionally permissive enhancer landscape in senescence.

bioRxiv preprint first posted online May. 9, 2019; doi: http://dx.doi.org/10.1101/633594. The copyright holder for this preprint (which was not peer-reviewed) is the author/funder, who has granted bioRxiv a license to display the preprint in perpetuity. All rights reserved. No reuse allowed without permission.

AP-1 pioneer TF bookmarking of senescence enhancer landscape foreshadows the senescence transcriptional program

Given our unexpected finding that most of the enhancer activation occurred *de novo* out of unmarked chromatin territories, *i.e.*, devoid of enhancer-related histone modifications H3K4me1 and H3K27ac and ending in an active H3K4me1$^+$/ H3K27ac$^+$ enhancer state at 144h, and that AP-1 TFs act as pioneers to shape the senescence enhancer landscape, we explored a possible role of AP-1 as a general bookmarking agent for future and past enhancer activity. Quantification of enhancer mark dynamics (Figure 3A and Supplementary Figures 3A-C) unveiled that for windows shifting from the "unmarked" state at T_0 to an "active enhancer" state (H3K4me1$^+$ / H3K27ac$^+$) at either 72 h or 144 h, i.e. "*de novo* enhancers", there is both a gradual increase in H3K4me1 and H3K27ac levels from initial levels (T_0) similar to steady-state unmarked regions but different from poised enhancers, to final levels (144 h) indistinguishable from constitutive enhancers (Figure 3A and Supplementary Figures 3A-B). By contrast, for windows shifting from an "active enhancer" state at T_0 to an "unmarked" state at either 72 h or 144 h, that we refer to as "remnant enhancers", there is a progressive decrease both in H3K4me1 and H3K27ac levels from initial levels indistinguishable from constitutive enhancers to final levels similar to unmarked regions and distinct from poised enhancers (Figure 3A and Supplementary Figures 3A and 3C). The dynamic behavior of each enhancer class on average associated with the expression profile of nearby genes, with constitutive enhancers displaying constant gene expression, *de novo* enhancers increasing and remnant enhancers decreasing gene expression (Supplementary Figure 3D). To directly show the functional role of *de novo* enhancers we used a CRISPR interference (CRISPRi) approach[32,33]. Expression of 4 different gRNA targeting the

bioRxiv preprint first posted online May. 9, 2019; doi: http://dx.doi.org/10.1101/633594. The copyright holder for this preprint (which was not peer-reviewed) is the author/funder, who has granted bioRxiv a license to display the preprint in perpetuity. All rights reserved. No reuse allowed without permission.

dCas9-KRAB transcriptional repressor to *de novo* enhancers in the IL1α /IL1β genomic locus (g7, -14, -15, and -61) significantly reduced the expression of IL1β when analyzed 8 days after oncogenic RAS induction (Figure 3B). Interestingly, IL1α expression was only mildly reduced by the two gRNAs (g61 and g7) adjacent to the IL1β promoter (Figure 3B). While similar results were observed 14 days after oncogenic RAS induction (Supplementary Figure 3E), a control gRNA (g54) targeting a genomic region just downstream of the IL1α /IL1β locus did not affect either expression, while control gRNA guides g2 and g48, targeting sequences in-between two *de novo* enhancers, had only very moderate effects (Supplementary Figure 3F). Together, we render ample evidence that *de novo* and remnant enhancers are novel senescence-associated *cis*-regulatory modules that define the senescence transcriptional program.

We next determined whether TFs bookmark *de novo* enhancers for future activation and also, whether TFs bookmark remnant enhancers after their inactivation as part of a molecular memory. Indeed, as shown in Figure 3C, we found that AP-1 is the predominant TF bookmarking *de novo* and remnant enhancers. Importantly, and highlighting the importance of AP-1 in bookmarking *de novo* enhancers for future activation, gRNAs chosen for CRISPRi were either overlapping with AP-1 binding sites (g14, g15 and g61) or in close proximity (g7), *i.e.* ~125bp outside of it (Figure 3B). Because CRISPRi can control repression over a length of two nucleosomes (~300bp)[34], it is highly probable that g7 also affects this AP-1 binding site. Moreover, a control gRNA (g2) targeting a non-enhancer AP-1 site (Supplementary Figure 3F) did not affect IL1 expression strongly suggesting that only enhancer-positioned AP-1 sites are functional. Finally, we validated the importance of AP-1 TFs for *de novo* and remnant enhancer bookmarking by examining their positioning also in cells undergoing replicative

bioRxiv preprint first posted online May. 9, 2019; doi: http://dx.doi.org/10.1101/633594. The copyright holder for this preprint (which was not peer-reviewed) is the author/funder, who has granted bioRxiv a license to display the preprint in perpetuity. All rights reserved. No reuse allowed without permission.

senescence, which demonstrated that AP-1 TFs here also play a leading role for bookmarking (Supplementary Figure 3G). We conclude that AP-1 bookmarking of *de novo* and remnant enhancers is independent of oncogenic RAS signaling and a novel and cardinal feature that reflects future and past transcriptional activities in senescence.

While performing this analysis, we noticed that only 2,480 out of 3,334 *de novo* enhancers were TF bookmarked, while the remainder (n=854) lacked any detectable TF binding activity (Figure 3D). Thus, *de novo* enhancers can be further divided into two subclasses: 1) “TF bookmarked *de novo* enhancers” and 2) “TF virgin *de novo* enhancers” that are reminiscent to previously described latent enhancers[15,35] expanding the senescence enhancer landscape. Next, we considered the chromatin state environment of the two *de novo* enhancer classes to further characterize them (Supplementary Figure 3H). While a chromatin state environment already rich in constitutive enhancers surrounded bookmarked *de novo* enhancers at T_0 (*i.e.*, pre-OIS stimulation; left top and bottom plots), a chromatin state environment poor in constitutive enhancer elements surrounded virgin *de novo* enhancers at T_0 (right top and bottom plots). Both AP-1 bookmarked and virgin *de novo* enhancers became progressively activated and expanded upon RAS-OIS induction. Given that AP-1 premarked *de novo* enhancers operate within pre-existing, active enhancer-rich *cis*-regulatory regions and virgin *de novo* enhancers in poor ones, we hypothesized that this might impact absolute gene expression levels and kinetics upon enhancer activation. Indeed, we observed that the nearest genes associated with bookmarked *de novo* enhancers were already expressed at higher basal levels (as were genes proximal to poised enhancers) and reached significantly higher absolute expression levels with faster kinetics after RAS-OIS induction. In contrast, virgin *de novo* enhancers showed only low-to-background

bioRxiv preprint first posted online May. 9, 2019; doi: http://dx.doi.org/10.1101/633594. The copyright holder for this preprint (which was not peer-reviewed) is the author/funder, who has granted bioRxiv a license to display the preprint in perpetuity. All rights reserved. No reuse allowed without permission.

basal expression levels and reached comparatively lower absolute expression levels with slower kinetics after RAS-OIS induction (Figure 3E). These results argue that TF bookmarking of *de novo* enhancers, similar to traditional enhancer poising[36], is a chromatin-priming event that impacts gene expression kinetics and absolute output. Contrary to latent enhancers, our newly identified virgin enhancers do not serve an adaptive role in mediating stronger and faster gene expression upon restimulation as observed in macrophages[15], but instead serve as novel enhancer elements for *de novo* gene expression. Finally, we plotted leading gene expression fold-changes against the number of *de novo* enhancers in a given prospective senescence enhancer region. Remarkably, we discovered that a single *de novo* enhancer element of 100 bp can substantially activate the expression of its nearest gene and that there exists a positive correlation between the number of *de novo* enhancer elements and the expression increase of their nearest genes (Supplementary Figure 3I).

Altogether, our results provide compelling evidence that *de novo* and remnant enhancers play a critical role for ensuring that genes pertinent for senescence are expressed at the correct time and the correct level and highlight the importance of AP-1 bookmarking for epigenetic memorization of past and future enhancer activity to define the senescence transcriptional program.

A hierarchical TF network defines the senescence transcriptional program

The combinatorial and dynamic binding of TFs to enhancers and their organization into TF networks are central to the spatiotemporal specificity of gene expression and a key determinant in cell fate decisions[37]. TF networks are frequently corrupted in disease and thus, a detailed understanding on TF networks has important implications for developing

bioRxiv preprint first posted online May. 9, 2019; doi: http://dx.doi.org/10.1101/633594. The copyright holder for this preprint (which was not peer-reviewed) is the author/funder, who has granted bioRxiv a license to display the preprint in perpetuity. All rights reserved. No reuse allowed without permission.

and improving new therapeutic strategies[38]. Currently, a TF network regulating senescence is not available, which precludes a deliberate therapeutic manipulation of the senescence phenotype. Importantly, TF networks deduced *in silico* from the integration of time-resolved multidimensional, genome-wide datasets improve the accuracy and predictive power of such networks.

To elucidate the combinatorial and dynamic binding of TFs to enhancers and their organization into TF networks, we first computed co-occurring pairs of TFs in enhancers (Figure 4A, Supplementary Figure 4A and Supplementary data: see under Code availability in Material and Methods) followed by a topic machine learning approach that dissects the complexity of combinatorial binding of many TFs into compact and easily interpretable regulatory modules or TF "lexicons" that form the thematic structures driving the RAS-OIS gene expression program (Figure 4B)[39,40]. These analyses illustrated two key points. First, as shown in the co-binding matrix of Figure 4A and heatmap of Figure 4B, AP-1 pioneer TFs interact genome-wide with most of the remaining non-pioneer TFs (*i.e.*, settlers and migrant TFs; Figure 4A), have the highest total number of binding sites (Figure 4B, grey colored box plot) and contribute to virtually all of the 54 TF lexicons (Figure 4B, green colored boxplot) with lexicon 22 being the most frequently represented lexicon genome-wide (Figure 4B, top orange colored box plot). Our interactive heatmap of Figure 4B (Supplementary data: see under Code availability in Material and Methods) provides a valuable resource for generating new hypotheses to functionally dissect TF interactions in cells undergoing RAS-OIS. Second, TF lexicon usage associates with specific chromatin states (Supplementary Figure 4B). For example, lexicons 21 and 22 are exclusively used for enhancers holding most of the AP-1 binding instances, while lexicon 50 is strongly related to polycomb repressor

bioRxiv preprint first posted online May. 9, 2019; doi: http://dx.doi.org/10.1101/633594. The copyright holder for this preprint (which was not peer-reviewed) is the author/funder, who has granted bioRxiv a license to display the preprint in perpetuity. All rights reserved. No reuse allowed without permission.

complex (PRC)-repressed regions and lexicons 44 and 52 predominantly associate with promoters. Interestingly among the most prominent TFs in lexicon 50 are the known PRC-interacting transcriptional co-repressor complex REST and insulator CTCF[41,42]. The latter implies that these proteins may recruit PRC to silence or structure genomic regions, an intriguing possibility that deserves further investigation. Moreover, the promoter-centric lexicon 52 holds many E2F TFs, which is in line with a primary role of E2Fs at promoters[43].

Next, we developed an algorithm, based on our temporal TF co-binding information and a previously published TF network (Supplementary Figure 4C)[44], to visualize the hierarchical structure of the senescence TF network. In Figure 4C we show a representative example of the TF network of SASP gene module VI. The network has a three-layered architecture: i) a top layer defined exclusively by the AP-1 family of pioneer TFs ii) a core layer composed mostly of other pioneer and settler TFs, and iii) a bottom layer characterized by settler and migrant TFs (Figures 4C and Cytoscape interactive maps in Supplementary Data: see under Code availability in Material and Methods). The core layer itself separates into a multi-level and single-level core, depending on the complexity of TF connectivity to the top and bottom layers (Figure 4C). Remarkably, the organizational logic of the TF network is highly similar, if not identical, for all gene expression modules despite high transcription factor diversity in the core and bottom layers (Supplementary data: see under Code availability in Material and Methods). The TF network topology for RAS-OIS is congruent with the biochemical and dynamic properties of each TF category (*i.e.*, pioneer, settler or migrant) in each layer of the network. As the interactions flow from the top to the bottom layer, there is an increasing dynamicity and number of TFs and a decreasing number of bound regions

bioRxiv preprint first posted online May. 9, 2019; doi: http://dx.doi.org/10.1101/633594. The copyright holder for this preprint (which was not peer-reviewed) is the author/funder, who has granted bioRxiv a license to display the preprint in perpetuity. All rights reserved. No reuse allowed without permission.

(Supplementary Figures 4D-E). Ranking the dynamicity index and the number of bound regions for all TFs in each network confirmed the hierarchical principles of their organization, with a common core of highly connected TFs from the top and core layers shared across all networks (Supplementary Figure 4F, black circle at center). Variability in the composition of the most dynamic TFs of the core and bottom layers defines the gene expression module specificity for each network and its corresponding specialized transcriptional output (Supplementary Figures 4G-I). Thus, TF network topology imposes and constrains the position of a given TF in the network and thus, its gene-regulatory contribution. Our data also revealed unanticipated plasticity in transcription factor binding leading to similar gene expression, thus, refuting the simple rule that co-expression behooves co-regulation[45].

Our hierarchical TF network model for RAS-OIS enhancers predicted that the number of direct target genes regulated by a given TF is a function of its position in the TF network hierarchy. To test this prediction, we performed transient RNA interference (siRNA) experiments targeting AP-1-cJUN (top layer), ETS1 (multi-level core layer) and RELA (single-level core layer) in fully senescent RAS-OIS cells (144 h), determined the global transcriptome profiles and compared them to the transcriptomes of cells transfected with a non-targeting siRNA (siCTRL) (Figure 4D). Consistent with the TF network hierarchy, silencing of AP-1-cJUN affected the most substantial number direct gene targets (n=5,089), followed by ETS1 (n=2,431) and RELA (n=2,224), thus, confirming the master regulatory role of AP-1 pioneer TFs at enhancers and in the execution of the RAS-OIS gene expression program. Specifically, 172 genes were co-regulated by the three TFs, while 987 were co-regulated by cJUN and ETS1, 520 by JUN and RELA, and 293 by ETS and RELA. Correspondence analysis (CA) revealed

bioRxiv preprint first posted online May. 9, 2019; doi: http://dx.doi.org/10.1101/633594. The copyright holder for this preprint (which was not peer-reviewed) is the author/funder, who has granted bioRxiv a license to display the preprint in perpetuity. All rights reserved. No reuse allowed without permission.

that perturbing the function of AP-1-cJUN, ETS1 or RELA could separate faithfully ($p = 1.8 \times 10^{-149}$) up-regulated (V-VII) from down-regulated gene expression modules (I-IV) (Figure 4E), which aligns perfectly, both with the CA for chromatin states (see Figures 2A-B) and the differential impact of the TFs on RAS-OIS-associated enhancer activation as predicted in the TF network analysis (Figure 4C and Supplementary data: see under Code availability in Material and Methods).

We conclude that the senescence response is encoded by a universal three-layered TF network architecture and relies strongly on the exploitation of an enhancer landscape implemented by AP-1 pioneer TFs to choreograph the OIS transcriptional program *via* local, diverse and dynamic interactions with settler and migrant TFs.

Hierarchy Matters: Functional Perturbation of AP-1 pioneer TF, but no other TF, reverts the senescence clock

Pioneer TFs have been identified as important drivers of cell fate changes during adaptive and cellular reprogramming as well as in cells undergoing malignant transformation[46,47]. As such, they represent attractive targets to manipulate cell fate for diverse research and therapeutic purposes[19].

The identification of AP-1-cJUN as a principal pioneer TF in fibroblasts undergoing RAS-OIS raised the possibility that perturbing its function could considerably change the transcriptional trajectory of the OIS cell fate, while perturbation of other TFs should not. To test this hypothesis, we depleted AP-1-cJUN, ETS1 and RELA at T_0, 72 h and 144 h following oncogenic RAS expression and compared global gene expression profiles with siCTRL treated cells at identical time-points. Capturing their transcriptional

bioRxiv preprint first posted online May. 9, 2019; doi: http://dx.doi.org/10.1101/633594. The copyright holder for this preprint (which was not peer-reviewed) is the author/funder, who has granted bioRxiv a license to display the preprint in perpetuity. All rights reserved. No reuse allowed without permission.

trajectories using PCA illustrated that functional perturbation of ETS1 and RELA shifted trajectories along the second principal component (PC2, which captures siRNA-related variability) at any given time-point compared to the control time course, but it did not affect the timely execution of the RAS-OIS gene expression program, since there is not shift along the first principal component (PC1, which captures time-related variability). By contrast, perturbing AP-1-cJUN function shifted trajectories both along PC1 and PC2 and effectively reverted the RAS-OIS transcriptional trajectory to a profile closely related to that of siCTRL-treated fibroblasts at 72 h after RAS-OIS induction. Silencing AP-1-cJUN expression at 72 h also pushed the transcriptional profile closer to control-treated cells at day T0 (Figure 5A, blue arrow). Functional overrepresentation analyses of the target genes (direct and/or indirect) of each TF further supported the siJUN-mediated reversion of the RAS-OIS transcriptional trajectory demonstrating that depletion of AP-1-cJUN strongly affected both the repression of the inflammatory response (*i.e.*, the SASP) and a partial reactivation of pro-proliferation genes (*i.e.,* E2F, G2M and mitotic spindle targets) (Figure 5B and Supplementary Figures 5A-C). A complete exit of senescence is not expected here, however, as AP-1 is absolutely required for proliferation[48,49].

To quantify and visualize the temporal overlaps in differentially expressed genes between siJUN and siCTRL-treated cells we used an UpSet plot (Supplementary Figures 5D) and expression heatmaps (Figure 5C and Supplementary Figures 5E-G). Congruent with a resetting of the senescence clock, a significant number of pro-proliferation E2F target genes (14%; *e.g. CCNB2* or *CDCA8*) were up-regulated (Supplementary Figure 5E) and NF-κB-regulated SASP target genes (*e.g. IL1B* or *IL6*)

bioRxiv preprint first posted online May. 9, 2019; doi: http://dx.doi.org/10.1101/633594. The copyright holder for this preprint (which was not peer-reviewed) is the author/funder, who has granted bioRxiv a license to display the preprint in perpetuity. All rights reserved. No reuse allowed without permission.

were down-regulated (60%) (Supplementary Figure 5F). cJUN-depleted RAS-OIS cells also shared a similar expression profile for a subset of genes (27%) of the Notch-1 intracellular domain (NC1ID)-induced senescence (NIS) transcriptional signature[50] that develops within the first 72-96 h of RAS-OIS (Supplementary Figure 5G). Thus, AP-1 inhibition is a powerful and save means to potently repress SASP expression in senescent cells without affecting their cell cycle arrest.

Altogether, these data identify AP-1 as a master regulator and molecular “time-keeper” of senescence. Our detailed description of the layered TF network architecture will facilitate targeted disruption of TFs to manipulate specific features of the senescence phenotype for future therapeutic benefit.

bioRxiv preprint first posted online May. 9, 2019; doi: http://dx.doi.org/10.1101/633594. The copyright holder for this preprint (which was not peer-reviewed) is the author/funder, who has granted bioRxiv a license to display the preprint in perpetuity. All rights reserved. No reuse allowed without permission.

DISCUSSION

Exploiting senescence targeting for treating age-related diseases and cancer requires a detailed knowledge of the transcriptional, epigenetic, and signaling mechanisms defining the basis and realization of the senescence program, which is currently missing. To fill this critical gap in our knowledge, we used a dynamic, multidimensional approach at high-resolution to define the gene-regulatory code driving the senescence cell fate.

A central finding of our study is that the senescence program is defined and driven by a predetermined enhancer landscape that is sequentially (in)activated during the senescence process. AP1 is instrumental for this predetermination by imprinting a prospective senescence enhancer landscape that, in the absence of traditional enhancer histone-modification marks, foreshadows future transcriptional activation. This is a surprising discovery given that AP-1 transcriptional activation has been traditionally linked to growth-factor and MAPK signaling[51]. There is, however, now accumulating evidence that AP-1 also plays an essential role as a pioneering factor for establishing cell type-specific enhancers and cellular identities[52,53]. In line with its role in pioneering and bookmarking enhancers, we show that AP-1 is also recruited *de novo* as a first line TF to “virgin” enhancers and that it serves as a molecular memory for enhancers that become inactivated during the senescence fate transition that we termed “remnant” enhancers. Based on these findings we propose a model by which “enhancer recycling” of AP1-bookmarked future and past enhancer activities is an evolutionary conserved mechanism that allows for modular and flexible, yet, efficient transcriptional responses to incoming signals. We stipulate that the senescence program is preserved through AP-1 binding to enhancer chromatin as part of epigenetic memory of the cell’s developmental (stress) history bypassing histone modification-dependent bookmarking

bioRxiv preprint first posted online May. 9, 2019; doi: http://dx.doi.org/10.1101/633594. The copyright holder for this preprint (which was not peer-reviewed) is the author/funder, who has granted bioRxiv a license to display the preprint in perpetuity. All rights reserved. No reuse allowed without permission.

to store genomic information. Further, given the pristine specificity of the newly identified prospective and remnant enhancers they can be used as urgently needed specific, rather than associated, senescence biomarkers and to predict a cell's potential to undergo senescence. This latter carries also important translational implications for identifying cancers that would respond positively to pro-senescence therapy. A natural question that arises from our data is whether the senescence program is universal to all inducing stimuli and cell types or if multiple senescence programs exist. Based on the data presented here and work in progress, we predict that the organizational principles of the senescence program we defined here hold for all cell types and inducers. Additional time-resolved studies of various inducers in different cell types are required and currently ongoing to answer this question definitively.

Another key finding is the reversibility of senescence by an informed intervention on network topology that we delineated in this study. Indeed, silencing the function of a single TF sitting atop the TF network hierarchy, AP-1, is sufficient to revert the "senescence clock". We thus define after the "telomere clock" a second, "epigenomic-enhancer clock" regulating the senescence process. Why does functional AP-1 perturbation not lead to complete senescence exit? Based on published[49] and our own results we surmise that AP1 depletion does not lead to a full cell cycle re-entry and proliferation, because AP1 plays important roles for proliferation. Thus, AP1 confines cells to their existing proliferative state and therefore may be viewed as a 'locking device' that restricts cells to their current state. However, we provide compelling evidence that functional inhibition of AP1 factors reverts the senescence transcriptional program and potently represses the expression of the pro-inflammatory senescence-associated secretory phenotype (SASP). This finding has great therapeutic potential, as

bioRxiv preprint first posted online May. 9, 2019; doi: http://dx.doi.org/10.1101/633594. The copyright holder for this preprint (which was not peer-reviewed) is the author/funder, who has granted bioRxiv a license to display the preprint in perpetuity. All rights reserved. No reuse allowed without permission.

pharmacological interference with AP1 using selective inhibitors (*e.g.* improved T-5224 derivatives) would allow to control effectively the detrimental effects of the SASP in promoting cancer and other age-related diseases[54-56]. In summary, we believe that AP1 is a prime target for therapeutic SASP modulation *in vivo*.

By determining the layered architecture/organizational principles of the TF network that orchestrate(s) the transition to OIS, we revealed the plasticity and stability of the senescent phenotype. We show that a highly flexible, combinatorial TF interactome establishes the senescence program, which is in line with the TF network dynamics during hematopoietic and stem cell differentiation[57,58]. In addition, we demonstrate that targeted engineering of specific nodes at different layers of the TF network disrupts gene expression with a corresponding magnitude, suggesting a path for the manipulation of the senescent phenotype *in vivo*. Pharmacological inhibition of TFs (see above for AP-1), signal transduction molecules, such as kinases or acetylases that converge in the activation of TFs, could represent a viable approach for manipulating the senescent phenotype *in vivo*[59]. Alternatively, small molecules that prevent TF-TF combinatorial interactions could also be envisioned[60].

In conclusion, the present work emphasizes the advantages of, and indeed the need for, integrating time-resolved genome-wide profiles to describe and interrogate the transition to senescence. This approach generates detailed knowledge necessary to develop strategies for manipulating/engineering the senescent cell fate (and other cell fate transitions) *in vivo* for research and therapeutic purposes. Overall, our study provides a comprehensive resource for the generation of novel hypotheses regarding senescence regulation, offers important mechanistic, regulatory insights that could

bioRxiv preprint first posted online May. 9, 2019; doi: http://dx.doi.org/10.1101/633594. The copyright holder for this preprint (which was not peer-reviewed) is the author/funder, who has granted bioRxiv a license to display the preprint in perpetuity. All rights reserved. No reuse allowed without permission.

translate to the study of other cell fate transitions and provide new inroads for the diagnosis and manipulation of the senescence state in age-related diseases and cancer.

bioRxiv preprint first posted online May. 9, 2019; doi: http://dx.doi.org/10.1101/633594. The copyright holder for this preprint (which was not peer-reviewed) is the author/funder, who has granted bioRxiv a license to display the preprint in perpetuity. All rights reserved. No reuse allowed without permission.

MATERIAL AND METHODS

Cell culture

WI-38 fibroblasts (purchased from ECCAC) were cultured in Dulbecco's Modified Eagle's medium (DMEM) containing 10% FBS and 1X Primocin (Invivogen) at 37ºC and 3% oxygen. WI-38-ER: RASV12 fibroblasts were generated by retroviral transduction as previously described[9]. Senescence was induced by addition of 400 nM 4-hydroxytamoxifen (4-OHT, Sigma Cat no. H7904-5MG) to the culture medium and samples were collected and processed at the time points indicated in the main text. Replicative senescent cells were generated by proliferative exhaustion and were used for experiments when cell cultures went through 1 population (PD) per 3 weeks, were >80% positive for senescence-associated beta galactosidase activity (SABG) and stained negative for EdU (see below for details). For the induction of quiescence, WI-38 fibroblasts were cultured in DMEM containing 0.2% FBS for up to 4 consecutive days and samples were collected and processed as described in the main text.

ATAC-seq

The transposition reaction and library construction were performed as previously described[24]. Briefly, 50,000 cells from each time point of the senescence time course (2 biological replicates) were collected, washed in 1X in PBS and centrifuged at 500 x *g* at 4ºC for 5 min. Nuclei were extracted by incubation of cells in Nuclear Extraction Buffer (NEB) containing 10 mM Tris-HCl, pH 7.4, 10 mM NaCl, 3 mM MgCl2, 0.1% IGEPAL CA-630 and immediately centrifuging at 500 x *g* at 4ºC for 5 min. The supernatant was carefully removed by pipetting, and the transposition was performed by resuspension of nuclei in 50 µL of Transposition Mix containing 1X TD Buffer (Illumina) and 2.5 µL Tn5

bioRxiv preprint first posted online May. 9, 2019; doi: http://dx.doi.org/10.1101/633594. The copyright holder for this preprint (which was not peer-reviewed) is the author/funder, who has granted bioRxiv a license to display the preprint in perpetuity. All rights reserved. No reuse allowed without permission.

(Illumina) for 30 min at 37ºC. DNA was extracted using the QIAGEN MinElute kit. Libraries were produced by PCR amplification (12-14 cycles) of tagmented DNA using the NEB Next High-Fidelity 2x PCR Master Mix (New England Biolabs). Library quality was assessed in an Agilent Bioanalyzer 2100. Paired-end sequencing was performed in an Illumina Hiseq 2500. Typically, 30-50 million reads per library are required for downstream analyses.

Histone modification and transcription factor ChIP-seq

WI-38-ER: RASV12 fibroblasts were treated with 400 nM 4-OHT for 0, 72 and 144 hours, and 10^7 cells (per time point, minimum two biological replicates) were fixed in 1% formaldehyde for 15 min, quenched in 2M glycine for additional 5 min and pelleted by centrifugation at 2,000 rpm, 4ºC for 4 min. For histone modification ChIP-seq, nuclei were extracted in Extraction Buffer 2 (0.25 M sucrose, 10 mM Tris-HCl pH 8.0, 10 mM $MgCl_2$, 1% Triton X-100 and proteinase inhibitor cocktail) on ice for 10 min followed by centrifugation at 3,000 x *g* at 4ºC for 10 min. The supernatant was removed and nuclei were resuspended in Nuclei Lysis Buffer (50 mM Tris-HCl pH 8.0, 10 mM EDTA, 1% SDS and proteinase inhibitor cocktail). Sonication was performed using a Diagenode Picoruptor until the desired average fragment size (100-500 bp) was obtained. Soluble chromatin was obtained by centrifugation at 11,500 rpm for 10 min at 4ºC and chromatin was diluted 10-fold. Immunoprecipitation was performed overnight at 4ºC with rotation using 1-2 x 10^6 cell equivalents per immunoprecipitation using antibodies (5 µg) against H3K4me1 (Abcam), H3K27ac (Abcam), H3K4me3 (Millipore), H3K27me3 (Millipore). Subsequently, 30 µL of Ultralink Resin (Thermo Fisher Scientific) was added and allowed to tumble for 4h at 4ºC. The resin was pelleted by centrifugation and washed

bioRxiv preprint first posted online May. 9, 2019; doi: http://dx.doi.org/10.1101/633594. The copyright holder for this preprint (which was not peer-reviewed) is the author/funder, who has granted bioRxiv a license to display the preprint in perpetuity. All rights reserved. No reuse allowed without permission.

three times in low salt buffer (150 mM NaCl, 0.1% SDS, 1% Triton X-100, 20 mM EDTA, 20 mM Tris-HCl pH 8.0), one time in high salt buffer (500 mM NaCl, 0.1% SDS, 1% Triton X-100, 20 mM EDTA, 20 mM Tris-HCl pH 8.0), two times in lithium chloride buffer (250 mM LiCl, 1% IGEPAL CA-630, 15 sodium deoxycholate, 1 mM EDTA, 10 mM Tris-HCl pH 8.0) and two times in TE buffer (10 mM Tris-HCl, 1 mM EDTA). For transcription factor ChIP-seq, fibroblasts were treated as described above except that chromatin was isolated using the enzymatic SimpleChIP kit (Cell Signaling) according to the manufacturer's instructions, obtaining chromatin with an average fragment length of 4-5 nucleosomes. Immunoprecipitation was performed overnight at 4ºC with rotation using 6-10 x 10^6 cell equivalents per immunoprecipitation using antibodies (5 µg) against cJUN, FOSL2 and RELA (Santa Cruz Biotechnologies) and processed as described above. Washed beads were resuspended in elution buffer (10 mM Tris-Cl pH 8.0, 5 mM EDTA, 300 mM NaCl, 0.5% SDS) treated with RNAse H (30 min, 37 ºC) and Proteinase K (2 h, 37ºC), 1 µL glycogen (20 mg/mL, Ambion) was added, and decrosslinked overnight at 65 ºC. For histone modifications, DNA was recovered by mixing the decrosslinked supernatant with 2.2X SPRI beads followed by 4 min incubation at RT. The SPRI beads were washed twice in 80% ethanol, allowed to dry, and DNA was eluted by in 35 µL 10 mM Tris-Cl pH 8.0. For transcription factors, DNA was eluted by phenol/chloroform extraction (2X) followed by ethanol precipitation overnight at -20ºC. The DNA pellet was washed with 70% ethanol, allowed to dry, and DNA was resuspended in 35 µL 10 mM Tris-Cl pH 8.0. Histone modification libraries were constructed using the NextFlex ChIP-seq kit (Bioo Scientific) according to the manufacturer's instructions. Libraries were amplified for 12 cycles. Transcription factor libraries were constructed using a modified protocol from the Accel-NGS 2S Plus DNA

bioRxiv preprint first posted online May. 9, 2019; doi: http://dx.doi.org/10.1101/633594. The copyright holder for this preprint (which was not peer-reviewed) is the author/funder, who has granted bioRxiv a license to display the preprint in perpetuity. All rights reserved. No reuse allowed without permission.

Library Kit (#21024), where we performed DNA extraction at each step using 25:24:1 phenol:chloroform:isoamyl alcohol followed by overnight ethanol precipitation of DNA at each step of the protocol. Additionally, we enriched for small DNA fragments using AMPure-XP beads (Beckman-Coulter (#A63881). Libraries were then resuspended in 20 µL of low EDTA-TE buffer. Libraries were quality controlled in an Agilent Technologies 4200 Tapestation (G2991-90001) and quantified using the Invitrogen Qubit DS DNA HS Assay kit (Q32854). Libraries were sequenced using an Illumina High-Seq 2500. Typically, 30-50 million reads were required for downstream analyses.

RNA and microarrays

RNA from each time point from the senescence and quiescence time series (2 biological replicates) was purified using the QIAGEN RNeasy Plus kit according to the manufacturer's instructions. 100 ng RNA per sample was analyzed using Affymetrix Human Transcriptome Arrays 2.0, according to the manufacturer's instructions.

EdU staining and senescence-associated beta galactosidase activity (SABG)

Representative samples from the senescent and quiescent time series were evaluated for EdU incorporation using the Click-iT EdU Alexa Fluor Imaging Kit (Thermo Fisher Scientific) according to the manufacturer's instructions. SABG activity was assessed as previously described[61]. Cells were imaged in a Zeiss confocal fluorescence microscope and images analyzed using the ZEN suite.

bioRxiv preprint first posted online May. 9, 2019; doi: http://dx.doi.org/10.1101/633594. The copyright holder for this preprint (which was not peer-reviewed) is the author/funder, who has granted bioRxiv a license to display the preprint in perpetuity. All rights reserved. No reuse allowed without permission.

RNA interference

Small interfering RNAs (20 µM) targeting JUN (QIAGEN, Ambion), ETS1 (QIAGEN) and RELA (QIAGEN) as well as non-targeting controls were transfected into WI-38-ER: RASV12 using siIMPORTER reagent (Millipore) according to the manufacturer's instructions (minimum 2 biological replicates per transcription factor per time course experiment). RAS-OIS was induced with 400 nM 4-OHT concomitantly with the addition of DMEM containing 20% FBS 4 hours after transfection and incubated overnight. Sixteen hours after transfection, cells were replenished with new media containing 10% FBS and 400 nM 4-OHT, and RNA was isolated at indicated time points and analyzed in Affymetrix Human Transcriptome Arrays 2.0.

Expression microarray pre-processing

Raw Affymetrix HTA 2.0 array intensity data were analyzed using open-source Bioconductor packages on R. The quiescence and the RAS-OIS time series data were normalized together (2 conditions, 2 biological replicates per condition, 6 time points per replicates) using the robust multi-array average normalization approach implemented in the *oligo* package. Internal control probe sets were removed and average expression deciles over time-points were independently defined for each treatment. Probes whose average expression was lower than the 4th expression decile in both conditions were removed for subsequent analyses. To remove sources of variation and account for batch effects, data were finally corrected with the *sva* package. To recover as much annotation information as possible, we combined Affymetrix HTA 2.0 annotations provided by Affymetrix and Ensembl through the packages *hta20sttranscriptcluster.db* and *biomaRt*. Principal component analysis and bi-clustering based on Pearson's

bioRxiv preprint first posted online May. 9, 2019; doi: http://dx.doi.org/10.1101/633594. The copyright holder for this preprint (which was not peer-reviewed) is the author/funder, who has granted bioRxiv a license to display the preprint in perpetuity. All rights reserved. No reuse allowed without permission.

correlation and Ward's aggregation criterion were used to confirm consistency between biological replicates and experimental conditions at each step of the pre-processing.

Self-organizing maps (SOM)

Normalized log-scaled and filtered expression values were processed using the unsupervised machine learning method implemented in *oposSOM*[25] to train a self-organizing map. This algorithm applies a neural network algorithm to project high dimensional data onto a two-dimensional visualization space. In this application, we used a two-dimensional grid of size 60 x 60 metagenes of rectangular topology. The SOM portraits were then plotted using a logarithmic fold-change scale. To define modules of co-expressed meta-genes, we used a clustering approach relying on distance matrix and implemented in *oposSOM*. Briefly, clusters of gene expression were determined based on the patterns of the distance map which visualizes the mean Euclidean distance of each SOM unit to its adjacent neighbors. This clustering algorithm – referred to as D-clustering – finds the SOM units referring to local maxima of their mean distance with respect to their neighbors. These pixels form halos edging the relevant clusters in the respective distance map and enable robust determination of feature clusters in the SOM. We finally performed a gene set over-representation analysis in each cluster considering the Molecular Signature Database (MSigDB) hallmark gene sets using a right-tail modified Fisher's exact test and the hypergeometric distribution to provide *p*-value.

bioRxiv preprint first posted online May. 9, 2019; doi: http://dx.doi.org/10.1101/633594. The copyright holder for this preprint (which was not peer-reviewed) is the author/funder, who has granted bioRxiv a license to display the preprint in perpetuity. All rights reserved. No reuse allowed without permission.

Correlation and multidimensional analyses

To highlight differences in expression profiles between quiescence and RAS-OIS through time, we used multi-dimensional scaling plot representing leading fold change, which is defined as the root-mean-square average of the log-fold-changes for the genes best distinguishing each pair of samples. To quantify the evolution of transcriptomic variability and noise through time, we looked at the gene expression density distributions for all possible pairs of treated *vs* T_0 transcriptomes. Distributions were estimated using kernel density estimation of all genes' expression in the ith T_0 transcriptome and the jth treated transcriptome. We also computed Pearson's correlation for each of these combinations. The Pearson's correlation between two transcriptomes, X and Y containing n gene expressions, is obtained by $R(X,Y) = \sum_{i=1}^{n}(x_i - \mu_X)\,(y_i - \mu_Y)/(\sigma_X \sigma_Y)$, where x_i and y_i are the ith observation in the vectors X and Y respectively, μ_X and μ_Y the average values of each transcriptome, and σ_X and σ_Y, the corresponding standard deviations.

Information theory – derived metrics

To evaluate transcriptome diversity and specialization, we used an approach based on information theory as described in [26].

Gene expression time series analysis

Normalized log-scaled and filtered expression data related to the quiescence and the OIS time series were further considered for differential analysis with *limma*[62]. To define an RAS-OIS specific transcriptomic signature, we proceeded in three steps, each relying

bioRxiv preprint first posted online May. 9, 2019; doi: http://dx.doi.org/10.1101/633594. The copyright holder for this preprint (which was not peer-reviewed) is the author/funder, who has granted bioRxiv a license to display the preprint in perpetuity. All rights reserved. No reuse allowed without permission.

on linear mixed model cubic B-splines, as nonlinear response patterns are commonly encountered in time course biological data. For each probe, and each treatment the expression was modeled as follow:

$$y = \beta_0 + \beta_1 x + \beta_2 x^2 + \beta_3 x^3 + \sum_{k=0}^{K-1} \gamma_k (x - \xi_k)^3 + \varepsilon$$

with $(x - \xi_k) = \begin{cases} 1 if x \leq \xi \\ x - \xi if x > \xi \end{cases}$

where $\beta_0$is the average probe expression over all samples in a given condition, β_{1-3} the model coefficients, K the number of knots, ξ_k the kth knot and ε the error term. First, we defined probes responding over time to RASV12 induction. Second, we considered all together the quiescence and the RAS-OIS time series, as well as the interaction between time and treatment, and defined probes responding to one or the other treatment over time, as well as probes responding differently between the two treatments at any time point. We finally defined the set of probes responding consistently to both treatment and time and removed these probes from the global set of probes responding to RASV12 induction defined at the first step. Moderated *F*-statistics that combine the empirical Bayes moderated *t*-statistics for all contrasts into an overall test of significance for each probe were used to assess the significance of the observed expression changes. At any step of this workflow, *p*-values were corrected for multiple testing using the FDR approach for a stringent significance level of 0.005. For validation purposes, we also wanted to compress the RAS-OIS time-series and achieve a volcano plot representation. To do so, we've computed the maximal absolute $\log_2$ fold change in expression in the RAS-OIS time series considering T_0 as the reference and selected up and down regulated probes using an absolute $\log_2$ fold change cutoff at 1.2 and a corrected *p*-value cutoff of 0.005. We then build a scatter-plot plotting the $\log_{10}$

bioRxiv preprint first posted online May. 9, 2019; doi: http://dx.doi.org/10.1101/633594. The copyright holder for this preprint (which was not peer-reviewed) is the author/funder, who has granted bioRxiv a license to display the preprint in perpetuity. All rights reserved. No reuse allowed without permission.

significance versus $\log_2$ fold-change on the y and x axes, respectively. Probes responding consistently to both ER: RASV12 induction and quiescence were finally over-plotted.

Gene expression unsupervised clustering

Probes constitutive of the RAS-OIS specific transcriptomic signature were clustered using the weighted gene correlated network analysis approach implemented in the *WGCNA* R package[63]. Standard WGCNA parameters were used for the analysis, with the exceptions of soft-thresholding power which was defined using methods described by and set at 18. The 7 co-expressed probe clusters identified were further functionally characterized using gene set over-representation tests. The same approach as previously described for the SOM-defined clusters was used.

Histone modification ChIP-seq data processing

Reads were cleaned and trimmed using *fastq-mcf* from the *ea-utils* suite v1.1.2 to remove adapters, low quality bases and reads, and discard reads shorter than 25 bp after filtering. Reads were then aligned to the human reference genome (hg19) with *bowtie* v1.1.1 using best matches parameters (bowtie -v 2 -m 1 --best --strata). Alignment files were further processed with *samtools* v1.2 and *PicardTools* v1.130 to flag PCR and optical duplicates and remove alignments located in Encode blacklisted regions. Fragment size was estimated *in silico* for each library using *spp* v1.10.1. Genome-wide consistency between replicates was checked using custom R scripts. Enriched regions were identified for each replicate independently with *MACS* v2.1.0 with non-IPed genomic DNA as a control (macs2 callpeak --nomodel --shiftsize --shift-control

bioRxiv preprint first posted online May. 9, 2019; doi: http://dx.doi.org/10.1101/633594. The copyright holder for this preprint (which was not peer-reviewed) is the author/funder, who has granted bioRxiv a license to display the preprint in perpetuity. All rights reserved. No reuse allowed without permission.

--gsize hs -p 1e-1). These relaxed peak lists were then processed through the irreproducible discovery rate (IDR) pipeline[64] to generate an optimal and reproducible set of peaks for each histone modification and each time point.

ATAC-seq data processing

Paired-ends reads were cropped to 100bp with *trimmomatic* v0.36[65] and cleaned using *cutadapt* v1.8.3[66] to remove Nextera adapters, low quality bases and reads, and discard reads shorter than 25 bp after filtering. Fragments were then aligned to the human reference genome (hg19) using *bowtie2* v2.2.3 discarding inconsistent pairs and considering a maximum insert size of 2kb (bowtie2 -N 0 --no-mixed --no-discordant --minins 30 --maxins 2000). Alignment files were further processed with *samtools* v1.2 and *PicardTools* v1.130 to flag PCR and optical duplicates and remove alignments located in Encode blacklisted regions. Accessible regions were identified using *MACS2* v2.1.0 without control (macs2 callpeak --gsize hs -p 1e-3). These relaxed peak lists were then processed through the irreproducible discovery rate (IDR) pipeline to generate an optimal and reproducible set of peaks for each time point.

Normalized ATAC-seq and ChIP-seq signal tracks

After verifying the consistency between biological replicates, time points and data type using *deepTools*[67], alignments related to biological replicates for a given assay and a given time point were combined. We then binned the genome in 200bp non-overlapping windows and generated genome-wide read count matrices for each assay

bioRxiv preprint first posted online May. 9, 2019; doi: http://dx.doi.org/10.1101/633594. The copyright holder for this preprint (which was not peer-reviewed) is the author/funder, who has granted bioRxiv a license to display the preprint in perpetuity. All rights reserved. No reuse allowed without permission.

independently. These matrices were finally quantile normalized with custom R script and further used to generate genome-wide signal tracts.

Histone modification ChIP-seq and ATAC-seq differential analysis

After assessing library saturation using *preseqR*, alignment and peak data were imported and pre-processed in R using the *DiffBind* package[68]. Briefly, for a given histone modification type, we first defined the global reproducible peak set as the union of each time-specific reproducible peak sets defined previously. We then counted the number of reads mapping inside each of these intervals at each time point and for each replicate. The raw count matrix was then normalized for sequencing depth using a non-linear full quantile normalization as implemented in the *EDASeq* package[69]. To remove sources of unwanted variation and consider batch effects, data were finally corrected with the *RUVSeq*[70] package considering 2 surrogate variables. Differential analyses for count data were performed using *edgeR*[71] considering time and batch in the design matrix, by fitting a negative binomial generalized log-linear model to the read counts for each peak. Peaks were finally annotated using *ChIPpeakAnno* considering annotations provided by Ensembl v86.

Chromatin state differential analysis

To quantify and define combinatorial chromatin state dynamics in space and time, we analyzed histone modification combinations with the *chromstaR* package[72]. Briefly, after partitioning the genome into 100bp non-overlapping bins and counting the number of reads mapping into each bin at each time point and for each histone modification, this

bioRxiv preprint first posted online May. 9, 2019; doi: http://dx.doi.org/10.1101/633594. The copyright holder for this preprint (which was not peer-reviewed) is the author/funder, who has granted bioRxiv a license to display the preprint in perpetuity. All rights reserved. No reuse allowed without permission.

algorithm relies on a univariate Hidden Markov Model (HMM) with two hidden states (unmodified, modified). This HMM is used to fit the parameters of the two-component mixture of zero-inflated negative binomial distribution considered to model read counts for every ChIP-seq experiments. A multivariate HMM is then used to assign every bin in the genome to one of the multivariate components considering $2^{(3 \text{ time points x 4 histone modifications})}$ possible states. To limit computational burden and focus on accurate differences, the analysis was run in differential mode with a 100bp resolution (*i.e.* smaller than a single nucleosome), such that every mark is first analyzed separately with all conditions combined while the full combinatorial state dynamics is rebuilt by combining the differential calls obtained for the four marks. We finally filtered out differential calls not overlapping with any histone modification and ATAC-seq reproducible peaks. To properly associate histone modification combinations with biologically meaningful mnemonics, we made an extensive comparison between the binning we obtained in WI38 fibroblasts undergoing RAS-OIS and IMR90 fetal lung fibroblasts chromatin states described in the scope of the Epigenomic Roadmap consortium. To test for association between changes in chromatin states through time and gene expression modules we ran a correspondence analysis. Briefly, genomic loci experiencing changes in chromatin states through time were first associated to the nearest gene. We then specifically focused on loci associated to genes belonging to any expression module and built a two-way contingency table summarizing the number of transition in states (considering all possible combinations) occurring in each expression module, further used as an input for a correspondence analysis using *FactoMineR*[73]. The significance of association between the two qualitative variables (transition in state and module) was assed using a χ^2 test. Results of the CA were visualized using a row-

bioRxiv preprint first posted online May. 9, 2019; doi: http://dx.doi.org/10.1101/633594. The copyright holder for this preprint (which was not peer-reviewed) is the author/funder, who has granted bioRxiv a license to display the preprint in perpetuity. All rights reserved. No reuse allowed without permission.

metric-preserving contribution asymmetric biplot and filtering for the top contributing and well-projected (squared cosine > 0.5) changes in chromatin states.

Motif enrichment analysis in active enhancers

For each time point independently, we defined the set of active enhancers as the overlap between H3K4me1, H3K27ac and ATAC-seq reproducible peaks using *bedtools*[74]. We then ran 3 independent motif enrichment analyses with *homer* v4.9[75] using default parameters.

Transcription factor footprinting

All transcription factor Position-Weight Matrices (PWM) representing eukaryote transcription factors were downloaded from the JASPAR database and used as an input for PIQ[21] to predict transcription factor binding sites from the genome sequence on down-sampled ATAC-seq alignments. For each motif, we retained only binding sites that were within the reproducible ATAC-seq peaks and passed the default purity cut-off (70%). We then computed pairwise PWM similarities based on Pearson's correlation, and clustered together PWMs sharing more than 90% similarity, defining a set of 310 non-redundant and distinct PWMs. The Pearson's correlation between two PWM P^1 and P^2 of length l was defined as:

$$r(P^1, P^2) = \frac{1}{l} \times \sum_{i=1}^{l} \frac{\sum_{b \in \{A,C,G,T\}} \left(P^1_{i,b} - 0.25\right)\left(P^2_{i,b} - 0.25\right)}{\sqrt{\sum_{b \in \{A,C,G,T\}} \left(P^1_{i,b} - 0.25\right)^2 \times \sum_{b \in \{A,C,G,T\}} \left(P^2_{i,b} - 0.25\right)^2}}$$

We further combined the bound instances identified with PIQ according to the PWM clustering.

bioRxiv preprint first posted online May. 9, 2019; doi: http://dx.doi.org/10.1101/633594. The copyright holder for this preprint (which was not peer-reviewed) is the author/funder, who has granted bioRxiv a license to display the preprint in perpetuity. All rights reserved. No reuse allowed without permission.

Transcription factor metrics

For each transcription factor, we computed the chromatin-opening index (COI), the motif dependence and the chromatin dependence (CD) following the approach described in [21].

Validation of PIQ predictions through ChIP-seq

To compare PIQ prediction with RELA, JUN and FOSL2 ChIP-seq data, we first used the approach suggested in [21], computing how many of the total ChIP-seq peaks are overlapping with any potential factor motif (since ChIP-Seq peaks can result from co-factor binding, and methods such as digital genomic footprinting are factor agnostic). We then used a more sophisticated approach aiming at correlating the ChIP-seq signal intensity with the bound / unbound status at PWM matches. For a given transcription factor (cJUN, FOSL2 or RELA,), we first considered all the PWM matches located inside ATAC-seq reproducible peaks, we selected all the PWM matches assigned with a purity score > 0.7 (the threshold used to define “bound” instances), and then randomly selected 3 times more PWM matches assigned to a purity score < 0.7 (considered as “unbound” instances) to obtain a global set containing 25% / 75% of bound / unbound instances for each TF. The selected regions were extended up to 2kb (1kb in each direction, from the middle of the match), and the 2kb intervals were binned in one hundred 20bp windows. We computed the normalized ChIP-seq and ATAC-seq signal inside each bin. The windows were finally ranked according to the summed ChIP-seq signal in the 10 most central bins (200bp). We finally run a set enrichment analysis with the *fgsea* package to assess whether bound / unbound PWM matches were enriched / depleted along this ranking and computed the enrichment score (ES, positive when

bioRxiv preprint first posted online May. 9, 2019; doi: http://dx.doi.org/10.1101/633594. The copyright holder for this preprint (which was not peer-reviewed) is the author/funder, who has granted bioRxiv a license to display the preprint in perpetuity. All rights reserved. No reuse allowed without permission.

bound instances are enriched for highest ChIP-seq signals, negative when unbound instances are depleted for highest ChIP-seq signals) and *p*-values which revealed the strength of the correlation. We performed 1,000 permutations to obtain *p*-values.

Distribution of transcription factor binding sites in space and time

Using the R package *annotatr* we first created an annotation datasets combining coordinates for hg19 promoters, 3'UTRs, exons, introns and intergenic regions as defined in UCSC, as well as our custom set of enhancers (intersection of the global sets of reproducible H3K4me1 peaks with global sets of reproducible H3K27ac peaks, to focus on enhancers that are active at least in one time point during RAS OIS in WI38 fibroblasts). We then annotated the PIQ binding occurrences for each of the PWM independently, and for the 6 time-points independently. Data were further normalized, to account for differences between time-points in the total number of bound occurrences summed across PWM, and finally they were converted to frequencies. We filtered TFs for which less than 100 binding sites were identified throughout the entire timecourse. TFs were ordered according to the proportions of binding sites located in promoters, introns or exons, and we finally computed the density in migrant, settler and pioneer factors along the ranking.

Transcription factor co-binding

For every cluster of PWM and time-point independently, we first removed all the bound instances identified outside enhancers. The remaining bound instances for all PWM were then combined for every time point using GEM *regulatory module discovery*[40]

bioRxiv preprint first posted online May. 9, 2019; doi: http://dx.doi.org/10.1101/633594. The copyright holder for this preprint (which was not peer-reviewed) is the author/funder, who has granted bioRxiv a license to display the preprint in perpetuity. All rights reserved. No reuse allowed without permission.

setting at 500 bp the minimal distance for merging nearby TF bound instances into co-binding regions and at 3 the minimum number of TF bound instances in a co-binding region.

Global pairwise co-binding heatmap. At this step, we obtained a set of contingency matrices M_{mt} of dimension $n_{mt} \times j$ with *i* the number of co-binding regions for the transcriptomic module *m* at the time point *t* and *j* = 310 PWM clusters, for each time point and each transcriptomic module. We then generated module- and time- specific normalized pairwise co-binding matrices C_{mt} by computing the normalized cross-product of matrices M_{mt} defined as:

$$C_{mt} = \frac{M_{mt} \times {}^{t}M_{mt}}{\sum_t \sum_m \sum_j a_{tmj}} \times 10^6$$

with a_{tmj} the number of bound instances for the PWM clusters *j*, in transcriptomic module *m*, at the time point *t*. To get a global picture of pairwise co-binding, we summed these matrices and tested for each combination of PWM clusters A and B whether the overlap between bound instances for A and B was significant using a hyper-geometric test defined as:

$$p(Q, M, n, k) = \sum_{m=k}^{min\,\{k,B\}} \frac{\binom{M}{m}\binom{Q-M}{n-m}}{\binom{Q}{m}}$$

where *Q* is the overall number of regions in the universe, *M* is the number of regions bound by A, *n* is the number of regions bound by B, and *k* the total number of regions bound by A and B. The *p*-values were further corrected for multiple testing using the Bonferroni strategy. We finally clustered the co-binding occurrence matrix using Ward's aggregation criterion and projected corresponding corrected *q*-values on this clustering.

bioRxiv preprint first posted online May. 9, 2019; doi: http://dx.doi.org/10.1101/633594. The copyright holder for this preprint (which was not peer-reviewed) is the author/funder, who has granted bioRxiv a license to display the preprint in perpetuity. All rights reserved. No reuse allowed without permission.

Pair-wise co-binding circos plots. To generate the co-binding circos plots, we used the global time- and, module-specific pair-wise normalized co-binding matrix C_{mt} described above, after a logarithmic transformation. For each time-point and module independently, we selected the top 500 interactions based on their occurrence *N*. The images were generated using the *Circos* suite[76].

Identification of TF regulatory modules

We used the data-sets generated using GEM regulatory module discovery described above. We applied a Hierarchical Dirichlet Process topic model which automatically determines the number of topics from the data, with the hyperparameter for the topic Dirichlet distribution set at 0.1 (encoding the assumption that most of the topics contains a few TFs) and the maximum number of iterations set at 2000. The lexicon usage for each time point and each transcriptomic was explored using a multiple factor analysis (MFA) with the R package *FactoMineR,* and lexicons were further selected based on their goodness of representation on the 3 first components (squared cosine > 0.5).

TF properties

With the aim of characterizing the binding properties of each TF, we computed the dynamicity, the total number of bound regions, the fraction of bound regions in enhancers and the fraction of bound regions before stimulation.

Dynamicity. We quantified the dynamicity of a TF accordingly to the following expression:

bioRxiv preprint first posted online May. 9, 2019; doi: http://dx.doi.org/10.1101/633594. The copyright holder for this preprint (which was not peer-reviewed) is the author/funder, who has granted bioRxiv a license to display the preprint in perpetuity. All rights reserved. No reuse allowed without permission.

$$d(A) = \frac{\sum \frac{n_t(A)}{TR_t}}{\sum \frac{t_t(A)}{TR_t}}$$

where $d(A)$ is the dynamicity of TF A; $n_t(A)$ is the number of regions bound by A for the first time at time point t ; $t_t(A)$ is the number of regions bound by A at time point t and TR_t is the number of regions bound by any TF in time point t. The factor TR_t was added to the expression to account for differences in the number of reads sequenced by the ATAC-seq protocol and normalizes the number of regions bound by TF A based on the number of bound regions detected at its corresponding time point. Notice that, if all samples have the same amount of TF binding events, this expression is reduced to the quotient of the sum of the regions first bound at each time point by the sum of all regions bound by the TF at each time point. By using this definition, the function $d(A)$ maps the activity of a TF to the interval $\left[\frac{1}{N_t}, 1\right]$, where N_t is the number of time points in the timecourse and is higher as the TF binds to previously not bound regions or leaves already bound regions. In the case of a TF that, for every time point, leaves all its previous bound regions and binds to only regions not previously bound, the numerator will be identical to the denominator, leading to $d(A) = 1$. Alternatively, if a TF remains on the same regions it has bound at $t = 0$, then $\sum n_t = n_0$ and $\sum t_t = N_t * n_0$, resulting in $d(A) = \frac{1}{N_t}$. One can observe that, if the same region is bound by TF A in different time points, it will contribute once to the numerator of the expression, while it will contribute to the denominator once for each time point it has been bound to.

Total number of bound regions. The number of bound regions was calculated by the following the expression:

bioRxiv preprint first posted online May. 9, 2019; doi: http://dx.doi.org/10.1101/633594. The copyright holder for this preprint (which was not peer-reviewed) is the author/funder, who has granted bioRxiv a license to display the preprint in perpetuity. All rights reserved. No reuse allowed without permission.

$$R(A) = \frac{\sum \frac{n_t(A)}{TR_t} \times \sum TR_t}{N_t}$$

where $R(A)$ is the normalized number of bound regions by TF A during the timecourse and $n_t(A)$, TR_t and N_t are defined as above. The first factor is a normalized sum of the regions bound by TF A, counting each region only once. The second factor scales the result by the mean of the number of regions bound by all TFs on each day.

TF percentage of binding at enhancers. The ratio of binding at enhancers, relative to all cis regulatory regions, was assessed by:

$$P_E(A) = \frac{R_E(A)}{R_E(A) + R_P(A)}$$

where $P_E(A)$ is the percentage of bound regions in enhancers for TF A, $R_E(A)$ is the number of regions bound by TF A marked as enhancers and $R_P(A)$ is the number of regions bound by TF A marked as promoters.

TF prestimulation binding. For each TF, we computed the ratio of regions bound at T_0, relative to the number of regions bound during the whole timecourse. We used the following definition for the prestimulation binding factor for each TF:

$$p(A) = \frac{\frac{n_{D0}(A)}{TR_{D0}}}{\sum \frac{n_t(A)}{TR_t}}$$

where $p(A)$ corresponds to the prestimulation binding of TF A and $n_t(A)$ and TR_t are defined as above. The numerator of this expression corresponds to the normalized number of regions bound by TF A at t = T_0, while the denominator is the normalized number of regions bound by TF A during the whole timecourse. Notice the denominator also corresponds to factor $R(A)$ before scaling.

bioRxiv preprint first posted online May. 9, 2019; doi: http://dx.doi.org/10.1101/633594. The copyright holder for this preprint (which was not peer-reviewed) is the author/funder, who has granted bioRxiv a license to display the preprint in perpetuity. All rights reserved. No reuse allowed without permission.

Hierarchical transcription factor network

In order to assess the TF chromatin binding hierarchy, i.e. TFs required for the binding of a specific TF, we generated a network for each gene module depicting the precedence of TF chromatin binding. The algorithms mentioned were implemented in R and all networks were visualized in CytoScape[77].

Computing precedence relationships. The edges in the generated networks represent the precedence relationship of TFs: an oriented edge from TF A to TF B, represented as (A, B), means that A was present in at least 30 % of the cis-regulatory regions bound by B at the same instant or before[44]. To account for the difference in the number of reads sequenced for each sample in the ATAC-seq, we normalized the number of regions bound based on the first day they appeared. The weight of an edge from A to B is given by:

$$w_{A\rightarrow B} = \frac{\sum \frac{R_t(A,B)}{R_t}}{\sum \frac{R_t(B)}{R_t}}$$

where $R_t(B)$ stands for the number of regions first bound by TF B at time point t ; $R_t(A,B)$, for the number of regions first bound by TF B at time point t that were bound by TF A at time point t or before; and R_t represents the total number of regions bound by any TF in time point t. In order to handle the networks, we used the *igraph* package[78].

Network simplification. Aiming to analyze the hierarchical relationship of TFs and simplify the interpretation of the network, we performed two operations over each gene module network: Vertex Sort and transitive reduction (TR)[79]. Briefly, the vertex sort algorithm assigns two parameters for each node in the network: the distance, in edges, between the node and the bottom of the network; and the distance between the node

bioRxiv preprint first posted online May. 9, 2019; doi: http://dx.doi.org/10.1101/633594. The copyright holder for this preprint (which was not peer-reviewed) is the author/funder, who has granted bioRxiv a license to display the preprint in perpetuity. All rights reserved. No reuse allowed without permission.

and the top of the network. Combined, those parameters allow for the topological ordering of the network, which consists in listing its nodes such that nodes at the top precede downstream nodes. We then defined the 'top layer' as the set of nodes with lowest distance to the top of the network, i.e., nodes that have no incoming edges or nodes that assemble a strongly connected component (SCC) with all upstream nodes. Analogously, the 'bottom layer' was defined as the set of nodes with lowest distance to the bottom of the network, i.e., nodes with no outgoing edges or that form a SCC with all downstream nodes. The 'core layer' comprises nodes that link top layer and bottom layer. Nodes in the core layer that are exactly one edge from both top and bottom layers constitute the 'single-level core layer', while nodes that link top and bottom through paths composed of more than one edge form the 'multi-level core layer'. The result of this procedure for each gene module can be seen in Figure 4 and supplementary data. The TR, in turn, simplifies the network visualization by generating the network with the smallest number of edges that keeps the reachability of the original network.

Network validation. We validated our approach by comparing the network produced when applying our method to the ChIP-seq data produced by [44] with the network they obtained. Transcription factor ChIP-seq peak files were retrieved from Gene Expression Omnibus (GSE36099, 23 TFs, and 4 time points; note that RUNX1 and ATF4 were discarded from the analysis since one and three time points, respectively, were missing on GEO for those TFs) and preprocessed as previously described to generated time resolved co-binding matrices, further used as an input for our networking algorithm. We computed the precedence relationships among TFs and generated the TF binding hierarchy networks for visualization. We compared the produced TF hierarchy network with the network shown in Figure S4 and in [44] using two metrics: sensitivity and

bioRxiv preprint first posted online May. 9, 2019; doi: http://dx.doi.org/10.1101/633594. The copyright holder for this preprint (which was not peer-reviewed) is the author/funder, who has granted bioRxiv a license to display the preprint in perpetuity. All rights reserved. No reuse allowed without permission.

specificity. Sensitivity is calculated as the ratio of edges described in this study over the edge number sum for both networks. Specificity is defined as the ratio of the number of edges that were described to not exist in the network produced by our software over the number of edges described to not occur in any of both studies.

Proportion of incoming edges based on the classification of the TF source node. Aiming to assess the hierarchy of TFs accordingly to their chromatin dependence and chromatin-opening index, we computed the number of edges connecting the sets of all TFs with a given classification for each gene module. We then divided those values by the number of edges that target TFs with a specific classification. Hence, the proportion of incoming edges based on TF classification is given by:

$$P_{C1\rightarrow C2} = \frac{|W_{C1\rightarrow C2}|}{\sum|W_{K\rightarrow C2}|}$$

where $P_{C1\rightarrow C2}$ is the proportion of edges from nodes with classification C1 to nodes with classification C2; $W_{C1\rightarrow C2}$ is the set of edges from nodes with classification C1 to nodes with classification C2; K can represent either pioneer, settler or migrant and |·| means the cardinality of a set, *i.e.* the number of elements it contains.

We assessed the classification precedence significance for TF interaction with a hyper-geometric test. We consider the sample space as all possible oriented edges in a network with the same number of nodes for each classification as the hierarchy network for a given transcriptional module. Formally:

$$p_{C1\rightarrow C2}(E, E_{C1\rightarrow C2}, W, W_{C1\rightarrow C2}) = \sum_{x=|W_{C1\rightarrow C2}|}^{|W|} \frac{\binom{E_{C1\rightarrow C2}}{x}\binom{E-E_{C1\rightarrow C2}}{|W|-x}}{\binom{E}{|W|}}$$

Where $E$is the number of edges on the sample space network, i.e., a fully connected network with the same number of nodes as the TF hierarchy network for a

bioRxiv preprint first posted online May. 9, 2019; doi: http://dx.doi.org/10.1101/633594. The copyright holder for this preprint (which was not peer-reviewed) is the author/funder, who has granted bioRxiv a license to display the preprint in perpetuity. All rights reserved. No reuse allowed without permission.

given transcriptional module (excluding self-loops), $E_{C1\rightarrow C2}$ is the number of edges from TFs with classification $C1$ to TFs with classification $C2$ in the sample space network, $|W|$ is the number of edges on the TF hierarchy network for a given transcriptional module and $|W_{C1\rightarrow C2}|$ is the number of edges in the same network connecting TFs with classification $C1$ to TFs with classification $C2$.

Network visualization. In order to visualize the network, we exported the adjacency matrices in the R environment to CytoScape using the CyREST API[80]. The networks' layout and style were automated with the help of packages RCy3[81] and RJSONIO.

Network mining

With the purpose of identifying key TFs in the transition to the senescent phenotype, we analyzed the TF binding characteristics with their relative location in the chromatin binding hierarchy networks for each gene module. The figures illustrating this analysis were generated with the help of the ggplot2 R package.

TF classification. For each network relative to a transcriptional gene module, the number of TF classified as either pioneer, settler or migrant was calculated for each layer, with the subdivision of the core layer as 'multi-level' and 'single-level' (see "*Network simplification*"). The overrepresentation of TFs with a specific classification in a given layer was evaluated by using a hypergeometric test. We calculated the *p*-value given by:

$$p(K,N,n,k) = \sum \frac{\binom{K}{x}\binom{N-K}{n-x}}{\binom{N}{n}}$$

where *K* is the number of TFs with a certain classification in the whole network, *N* is the number of TFs in the network; *n* is the number of TFs that belong to a specific layer and

bioRxiv preprint first posted online May. 9, 2019; doi: http://dx.doi.org/10.1101/633594. The copyright holder for this preprint (which was not peer-reviewed) is the author/funder, who has granted bioRxiv a license to display the preprint in perpetuity. All rights reserved. No reuse allowed without permission.

k is the number of TFs that belong to the same layer and have the referred classification. The *p*-values were corrected for multiple testing with FDR and a corrected $p = 0.05$ was considered an indicative of enrichment for that specific classification in the corresponding layer.

TF dynamicity. For each network relative to a transcriptional gene module, we compared the distribution of the dynamicity of TFs belonging to a certain layer with the distribution of the dynamicity of TFs belonging to the rest of the network. We used the dynamicity index defined previously for each TF, considering only the regions marked as enhancers belonging only to the gene module relative to the network. For each layer in the network, we applied the Kolmogorov-Smirnov test to compare the TF dynamicity distribution for the chosen layer with the dynamicity distribution relative to the TFs belonging to three other layers in the respective network. To account for multiple hypothesis testing, we also performed an FDR correction, considering values of $p = 0.05$ as an indicative of statistical significance.

TF number of binding regions. We performed the same analysis as described in the previous section ("*TF dynamicity*") for the number of bound regions defined in section "*Total number of bound regions*", instead of the dynamicity index.

TF binding characteristics and transcriptional modules. In order to characterize the binding activity of each TF for the different gene modules, we ranked them accordingly to their dynamicity and their number of bound regions. Both parameters for each gene module are shown in Supplementary Figure 4E, which was generated with the *ComplexHeatmap*[82] and *circlize*[83] R packages. We used the mean of the ratio dynamicity - number of bound regions to order the TFs. We assessed the significance of pioneer (respectively, migrant) TF enrichment at the top (respectively, bottom) of the

bioRxiv preprint first posted online May. 9, 2019; doi: http://dx.doi.org/10.1101/633594. The copyright holder for this preprint (which was not peer-reviewed) is the author/funder, who has granted bioRxiv a license to display the preprint in perpetuity. All rights reserved. No reuse allowed without permission.

ranked clustered list by employing a set enrichment analysis implemented in the package fgsea.

TF chromatin binding hierarchy networks overlap. To analyze the similarity between the networks for different transcriptional gene modules, we generated a 7-set Euler diagram, where each set contains the edges present in the TF hierarchy network relative to a gene module. Edges in two different networks are considered equal if they link nodes corresponding to the same TFs in their respective networks. We used the package Vennerable to compute the intersections of all possible network combinations and to create the Euler diagram in Supplementary Figures 4F-I. In this figure, the area of each region is proportional to the number of edges shared by the networks corresponding to the sets that contain the referred region and was calculated using the Chow-Ruskey algorithm[84]. A Euler diagram is similar to a Venn diagram, with the difference that the area of a region representing a set is proportional to the number of elements in the set.

Analysis of *de novo* and remnant enhancers

To track combinatorial chromatin state dynamics in space and time, we integrated histone modification ChIP-seq signals at a sub-nucleosomal resolution considering non-overlapping 100bp windows genome-wide using chromstaR (see above), which converts quantitative ChIP-seq data to qualitative chromatin states. For subsequent analysis, since these 100bp windows can be either isolated or organized in stretches experiencing consistent changes in states, we summarized the information at a higher level, and linked them with the histone modification peaks identified using the more classical ChIP-seq and ATAC-seq peak-calling approach (see flowchart). Briefly, after merging all the peaks identified for all the time-points, for all the histone modification and

bioRxiv preprint first posted online May. 9, 2019; doi: http://dx.doi.org/10.1101/633594. The copyright holder for this preprint (which was not peer-reviewed) is the author/funder, who has granted bioRxiv a license to display the preprint in perpetuity. All rights reserved. No reuse allowed without permission.

for the ATAC-seq data sets defining *cis*-regulatory regions, we determined the overlap between "poised enhancers"-, "*de novo* enhancers"-, "remnant enhancer" or "constitutive enhancers"-flagged 100bp windows. When an overlap was found, the entire *cis*-regulatory regions were annotated according to the 100bp window it is overlapping with. This operation rendered a list of annotated *cis*-regulatory regions with *de novo*, constitutive, poised or remnant enhancer elements. We finally considered the center +/- 10kb of these elements.

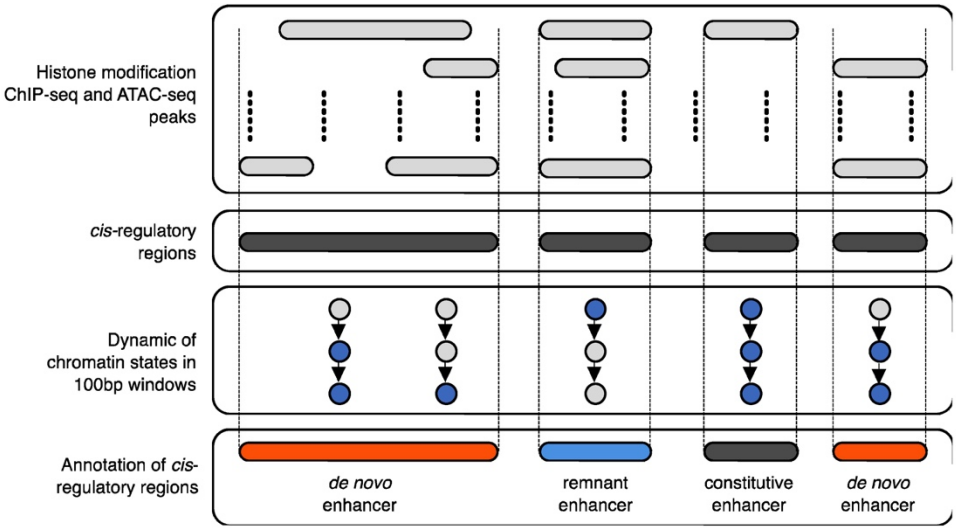

CRISPR interference (CRISPRi)

hU6-gRNA-hUbc-dCas9-KRAB plasmid was a kind gift from Charles Gerbach (Addgene 71236). gRNA cloning was as published [34]. Briefly, the plasmid was digested with BsmBI and dephosphorylated before ligation with phosphorylated oligo pairs. The gRNA sequences were listed in the Table 1. The plasmid was then transfected in HEK293T cells, together with packaging plasmids psPAX2 and pMD2.G. 24 hours after fresh

bioRxiv preprint first posted online May. 9, 2019; doi: http://dx.doi.org/10.1101/633594. The copyright holder for this preprint (which was not peer-reviewed) is the author/funder, who has granted bioRxiv a license to display the preprint in perpetuity. All rights reserved. No reuse allowed without permission.

medium was added and the medium containing lentivirus was collected and filtered subsequently. Cells were infected for 3 hours. 3 days post infection, cells were passaged and selected with puromycin and used for analyses.

Table 1. gRNA sequences

gRNA	Sequence	
ctrl	caccgGTATTACTGATATTGGTGGG	aaacCCCACCAATATCAGTAATACc
2	caccgAGATGAGGTGTTGCGTGTCT	aaacAGACACGCAACACCTCATCTc
7	caccgTCTGCTCATTGGGGATCGGA	aaacTCCGATCCCCAATGAGCAGAc
14	caccgAAGGCGAAGAAGACTGACTC	aaacGAGTCAGTCTTCTTCGCCTTc
15	caccgCAATGAAATGACTCCCTCTC	aaacGAGAGGGAGTCATTTCATTGc
48	caccgGGAGAACAGTCGCATGAACA	aaacTGTTCATGCGACTGTTCTCCc
54	caccgTTCCAGGGAGTCACCTGTCC	aaacGGACAGGTGACTCCCTGGAAc
61	caccgTTGAAGCAGCACTAGTATCC	aaacGGATACTAGTGCTGCTTCAAc

Immunofluorescence staining and imaging of cells

Immunofluorescence staining was performed as previously published[85]. Cells grown in 96-well plates were fixed with 4% PFA and permeabilised with 0.2% Triton-X in PBS. After blocking, the cells were incubated with primary antibody for 1 hour, and then Alexa Fluor secondary antibody for 30 min. Nuclei were counterstained with DAPI. The antibodies were listed in Table 2. The imaging was carried out by IN Cell Analyzer 2000 (GE Healthcare) with the 20x objective and the quantification was processed using IN Cell Investigator 2.7.3 software.

bioRxiv preprint first posted online May. 9, 2019; doi: http://dx.doi.org/10.1101/633594. The copyright holder for this preprint (which was not peer-reviewed) is the author/funder, who has granted bioRxiv a license to display the preprint in perpetuity. All rights reserved. No reuse allowed without permission.

Table 2. Antibodies

Antibody	Dilution	Cat. No.
IL1α	1:100	R&D MAB200
IL1β	1:100	R&D MAB201
IL8	1:100	R&D MAB208

Quantitative RT-qPCR

RNA was extracted with TRIzol (Ambion) and RNAeasy Mini Kit (Qiagen) according to the manufacturer's protocol. Reverse transcription was carried out with SuperScript II RT kit (Invitrogen). Samples were analysed with SYBR Green PCR Master Mix (Applied Biosystems) in CFX96™ Real-Time PCR Detection system (Bio-Rad). Ribosomal protein S14 (RPS14) was used as the housekeeping gene. Primers are listed in Table 3.

Table 3. qPCR primer sequence

Gene	Sequence	
RPS14	CTGCGAGTGCTGTCAGAGG	TCACCGCCCTACACATCAAACT
IL1α	AGTGCTGCTGAAGGAGATGCCTGA	CCCCTGCCAAGCACACCCAGTA
IL1β	GGAGATTCGTAGCTGGATGC	AGCTGATGGCCCTAAACAGA
IL8	GAGTGGACCACACTGCGCCA	TCCACAACCCTCTGCACCCAGT

bioRxiv preprint first posted online May. 9, 2019; doi: http://dx.doi.org/10.1101/633594. The copyright holder for this preprint (which was not peer-reviewed) is the author/funder, who has granted bioRxiv a license to display the preprint in perpetuity. All rights reserved. No reuse allowed without permission.

Data availability

All transcriptome data are hosted on Gene Expression Omnibus (BioProject PRJNA439263, accession n°GSE112084). ATAC-seq, and ChIP-seq data (histone modification and transcription factor) are hosted on SRA (BioProject PRJNA439280).

Code availability for reproducible science

Interactive maps, circus plots, workflows, scripts and software developed to pre-process raw data, perform statistical analyses as well as data mining and integration are available as .html, and R Markdown files provided in Supplementary data hosted on Zenodo (https://zenodo.org, DOI : 10.5281/zenodo.1493872). This archive collapses all the material (including processed data) required to reproduce figures presented in the manuscript.

ACKNOWLEDGMENTS

We thank all members, in particular Nir Rozenblum, of the O.B. laboratory for fruitful discussions and suggestions through the course of this work. We would like to thank the Transcriptome and Epigenome facility of Institut Pasteur. We thank Claudia Chica for expert advice on ChIP-seq data processing. We thank Ido Amit and Deborah Winter for valuable discussion and technical support. We thank Benno Schwikowski for key insights and technical advice. We also thank Lars Zender, Eric Gilson, and Hinrich Gronemeyer for valuable intellectual input. R.I.M-Z. was supported by La Ligue Nationale Contre le Cancer and was a Mexican National Scientific and Technology Council (CONACYT) and Mexican National Researchers System (SNI) fellow. Lucas

bioRxiv preprint first posted online May. 9, 2019; doi: http://dx.doi.org/10.1101/633594. The copyright holder for this preprint (which was not peer-reviewed) is the author/funder, who has granted bioRxiv a license to display the preprint in perpetuity. All rights reserved. No reuse allowed without permission.

Robinson was supported by the Pasteur - Paris University (PPU) International PhD Program and by the Fondation pour la Recherche Médicale (FRM). J.A.N.L.F.F. was supported by La Ligue Nationale Contre le Cancer. O.B was supported by the Pasteur-Weizmann Foundation, ANR-BMFT, Fondation ARC pour la recherche sur le Cancer, La Ligue Nationale Contre le Cancer, INSERM-AGEMED. Research reported in this publication was supported by the National Cancer Institute of the National Institutes of Health under Award Number R01CA136533. The content is solely the responsibility of the authors and does not necessarily represent the official views of the National Institutes of Health. O.B. is a CNRS Research Director DR2.

AUTHOR CONTRIBUTIONS

R.I.M-Z, P.-F.R and O.B conceived of the study and conceptual ideas. R.I.M-Z, P.-F.R and O.B. planned, designed experiments, interpreted data and wrote the manuscript. All authors discussed the results and contributed to the final manuscript. R.I.M-Z generated the cell culture system and performed ChIP-seq, ATAC-seq and RNAi experiments. P-F.R performed computational analyses, designed bioinformatics pipelines and prepared figures. L.R. performed senescence characterization studies and performed ChIP-seq experiments. J.A.N.L.F.F. generated TF networks. G.D. generated Affymetrix microarray data. B.S. and J.G. performed CRISPRi experiments. U.H. supported the study. O.B. supervised, managed and obtained funding for the study.

DECLARATION OF INTERESTS

The authors declare no conflict of interest.

bioRxiv preprint first posted online May. 9, 2019; doi: http://dx.doi.org/10.1101/633594. The copyright holder for this preprint (which was not peer-reviewed) is the author/funder, who has granted bioRxiv a license to display the preprint in perpetuity. All rights reserved. No reuse allowed without permission.

REFERENCES

1. Martinez-Zamudio, R.I., Robinson, L., Roux, P.F. & Bischof, O. SnapShot: Cellular Senescence in Pathophysiology. *Cell* **170**, 1044-1044 e1 (2017).

2. Kirkland, J.L. & Tchkonia, T. Cellular Senescence: A Translational Perspective. *EBioMedicine* **21**, 21-28 (2017).

3. Martinez-Zamudio, R.I., Robinson, L., Roux, P.F. & Bischof, O. SnapShot: Cellular Senescence Pathways. *Cell* **170**, 816-816 e1 (2017).

4. Coppe, J.P., Desprez, P.Y., Krtolica, A. & Campisi, J. The senescence-associated secretory phenotype: the dark side of tumor suppression. *Annu Rev Pathol* **5**, 99-118 (2010).

5. Franceschi, C. & Campisi, J. Chronic inflammation (inflammaging) and its potential contribution to age-associated diseases. *J Gerontol A Biol Sci Med Sci* **69 Suppl 1**, S4-9 (2014).

6. Schosserer, M., Grillari, J. & Breitenbach, M. The Dual Role of Cellular Senescence in Developing Tumors and Their Response to Cancer Therapy. *Front Oncol* **7**, 278 (2017).

7. Benhamed, M., Herbig, U., Ye, T., Dejean, A. & Bischof, O. Senescence is an endogenous trigger for microRNA-directed transcriptional gene silencing in human cells. *Nat Cell Biol* **14**, 266-75 (2012).

8. Shah, P.P. *et al.* Lamin B1 depletion in senescent cells triggers large-scale changes in gene expression and the chromatin landscape. *Genes Dev* **27**, 1787-99 (2013).

9. Puvvula, P.K. *et al.* Long noncoding RNA PANDA and scaffold-attachment-factor SAFA control senescence entry and exit. *Nat Commun* **5**, 5323 (2014).

bioRxiv preprint first posted online May. 9, 2019; doi: http://dx.doi.org/10.1101/633594. The copyright holder for this preprint (which was not peer-reviewed) is the author/funder, who has granted bioRxiv a license to display the preprint in perpetuity. All rights reserved. No reuse allowed without permission.

10. Rai, T.S. *et al.* HIRA orchestrates a dynamic chromatin landscape in senescence and is required for suppression of neoplasia. *Genes Dev* **28**, 2712-25 (2014).

11. Tasdemir, N. *et al.* BRD4 Connects Enhancer Remodeling to Senescence Immune Surveillance. *Cancer Discov* **6**, 612-29 (2016).

12. Sen, P. *et al.* Histone Acetyltransferase p300 Induces De Novo Super-Enhancers to Drive Cellular Senescence. *Mol Cell* **73**, 684-698 e8 (2019).

13. Heinz, S., Romanoski, C.E., Benner, C. & Glass, C.K. The selection and function of cell type-specific enhancers. *Nat Rev Mol Cell Biol* **16**, 144-54 (2015).

14. Creyghton, M.P. *et al.* Histone H3K27ac separates active from poised enhancers and predicts developmental state. *Proc Natl Acad Sci U S A* **107**, 21931-6 (2010).

15. Ostuni, R. *et al.* Latent enhancers activated by stimulation in differentiated cells. *Cell* **152**, 157-71 (2013).

16. van Oevelen, C. *et al.* C/EBPalpha Activates Pre-existing and De Novo Macrophage Enhancers during Induced Pre-B Cell Transdifferentiation and Myelopoiesis. *Stem Cell Reports* **5**, 232-47 (2015).

17. Huggins, C.J. *et al.* C/EBPgamma suppresses senescence and inflammatory gene expression by heterodimerizing with C/EBPbeta. *Mol Cell Biol* **33**, 3242-58 (2013).

18. Nardella, C., Clohessy, J.G., Alimonti, A. & Pandolfi, P.P. Pro-senescence therapy for cancer treatment. *Nat Rev Cancer* **11**, 503-11 (2011).

19. Drouin, J. Minireview: pioneer transcription factors in cell fate specification. *Mol Endocrinol* **28**, 989-98 (2014).

20. Soufi, A. *et al.* Pioneer transcription factors target partial DNA motifs on nucleosomes to initiate reprogramming. *Cell* **161**, 555-568 (2015).

bioRxiv preprint first posted online May. 9, 2019; doi: http://dx.doi.org/10.1101/633594. The copyright holder for this preprint (which was not peer-reviewed) is the author/funder, who has granted bioRxiv a license to display the preprint in perpetuity. All rights reserved. No reuse allowed without permission.

21. Sherwood, R.I. *et al.* Discovery of directional and nondirectional pioneer transcription factors by modeling DNase profile magnitude and shape. *Nat Biotechnol* **32**, 171-178 (2014).

22. Takahashi, K. & Yamanaka, S. Induction of pluripotent stem cells from mouse embryonic and adult fibroblast cultures by defined factors. *Cell* **126**, 663-76 (2006).

23. Martin, N. *et al.* Physical and functional interaction between PML and TBX2 in the establishment of cellular senescence. *EMBO J* **31**, 95-109 (2012).

24. Buenrostro, J.D., Giresi, P.G., Zaba, L.C., Chang, H.Y. & Greenleaf, W.J. Transposition of native chromatin for fast and sensitive epigenomic profiling of open chromatin, DNA-binding proteins and nucleosome position. *Nat Methods* **10**, 1213-8 (2013).

25. Loffler-Wirth, H., Kalcher, M. & Binder, H. oposSOM: R-package for high-dimensional portraying of genome-wide expression landscapes on bioconductor. *Bioinformatics* **31**, 3225-7 (2015).

26. Martinez, O. & Reyes-Valdes, M.H. Defining diversity, specialization, and gene specificity in transcriptomes through information theory. *Proc Natl Acad Sci U S A* **105**, 9709-14 (2008).

27. Patel, P.L., Suram, A., Mirani, N., Bischof, O. & Herbig, U. Derepression of hTERT gene expression promotes escape from oncogene-induced cellular senescence. *Proc Natl Acad Sci U S A* **113**, E5024-33 (2016).

28. Milanovic, M. *et al.* Senescence-associated reprogramming promotes cancer stemness. *Nature* **553**, 96-100 (2018).

29. Zhang, B. & Horvath, S. A general framework for weighted gene co-expression network analysis. *Stat Appl Genet Mol Biol* **4**, Article17 (2005).

bioRxiv preprint first posted online May. 9, 2019; doi: http://dx.doi.org/10.1101/633594. The copyright holder for this preprint (which was not peer-reviewed) is the author/funder, who has granted bioRxiv a license to display the preprint in perpetuity. All rights reserved. No reuse allowed without permission.

30. Yosef, N. & Regev, A. Impulse control: temporal dynamics in gene transcription. *Cell* **144**, 886-96 (2011).

31. Deng, T. & Karin, M. c-Fos transcriptional activity stimulated by H-Ras-activated protein kinase distinct from JNK and ERK. *Nature* **371**, 171-5 (1994).

32. Thakore, P.I. *et al.* Highly specific epigenome editing by CRISPR-Cas9 repressors for silencing of distal regulatory elements. *Nat Methods* **12**, 1143-9 (2015).

33. Klann, T.S. *et al.* CRISPR-Cas9 epigenome editing enables high-throughput screening for functional regulatory elements in the human genome. *Nat Biotechnol* **35**, 561-568 (2017).

34. Gilbert, L.A. *et al.* Genome-Scale CRISPR-Mediated Control of Gene Repression and Activation. *Cell* **159**, 647-61 (2014).

35. Kaikkonen, M.U. *et al.* Remodeling of the enhancer landscape during macrophage activation is coupled to enhancer transcription. *Mol Cell* **51**, 310-25 (2013).

36. Wang, A. *et al.* Epigenetic priming of enhancers predicts developmental competence of hESC-derived endodermal lineage intermediates. *Cell Stem Cell* **16**, 386-99 (2015).

37. Zinzen, R.P., Girardot, C., Gagneur, J., Braun, M. & Furlong, E.E. Combinatorial binding predicts spatio-temporal cis-regulatory activity. *Nature* **462**, 65-70 (2009).

38. Wilkinson, A.C., Nakauchi, H. & Gottgens, B. Mammalian Transcription Factor Networks: Recent Advances in Interrogating Biological Complexity. *Cell Syst* **5**, 319-331 (2017).

39. Neph, S. *et al.* An expansive human regulatory lexicon encoded in transcription factor footprints. *Nature* **489**, 83-90 (2012).

bioRxiv preprint first posted online May. 9, 2019; doi: http://dx.doi.org/10.1101/633594. The copyright holder for this preprint (which was not peer-reviewed) is the author/funder, who has granted bioRxiv a license to display the preprint in perpetuity. All rights reserved. No reuse allowed without permission.

40. Guo, Y. & Gifford, D.K. Modular combinatorial binding among human trans-acting factors reveals direct and indirect factor binding. *BMC Genomics* **18**, 45 (2017).

41. Ren, X. & Kerppola, T.K. REST interacts with Cbx proteins and regulates polycomb repressive complex 1 occupancy at RE1 elements. *Mol Cell Biol* **31**, 2100-10 (2011).

42. Li, T. *et al.* CTCF regulates allelic expression of Igf2 by orchestrating a promoter-polycomb repressive complex 2 intrachromosomal loop. *Mol Cell Biol* **28**, 6473-82 (2008).

43. Weinmann, A.S., Bartley, S.M., Zhang, T., Zhang, M.Q. & Farnham, P.J. Use of chromatin immunoprecipitation to clone novel E2F target promoters. *Mol Cell Biol* **21**, 6820-32 (2001).

44. Garber, M. *et al.* A high-throughput chromatin immunoprecipitation approach reveals principles of dynamic gene regulation in mammals. *Mol Cell* **47**, 810-22 (2012).

45. Novershtern, N. *et al.* Densely interconnected transcriptional circuits control cell states in human hematopoiesis. *Cell* **144**, 296-309 (2011).

46. Zaret, K.S. & Carroll, J.S. Pioneer transcription factors: establishing competence for gene expression. *Genes Dev* **25**, 2227-41 (2011).

47. Jozwik, K.M. & Carroll, J.S. Pioneer factors in hormone-dependent cancers. *Nat Rev Cancer* **12**, 381-5 (2012).

48. Wisdom, R., Johnson, R.S. & Moore, C. c-Jun regulates cell cycle progression and apoptosis by distinct mechanisms. *EMBO J* **18**, 188-97 (1999).

49. Weitzman, J.B., Fiette, L., Matsuo, K. & Yaniv, M. JunD protects cells from p53-dependent senescence and apoptosis. *Mol Cell* **6**, 1109-19 (2000).

bioRxiv preprint first posted online May. 9, 2019; doi: http://dx.doi.org/10.1101/633594. The copyright holder for this preprint (which was not peer-reviewed) is the author/funder, who has granted bioRxiv a license to display the preprint in perpetuity. All rights reserved. No reuse allowed without permission.

50. Hoare, M. *et al.* NOTCH1 mediates a switch between two distinct secretomes during senescence. *Nat Cell Biol* **18**, 979-92 (2016).

51. Duronio, R.J. & Xiong, Y. Signaling pathways that control cell proliferation. *Cold Spring Harb Perspect Biol* **5**, a008904 (2013).

52. Biddie, S.C. *et al.* Transcription factor AP1 potentiates chromatin accessibility and glucocorticoid receptor binding. *Mol Cell* **43**, 145-55 (2011).

53. Vierbuchen, T. *et al.* AP-1 Transcription Factors and the BAF Complex Mediate Signal-Dependent Enhancer Selection. *Mol Cell* **68**, 1067-1082 e12 (2017).

54. Krtolica, A., Parrinello, S., Lockett, S., Desprez, P.Y. & Campisi, J. Senescent fibroblasts promote epithelial cell growth and tumorigenesis: a link between cancer and aging. *Proc Natl Acad Sci U S A* **98**, 12072-7 (2001).

55. van Deursen, J.M. The role of senescent cells in ageing. *Nature* **509**, 439-46 (2014).

56. Eggert, T. *et al.* Distinct Functions of Senescence-Associated Immune Responses in Liver Tumor Surveillance and Tumor Progression. *Cancer Cell* **30**, 533-547 (2016).

57. Tsankov, A.M. *et al.* Transcription factor binding dynamics during human ES cell differentiation. *Nature* **518**, 344-9 (2015).

58. Goode, D.K. *et al.* Dynamic Gene Regulatory Networks Drive Hematopoietic Specification and Differentiation. *Dev Cell* **36**, 572-87 (2016).

59. Xu, M. *et al.* Senolytics improve physical function and increase lifespan in old age. *Nat Med* **24**, 1246-1256 (2018).

60. Overman, J. *et al.* Pharmacological targeting of the transcription factor SOX18 delays breast cancer in mice. *Elife* **6**(2017).

bioRxiv preprint first posted online May. 9, 2019; doi: http://dx.doi.org/10.1101/633594. The copyright holder for this preprint (which was not peer-reviewed) is the author/funder, who has granted bioRxiv a license to display the preprint in perpetuity. All rights reserved. No reuse allowed without permission.

61. Itahana, K., Campisi, J. & Dimri, G.P. Methods to detect biomarkers of cellular senescence: the senescence-associated beta-galactosidase assay. *Methods Mol Biol* **371**, 21-31 (2007).

62. Ritchie, M.E. *et al.* limma powers differential expression analyses for RNA-sequencing and microarray studies. *Nucleic Acids Res* **43**, e47 (2015).

63. Langfelder, P. & Horvath, S. WGCNA: an R package for weighted correlation network analysis. *BMC Bioinformatics* **9**, 559 (2008).

64. Landt, S. G. *et al.* ChIP-seq guidelines and practices of the ENCODE and modENCODE consortia. *Genome Res.* **22,** 1813–31 (2012).

65. Bolger, A. M., Lohse, M. & Usadel, B. Trimmomatic: a flexible trimmer for Illumina sequence data. *Bioinformatics* **30,** 2114–20 (2014).

66. Martin, M. Cutadapt removes adapter sequences from high-throughput sequencing reads. *EMBnet.journal* **17,** 10–12 (2011).

67. Ramírez, F. *et al.* deepTools2: a next generation web server for deep-sequencing data analysis. *Nucleic Acids Res.* **44,** W160–W165 (2016).

68. Ross-Innes, C. S. *et al.* Differential oestrogen receptor binding is associated with clinical outcome in breast cancer. *Nature* **481,** 389–93 (2012).

69. Risso, D., Schwartz, K., Sherlock, G. & Dudoit, S. GC-content normalization for RNA-Seq data. *BMC Bioinformatics* **12,** 480 (2011).

70. Risso, D., Ngai, J., Speed, T. P. & Dudoit, S. Normalization of RNA-seq data using factor analysis of control genes or samples. *Nat. Biotechnol.* **32,** 896–902 (2014).

71. Robinson, M. D., McCarthy, D. J. & Smyth, G. K. edgeR: a Bioconductor package for differential expression analysis of digital gene expression data. *Bioinformatics* **26,** 139–40 (2010).

bioRxiv preprint first posted online May. 9, 2019; doi: http://dx.doi.org/10.1101/633594. The copyright holder for this preprint (which was not peer-reviewed) is the author/funder, who has granted bioRxiv a license to display the preprint in perpetuity. All rights reserved. No reuse allowed without permission.

72. Taudt, A., Nguyen, M. A., Heinig, M., Johannes, F. & Colome-Tatche, M. chromstaR: Tracking combinatorial chromatin state dynamics in space and time. *bioRxiv* 038612 (2016). doi:10.1101/038612

73. Lê, S., Josse, J. & Husson, F. FactoMineR: An R package for multivariate analysis. **25,** 1–18 (2008).

74. Quinlan, A. R. & Hall, I. M. BEDTools: a flexible suite of utilities for comparing genomic features. *Bioinformatics* **26,** 841–2 (2010).

75. Heinz, S. *et al.* Simple Combinations of Lineage-Determining Transcription Factors Prime cis-Regulatory Elements Required for Macrophage and B Cell Identities. *Mol. Cell* **38,** 576–589 (2010).

76. Krzywinski, M. *et al.* Circos: an information aesthetic for comparative genomics. *Genome Res.* **19,** 1639–45 (2009).

77. Shannon, P. *et al.* Cytoscape: A Software Environment for Integrated Models of Biomolecular Interaction Networks. *Genome Res.* **13,** 2498–2504 (2003).

78. Csárdi, G. & Nepusz, T. The igraph software package for complex network research.

79. Aho, A. V., Garey, M. R. & Ullman, J. D. The Transitive Reduction of a Directed Graph. *SIAM J. Comput.* **1,** 131–137 (1972).

80. Ono, K., Muetze, T., Kolishovski, G., Shannon, P. & Demchak, B. CyREST: Turbocharging Cytoscape Access for External Tools via a RESTful API. *F1000Research* **4,** 478 (2015).

81. Shannon, P. T., Grimes, M., Kutlu, B., Bot, J. J. & Galas, D. J. RCytoscape: tools for exploratory network analysis. *BMC Bioinformatics* **14,** 217 (2013).

82. Gu, Z., Eils, R. & Schlesner, M. Complex heatmaps reveal patterns and

bioRxiv preprint first posted online May. 9, 2019; doi: http://dx.doi.org/10.1101/633594. The copyright holder for this preprint (which was not peer-reviewed) is the author/funder, who has granted bioRxiv a license to display the preprint in perpetuity. All rights reserved. No reuse allowed without permission.

correlations in multidimensional genomic data. *Bioinformatics* **32,** 2847–2849 (2016).

83. Gu, Z., Gu, L., Eils, R., Schlesner, M. & Brors, B. Circlize implements and enhances circular visualization in R. *Bioinformatics* **30,** 2811–2812 (2014).

84. Chow, S. & Ruskey, F. Drawing Area-Proportional Venn and Euler Diagrams. in 466–477 (Springer, Berlin, Heidelberg, 2004). doi:10.1007/978-3-540-24595-7_44

85. Georgilis, A. *et al.* PTBP1-Mediated Alternative Splicing Regulates the Inflammatory Secretome and the Pro-tumorigenic Effects of Senescent Cells. *Cancer Cell* **34,** 85–102.e9 (2018).

bioRxiv preprint first posted online May. 9, 2019; doi: http://dx.doi.org/10.1101/633594. The copyright holder for this preprint (which was not peer-reviewed) is the author/funder, who has granted bioRxiv a license to display the preprint in perpetuity. All rights reserved. No reuse allowed without permission.

FIGURE 1:

Multi-state establishment of the senescence transcriptional program

(a) Schematic overview for defining the gene-regulatory code of RAS-OIS using time-resolved, high-throughput transcriptome (microarray) and epigenome (ChIP-seq, and ATAC-seq) data sets.

(b) Self-organizing maps (SOMs) of gene expression profiles for quiescence and RAS-OIS time-series experiments as logarithmic fold-change. Red spots mark overexpression, blue spots underexpression.

(c) Multidimensional scaling (MDS) analysis scatter plot visualizing the level of similarity/dissimilarity between normalized quiescence and RAS-OIS time-series transcriptomes. Distances between samples represent leading logarithmic fold-changes defined as the root-mean-squared average of the logarithmic fold-changes for the genes best distinguishing each pair of samples.

(d) Scatter plot depicting the evolution of transcriptome diversity (H_j) *vs.* transcriptome specialization (σ_j) in cells undergoing quiescence or RAS-OIS. For each time-point and treatment, the average H_j and σ_j values across biological replicates are given. T_0 is start of time-course.

(e) Heatmap showing seven modules (I-VII) of temporally co-expressed genes specific for RAS-OIS using an unsupervised WGCNA clustering approach. Data are expressed as raw Z-scores.

(f) Functional over-representation map depicting Molecular Signatures Database (MSigDB) hallmark gene sets associated to each transcriptomic cluster. Dots are color-coded according to the FDR corrected *p*-value based on the hypergeometric distribution. Size is proportional to the percentage of genes in the gene set belonging to the cluster.

bioRxiv preprint first posted online May. 9, 2019; doi: http://dx.doi.org/10.1101/633594. The copyright holder for this preprint (which was not peer-reviewed) is the author/funder, who has granted bioRxiv a license to display the preprint in perpetuity. All rights reserved. No reuse allowed without permission.

FIGURE 2:

A dynamic enhancer program shapes the senescence transcriptome

(a) Arc plot visualizing dynamic chromatin state transitions for the indicated intervals. Edge width is proportional to the number of transitions.

(b) Histogram showing the total number of windows of the top 15 chromatin states transitions. Chromatin state transitions corresponding to *de novo* enhancer activation are highlighted as white bars.

(c) Chromatin dependence (CD) versus chromatin opening index (COI) are plotted for high-confidence TF sequence motifs used in our study (see Materials and Methods for details). Pioneer, settler and migrant TFs as defined by their COI and CD property are color-coded and select members of each TF class are listed. Same color code is used in all figures.

(d) Biplot for principal component analysis performed with select TF binding parameters: dynamicity, total number of bound windows (N), percentage of binding at enhancers, pioneer index (referred to as the number of bound windows pre-stimulation), chromatin opening index (COI) and chromatin dependence (CD). The plot depicts the projections of the TFs and the loading of the different covariates for the first two principle components which explain 76.9% of the total inertia. The ellipses delineate the 95% confidence intervals for AP1 pioneers (blue with black outline), non-AP1 pioneers (blue), settlers (red), and migrants (green).

bioRxiv preprint first posted online May. 9, 2019; doi: http://dx.doi.org/10.1101/633594. The copyright holder for this preprint (which was not peer-reviewed) is the author/funder, who has granted bioRxiv a license to display the preprint in perpetuity. All rights reserved. No reuse allowed without permission.

FIGURE 3:

AP-1 pioneer TF bookmarking of senescence enhancer landscape foreshadows the senescence transcriptional program

(a) Distribution of fold-change in normalized enhancer marks H3K27ac and H3K4me1 ChIP-seq signals over input in the "unmarked"-, "constitutive"-, "poised"-, "*de novo"*-, and "remnant enhancers"-flagged genomic bins at indicated time-points (see Material and Methods for details). The cartoon at the top illustrates the temporal rules used to flag genomic bins. Bottom specifies the genomic coverage in mega bases (Mb) for each category and the corresponding number of enhancers.

(b) WI38-ER: RASV12 were super-infected with dCas9-KRAB and individual guides (g14, 15, g61 and g7) targeting two *de novo* enhancers. Cells were pharmacologically selected and induced into RAS-OIS by 4-OHT. 8 days after RAS-OIS induction cells were stained by indirect immunofluorescence for IL1β or analyzed by RT-qPCR for the expression of IL1α or IL1β. WI38-ER: RASV12 treated with 4-OHT or DMSO served as positive and negative controls. Data represent mean ± SD (n=3). *$p<0.05$, ***$p<0.001$. Comparison with ctrl 4-OHT, one-way ANOVA (Dunnett's test). Scale bar, 100 µm.

(c) Rank plot depicting the summed occurrences for TF binding in *de novo* enhancers before RAS-OIS induction (left) and remnant enhancers after RAS-OIS (6 days) induction (right). Top ten TFs are indicated.

(d) Distribution of total number (N) of TFs bound per enhancer for constitutive enhancers (grey), TF pre-marked *de novo* enhancers (yellow) and TF virgin *de novo* enhancers (orange).

(e) Average absolute expression level (log_2 scale) kinetics for genes associated with: poised (blue), TF pre-marked *de* novo (yellow), and TF virgin *de novo* enhancers

bioRxiv preprint first posted online May. 9, 2019; doi: http://dx.doi.org/10.1101/633594. The copyright holder for this preprint (which was not peer-reviewed) is the author/funder, who has granted bioRxiv a license to display the preprint in perpetuity. All rights reserved. No reuse allowed without permission.

(orange). Dots depict the average absolute expression level, and bars depict the standard error of the mean. Inset histogram illustrates the average leading $\log_2$ fold-change in expression (+/- standard error of the mean) for genes associated with constitutive (black), poised (light blue), TF pre-marked *de novo* (yellow) and TF virgin *de novo* (orange), and remnant enhancers (dark blue).

FIGURE 4:

A hierarchical TF network defines the senescence transcriptional program

(a) Genome-wide transcription factor co-binding occurrence matrix summed across all time-points (left, shades from blue to yellow, in $\log_{10}$ scale). Overlap significance was calculated by a hyper-geometric test (right, shades from blue to red, in $-\log_{10}$ scale). The co-binding occurrence matrix was clustered using Ward's aggregation criterion and corresponding, corrected *q*-values were projected on this clustering. The graphs on the left and bottom show the density in pioneer, migrant and settler TFs along each axis of the matrix.

(b) Heatmap describing the association between individual TFs (row) and TF lexicons (columns). Four boxed out insets provide detailed information on TF composition of lexicons. A comprehensive, high-resolution and interactive heatmap is shown in Supplementary Data (see under Code availability in Material and Methods). The right bar plot shows the total number of binding sites for each TF. The top bar plot shows the total number of regions for each regulatory module. The bottom bar plot shows the average proportion of AP1 binding sites inside each regulatory module.

(c) Graphical representation of the hierarchical TF network for transcriptomic module VI. Nodes (circles) represent TFs and an oriented edge (line) connecting TFs A and B

bioRxiv preprint first posted online May. 9, 2019; doi: http://dx.doi.org/10.1101/633594. The copyright holder for this preprint (which was not peer-reviewed) is the author/funder, who has granted bioRxiv a license to display the preprint in perpetuity. All rights reserved. No reuse allowed without permission.

means that at least 30 % of the regions bound by B were also bound by A at the same time point or before. In order to simplify the visualization, we represent strongly connected components (SCCs) as a single node and performed a transitive reduction (TR). Node color is based on the average dynamicity of the SCC members. Node border color indicates their classification as pioneer (blue), settler (red) or migrant (green). Node border thickness encodes the percentage of bound regions before RAS stimulation. Edge color was calculated accordingly to the relative coverage of the outgoing TF over the incoming TF. The network has three layers: top, core and bottom. Nodes in the top have no incoming edges and nodes in the bottom have no outgoing edges. The core layer comprises TFs that have both incoming and outgoing edges. Interactive Cytoscape graphs are accessible as Supplementary data (see under Code availability in Material and Methods).

(d) Venn diagram showing the specificities and overlaps in differentially expressed direct target genes upon siRNA-mediated AP-1-c*JUN, ETS1,* and *RELA* depletion in RAS-OIS cells at day 6 (fully senescent cells). Genes are considered as direct targets of a given TF when PIQ predicts that the TF bound to an enhancer associates to this gene (see Materials and Methods for details). Promoters were excluded from the analysis.

(e) Asymmetric biplot for correspondence analysis between transcriptomic clusters and the number of up-, down-, up-or-down- or nonregulated (stable) genes upon siRNA-mediated AP-1-c*JUN*, *ETS1* or *RELA* depletion. The *p*-value reflects the strength of the association as assessed with a χ^2 test.

bioRxiv preprint first posted online May. 9, 2019; doi: http://dx.doi.org/10.1101/633594. The copyright holder for this preprint (which was not peer-reviewed) is the author/funder, who has granted bioRxiv a license to display the preprint in perpetuity. All rights reserved. No reuse allowed without permission.

FIGURE 5:

Hierarchy Matters: Functional Perturbation of AP-1 pioneer TF, but no other TF, reverts the senescence clock

(a) Principal component analysis (PCA) on transcriptomes obtained from siRNA-mediated depletion of AP-1-c*JUN*, *ETS1* or *RELA* at indicated timepoints of the RAS-OIS timecourse. Horizontal and vertical bars show minimal and maximal coordinates for each siRNA and time-point on principal components one (PC1, horizontal axis) and two (PC2, vertical axis).

(b) Functional overrepresentation map showing Molecular Signature Database (MSigDB) hallmark pathways associated to “All, Direct Target and Indirect Target” genes differentially expressed after siRNA-mediated AP-1-c*JUN*, *ETS1* or *RELA* depletion. Genes are considered as direct targets when a PIQ prediction for the given TF is falling inside an enhancer associated to this specific gene. Promoters are excluded from the analysis. The size of dots is proportional to the $-\log_{10}$ *q*-value based on the hypergeometric distribution obtained when testing for over-representation, and their color denote whether the term is enriched for an up or down-regulated gene list.

(c) Heatmap comparing gene expression profiles of siRNA-Control-treated (siCTRL) cells at indicated time-points of OIS and siRNA-cJUN treated senescent RAS-OIS cells at day 6 (144h).

Figure S1:

Multi-state establishment of the senescence transcriptional program

(a-b) Characterization of quiescence and RAS-OIS cells. **(a)** Representative DAPI, EdU, SABG (from left to right) indirect fluorescence and phase contrast microscopy images of

bioRxiv preprint first posted online May. 9, 2019; doi: http://dx.doi.org/10.1101/633594. The copyright holder for this preprint (which was not peer-reviewed) is the author/funder, who has granted bioRxiv a license to display the preprint in perpetuity. All rights reserved. No reuse allowed without permission.

WI38 fibroblasts undergoing quiescence at indicated time-points. Proliferative capacity is % of EdU-positive staining cells. Scale bar, 100µm. **(b)** Representative DAPI, EdU, SABG (from left to right) indirect fluorescence and phase contrast microscopy images of WI38 fibroblasts undergoing OIS at indicated time-points. Scale bar, 100µm.

(c) Distribution of gene expression levels as kernel density estimates for time-resolved quiescence and RAS-OIS transcriptomes. Pearson's correlation coefficient (R^2) is shown.

(d) Volcano plot of RAS-OIS time-series transcriptome data. Dark grey dots highlight genes sharing a common gene expression pattern between quiescence and OIS time-series experiments and were removed to define the RAS-OIS specific temporal transcriptomic signature used for all further downstream analyses.

(e) Boxplot depicting expression patter for each of the RAS-OIS transcriptomic modules. Data are expressed as row Z-score.

Figure S2:

A dynamic enhancer program shapes the senescence transcriptome

(a) Histogram showing the percentage of genome covered by each chromatin state at indicated time. Bottom table assigns histone modification combinations (grey: presence, white: absence) to biologically meaningful mnemonics. Venn diagrams highlight the specificities and overlaps in chromatin states associated with active (left) and poised enhancers (right) at indicated time-points.

(b) Boxplots showing the distribution of relative gene expression (row Z-score) through time for genes associated to regions undergoing different chromatin state changes. The

bioRxiv preprint first posted online May. 9, 2019; doi: http://dx.doi.org/10.1101/633594. The copyright holder for this preprint (which was not peer-reviewed) is the author/funder, who has granted bioRxiv a license to display the preprint in perpetuity. All rights reserved. No reuse allowed without permission.

pictogram at the top of each graph describes the class of chromatin state change considered.

(c) Asymmetric biplot for correspondence analysis between changes in chromatin states and gene expression modules. The *p*-value reflects the strength of the association using a χ^2 test. Only the top 20 contributing and best projected (squared cosine > 0.5) chromatin state changes are shown.

(d-f) Most enriched sequence motifs in **(d)** active enhancers or **(e-f)** ATAC-seq peaks at each time point for the **(d)** RAS-OIS, **(e)** replicative senescence**,** and **(f)** quiescence time courses. **(d)** Motif logos are shown on left of the histogram. Black, dotted boxes highlight the core motif for AP1 transcription factor family members. Note that the transcriptional repressor BACH shares this motif.

(g-i) ATAC-seq (grey lines for forward, black lines for reverse reads) and nucleosome (red line) footprints for **(g)** AP-1 FOSL1 (pioneer), **(h)** RELA (settler), and **(i)** SREBF1 (migrant).

(j) Comparison between PIQ predictions and RELA (left), AP-1-JUN (middle) and AP-1-FOSL2 (right) ChIP-seq. The two density heatmaps at the center of each panel illustrate ChIP-seq (left) and ATAC-seq (right) signals computed in 10bp non-overlapping windows at selected bound- (25%) and unbound- (75%) predicted PWM hits ± 1kb ranked according to the ChIP-seq signal in the most central 100bp. The stack histogram on the left shows the distribution of bound (red) and unbound (green) PWM hits as defined by PIQ along the ranking. The curves on the right depict the evolution of the enrichment score (ES) along the ranking as defined with a set enrichment analyses (SEA) comparing the ChIP-seq signal and the bound (red) and unbound (green) status

bioRxiv preprint first posted online May. 9, 2019; doi: http://dx.doi.org/10.1101/633594. The copyright holder for this preprint (which was not peer-reviewed) is the author/funder, who has granted bioRxiv a license to display the preprint in perpetuity. All rights reserved. No reuse allowed without permission.

of the PWM hit. For each SEA, we performed 1 000 permutations and provide the associated Benjamini–Hochberg adjusted *p*-value and ES score.

Figure S3:

AP-1 pioneer TF bookmarking of senescence enhancer landscape foreshadows the senescence transcriptional program

(a) Density heatmaps of normalized H3K27ac and H3K4me1 ChIP-seq signals computed in 10bp non-overlapping windows at enhancers +/- 10kb grouped by enhancer status (constitutive, *de novo* or remnant) at indicated time-points after RAS-OIS induction.

(b-c) Representative genome browser screenshots of normalized H3K4me1 (pink), H3K27ac (orange), H3K4me3 (blue) and H3K27me3 (green) ChIP-seq and ATAC-seq (light grey) profiles and chromatin states at **(b)** *IL1ß* and **(c)** *CDC6* gene loci. Red boxes single-out **(b)** IL1ß *de novo* and **(c)** CDC6 remnant enhancers.

(d) Boxplots depicting the distribution of relative gene expression (row Z-score) through time for genes associated with constitutive (left), *de novo* (middle) and remnant (left) enhancer windows.

(e) RAS-OIS cells at day 14 infected with dCas9-KRAB and individual guides (g14, g15, g61, and g7) and analyzed by RT-qPCR for the expression of IL1α or IL1β as described in Figure 3b. Data represent mean ± SD (n=3). *p<0.05, ***p<0.001. Comparison with ctrl 4OHT, one-way ANOVA (Dunnett's test).

(f) RAS-OIS cells were infected with dCas9-KRAB and individual guides (g2, g48 and g54) for non-enhancer regions (outside *de novo* enhancers) as described in Figure 3b. 8 or 14 days after infection, cells were stained for IL1α or IL1β by indirect

bioRxiv preprint first posted online May. 9, 2019; doi: http://dx.doi.org/10.1101/633594. The copyright holder for this preprint (which was not peer-reviewed) is the author/funder, who has granted bioRxiv a license to display the preprint in perpetuity. All rights reserved. No reuse allowed without permission.

immunofluorescence and percentage positive cells were quantified (n=3 for 8 days and n=2 for 14 days). Data represent mean ± SD. *p<0.05, **p<0.01, ***p<0.001. Comparison with ctrl 4OHT, one-way ANOVA (Dunnett's test).

(g) Rank plot depicting the summed occurrences for TFs binding in proliferating cells (T_0) in *de novo* enhancers (left) and after replicative senescence in remnant enhancers (right). Top ten TFs are highlighted.

(h) Metaprofiles showing the density in "active enhancer"-flagged genomic bins (top) and "constitutive enhancer"-flagged genomic bins (bottom) in the vicinity (+/- 50kb) of TF bookmarked *de novo* (left) and TF virgin *de novo* enhancers (right). The density in "active enhancer"-flagged genomic bins is provided for the indicated time points.

(i) Boxplot showing the correlation between absolute leading $\log_2$ expression fold-change and the number of genomic bins flagged as "*de novo"* enhancers per enhancer. *** : *p*-value < 10^{-3}, Student's *t*-test considering regions with 0 "*de novo"* enhancers bins as a control.

Figure S4:

A hierarchical TF network defines the senescence transcriptional program

(a) Representative circos plots summarizing pairwise transcription factor co-binding at enhancers for down-regulated transcriptomic module (IV, top) and up-regulated transcriptomic module (VI, bottom) at indicated time-points. Co-interactions involving AP1 are shown in black. Selected examples of gained (green) and lost (orange) interactions are highlighted. Pioneer TFs blue, settler TFs red, migrant TFs green. See also dynamic circos plot movies in Supplementary Data (see under Code availability in Material and Methods).

bioRxiv preprint first posted online May. 9, 2019; doi: http://dx.doi.org/10.1101/633594. The copyright holder for this preprint (which was not peer-reviewed) is the author/funder, who has granted bioRxiv a license to display the preprint in perpetuity. All rights reserved. No reuse allowed without permission.

(b) Heatmap showing the overlap between TF lexicons (rows) and chromatin states, ChIP-seq and ATAC-seq peaks (columns). The dendrograms were computed by applying hierarchical clustering on the fraction matrix with Pearson's correlation and average linkage.

(c) Validation of TF network algorithm using TF ChIP-seq published data sets (Garber *et al.*, 2012). Edges colored in gray were detected in both studies and edges colored in red were found only the analysis performed by Garber *et al.*. The displayed edge set is the same as in Figure 5A (Garber *et al.*, 2012). We employed a transitive reduction step in order to facilitate visualization. Comparison of the two networks resulted in a sensitivity of 88,9 % and a specificity of 100 %.

(d) Ratio of incoming edges based on the classification of the TF source node. The relative and absolute number of edges corresponding to all seven modules are displayed inside the nodes, which are colored accordingly to TF classification as in previous panels. The thickness of links is proportional to the relative number of TF hierarchy edges connecting nodes with the corresponding classification.

(e) Number of bound regions and dynamicity index for each TF (rows) across all gene modules (columns). The left heatmap depicts the dynamicity index scaled by column. The middle heatmap depicts the square root of number of bound regions scaled by column. The right single-column heatmap illustrates TF classification.

(f) Venn diagram showing specificities and overlaps of TF interactions in each gene module. Each set corresponds to the TF-TF network edges identified for a given transcriptomic module. The global area of each set is proportional to the number of edges in its respective transcriptomic module and was calculated with the Chow-Ruskey algorithm.

bioRxiv preprint first posted online May. 9, 2019; doi: http://dx.doi.org/10.1101/633594. The copyright holder for this preprint (which was not peer-reviewed) is the author/funder, who has granted bioRxiv a license to display the preprint in perpetuity. All rights reserved. No reuse allowed without permission.

(g-i) Chow-Ruskey diagrams for edges **(g)** originating only from TFs at the top of hierarchy, **(h)** connecting only TFs at the core layer or **(i)** reaching only TFs at the bottom. Note that edges at the top of the hierarchy are shared among the gene modules while edges towards the bottom of the hierarchy are module-specific.

Figure S5:

Hierarchy Matters: Functional Perturbation of AP-1 pioneer TF, but no other TF, reverts the senescence clock

(a-c) Volcano plots depicting the -$\log_{10}$ *p*-value as a function of the $\log_2$ fold-change in gene expression defined by a differential analysis conducted with *limma* to highlight the effect of siRNA-mediated **(a)** AP-1-c*JUN*, **(b)** *ETS*1 and **(c)** *RELA* depletion in senescent RAS-OIS cells at day 6 (144h). Blue dots in respective plots indicate probes corresponding to AP-1-c*JUN*, *ETS*1 and *RELA*. Black outlined dots highlight direct targets of AP-1-c*JUN*, *ETS*1 and *RELA*.

(d) Upset plot depicting specificities and overlaps in differentially expressed genes of siRNA-Control and siRNA-*JUN* silenced OIS fibroblasts at indicated time-points. The yellow dots highlight gene sets specific to a single comparison set, while green dots highlight gene sets find in two different pair-wise comparison.

(e-g) Venn diagrams (top) and heatmaps (bottom) depicting the overlap between genes belonging to **(e)** E2F-, **(f)** NFκB target, and **(g)** N1ICD-induced senescence (NIS) gene signatures. Venn diagrams show the overlap of up-regulated genes after siRNA-mediated AP-1-c*JUN* knock-down for upregulated E2F- (*i.e.* pro-proliferation genes), NIS- (*i.e.* early SASP genes), and downregulated NFκB target genes (*i.e.* late SASP genes) RAS-OIS cells at day 6 (144h). Bottom heatmaps show the comparison of gene

bioRxiv preprint first posted online May. 9, 2019; doi: http://dx.doi.org/10.1101/633594. The copyright holder for this preprint (which was not peer-reviewed) is the author/funder, who has granted bioRxiv a license to display the preprint in perpetuity. All rights reserved. No reuse allowed without permission.

expression profiles of siRNA-Control (siCtrl) and siRNA-cJUN treated cells undergoing RAS-OIS at indicated time-points. Data are expressed as row Z-score. E2F targets and NFκB targets were defined according to Molecular Signature Database (MSigDB).

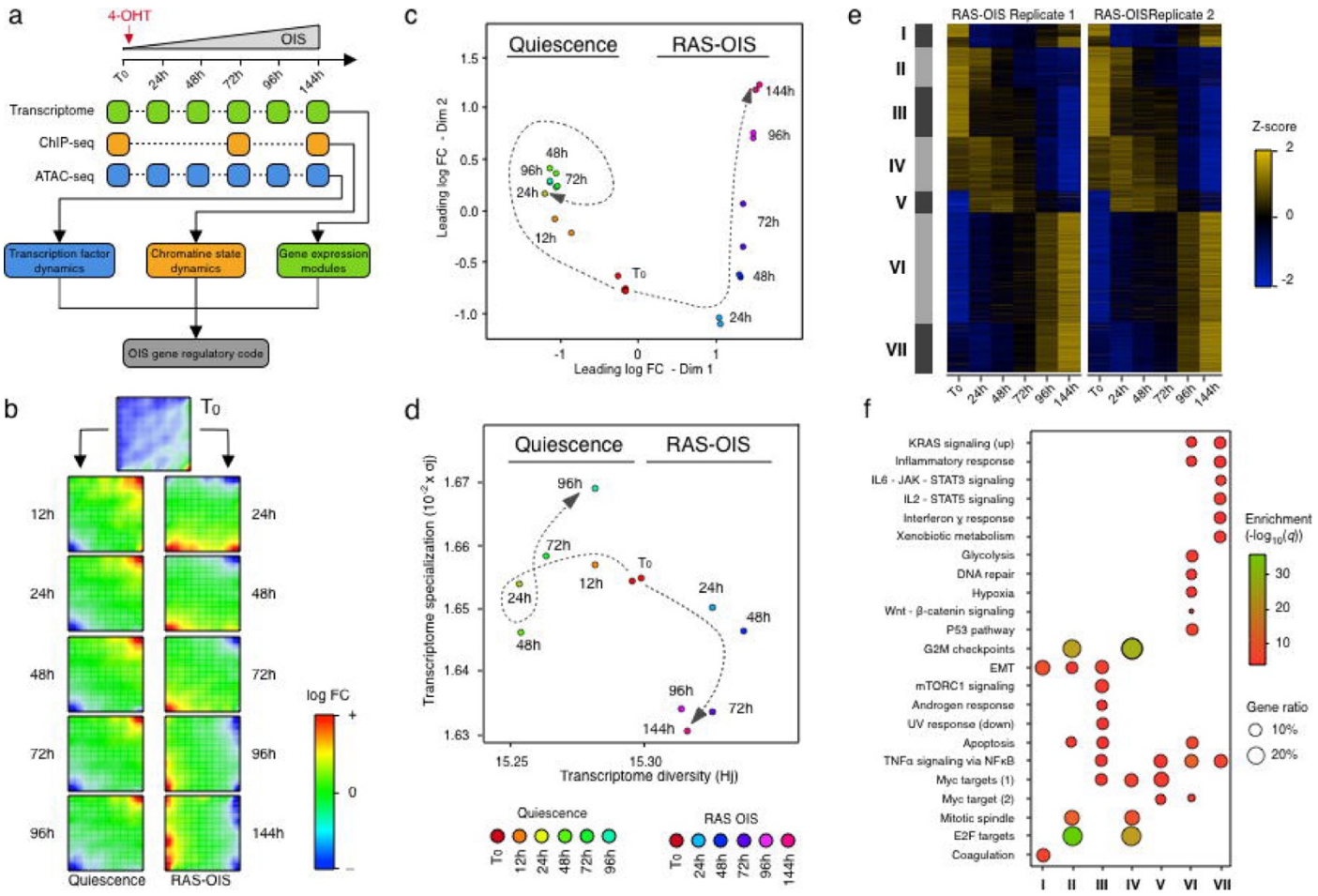
a
4-OHT
OIS
T0
24h
48h
72h
96h
144h
Transcriptome
ChIP-seq
ATAC-seq
Transcription factor dynamics
Chromatine state dynamics
Gene expression modules
OIS gene regulatory code
b
T0
12h
24h
48h
72h
96h
144h
Quiescence
RAS-OIS
log FC
c
Quiescence
RAS-OIS
Leading log FC - Dim 2
Leading log FC - Dim 1
d
Quiescence
RAS-OIS
Transcriptome specialization (10^-2 x σj)
Transcriptome diversity (Hj)
e
RAS-OIS Replicate 1
RAS-OISReplicate 2
Z-score
f
KRAS signaling (up)
Inflammatory response
IL6 - JAK - STAT3 signaling
IL2 - STAT5 signaling
Interferon γ response
Xenobiotic metabolism
Glycolysis
DNA repair
Hypoxia
Wnt - β-catenin signaling
P53 pathway
G2M checkpoints
EMT
mTORC1 signaling
Androgen response
UV response (down)
Apoptosis
TNFα signaling via NFκB
Myc targets (1)
Myc target (2)
Mitotic spindle
E2F targets
Coagulation
Enrichment (-log10(q))
Gene ratio
10%
20%

Figure 1

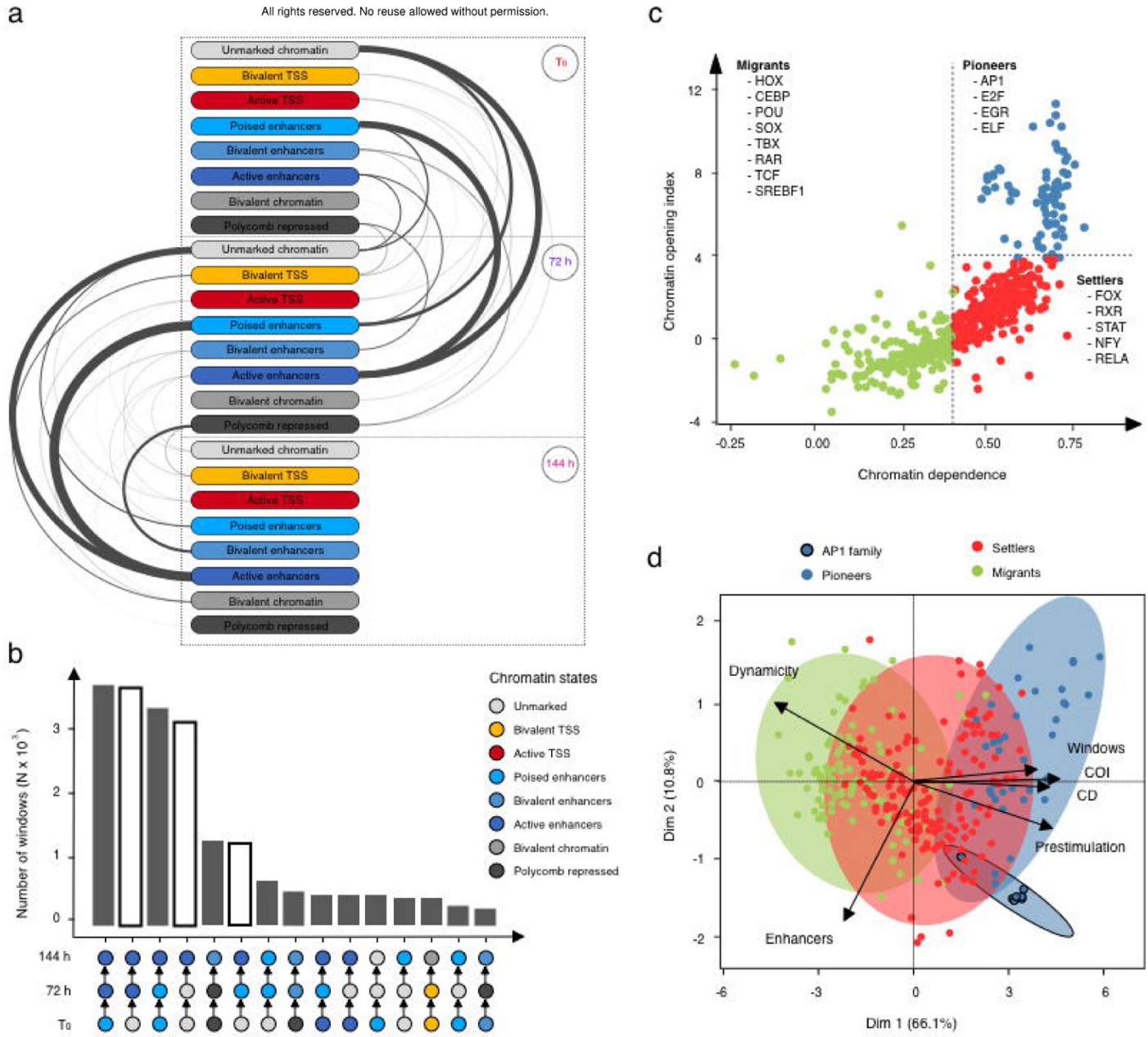
a
All rights reserved. No reuse allowed without permission.
Unmarked chromatin
Bivalent TSS
Active TSS
Poised enhancers
Bivalent enhancers
Active enhancers
Bivalent chromatin
Polycomb repressed
T0
72 h
144 h
b
Number of windows (N x 10^3)
Chromatin states
Unmarked
Bivalent TSS
Active TSS
Poised enhancers
Bivalent enhancers
Active enhancers
Bivalent chromatin
Polycomb repressed
144 h
72 h
T0
c
Migrants
- HOX
- CEBP
- POU
- SOX
- TBX
- RAR
- TCF
- SREBF1
Pioneers
- AP1
- E2F
- EGR
- ELF
Settlers
- FOX
- RXR
- STAT
- NFY
- RELA
Chromatin opening index
Chromatin dependence
d
AP1 family
Pioneers
Settlers
Migrants
Dynamicity
Windows
COI
CD
Prestimulation
Enhancers
Dim 2 (10.8%)
Dim 1 (66.1%)

Figure 2

bioRxiv preprint first posted online May. 9, 2019; doi: http://dx.doi.org/10.1101/633594. The copyright holder for this preprint (which was not peer-reviewed) is the author/funder, who has granted bioRxiv a license to display the preprint in perpetuity. It is made available under aCC-BY-NC-ND 4.0 International license.

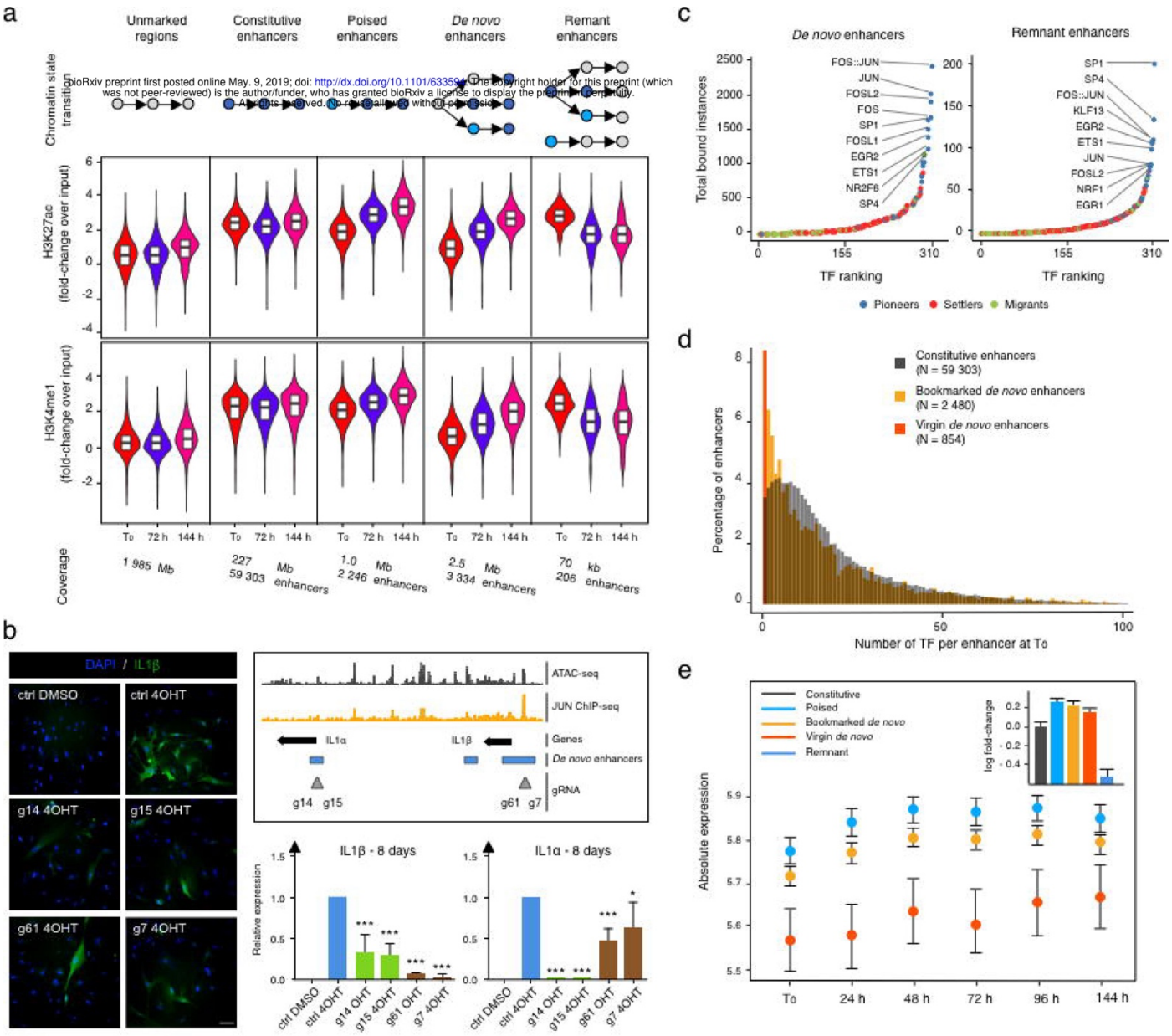

Figure 3

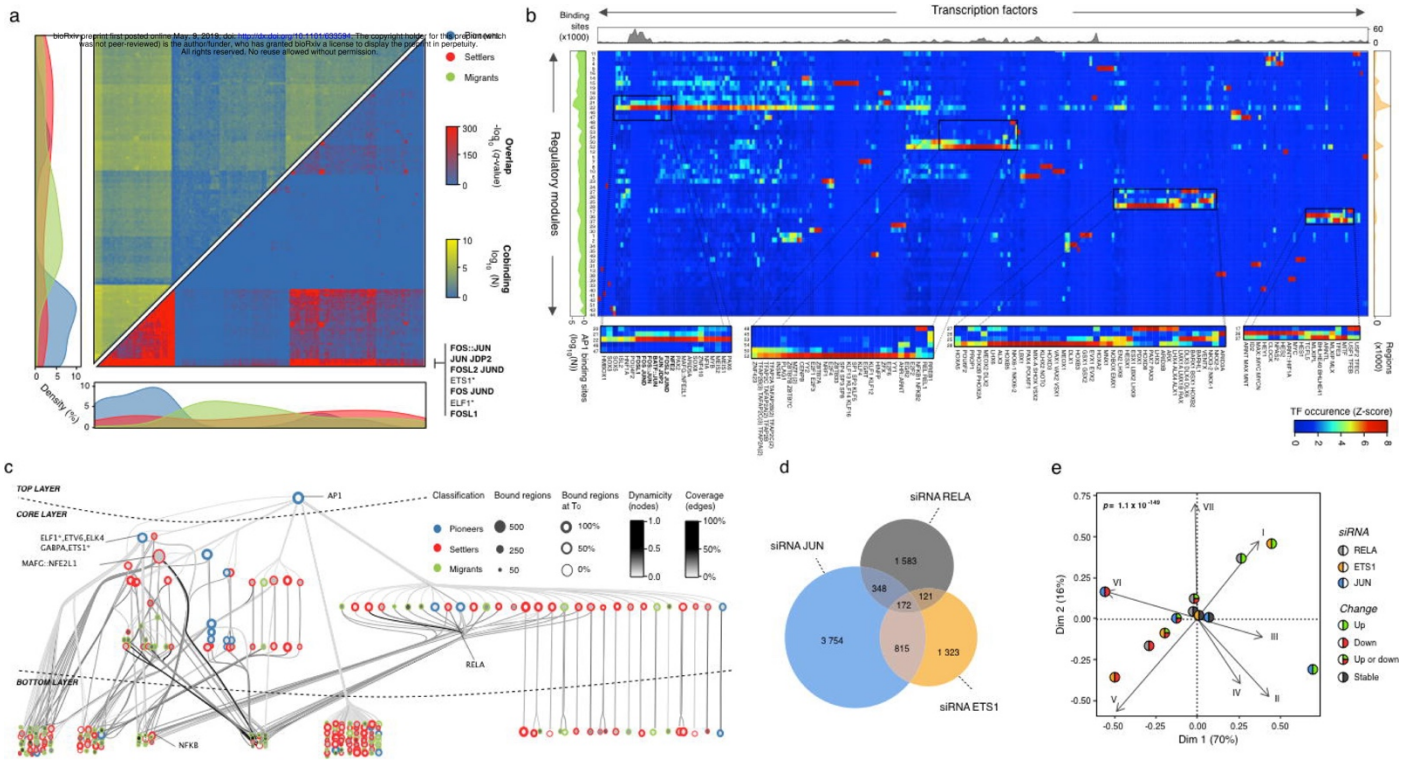
a
Settlers
Migrants
Overlap
Cobinding
FOS::JUN
JUN JDP2
FOSL2 JUND
ETS1*
FOS JUND
ELF1*
FOSL1
Density (%)
b
Transcription factors
Binding sites (x1000)
Regulatory modules
AP1 binding sites
Regions (x1000)
TF occurence (Z-score)
c
TOP LAYER
CORE LAYER
BOTTOM LAYER
AP1
ELF1*,ETV6,ELK4
GABPA,ETS1*
MAFC::NFE2L1
RELA
NFKB
Classification
Pioneers
Settlers
Migrants
Bound regions
Bound regions at To
Dynamicity (nodes)
Coverage (edges)
d
siRNA RELA
siRNA JUN
siRNA ETS1
1 583
348
121
172
3 754
815
1 323
e
Dim 1 (70%)
Dim 2 (16%)
siRNA
RELA
ETS1
JUN
Change
Up
Down
Up or down
Stable

Figure 4

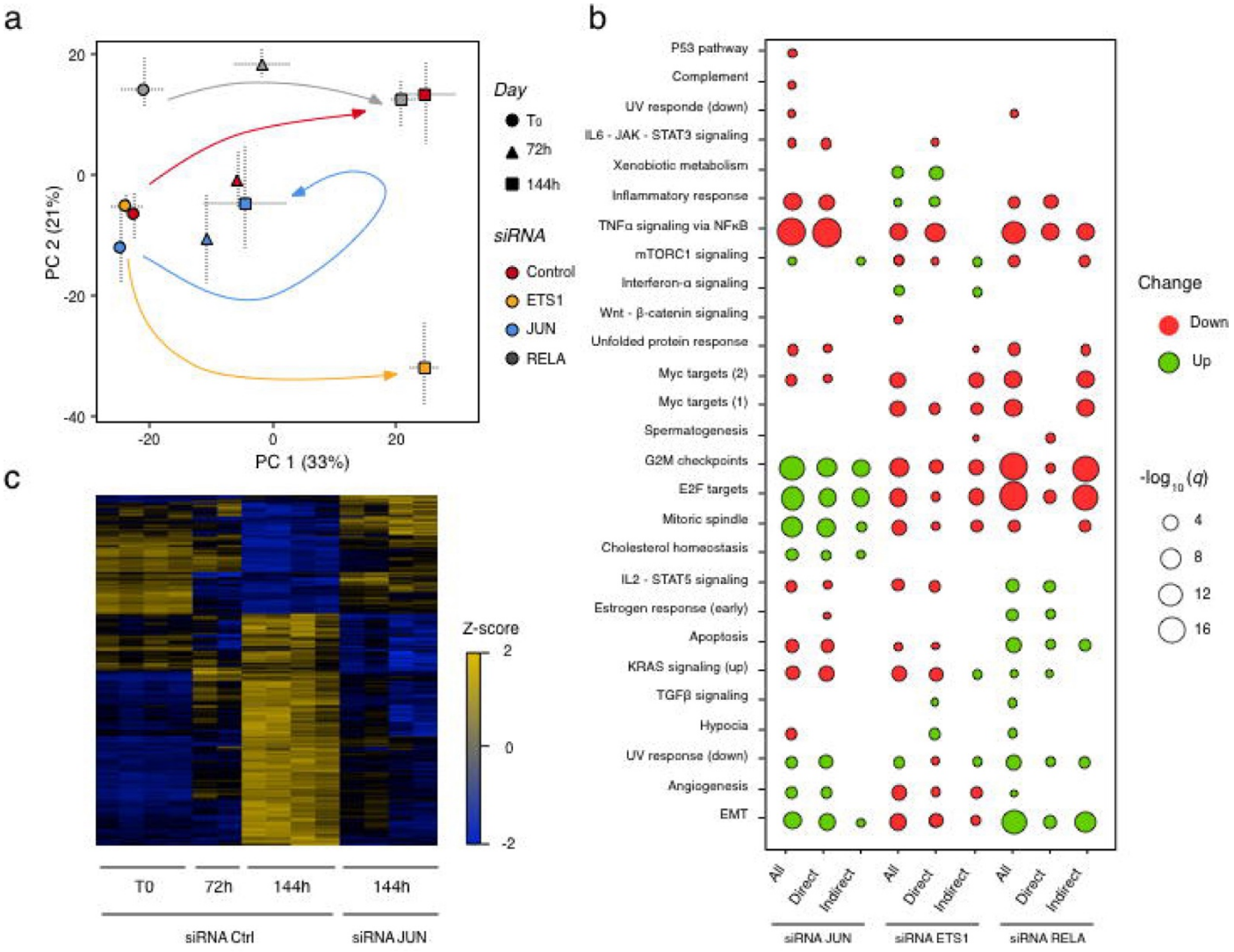
a
PC 2 (21%)
PC 1 (33%)
Day
T0
72h
144h
siRNA
Control
ETS1
JUN
RELA
b
P53 pathway
Complement
UV responde (down)
IL6 - JAK - STAT3 signaling
Xenobiotic metabolism
Inflammatory response
TNFα signaling via NFκB
mTORC1 signaling
Interferon-α signaling
Wnt - β-catenin signaling
Unfolded protein response
Myc targets (2)
Myc targets (1)
Spermatogenesis
G2M checkpoints
E2F targets
Mitotic spindle
Cholesterol homeostasis
IL2 - STAT5 signaling
Estrogen response (early)
Apoptosis
KRAS signaling (up)
TGFβ signaling
Hypocia
UV response (down)
Angiogenesis
EMT
All
Direct
Indirect
siRNA JUN
siRNA ETS1
siRNA RELA
Change
Down
Up
-log10(q)
4
8
12
16
c
Z-score
2
0
-2
T0
72h
144h
144h
siRNA Ctrl
siRNA JUN

Figure 5

bioRxiv preprint first posted online May. 9, 2019; doi: http://dx.doi.org/10.1101/632554. The copyright holder for this preprint (which was not certified by bioRxiv) is the author/funder. It is made available under a CC-BY-NC-ND 4.0 International license. bioRxiv a license to display the preprint in perpetuity. It is made available under a CC-BY-NC-ND 4.0 International license. allowed without permission.

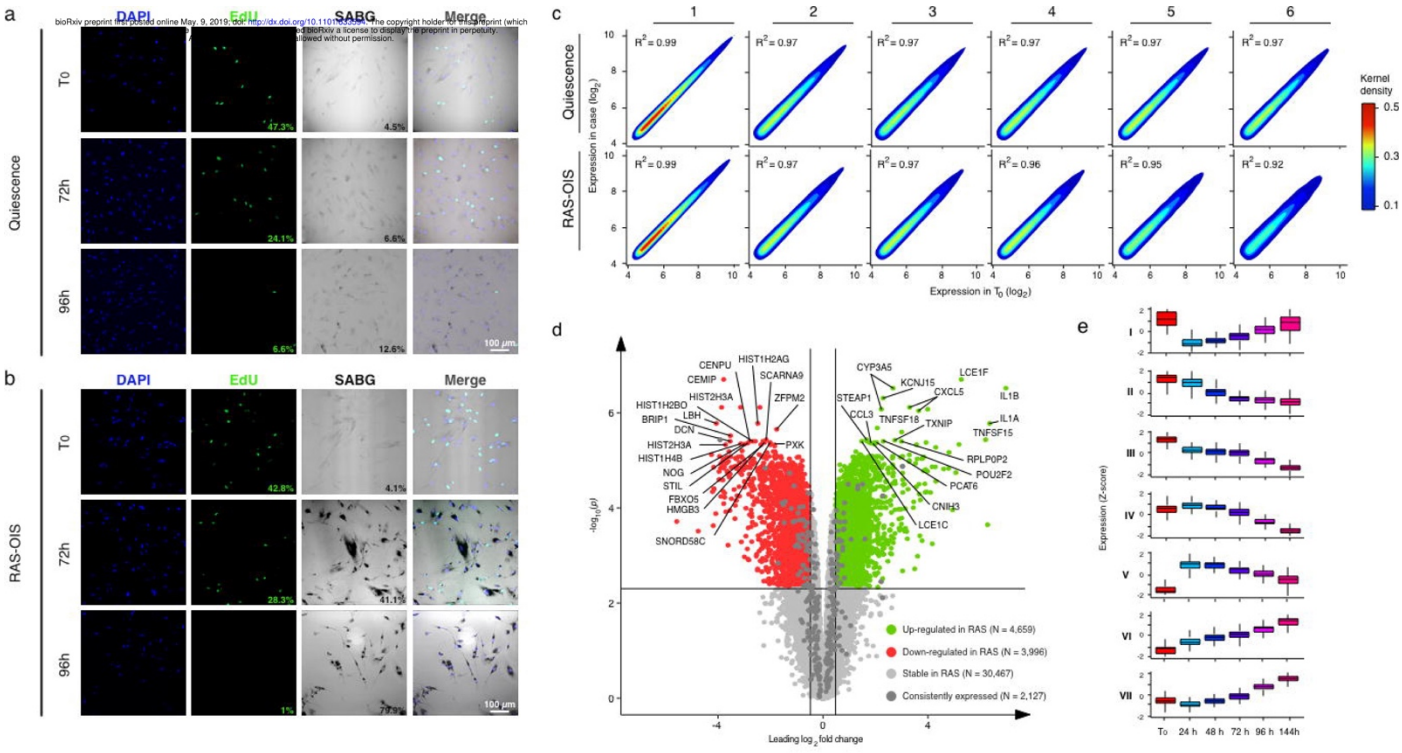

Figure S1

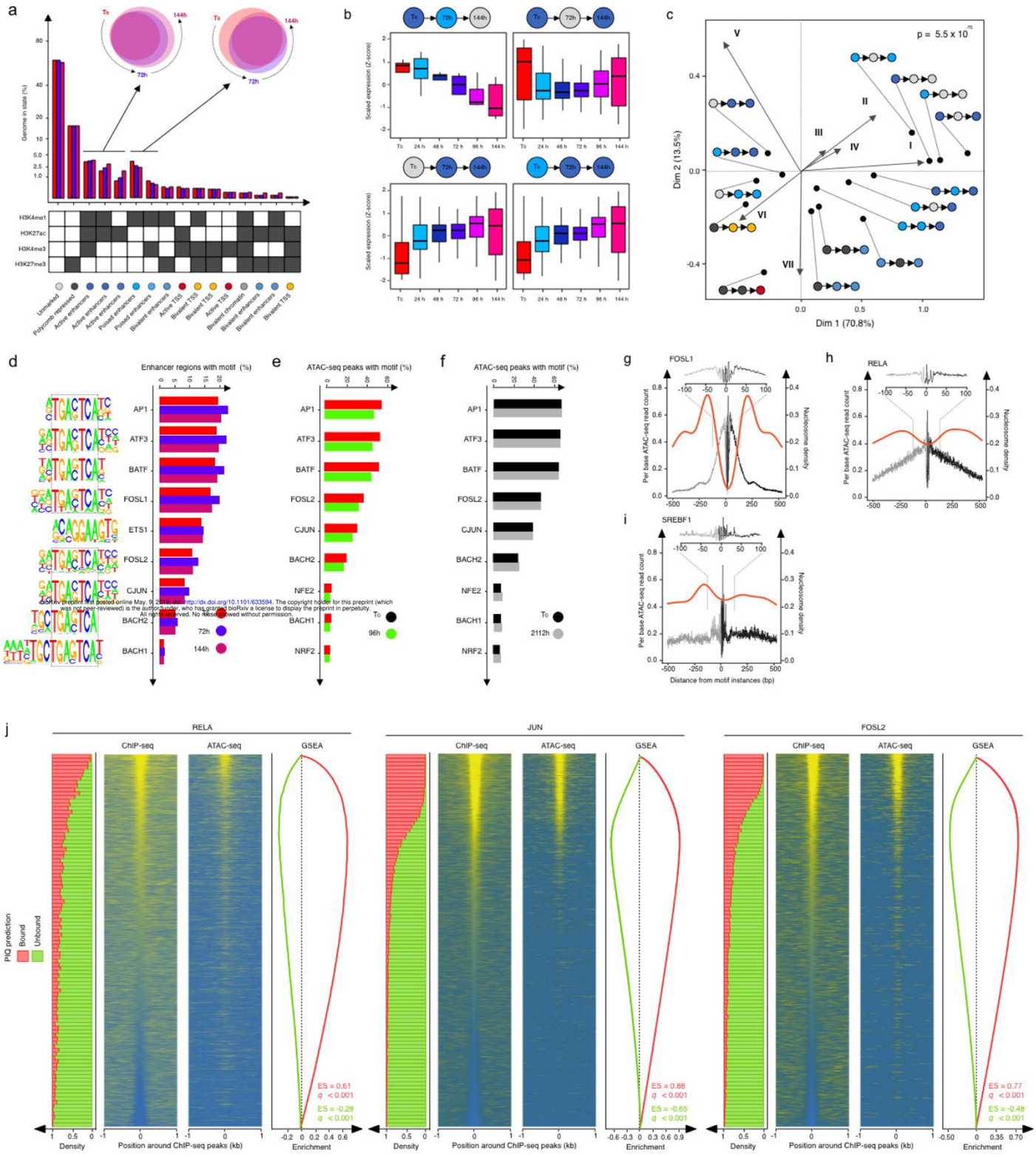

bioRxiv preprint first posted online May. 3, 2019; doi: http://dx.doi.org/10.1101/633594. The copyright holder for this preprint (which was not peer-reviewed) is the author/funder, who has granted bioRxiv a license to display the preprint in perpetuity. All rights reserved. No reuse allowed without permission.

Figure S2

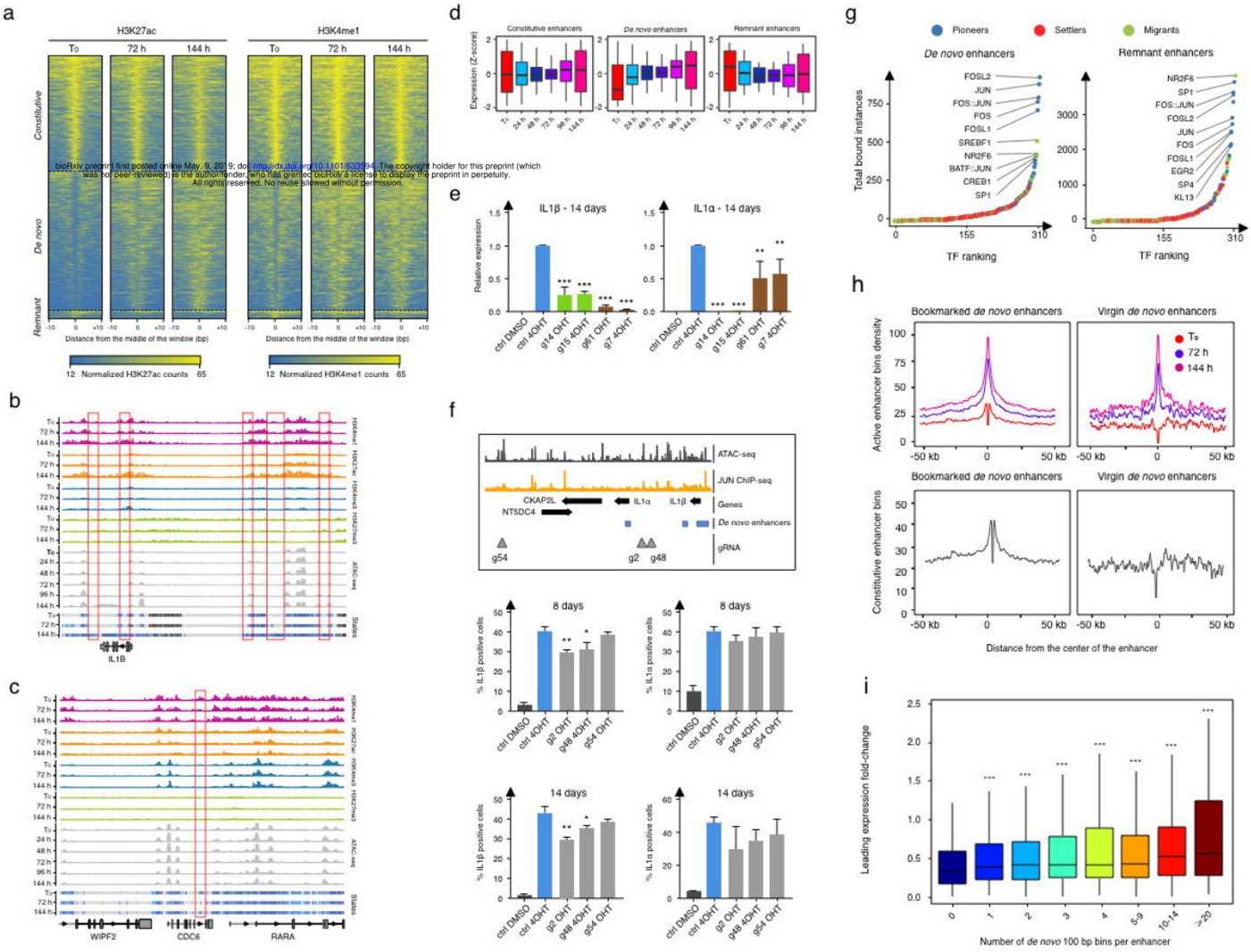

Figure S3

bioRxiv preprint first posted online May. 9, 2019; doi: http://dx.doi.org/10.1101/633594. The copyright holder for this preprint (which was not peer-reviewed) is the author/funder, who has granted bioRxiv a license to display the preprint in perpetuity. All rights reserved. No reuse allowed without permission.

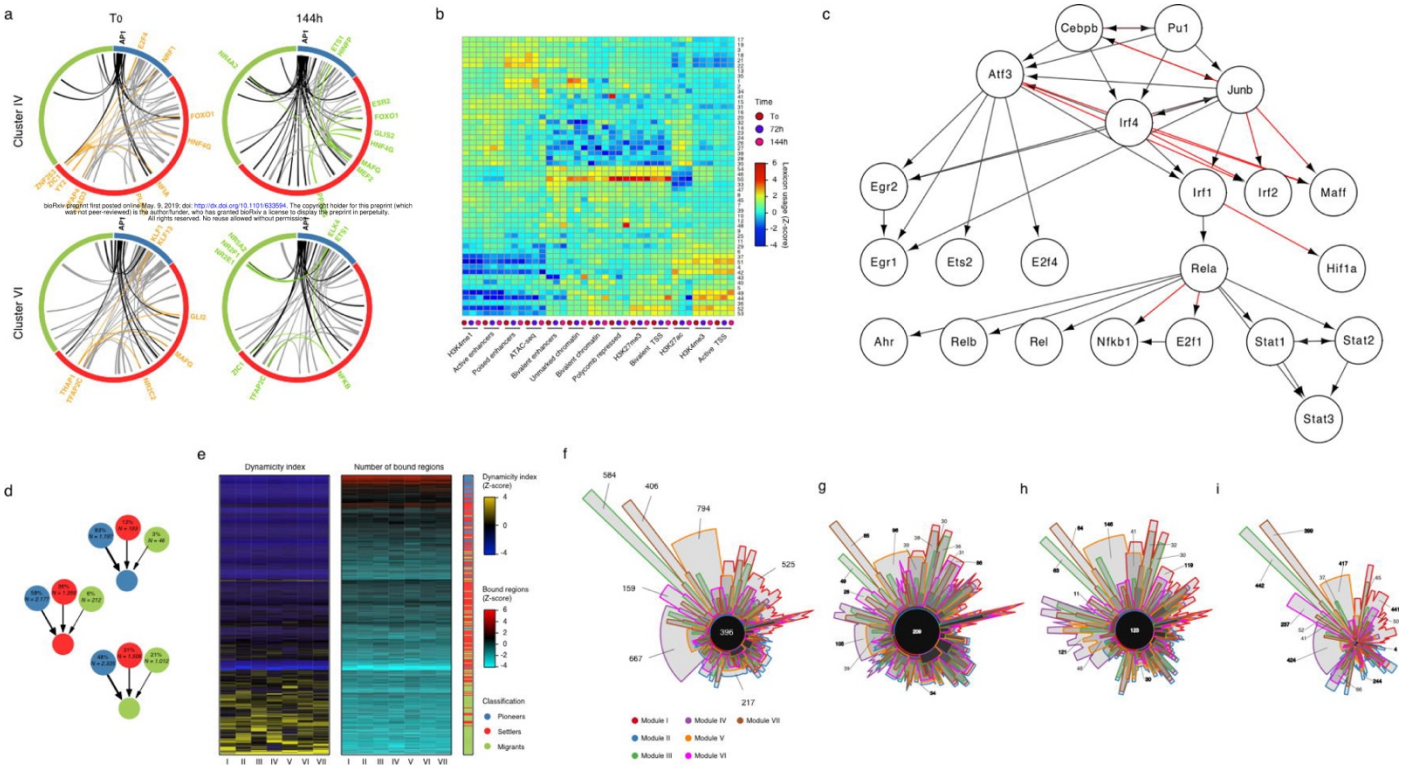

bioRxiv preprint first posted online May. 9, 2019; doi: http://dx.doi.org/10.1101/630594. The copyright holder for this preprint (which was/not peer-reviewed) is the author/funder, who has granted bioRxiv a license to display the preprint in perpetuity. All rights reserved. No reuse allowed without permission.

Figure S4

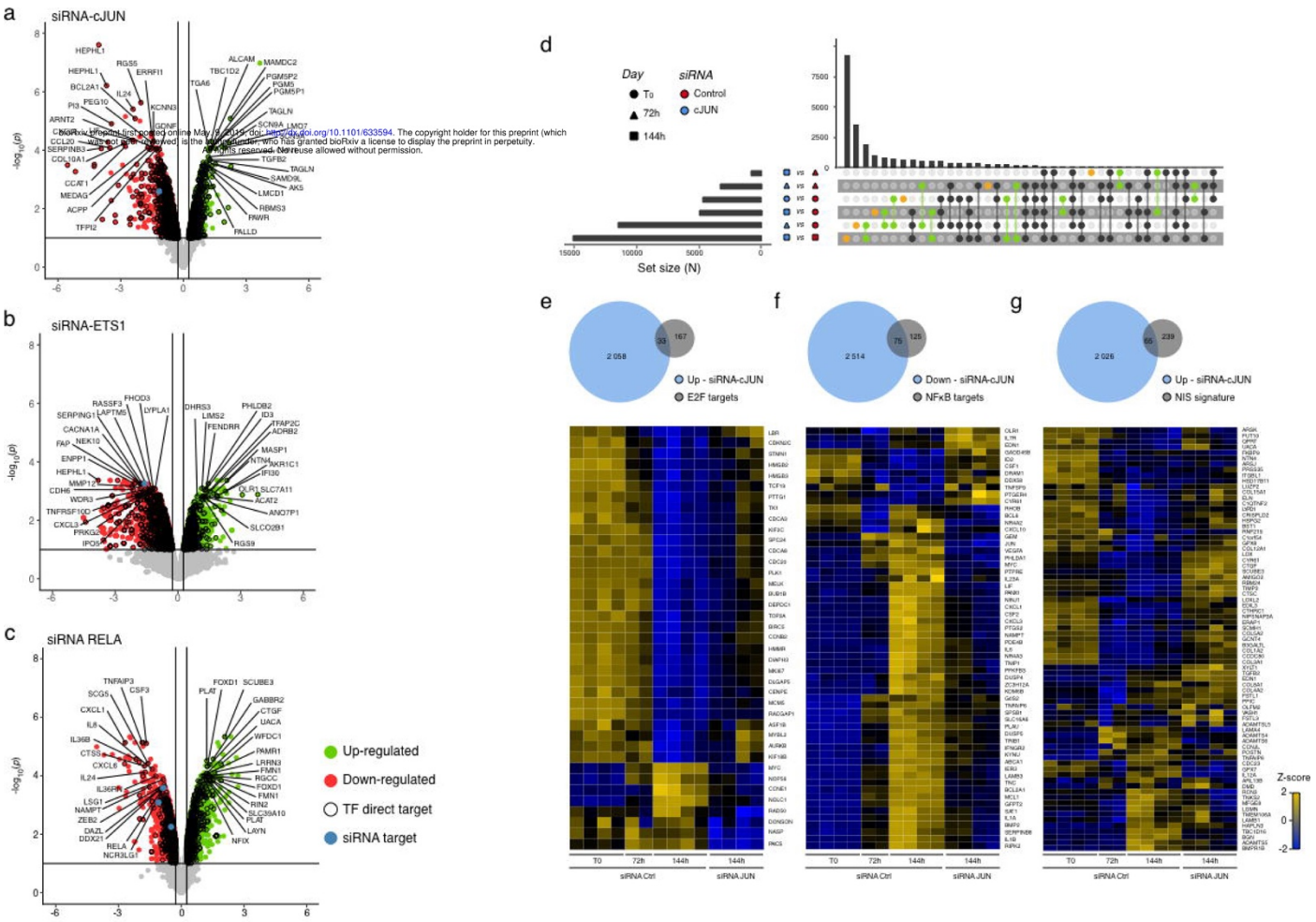

bioRxiv preprint first posted online May 17, 2019; doi: https://doi.org/10.1101/633594. The copyright holder for this preprint (which was not peer reviewed) is the author/funder, who has granted bioRxiv a license to display the preprint in perpetuity. All rights reserved. No reuse allowed without permission.

Figure S5

8.1.2 Necroptosis Microenvironment Directs Lineage Commitment in Liver Cancer

Appendix 8.1.2 is removed from this version of the manuscript. Due to unauthorized distribution of the following article the pages are left vacant so that the layout and pagination of the thesis will remain unchanged.

See article:
Seehawer, M., Heinzmann, F., D'Artista, L., Harbig, J., Roux, P.-F., Hoenicke, L., Dang, H., Klotz, S., Robinson, L., Doré, G., et al. (2018). Necroptosis microenvironment directs lineage commitment in liver cancer. Nature *562*, 69–75.

8.1.3 Cell Snapshot: Cellular Senescence Pathways

SnapShot: Cellular Senescence Pathways

Cell

Ricardo Iván Martínez-Zamudio, Lucas Robinson, Pierre-Francois Roux, and Oliver Bischof
INSERM, U993, 75015 Paris, France; Equipe Labellisée Fondation ARC pour la recherche sur le cancer, 94803 Villejuif, France;
Institut Pasteur, Molecular and Cellular Biology of Cellular Senescence and Age-Related Pathologies Group,
Nuclear Organization and Oncogenesis Unit, Department of Cell Biology and Infection, 75015 Paris, France

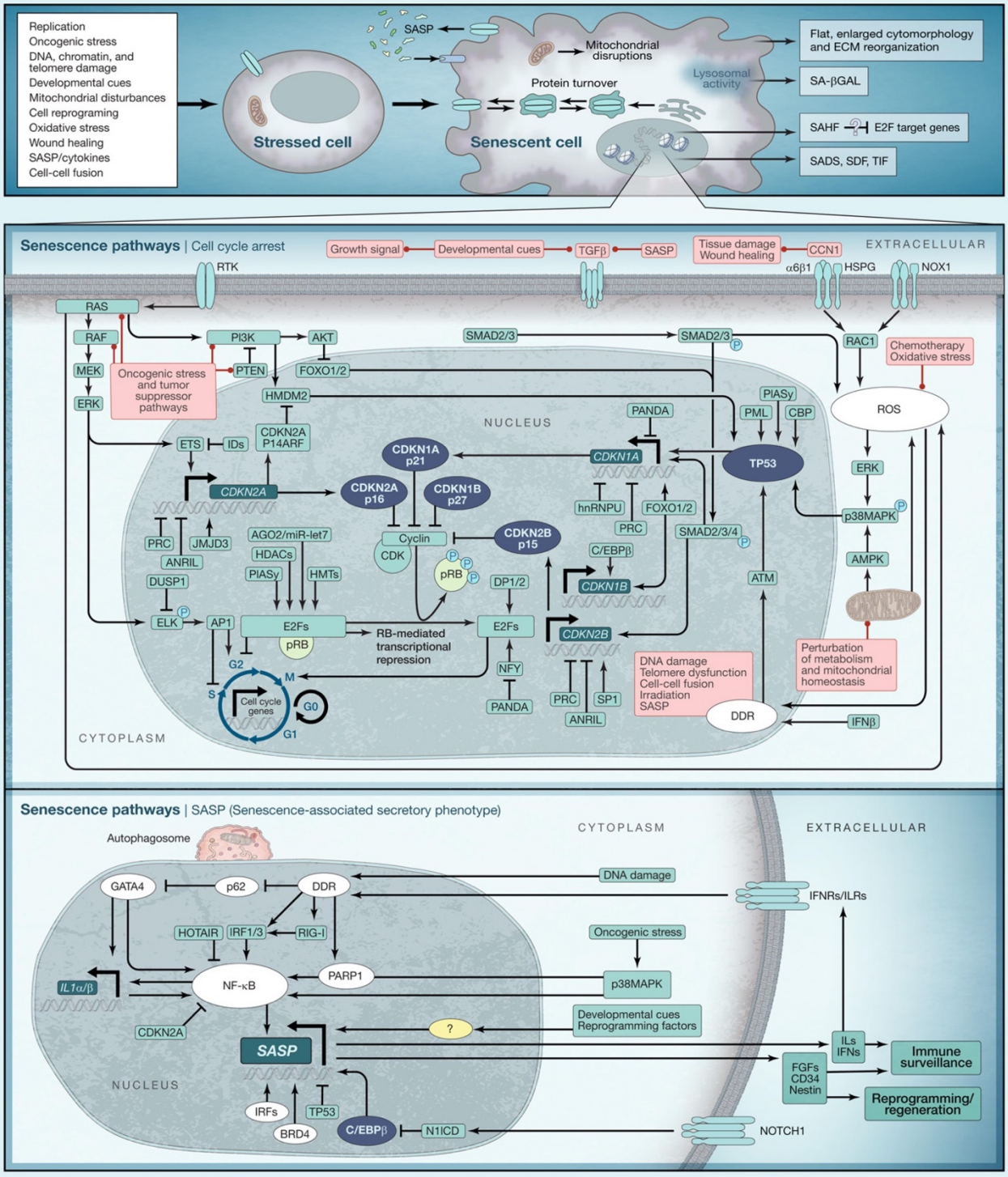

816 Cell *170*, August 10, 2017 © 2017 Elsevier Inc. DOI http://dx.doi.org/10.1016/j.cell.2017.07.049

See online version for legends and references

SnapShot: Cellular Senescence Pathways

Cell

Ricardo Iván Martínez-Zamudio, Lucas Robinson, Pierre-Francois Roux, and Oliver Bischof
INSERM, U993, 75015 Paris, France; Equipe Labellisée Fondation ARC pour la recherche sur le cancer, 94803 Villejuif, France;
Institut Pasteur, Molecular and Cellular Biology of Cellular Senescence and Age-Related Pathologies Group,
Nuclear Organization and Oncogenesis Unit, Department of Cell Biology and Infection, 75015 Paris, France

Causes and Characteristics of Cellular Senescence–Top Panel

The stressors/stimuli leading to senescence include telomere shortening due to replicative exhaustion (replicative senescence, RS), oncogene hyperactivation (oncogene-induced senescence, OIS), tumor suppressor loss, damage to DNA or chromatin structure (including from anti-cancer therapy), developmental cues, mitochondrial dysfunction, reprogramming factors, oxidative stress, wound healing, cell-cell fusion, and certain cytokines (including the senescence-associated secretory phenotype itself [SASP]). Senescence arrest occurs mostly in the G_1 phase of the cell cycle, distinguishing it from G_0-arrested quiescent cells. The arrest is mediated by cyclin-dependent kinase inhibitors and is dependent on the TP53 and pRB tumor suppressor pathways. The SASP modulates immune surveillance during development, tissue regeneration, and pro- and anti-tumoral responses and enhances cellular reprogramming. The composition of the SASP is stimulus-dependent and includes pro- and anti-inflammatory cytokines, chemokines, stemness factors, and matrix metalloproteinases.

The archetypical senescence biomarker is acidic lysosomal SA-ßGal activity, indicative of augmented autophagy and enlargement of the lysosomal compartment. Senescent cells undergo changes in chromatin architecture epitomized by the appearance of senescence-associated heterochromatin foci (SAHF), regions of condensed chromatin containing repressive histone marks. The formation of these foci depends on the CDKN2A-pRB pathway. The persistent DNA damage response (DDR) in senescent cells leads to senescence DNA damage foci (SDF) and telomere-dysfunction-induced foci (TIF). SDF and TIF are identified by the colocalization of DDR-associated proteins 53BP1, γH2AX, and ATM. Senescent cells also display distension of peri- and centromeric satellites (SADS). Senescent cells exhibit increased protein turnover and massive proteotoxic stress due to augmented autophagy and SASP component synthesis. This is partially explained by the colocalization of autophagic, lysosomal, and nascent proteins in the TOR-autophagy spatial coupling compartment, coupling protein catabolism and anabolism. Senescence is associated with increased rates of mitochondrial metabolic activity, including the tricarboxylic acid cycle, oxidative phosphorylation, and glycolytic pathways. Senescent cells have increased AMP/ADP:ATP and NAD^+/NADH ratios, activating AMPK, which reinforces a TP53-dependent cell-cycle arrest. Senescent cells undergo notable changes in their extracellular matrix organization, which are reflected in their enlarged and flat morphology.

Regulation of the Cell Cycle Arrest–Middle Panel

Most senescence inducers activate the tumor suppressor pathways TP53/CDKN1A and/or pRB/CDKN2A. TP53 integrates signals for DNA-damage-induced senescence, imposing a CDKN1A-mediated cell-cycle arrest. DNA damage caused by genotoxic agents or reactive oxygen species (ROS) activates TP53 via the p38MAPK and ATM pathways. Generation of ROS occurs via tissue damage-activated RAC1, dysfunctional mitochondria, OIS, or SASP signaling. Dysfunctional mitochondria and other metabolic perturbations also induce a TP53-dependent arrest via AMPK activation. TP53-dependent upregulation of CDKN1A overrides the repression of the *CDKN1A* locus by Polycomb repressor complexes (PRC) 1 and 2, the long non-coding RNA PANDA, and the scaffolding factor hnRNPU. Additional regulation of the TP53-mediated senescence arrest occurs through acetylation by CBP and sumoylation by E3 SUMO ligase PIASγ .

During senescence, E2F7 and pRB act to repress pro-proliferation genes. *E2F7* is a TP53 target gene and is the only E2F transcription factor (TF) family member that is strongly upregulated in senescence. The activity of pRB is tightly regulated by CDK-mediated phosphorylation. In senescence, CDK inhibitors, such as CDKN2A or –1A, maintain pRB in an active, hypophosphorylated state, leading to its association with and inhibition of E2F1-3, promoting the senescence arrest. E2F7 and pRB reinforce the repression of E2F target genes by promoting local heterochromatinization via the recruitment of histone deacetylases (HDACs), histone methyl transferases (HMTs), and PIASγ. The RNA interference machinery also contributes to the repression of a subset of E2F target genes. This is mediated by a microRNA (miR)-loaded AGO2 dimeric complex, which facilitates formation and binding of the pRB co-repressor complex to a subset of E2F targets to deposit repressive chromatin marks. In addition, OIS signaling through the MAPK pathway activates JunB-containing AP1 dimers to repress expression of *CCND1* and strengthen the cell cycle arrest. Finally, increased promoter methylation, particularly flanking CpG islands, is associated with repression of cell cycle genes in senescence.

In proliferating cells, the *INK4* locus (encoding for CDKN2A, -2B, and $p14^{ARF}$) is maintained in a repressive chromatin state through lncRNA *ANRIL*-mediated recruitment of PRC1/2, catalyzing repressive histone methylation. Transcriptional activation of the *CDKN2A* gene and increased levels of CDKN2A are observed during senescence and aging, and thus, it is now considered an aging biomarker. The $p14^{ARF}$ protein also contributes to senescence by stabilizing TP53 levels through inhibition of the HMDM2 ubiquitin ligase. Increased expression of the *CDKN2B* gene has been observed in developmentally programmed, SASP-mediated, DNA-damage- and oncogene-induced senescence. Increased levels of CDKN2B are dependent on TGF-β-SMAD and PI3K-FOXO signaling and IL6-mediated activation of C/EBPß. TP53-independent CDKN1A induction is central to developmentally programmed senescence. As with CDKN2B, *CDKN1A* induction during development is dependent upon TGF-β-SMAD and PI3K-FOXO signaling in the absence of detectable DNA damage. Increased levels of *CDKN1B* are also observed in this context. The mechanisms underlying the derepression of the *INK4* locus include H3K27me3 demethylation, displacement of PRC complexes, and activation of TFs ETS1/2. In addition, ID proteins inhibit ETS TFs.

Regulation of the Inflammatory SASP–Bottom Panel

SASP induction relies on the activation of the inflammatory TFs NF-κB and C/EBPß, a chronic DNA damage response, and on the p38MAPK pathway. Many *cis*-regulatory regions of SASP genes contain NF-κB and C/EBPß binding sites, and their increased expression promotes a positive feedback loop that reinforces the senescent state through intra-, auto-, and paracrine signaling. In response to DNA damage, a DDR-activated PARP1-NF-κB axis induces the expression of a CCL2-dominated inflammatory SASP that confers metastatic properties in vivo. DDR-driven senescence involves stabilization of GATA4 by inhibiting its degradation through p62-mediated autophagy, which in turn leads to activation of NF-κB and transcription of inflammatory cytokines. OIS-induced SASP is dynamic, with an initial secretion dominated by NOTCH1, whose intracellular domain N1ICD restrains the inflammatory SASP by inhibiting the activity of C/EBPß. In this context, the super enhancer (SE) landscape is remodeled to facilitate the expression of inflammatory cytokines. This process requires the concerted binding of NF-κB and BRD4 at later stages of OIS, which promote activation of SASP-associated SEs. The NF-κB pathway is also activated through the RIG-I and IRF pathways in response to DNA damage. In this context, IRF3 contributes to the SASP by directly transcribing the *IFNß* gene. The majority of TFs involved in SASP transcriptional activation during development and reprogramming remain to be identified.

ACKNOWLEDGMENTS

This work was supported by grants from ANR-BMFT, Fondation ARC pour la recherche sur le Cancer, Association La Ligue National Contre le Cancer LNCC, INSERM, and the National Cancer Institute of the National Institutes of Health under Award Number R01CA136533. R.I.M.-Z. is a member of the Mexican National Investigator System (SNI). O.B. is a CNRS fellow.

REFERENCES

Acosta, J.C., Banito, A., Wuestefeld, T., Georgilis, A., Janich, P., Morton, J.P., Athineos, D., Kang, T.-W., Lasitschka, F., Andrulis, M., et al. (2013). Nat. Cell Biol. *15*, 978–990.

Benhamed, M., Herbig, U., Ye, T., Dejean, A., and Bischof, O. (2012). Nat. Cell Biol. *14*, 266–275.

Campisi, J., 2013. Annu. Rev. Physiol. *75*, 17.1-17.21.

Muñoz-Espín, D., and Serrano, M. (2014). Nat. Rev. Mol. Cell Biol. *15*, 482–496.

Narita, M., Nũnez, S., Heard, E., Narita, M., Lin, A.W., Hearn, S.A., Spector, D.L., Hannon, G.J., and Lowe, S.W. (2003). Cell *113*, 703–716.

Ritschka, B., Storer, M., Mas, A., Heinzmann, F., Ortells, M.C., Morton, J.P., Sansom, O.J., Zender, L., and Keyes, W.M. (2017). Genes Dev. *31*, 1–12.

Kuilman, T., Michaloglou, C., Mooi, W.J., and Peeper, D.S. (2010). Genes Dev. *24*, 2463–2479.

 Cell *170*, August 10, 2017 © 2017 Elsevier Inc. DOI http://dx.doi.org/10.1016/j.cell.2017.07.049

8.1.4 Cell Snapshot: Cellular Senescence in Pathophysiology

SnapShot: Cellular Senescence in Pathophysiology

Cell

Ricardo Iván Martínez-Zamudio, Lucas Robinson, Pierre-François Roux, and Oliver Bischof
INSERM, U993, 75015 Paris, France; Equipe Labellisée Fondation ARC pour la recherche sur le cancer, 94803 Villejuif, France; Institut Pasteur, Molecular and Cellular Biology of Cellular Senescence and Age-Related Pathologies Group, Nuclear Organization and Oncogenesis Unit, Department of Cell Biology and Infection, 75015 Paris, France

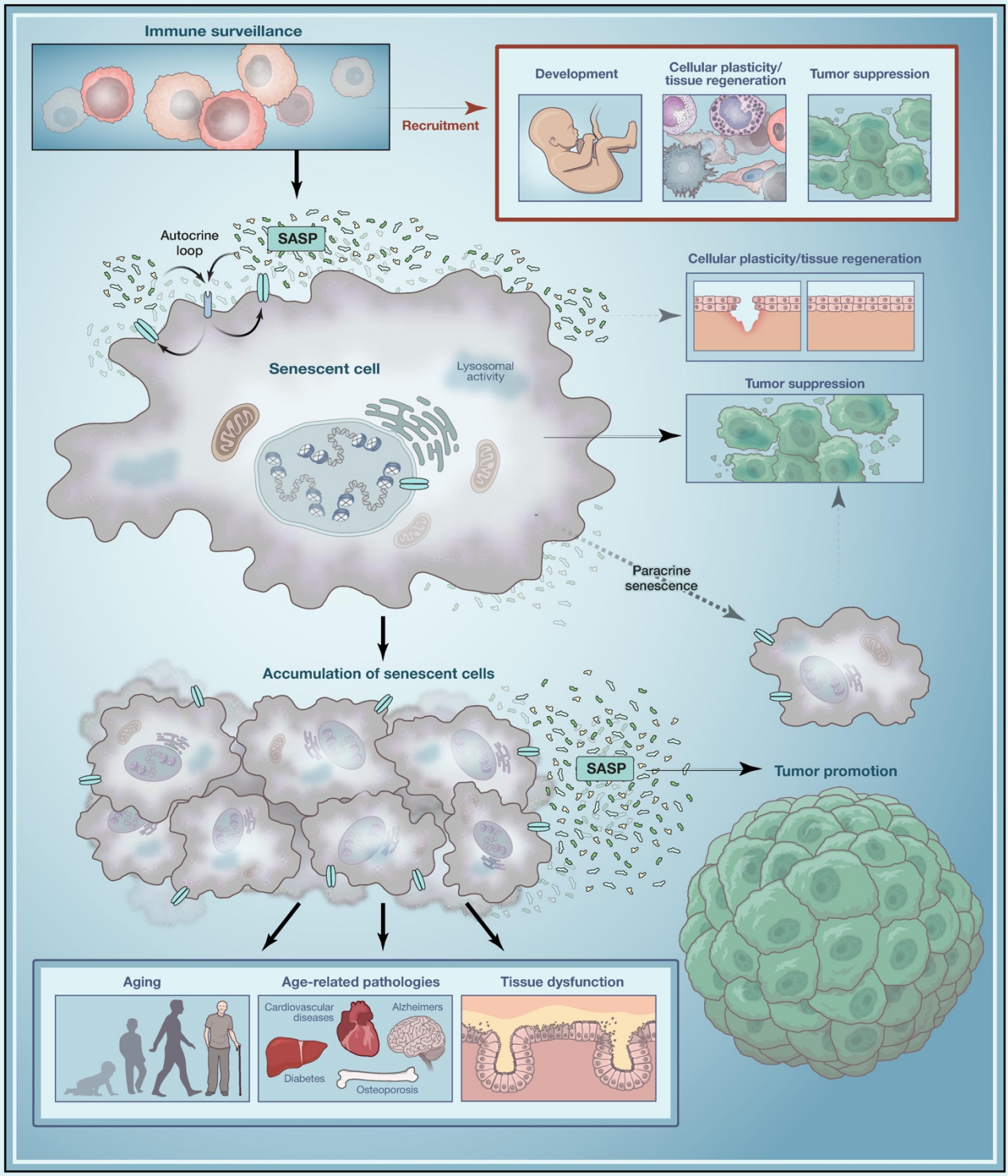

1044 Cell *170*, August 24, 2017 © 2017 Elsevier Inc. DOI http://dx.doi.org/10.1016/j.cell.2017.08.025

See online version for legends and references

SnapShot: Cellular Senescence in Pathophysiology

Cell

Ricardo Iván Martínez-Zamudio, Lucas Robinson, Pierre-François Roux, and Oliver Bischof
INSERM, U993, 75015 Paris, France; Equipe Labellisée Fondation ARC pour la recherche sur le cancer, 94803 Villejuif, France; Institut Pasteur, Molecular and Cellular Biology of Cellular Senescence and Age-Related Pathologies Group, Nuclear Organization and Oncogenesis Unit, Department of Cell Biology and Infection, 75015 Paris, France

Cellular Senescence in (Patho)physiology and Aging

Cellular senescence plays important roles during development, modulation of the (pre)cancerous state, and reprogramming/regeneration and is implicated in aging and age-related pathologies. In many instances, senescent cells exert their effects through the senescence associated secretory phenotype (SASP).

Development

Senescent cells have been observed in transient developmental structures, including the mesonephros, the apical ectodermal ridge (AER), the endolymphatic sac, and the neural roof plate, where they are thought to facilitate tissue growth and patterning, after which they are cleared by macrophages through a SASP-dependent mechanism.

Cellular Plasticity

The SASP enhances cellular plasticity and tissue regeneration in the context of senescence induced by cellular reprograming and oncogene induced senescence (OIS). These processes are generally completed with the removal of senescent cells by the immune system.

Cancer

Senescence is a potent, cell-autonomous tumor-suppressor mechanism effectively arresting the proliferation of pre-cancerous cells. Through the SASP, it further limits tumorigenic risk, cell non-autonomously, via paracrine senescence and immune surveillance. However, many SASP factors secreted by senescent cells can promote tumor development in vivo and malignant phenotypes such as proliferation and invasiveness in cell culture models. Thus, the role of senescence in cancer is time- and context-dependent.

Aging and Age-Related Pathologies

Diverse tissues of aging organisms accumulate CDNK2A-expressing senescent cells, which can compromise tissue function by loss of structural integrity and/or depletion of tissue-specific stem cell pools, thus contributing to age-related pathology and morbidity. Remarkably, depletion of CDKN2A-expressing cells in mice promotes tissue fitness and prolongs lifespan.

Perspective

It is becoming increasingly clear that senescence cannot be treated as a single-cell fate. Rather, it is a collection of phenotypes that share certain key features but otherwise are specific to the triggering stimulus and follow specific kinetics. As such, it is likely that these specific senescence programs are reflected in the physiological and pathological consequences of the senescence phenotype. Collectively, our present knowledge suggests that the senescence phenotype has its evolutionary origins in tissue regeneration and has been co-opted successively to other physiological processes. Finally, senescence therapies hold great potential to substantially improve health-span.

ACKNOWLEDGMENTS

This work was supported by grants from ANR-BMFT, Fondation ARC pour la recherche sur le Cancer, Association La Ligue National Contre le Cancer LNCC, INSERM, and the National Cancer Institute of the National Institutes of Health under Award Number R01CA136533. R.I.M.-Z. is a member of the Mexican National Investigator System (SNI). O.B. is a CNRS fellow.

REFERENCES

Acosta, J.C., Banito, A., Wuestefeld, T., Georgilis, A., Janich, P., Morton, J.P., Athineos, D., Kang, T.-W., Lasitschka, F., Andrulis, M., et al. (2013). Nat. Cell Biol. *15*, 978–990.

Baker, D.J., Childs, B.G., Durik, M., Wijers, M.E., Sieben, C.J., Zhong, J., Saltness, R.A., Jeganathan, K.B., Verzosa, G.C., Pezeshki, A., et al. (2016). Nature *530*, 184–189.

Dörr, J.R., Yu, Y., Milanovic, M., Beuster, G., Zasada, C., Däbritz, J.H.M., Lisec, J., Lenze, D., Gerhardt, A., Schleicher, K., et al. (2013). Nature *501*, 421–425.

Kuilman, T., Michaloglou, C., Mooi, W.J., and Peeper, D.S. (2010). Genes Dev. *24*, 2463–2479.

Muñoz-Espín, D., and Serrano, M. (2014). Nat. Rev. Mol. Cell Biol. *15*, 482–496.

Ritschka, B., Storer, M., Mas, A., Heinzmann, F., Ortells, M.C., Morton, J.P., Sansom, O.J., Zender, L., and Keyes, W.M. (2017). Genes Dev. *31*, 1–12.

Xue, W., Zender, L., Miething, C., Dickins, R.A., Hernando, E., Krizhanovsky, V., Cordon-Cardo, C., and Lowe, S.W. (2007). Nature *445*, 656–660.

1044.e1 Cell *170*, August 24, 2017 © 2017 Elsevier Inc. DOI http://dx.doi.org/10.1016/j.cell.2017.08.025

Titre : Décryptage les Processus Transcriptionelle dans la Sénescence Cellulaire: Le Rôle de PARP1 dans la Régulation de l'Expression Génique Associée à La Sénescence

Résumé :
La sénescence cellulaire est une réaction de stress complexe qui arrête la prolifération cellulaire et s'accompagne de bouleversements généralisés du métabolisme, de la structure de la chromatine et de l'expression des gènes, y compris la surexpression et la sécrétion de facteurs inflammatoires. La sénescence cellulaire a des effets bénéfiques en tant que mécanisme suppresseur de tumeurs et facilite le développement embryonnaire ainsi que la régénération tissulaire. Cependant, ce processus est également considéré comme un acteur important du vieillissement et des maladies liées à l'âge, principalement par son phénotype inflammatoire, appelé SASP (Senescence-associated secretory phenotype).

Les recherches actuelles pointent vers un rôle de PARP1 (poly(ADP-ribose) polymérase 1) dans la régulation transcriptionnelle des processus inflammatoires et la modulation de la structure de la chromatine. Néanmoins, les mécanismes exacts par lesquels PARP1 exerce ses fonctions de régulation et ses rôles dans le contexte de la régulation transcriptionnelle de la sénescence demeurent peu connus.

Dans ma thèse, j'ai entrepris de définir le rôle fonctionnel des activités catalytique et de liaison à la chromatine de PARP1 dans la régulation transcriptionnelle et la structure de la chromatine dans les cellules en sénescence. J'ai réalisé des analyses transcriptomiques à résolution temporelle, des études d'accessibilité de la chromatine et du paysage chromatinien de PARP1 par ChIP-Seq, ainsi que de la chromatine ADP-ribosylée en développant une nouvelle technique le CRAP-seq (Chromatin-Ribosylation-Affinity-Pulldown).

Ces analyses ont permis d'identifier une dichotomie de la fonction de PARP1 - l'une liée à son activité enzymatique d'ADP-ribosylation et l'autre à son activité de liaison à la chromatine non enzymatique - avec des impacts distincts sur le programme transcriptionnel de la sénescence. Sur la base de ces résultats, j'ai pu définir un nouveau rôle global pour PARP1 dans la modulation de la structure de la chromatine, d'une part par la stabilisation du positionnement des nucléosomes au niveau des promoteurs géniques et d'autre part par l'ADP-ribosylation des éléments régulateurs en *cis* pour finement réguler la transcription des gènes peu exprimés. Ainsi, ces recherches permettent d'envisager le rôle des inhibiteurs de PARP dans les thérapies ciblant la sénescence (thérapies sénolytiques) pour le traitement des pathologies liées au vieillissement.
Mots clefs : Sénescence, cancer, vieillissement, Epigénetique

Title : Deciphering Gene-regulatory Processes in Cellular Senescence: The Role of PARP1 in the Regulation of Senescence-Associated Gene Expression

Abstract :
Cellular senescence is a complex stress response that arrests cell proliferation and is accompanied by widespread changes in metabolism, chromatin structure, and gene-expression, including the overexpression and secretion of inflammatory factors. Cellular senescence is health-promoting as a tumor-suppressive mechanism, facilitating embryonic development and tissue regeneration. However, it is also considered a major contributor to aging and age-related diseases, mostly through its inflammatory phenotype, the so-called SASP (senescence-associated secretory phenotype).

Current research supports the role of PARP1 (Poly (ADP-ribose) polymerase 1) in the transcriptional regulation of inflammatory processes and modulation chromatin structure. However, the exact mechanisms by which PARP1 exerts its regulatory functions, and its roles in the context of regulating senescence gene-expression are underexplored.

In my thesis, I set out to define the functional role of PARP1 catalytic and chromatin binding activities in gene regulation and chromatin structure in cells undergoing senescence. I performed time-resolved transcriptomics, chromatin-accessibility studies, and mapping of the genome-wide locations of PARP1 using ChIP-seq and ADP-ribosylated chromatin using a novel technique CRAP-seq (Chromatin-Ribosylation-Affinity-Pulldown).

Together, I identified a dichotomy of PARP1 function – one related to its enzymatic ADP-ribosylation activity and the other related to its non-enzymatic chromatin binding activity – with distinct impacts on the senescence transcriptional program. Based on these findings, I can define a novel and global role for PARP1 in and chromatin structure modulation by stabilizing nucleosomes positioning at gene promoters and ADP-ribosylation of *cis*-regulatory modules to fine-tune transcription of lowly expressed genes. Indeed, based on my investigations, the role of PARP-inhibitors in senescence targeting therapies (senolytic therapies) for the treatment of age-related pathologies can be envisioned.
Keywords : Senescence, Aging, Cancer, Epigenetics